Anexo I.

Modelos teóricos de análisis de sistemas de valencia mixta.

1. MODELOS TEÓRICOS.

Para entender el comportamiento de un sistema de valencia mixta se han propuesto distintos modelos que son capaces de explicar de manera más o menos simplificada y con más o menos éxito sus características principales, e incluso llegar a determinar el acoplamiento electrónico del sistema.

1.1. Modelo de Robin y Day.

El modelo de Robin y Day constituye sólo una primera aproximación. Según este modelo, la existencia de acoplamiento electrónico entre los dos centros redox tiene como consecuencia la aparición de dos nuevos estados, con energías W_1 y W_2, cuya separación es función de la magnitud del acoplamiento electrónico. Este es un modelo muy simplificado, y su principal defecto es que no es capaz de explicar la observación de localización de carga en sistemas homonucleares (A-A*).

1.2. Modelo de PKS.

Ya hemos comentado que el modelo de Robin y Day no era capaz de explicar la localización de carga en sistemas homonucleares A-A*. Esta deficiencia fue superada con el modelo de Piepho-Krausz-Schatz o PKS,[1,2,3] ya que tiene en cuenta los movimientos vibracionales de los núcleos de manera que considera la influencia de la geometría nuclear en las propiedades electrónicas del sistema.

1.3. Modelo de Marcus y Hush.

El modelo de Transferencia Electrónica Intramolecular clásico de Marcus y Hush[4,5,6] inicialmente se desarrolló para la interpretación de las bandas de transferencia de carga en sólidos, y posteriormente se extendió y se aplicó a

transferencias de carga en compuestos de valencia mixta organometálicos[7,8] y orgánicos[9,10], así como también en transferencias de carga ligando-metal o metal-ligando.[11,12]

La validez del modelo de Hush (publicado a finales de los años 60)[5] se limita a sistemas de valencia mixta poco acoplados electrónicamente (Clase II). De hecho, considera que los estados electrónicos del sistema se pueden aproximar mediante las funciones de onda de los centros por separado. Sin embargo, a diferencia del modelo de Robin y Day, el modelo de Hush tiene en cuenta que la energía del sistema depende de la geometría de los núcleos.

El marco conceptual que se usa para entender la transferencia electrónica térmica u ópticamente inducida se ilustra mediante un diagrama de energía potencial clásico. El caso más simple para una transferencia electrónica (donde el electrón se acopla entre el dador y el aceptor por una sola oscilación teniendo la misma frecuencia en los dos estados inicial y final), se ilustra en la Figura 1. Tanto en las Figura 1a (sistema simétrico) como en la Figura 1b (sistema asimétrico), la curva de la izquierda corresponde al estado inicial mientras que la de la derecha corresponde al estado final. En los sistemas simétricos no hay diferencia de energía entre el estado inicial y el final ($\Delta G^o = 0$), al contrario que en los sistemas asimétricos (($\Delta G^o > 0$).

La transición vertical entre los estados inicial y final ($E_{opt} = \lambda$) es la energía requerida para fotoexcitar un electrón entre estos estados. Una transferencia electrónica térmicamente inducida proviene del acoplamiento vibrónico de los estados inicial y final, y tiene la energía de activación E_{term}.

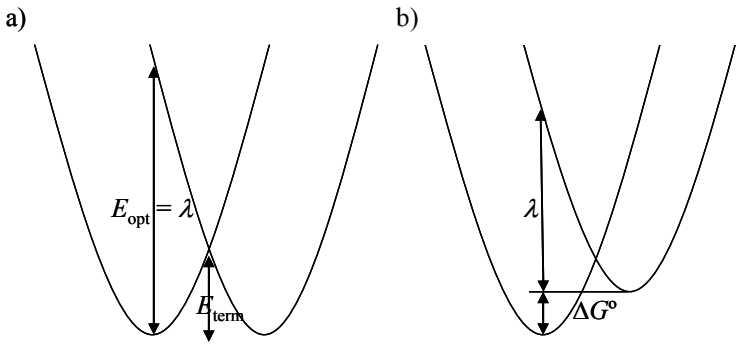

Figura 1 *Diagramas de curvas de energía potencial de los estados inicial y final de una TEI para (a) un complejo de valencia mixta simétrico (b) un sistema de valencia mixta asimétrico.*

Cuando el dador y el aceptor interactúan (débilmente: sistema de Clase II), los estados inicial y final se mezclan o combinan causando una distorsión en la curva de energía potencial. La energía de activación térmica ($E_{term} = \Delta G^{\#}$) se hace más pequeña, aumentando la magnitud de la integral de resonancia de intercambio V_{ab}, (Figura 2). La teoría de Marcus utilizó este marco conceptual para entender la dependencia de E_{term} con la naturaleza de compuestos dador-aceptor débilmente acoplados. Fue Hush quien lo aplicó al problema de las transiciones de intervalencia.

En la Figura 2 los niveles vibracionales se han omitido para simplificar el diagrama, y la energía ΔG^{o} es nula puesto que se trata de un compuesto homonuclear. El mínimo de la parte izquierda de la curva corresponde a la geometría en equilibrio en la que el electrón está situado en el centro redox de la izquierda ($M\text{-}M^{+}$), mientras que el mínimo de la parte derecha corresponde a la geometría en equilibrio en la que el electrón está localizado en el centro redox de la derecha ($M^{+}\text{-}M$). Este modelo también se llama modelo de dos estados de Hush, puesto que tiene en cuenta los dos estados que acabamos de mencionar.

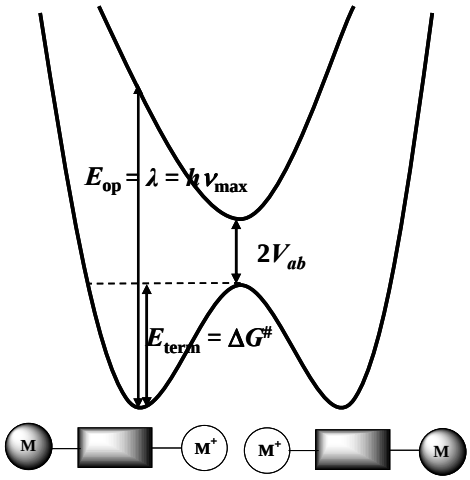

Figura 2 *Diagrama de curvas de energía potencial de un complejo de valencia mixta simétrico de Clase II.*

Para tener una Transferencia Electrónica Intramolecular estimulada térmicamente, el electrón debe moverse de izquierda a derecha a lo largo de la coordenada nuclear sin cambiar el estado electrónico, sobrepasando la barrera de energía térmica ($E_{term} = \Delta G^{\#}$), que surge de la reorganización nuclear requerida

antes de que tenga lugar la transferencia electrónica. En otras palabras, la TEI ocurre a través de un estado intermedio donde las distancias de enlace de alrededor de M y M^+ son equivalentes y con valores entre ambos estados de equilibrio.

Cuando se suministra suficiente energía térmica, la reacción es adiabática y el sistema pasa de un pozo de potencial al otro con una probabilidad (k) de la unidad. Cuando la interacción se hace más pequeña, k tiene un valor mucho menor que 1, y la reacción se vuelve no-adiabática, como en sistemas de Clase I.

Por otro lado, la Transferencia Electrónica Intramolecular ópticamente inducida (E_{opt}), de acuerdo con el principio de Frank-Condon, tiene lugar a través de un estado excitado (M^+-M)* donde ni el disolvente ni la geometría interna pueden contribuir a relajar. En otras palabras, el nuevo centro oxidado M^+ retiene las distancias de enlace y la esfera de solvatación del centro neutro, M, mientras que el nuevo centro M retiene las distancias de enlace y la esfera de solvatación del centro oxidado M^+. Como consecuencia, se observa en el espectro de absorción óptica una banda de *transición de intervalencia* correspondiente a la excitación vertical o fotoexcitación. Como se verá en detalle, con la posición, la intensidad y la anchura de la banda de intervalencia (que aparece normalmente en la región del infrarrojo cercano, NIR),[6a, 13] se puede caracterizar la Transferencia Electrónica Intramolecular.

En compuestos de valencia mixta de Clase II, donde la distorsión (V_{ab}) es pequeña (Figura 2), basándose en las propiedades de la banda de intervalencia, Hush desarrolló las siguientes expresiones:

En el caso de sistemas simétricos,

$$E_{opt} = h\nu_{max} = \lambda = 4\,E_{term}, \tag{1}$$

$$\Delta\bar{\nu}_{1/2} = (2310 \cdot h\nu_{max})^{1/2}. \tag{2}$$

Para sistemas asimétricos:

$$E_{opt} = h\nu_{max} = \lambda + \Delta G^{o}, \tag{3}$$

$$\Delta\bar{\nu}_{1/2} = (2310 \cdot \lambda)^{1/2}. \tag{4}$$

λ es la energía de reorganización total y $\Delta\bar{\nu}_{1/2}$ es la anchura de la banda de intervalencia a altura mitad. En estas expresiones se ha asumido que la banda tiene forma Gaussiana.

La energía de reorganización total, λ, puede expresarse como la suma de dos contribuciones independientes: la reorganización de los modos nucleares interiores, es decir, la alteración interna de la longitud de los enlaces o cambios vibracionales que experimenta la molécula durante la TEI, (λ_v) y la reorganización de los modos nucleares exteriores, que se origina por la reorientación de la capa de solvatación que rodea los dos centros redox (λ_{out}).[14,15]

$$\lambda = \lambda_v + \lambda_{out}. \tag{5}$$

Para sistemas débilmente acoplados, Hush demostró que la intensidad de una transición de intervalencia estaba relacionada con la amplitud del acoplamiento electrónico entre dador y aceptor (V_{ab}). A esta relación se llega partiendo de la expresión teórica de la fuerza de oscilación: [16]

$$f = 1{,}085\times10^{11}\cdot G\cdot\bar{\nu}_{max}\cdot D, \tag{6}$$

donde G hace referencia a la degeneración de los estados, $\bar{\nu}_{max}$ se asume como la energía de la banda de intervalencia cuando el coeficiente de extinción molar ε_{max} es máximo, y D es la fuerza dipolar que, para un solo electrón, está relacionada con el momento dipolar de la transición de transferencia de carga, M, mediante la siguiente expresión:

$$M = \langle\psi_g|er|\psi_e\rangle = e\cdot D^{1/2}, \tag{7}$$

En la que ψ_g es la función de onda del estado fundamental, ψ_e es la función de onda del estado excitado y er es el operador de la transición dipolar.

Si tenemos en cuenta un acoplamiento débil entre el dador y el aceptor, las funciones de onda del dador ϕ_d y del aceptor ϕ_a se pueden considerar aisladas; los coeficientes de combinación de las funciones de onda son α_{ad} = - α_{da} = α, y por teoría de perturbaciones se tiene que

$$\alpha = V_{ad}/E_d\text{-}E_a \approx V_{ad}/\bar{\nu}_{max}, \tag{8}$$

donde V_{ad} es la integral de resonancia de intercambio, que es una medida del acoplamiento electrónico entre los dos centros redox, y E_d-E_a es la diferencia de energía entre las funciones de onda del dador y el aceptor, que aproximadamente es $\bar{\nu}_{max}$.

Teniendo en cuenta todas estas simplificaciones, se obtiene que el momento dipolar de transferencia de carga se puede expresar como: [17]

$$M \cong \alpha \cdot e \cdot R \cong (V_{ad}/\bar{\nu}_{max}) \cdot e \cdot R, \quad (9)$$

donde R es la longitud de la transición dipolar (es decir, la distancia a través de la cual es tranportada la carga).

Substituyendo el valor de M (Ecuación 9) en la Ecuación 7 obtenemos la fuerza dipolar D, lo que nos permite formular la fuerza de oscilación en la Ecuación 6, como:

$$f = 1{,}085\times10^{11} \cdot G \cdot V_{ad}{}^2 \cdot R^2/\bar{\nu}_{max}. \quad (10)$$

Y si además consideramos que la banda es Gaussiana, podemos determinar también la fuerza de la oscilación de forma experimental:

$$f = 4{,}6\times10^{-9} \cdot \varepsilon_{max} \cdot \Delta\bar{\nu}_{1/2}. \quad (11)$$

Finalmente, a partir de las Ecuaciones 10 y 11 se obtiene la expresión:

$$V_{ad} = \left[2{,}05\times10^{-2}\sqrt{\varepsilon_{max}\bar{\nu}_{max}\Delta\bar{\nu}_{1/2}}\right]R^{-1}, \quad (12)$$

en la que R es la separación efectiva entre los dos centros redox, en Å, ε_{max} es el coeficiente de extinción molar máximo de la banda de absorción de intervalencia, en $M^{-1}\cdot cm^{-1}$, $\bar{\nu}_{max}$ es la energía de la transición, en cm^{-1} y $\Delta\bar{\nu}_{1/2}$ es la anchura de la banda a altura mitad, en cm^{-1}.[6b,18]

Por lo tanto, si se observa experimentalmente una banda de intervalencia en el espectro de UV-Vis-NIR y conocemos la ditancia entre centros redox, R, el modelo de Hush nos permite estimar el grado de acoplamiento electrónico entre el dador y el aceptor de nuestra especie de valencia mixta, mediante los parámetros V_{ad} (o simplemente V_{ab}) y α.

Región normal e invertida de Marcus:

Dependiendo de las condiciones bajo las cuales tiene lugar la transferencia electrónica, se pueden distinguir distintos regímenes.

En las especies de valencia mixta simétricas (con asimetría redox ΔG^o despreciable) que muestran transferencia de carga, la cinética de la transferencia de carga está governada por la región normal de Marcus (*Marcus normal-region*), donde $-\Delta G^o \leq \lambda$. En este caso, la constante de velocidad de la transferencia electrónica aumenta cuando aumenta la fuerza motriz $-\Delta G^o$ y muestra un comportamiento nomal con la temperatura: cuando se aumenta la temperatura, aumenta la probabilidad de alcanzar el estado de transición seguido por la transferencia electrónica.

Sin embargo, algunas especies asimétricas pueden mostrar una asimetría redox tan grande que se sitúan en la región invertida de Marcus (*Marcus inverted-region*), donde $-\Delta G^o > \lambda$.[19,20] En este caso, la constante de velocidad de la transferencia electrónica disminuye cuando aumenta la fuerza motriz $-\Delta G^o$.

1.4. Otros Modelos.

El modelo de Hush es el método de análisis de complejos de valencia mixta preferido por la mayoría de investigadores porque es sencillo, se superpone con la teoría de Marcus y es de fácil aplicación. Otras teorías como las desarrolladas por Levich[21] o Jortner[22] llegan a las misma relaciones que el modelo de Hush.

Sin embargo, el modelo de Marcus y Hush sólo es aplihilo en compuestos de Clase II.

El modelo de PKS se puede aplicar a complejos de valencia mixta de Clase II y III, pero no tiene en cuenta el medio. Buhks,[23] Wong y Schatz[24] ampliaron el modelo PKS para contemplar la influencia del disolvente.

Curtis y colaboradores[25] desarrollaron un análisis del acoplamiento electrónico en complejos de valencia mixta que combina resultados electroquímicos con una extensión de la teoría de Mulliken de las interacciones dador-aceptor. Este estudio se puede aplicar a complejos de Clase II y a complejos próximos a Clase III.

El modelo de tres estados de Creutz, Newton y Sutin (el llamado modelo o aproximación CNS) hace una estimación razonable del grado de acoplamiento en complejos que están en la frontera entre la Clase II y la Clase III.[26] Es un modelo que tiene en cuenta no solamente los dos centros redox sino también la contribución del puente a la transferencia de carga.[27,28]

2. EQUILIBRIO DE COMPROPORCIÓN.

Para obtener una especie de valencia mixta tenemos que oxidar (o reducir) un solo centro electroactivo de la especie inicial. En el proceso de oxidación (o reducción) se parte de la especie de partida simbolizada como (M^{II}-M^{II}) en el Esquema 1, cuando se ha oxidado (o reducido) el 50 % de la especie inicial obtenemos el máximo de concentración de especie de valencia mixta (M^{II}-M^{III}). Finalmente, el proceso redox termina cuando la especie está totalmente oxidada (o reducida): M^{III}-M^{III}.

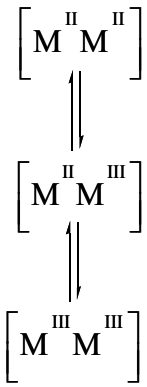

Esquema 1

Por lo tanto, la especie de valencia mixta está en equilibrio con la especie inicial y la especie totalmente oxidada (o reducida), y este equilibrio se denomina equilibrio de comproporción.

La constante del equilibrio de comproporción definido por la Ecuación 13, K_c, y la energía libre de comproporción, ΔG^{o}_{c}, son una alternativa para determinar el grado de deslocalización electrónica.[a,29]

La constante de comproporción (K_c) para complejos de Clase I y II se obtiene del equilibrio de comproporción siguiente:

$$\left[M^{II}M^{II}\right]+\left[M^{III}M^{III}\right] \overset{K_c}{\rightleftharpoons} 2\left[M^{II}M^{III}\right]. \quad (13)$$

El valor de la constante del equilibrio de comproporción expresa la estabilidad de la especie de valencia mixta [M^{II} M^{III}] frente a las especies [M^{II} M^{II}] y [M^{III} M^{III}], donde:

$$K_c = \frac{\left[M^{II}M^{III}\right]^2}{\left[M^{II}M^{II}\right]\left[M^{III}M^{III}\right]}. \quad (14)$$

Para especies de Clase III el equilibrio de comproporción se determina de:

$$\left[M^{II}M^{II}\right]+\left[M^{III}M^{III}\right] \overset{K_c}{\rightleftharpoons} 2\left[M^{II1/2}M^{II1/2}\right]. \quad (15)$$

El valor de K_c se puede establecer electroquímicamente a partir de la separación de las ondas de potencial redox de los dos centros electroactivos, ΔE^o, por medio de la ecuación siguiente:

$$K_c = \exp(\Delta E^o F/RT), \quad (16)$$

$$\Delta G_c^o = -RT\ln K_c = -\Delta E^o F. \quad (17)$$

Donde F es la constante de Faraday y F/RT tiene un valor de 38,92 V^{-1} a 298 K.[6a,29] Si la separación de las ondas de potencial redox es pequeña, o están mal resueltas, el valor de K_c sólo se puede obtener a partir de una valoración redox, representando la densidad óptica *vs x* (número de electrones añadidos u extraídos del sistema).[6a,29,30]

Para obtener aislado el complejo en su estado de valencia mixta es fundamental tener valores grandes de ΔE^o y K_c. Si esto es así, entonces la proporción de la especie de valencia mixta cuando se ha oxidado o reducido totalmente un centro redox (P) es del 100 %, siendo:

$$P = K_c^{1/2} / (2 + K_c^{1/2}). \quad (18)$$

Sin embargo, si el valor de K_c es pequeño, cuando se ha oxidado o reducido la mitad de la especie inicial, la proporción P de la especie de valencia mixta ya no

es del 100 %, por lo tanto esto se tiene que tener en cuenta para corregir su espectro de UV-Vis-NIR.

Hay cuatro factores que contribuyen a la magnitud de ΔG_c^o: un factor entrópico o contribución estadística ($1/2RTln1/4$), un factor electrostático (ΔG_e^o) originado por la repulsión de cargas de los centros metálicos, un factor inductivo de estabilización de los centros M^{II} y M^{III} o viceversa (ΔG_i^o) y un factor de estabilización por intercambio de resonancia (ΔG_r^o) debido a la deslocalización electrónica.

$$\Delta G_c^o = 1/2RTln1/4 + \Delta G_e^o + \Delta G_i^o + \Delta G_r^o. \quad (19)$$

En especies de Clase II las tres primeras contribuciones se pueden determinar.[6,29, 31] ΔG_r^o es el único componente que representa realmente el acoplamiento entre los dos centros redox, y está relacionado con V_{ab} por las Ecuaciones 20a y 20b para sistemas localizados y deslocalizados, respectivamente.[27,32]

$$-\Delta G_r^o = 2V_{ab}/\lambda, \quad (20a)$$

$$-\Delta G_r^o = 2(V_{ab} - \lambda/4). \quad (20b)$$

En cualquier caso, hay que ser cautos con la interpretación de los datos electroquímicos, puesto que puede haber una dependencia significativa de los potenciales redox con la naturaleza del disolvente y del contraión del electrolito.[33]

3. ANÁLISIS DE ESPECIES ENTRE CLASE II Y CLASE III.

Como ya se ha comentado, existen especies de valencia mixta que se encuentran en el régimen llamado de Clase II-III.

La apariencia de la banda de intervalencia y la dependencia con el disolvente es la información experimental más valiosa para distinguir entre la Clase II, donde la banda es ancha, poco intensa, con forma Gaussiana y dependiente del disolvente y la Clase II-III, con bandas más estrechas e intensas, asimétricas e independientes del disolvente utilizado.

El que la anchura de la banda de intervalencia a altura mitad determinada experimentalmente $\Delta\bar{\nu}_{1/2}{}^{0}$ sea menor que la que se predice teóricamente $\Delta\bar{\nu}_{1/2}$ = $(2310\times\lambda)^{1/2}$ [34] según el modelo de Hush de dos estados,[5,6a,26] es un indicio de que el grado de deslocalización es considerable en la especie de valencia mixta.[35]

Brunschwig, Creutz y Sutin introdujeron un criterio para clasificar las especies (Clase II débilmente o moderadamente acoplada, Clase II-III o Clase III) basado en la anchura de la banda de intervalencia a altura mitad experimental y predicha, mediante el parámetro Γ: $\Gamma = 1 - (\Delta\bar{\nu}_{1/2}{}^{o}/\Delta\bar{\nu}_{1/2})$.[36]

4. EFECTO DEL DISOLVENTE.

La teoría de Marcus y Hush permite correlacionar la energía de una absorción óptica debida a una transición de transferencia de carga (E_{opt} o $h\nu_{max}$) con los cambios de energía libre que la molécula experimenta durante la Transferencia Electrónica Intramolecular: λ_v y λ_{out}. Si el compuesto es asimétrico se añade, además, la asimetría redox o asimetría energética ΔG^o, (Ecuación 21, combinación de las Ecuaciones 3 y 5).

$$E_{opt} = h\nu_{max} = \lambda_v + \lambda_{out} + \Delta G^o (+ \Delta E') . \qquad (21)$$

$\Delta E'$ se refiere a cualquier energía adicional asociada a la excitación.[6a,37]

La energía de reorganización de los modos nucleares exteriores (λ_{out}) se origina por la reorientación de la capa de solvatación de alrededor de los dos centros redox, que difiere antes y después de que tenga lugar la TEI. Su valor se puede estimar mediante la ecuación siguiente:

$$\lambda_{out} = e^2\left(\frac{1}{\varepsilon_{opt}} - \frac{1}{\varepsilon_s}\right)\left(\frac{1}{2r_a} + \frac{1}{2r_b} - \frac{1}{R}\right), \qquad (22)$$

donde e es la carga electrónica, ε_{opt} y ε_s son las constantes dieléctricas óptica y estática del disolvente, r_a y r_b son los radios de los reactivos, y R es la distancia entre los dos centros redox.

Entonces, en compuestos simétricos, la dependencia del disolvente con la energía óptica de la banda de transferencia de carga viene determinada por el

término λ_{out}, mientras que en compuestos asimétricos viene determinada por λ_{out} y la asimetría redox, ΔG^o. En complejos de valencia mixta simétricos débilmente acoplados (Clase II) donde los términos λ_v y $\Delta E'$ se pueden considerar independientes respecto al disolvente, el desplazamiento de E_{opt} con la naturaleza del disolvente debería mostrar una correlación lineal con $\left(\frac{1}{\varepsilon_{opt}} - \frac{1}{\varepsilon_s}\right)$, aunque en realidad esto es una aproximación, como se verá ahora.

Una manera habitual de describir la polaridad de un disolvente es por medio de los modelos que tienen en cuenta el disolvente como un continuo (*solvent continuum models*) y sus propiedades se definen solamente por las constantes dieléctricas estática ε_s y óptica $\varepsilon_{opt} = n^2$ (siendo n el índice de refracción). Dependiendo del modelo geométrico escogido, la dependencia de las distintas energías individuales con el disolvente puede describirse por funciones de polaridad del disolvente basadas en diferentes combinaciones de ε_s y n^2.[38]

En estos modelos no se tienen en cuenta las interacciones específicas solvente/soluto y se asume que el disolvente tiene momento dipolar pero un momento multipolar despreciable. Para tener en cuenta las interacciones específicas solvente/soluto y explicar los comportamientos solvatocrómicos, se han utilizado diversos métodos empíricos,[39, 40] uno de los más usados es la aproximación multiparamétrica LSER, acrónimo de Linear Solvent Energy Relationship, desarrollada por Kamlet, Taft y colaboradores.[41]

5. BIBLIOGRAFÍA.

1. S. B. Piepho, E. R. Krausz, P. N. Schatz, *J. Am. Chem. Soc.* **1978**, *100*, 2996.

2. P. N. Schatz , S. B. Piepho, E. R. Krausz, *Chem. Phys. Lett.* **1978**, *55*, 539.

3. K. Y. Wong, P. N. Schatz, S. B. Piepho, *J. Am. Chem. Soc.* **1979**, *101*, 2793.

4. a) R. A. Marcus, *J. Chem. Phys.* **1956**, *24*, 966. b) R. A. Marcus, *J. Chem. Phys.* **1957**, *26*, 867. c) R. A. Marcus, *Annu. Rev. Phys. Chem*. **1964**, *15*, 155. (d) R. A. Marcus, N. Sutin, *Biochim. Biophys. Acta* **1985**, *811*, 265. e) R. A. Marcus, P. Siders, *J. Phys. Chem*. **1982**, *86*, 622. (f) R. A. Marcus, N. Sutin, *Inorg. Chem*. **1975**, *14*, 213. (g) N. Sutin, *J. Photochem*. **1979**, *10*, 19. (h) R. A. Marcus, *J. Phys. Chem*. **1965**, *43*, 679. (i) R. A. Marcus, *Angew. Chem. Int. Ed.* **1956**, *24*, 966.

5. a) N. S. Hush, *Prog. Inorg. Chem*. **1967**, *8*, 391. b) N. S. Hush, *Trans. Faraday Soc.* **1961**, *57*, 557. c) N. S. Hush, *Electrochim. Acta* **1968**, *13*, 1005. d) N. S. Hush, *Coord. Chem. Rev*. **1985**, *64*, 135. e) R. S. Mulliken, *J. Am. Chem. Soc.* **1952**, *64*, 811. f) R. S. Mulliken, W. B. Person, *Molecular Complexes* (Wiley, New York, **1969**).

6. a) R. J. Crutchley, *Adv. Inorg. Chem.* **1994**, *41*, 273. b) S. Barlow, D. O'Hare, *Chem. Rev.* **1997**, *97*, 637.

7. M. C. B. Colbert, J. Lewis, N. J. Long, P. R. Raithby, M. Younus, A. J. P. White, D. J. Williams, N. N. Payne, L. Yellowlees, D. Beljonne, N. Chawdhury, R. H. Friend, *Organometallics* **1998**, *17*, 3034.

8. Y. Zhu, O. Clot, M. O. Wolf, G. P. A. Yap, *J. Am. Chem. Soc*. **1998**, *120*, 1812.

9. S. F. Nelsen, H. Q. Tran, M. A. Nagy, *J. Am. Chem. Soc*. **1998**, *120*, 298.

10. C. Lambert, G. Nöll, *J. Am. Chem. Soc*. **1999**, *121*, 8434.

11. a) P. Desjardins, G. P. A. Yap, R. J. Crutchley, *Inorg. Chem*. **1999**, *38*, 5901. b) C. E. B. Evans, M. L. Naklicki, R. J. Crutchley, *Inorg. Chem*. **1995**, *34*, 1350.

12. T. Ito, N. Imai, T. Yamagushi, T. Hamaguchi, C. H. Londergan, C. P. Kubiak, *Angew. Chem. Int. Ed.* **2004**, *43*, 1376 y referencias citadas en él.

13. R. J. Crutchley, *Adv. Inorg. Chem.* **1994**, *41*, 273.

14. R. A. Marcus, *Angew. Chem.* **1993**, *32*, 1111 y referencias citadas.

15. J. P. Sauvage, J.-P. Collin, J.-C. Chambron, S. Guillerez, C. Coudret, *Chem. Rev.* **1994**, *94*, 993 y referencias citadas.

16. N. Mataga, T. Kubota, "*Molecular Interactions and Electronic Spectra*". Dekker, New York, **1970**.

17. P. Chen, M. Curry, T. J. Meyer, *Inorg. Chem.* **1989**, *28*, 2271.

18. K. Y. Wong, P. N. Schatz, "*A progress in Inorganic Chemistry*" 369. Wiley, New York.

19. a) S. Utamapanya, A. Rajca *J. Am. Chem. Soc.* **1991**, *113*, 9242. b) J. P. Telo, C. B. L. Shohoji, B. Herold, G. Grampp *J. Chem. Soc. Faraday Trans.* **1992**, *88*, 47. c) L. Hviid, A. M. Brouwer, M. N. Paddon-Row, J. W. Verhoeven *Chem. Phys. Chem*. **2001**, *2*, 232. d) K. A. Jolliffe, T. D. M. Bell, K. P. Ghiggino, S. J. Langford, M. N. Paddon-Row *Angew. Chem. Int. Ed*. **1998**, *37*, 916. e) T. D. M. Bell, K. P. Ghiggino, K. A. Jolliffe, M. G. Ranasinghe, S. J. Langford, M. J. Shephard, M. N. Paddon-Row *J. Phys. Chem. A*. **2002**, *106*, 10079. f) A. S. D. Sandanayaka, H. Sasabe, Y. Araki, Y. Furusho, O. Ito, T. Takata *J. Phys. Chem. A*. **2004**, *108*, 5145.

20. a) G. L. Closs, J. R. Miller *Science* **1988**, *240*, 440. b) G. L. Closs, L. T. Calcaterra, N. J. Green, K. W. Penfield, J. R. Miller *J. Phys. Chem.* **1986,** *90*, 3673. c) J. R. Miller, L. T. Calcaterra, G. L. Closs *J. Am. Chem. Soc.* **1984**, *106*, 3047.

21. V. G. Levich, R. R. Dogonadze, *Collect Czech. Chem. Commun.* **1961**, *26*, 193.

22. J. Jortner, *J. Chem. Phys.* **1976**, *64*, 4860.

23. E. Buhks, *Tesis*, Tel Aviv University, Tel Aviv, **1980**.

24. K. Y. Wong, P. N. Schatz, *Mechanistic Aspects of Inorganic Reactions* cap. 12, p. 281. American Chemical Society, Washington, D. C., **1982**.

25. F. Salaymeh, S. Berhane, R. Yusof, R. de la Rosa, E. Y. Fung, R. Matamoros, K. W. Lau, Q. Zheng, E. M. Kober, J. C. Curtis, *Inorg. Chem.* **1993**, *32*, 3895.

26. S. F. Nelsen, *Chem. Eur. J*. **2000**, *6*, 581.

27. B. S. Brunschwig, N. Sutin, *Coord*. *Chem. Rev.* **1999**, *187*, 233.

28. C. Creutz, M. D. Newton, N. Sutin, *J. Photochem.* **1994**, *82*, 47.

29. D. E. Richardson, H. Taube, *Coord. Chem. Rev.* **1984**, *60*, 107.

30. A. C. Ribou, J. P. Launay, K. Takhashi, T. Nihira, S. Tarutani, C. W. Spangler, *Inorg. Chem.* **1994**, *33*, 1325.

31. M. D. Ward, *Chem. Soc. Rev.* **1995**, *24*, 121.

32. J. E. Sutton, H. Taube, *Inorg. Chem.* **1981**, *20*, 3125.

33. a) C. Pataoux, C. Coudret, J. P. Launay, C. Joachim, A. Gourdon, *Inorg. Chem.* **1997**, *36*, 5037. b) J. P. Launay, *Chem. Soc. Rev.* **2001**, *30*, 386.

34. a) C. M. Elliot, D. L. Derr, D. V. Matyushov, M. D. Newton, *J. Am. Chem. Soc*. **1998**, *120*, 11714. b) J. C. Curtis, T. J. Meyer, *Inorg. Chem*. **1982**, *21*, 1562.

35. K. D. Demadis, C. M. Hartshorn, T. J. Meyer, *Chem. Rev*. **2001**, *101*, 2655.

36. a) B. S. Brunschwig, C. Creutz, N. Sutin, *Chem. Soc. Rev*. **2002**, *31*, 168. b) D. M. D´Alessandro, F. K. Keene, *Chem. Soc. Rev.* **2006**, *35*, 424.

37. J. T. Huup, T. J. Meyer, *Inorg. Chem.* **1986**, *26*, 2332.

38. a) B. S. Brunschwig, S. Ehrenson, N. Sutin *J. Phys. Chem*. **1987**, *91*, 4714. b) M. M. Karelson, M. C. Zerner *J. Phys. Chem*. **1992**, *96*, 6949.

39. A. R. Katritzky, D. C. Fara, H. Yang, K. Tämm *Chem. Rev*. **2004**, *104*, 175.

40. a) M. J. Kamlet, R. W. Taft *J. Am. Chem. Soc.* **1976**, *98*, 377, 2886. b) M. J. Kamlet, J.-L. Abboud, R. W. Taft *Prog. Phys. Org. Chem*. **1981**, *13*, 481. c) C. Laurence, P. Nicolet, M. T. Dalati, J.-L. M. Abboud, R. Notario *J. Phys. Chem*. **1994**, *98*, 5807.

41. a) J.-L. M. Abboud, M. J. Kamlet, R. W. Taft, *J. Am. Chem. Soc.* **1977**, *99*, 8325. b) M. J. Kamlet, R. W. Taft, M. H. Abraham, R. M. Doherty, *J. Am.*

Chem. Soc. **1984**, *106*, 464. c) C. Reichardt, "*Solvent and Solvent Effects in Organic Chemistry*", 2nd. Ed.; VCH: New York, **1990**, Chapter 7. d) R. W. Taft, J. L. M. Abboud, M. J. Kamlet, M. H. Abraham, *J. Solut. Chem.* **1985**, *14*, 153.

Anexo II.

Resonancia Paramagnética Electrónica.

1. INTRODUCCIÓN A LA RESONANCIA PARAMAGNÉTICA ELECTRÓNICA.

La Resonancia Paramagnética Electrónica es una potente herramienta a la hora de caracterizar radicales orgánicos, proporcionando diferentes tipos de información en función del diseño del experimento y de las características de la muestra: Espectros de radicales aislados en condiciones isótropas (disoluciones diluidas) en los que se pueden determinar las constantes de acoplamiento hiperfino, el factor de Landé, la forma y anchuras de línea, la densidad de espín en muchos de los núcleos que forman el radical, la influencia de factores extrínsecos como la concentración, la temperatura, la viscosidad, etc., o en condiciones anisótropas (disoluciones diluidas sólidas) en los que se pueden determinar anisotropías del tensor *g* y del tensor acoplamiento hiperfino. También se pueden estudiar procesos dinámicos (fenómenos de ensanchamiento de línea tanto homogéneos como heterogéneos).

En los espectros de agregados supramoleculares de radicales, cuando son agregados discretos, (dímeros, trímeros) o se trata de bi, tri o poliradicales, especialmente en las denominadas moléculas de alto espín, se pueden estudiar las interacciones anisótropas dipolares y las interacciones isótropas de canje. En el caso de agregados extensos (sólidos moleculares cristalinos) la RPE proporciona datos sobre la anisotropía magnética de los radicales que lo componen, así como de la dimensionalidad y tipo de las interacciones magnéticas de canje intermoleculares en los cristales. En sistemas que presenten propiedades conductoras la RPE puede dar información sobre la anisotropía de la conductividad eléctrica en el cristal, y en general, también se puede obtener información sobre transiciones estructurales, cambios de fase, etc. Para profundizar en los fundamentos espectroscópicos sugerimos al lector bibliografía especializada.[1,2,3]

2. DESCRIPCIÓN DE LA RPE.

Las resonancias magnéticas son espectroscopías, en las que un campo magnético oscilante induce transiciones magnéticas entre niveles de energía de un sistema paramagnético, al desdoblarse estos por la aplicación de un campo magnético estático. En particular, la Resonancia Paramagnética Electrónica estudia los dipolos magnéticos de origen electrónico y, dado que la magnitud que los gobierna es el magnetón de Bohr, habitualmente se manifiesta en la zona de las microondas (10^9 – 10^{11} Hz, para la banda X), mientras que para la Resonancia Magnética Nuclear, que se focaliza en espines de origen nuclear, la diferencia de energías es del orden de las radiofrecuencias (10^6 – 10^9 Hz).

Para describir el comportamiento de un sistema paramagnético aislado (espín localizado) sometido a un campo magnético **B**, en lo que a su espectro de RPE se refiere, se hace uso del formalismo del Hamiltoniano de espín. Si tenemos en cuenta la existencia de núcleos con un momento angular $I \neq 0$ además del electrón desapareado en el sistema paramagnético, el Hamiltoniano de espín puede escribirse como:

$$H = \mu_B \overline{B}\,\overline{g}\,\overline{S} - \mu_N \overline{B}\,\overline{g}_N\,\overline{I} + \overline{I}\,\overline{A}\,\overline{S} + \overline{S}\,\overline{D}\,\overline{S}$$

Expresión en la que figuran las cuatro interacciones más importantes: la interacción Zeeman electrónica entre el electrón desapareado y el campo magnético, la interacción Zeeman nuclear entre los núcleos con $I \neq 0$ y el campo magnético, la interacción hiperfina entre el espín electrónico y los núcleos con $I \neq 0$ y la interacción dipolar o desdoblamiento a campo cero entre dos o más electrones desapareados entre sí.

3. ESPECTROS EN CONDICIONES ISÓTROPAS. DISOLUCIONES DILUIDAS.

Los espectros de RPE de radicales en disolución, en especial los de radicales orgánicos, son los más sencillos de interpretar por lo que comenzaremos con su estudio. En el caso de un radical con un electrón desapareado y en condiciones isótropas, la expresión del Hamiltoniano de espín queda reducida a:

$$H = \mu_B B g \bar{S}$$

y puesto que la energía E, es proporcional al momento magnético, la cuantización del momento angular de espín ($m_S = \pm 1/2$) determina la cuantización de los niveles de energía del electrón en un campo magnético, obteniéndose en este caso dos niveles:

$$E_\alpha = +\tfrac{1}{2} g\mu_\beta$$

$$E_\beta = -\tfrac{1}{2} g\mu_\beta$$

siendo la ecuación de resonancia correspondiente a la transición entre estados β y α (ver Figura 1) la siguiente:

$$\Delta E = E_\alpha - E_\beta = g\mu_B B = h\nu$$

por lo que aparecerá en el espectro una única línea centrada en el campo de resonancia correspondiente, con un factor g y una anchura de línea características del radical.

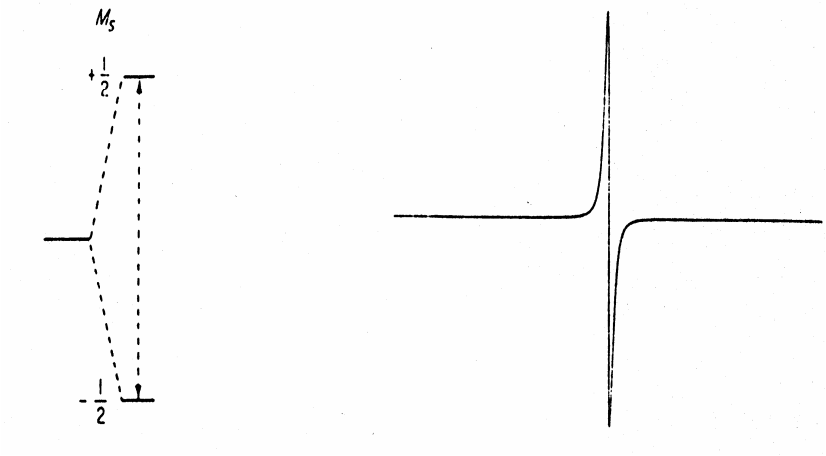

Figura 1 *Representación de la separación energética de un espín electrónico sometido a un campo magnético B y el espectro de RPE correspondiente.*

Si en el sistema paramagnético, por ejemplo un radical orgánico, que tiene núcleos con $I \neq 0$, habrá que tener en cuenta también la interacción hiperfina, que en disolución, o lo que es lo mismo, cuando el radical está girando con respecto al campo magnético lo suficientemente rápido como para observar sólo el promedio, ésta interacción es isótropa. Un radical que tenga un solo núcleo (n=1) con I = ½,

como es el caso del hidrógeno presentará 2nI+1=2 líneas, con un desdoblamiento hiperfino, *a*, que será proporcional a la densidad de espín del electrón sobre dicho átomo. En el caso del radical fenil α-nitronil nitróxido, que presenta dos N equivalentes (I=1), 12 H equivalentes de los cuatro grupos metilo y 5 H del anillo aromático; 2 H*orto*, 2 H*meta* y 1 H*para*, el espectro presentará un total de $\Pi_j(2\ N_j\ I_j + 1)$=1170 líneas distribuidas en 5 grupos de líneas muy solapadas entre sí. Los espectros experimental y simulado se muestran en la Figura 2 siendo las constantes de acoplamiento (en Gauss) determinadas por simulación, las siguientes: *a*N: 7,43; aH_{CH3}: 0,21; aH_o: 0,49; aH_m: 0,17; aH_p: 0,42 y $a^{13}C_\alpha$: 12,0.

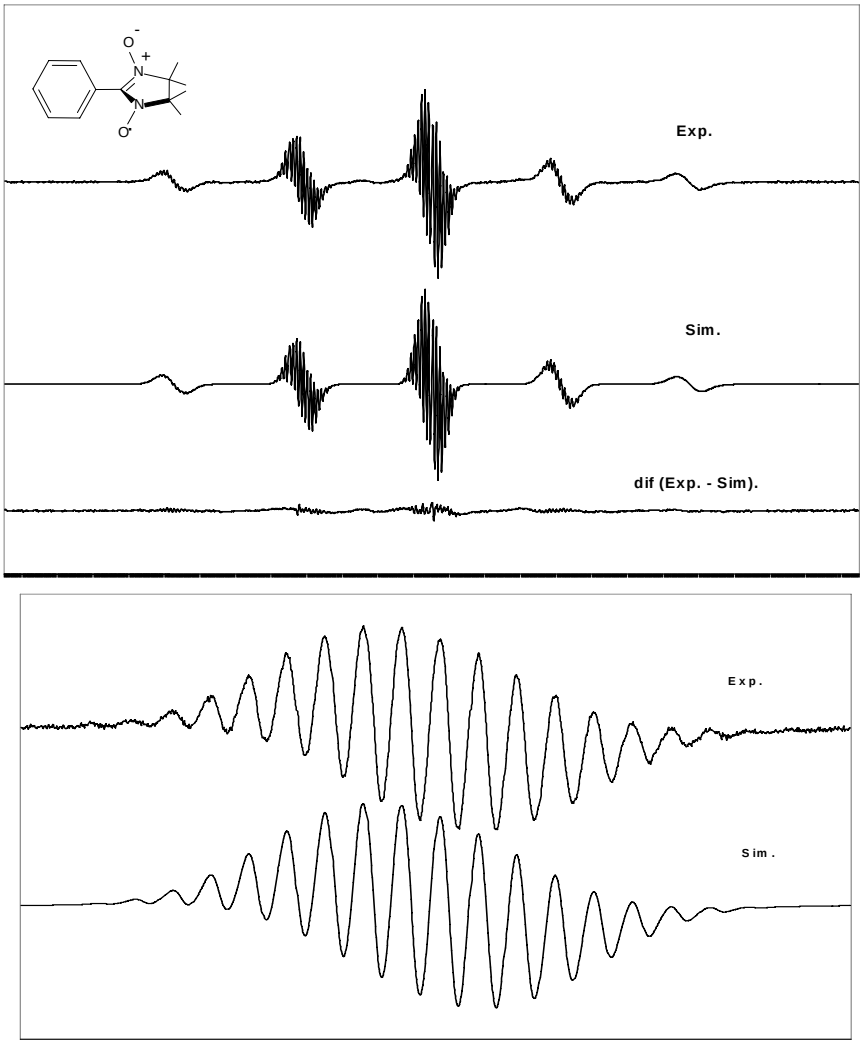

Figura 2 *Espectro experimental y simulado del radical fenil α-nitronil nitróxido (arriba) y detalle del conjunto de líneas centrales experimentales y simuladas (abajo) en condiciones de alta resolución.*

En general, existen unas reglas de interpretación de espectros de RPE en disolución, y se cumplen siempre que haya condiciones isótropas y desdoblamientos de primer orden. Las más importantes son las siguientes:

1- El espectro debe ser simétrico con respecto a un punto central.
2- La falta de señal central indica un número de núcleos equivalentes impar.
3- La separación entre las dos líneas exteriores, siempre da el valor de desdoblamiento hiperfino más pequeño.
4- Cuando sólo hay núcleos con I = ½, la suma $\Sigma_j\ n_j\ |a_j|$ es igual a la extensión total del espectro. Donde n_j es el número de núcleos con desdoblamiento hiperfino a_j.
5- El número máximo de líneas posible viene dado por la expresión: $\Pi_j(2\ N_j\ I_j + 1)$. Donde N_j es el número de núcleos equivalentes con espín I_j.
6- La mejor prueba de una correcta interpretación es la simulación del espectro.

La reorientación rápida de los radicales en disolución promedia cualquier anisotropía en el factor g y en las constantes de acoplamiento hiperfino. Esto, junto con la simetría y la alta resolución del espectro así obtenido, facilita la identificación del radical, mientras que la interpretación del espectro, permite asignar las constantes de acoplamiento hiperfino y conocer así la densidad de espín del electrón desapareado por toda la molécula.

En disolución también se puede estudiar la influencia en la forma del espectro de factores como la concentración del radical, la temperatura, la viscosidad etc., y estudiar procesos dinámicos como cinéticas de reacción, equilibrios monómero - dímero u otros muchos.

4. EFECTOS DINÁMICOS.

Podemos decir de forma general que, cualquier proceso dinámico en el entorno de un centro paramagnético, puede afectar la forma de las líneas de un espectro y provocar fenómenos de ensanchamiento que se apartan del comportamiento típico de un radical en condiciones isótropas. Así, cualquier proceso dinámico molecular como cambios conformacionales, interacciones con otras moléculas paramagnéticas, reacciones químicas que impliquen, por ejemplo,

transferencias protón o equilibrios ácido-base, volteo molecular lento debido a la viscosidad del medio, etc., y por supuesto, Transferencias Electrónicas Intramoleculares, puede presentar fenómenos de ensanchamiento de línea homogéneo. El efecto suele ser un ensanchamiento de las líneas del espectro provocado por fluctuaciones dinámicas en el campo magnético local al que está sometido el electrón desapareado. Si los cambios se desarrollan lo suficientemente despacio, es decir, la velocidad es inferior al tiempo de respuesta de la técnica, se observan líneas asignables a las distintas especies del sistema (por ejemplo distintos confórmeros, distintos entornos etc.). A medida que la velocidad de las fluctuaciones aumenta, las líneas del espectro se ensanchan y finalmente, cuando la velocidad del proceso es superior al tiempo de respuesta de la técnica, coalescen en una única línea, o grupo de líneas, y su posición es promedio de la posición de las líneas originales.

En la Figura 3 se ilustra el efecto dinámico de forma geneal.[2] Existen muchos modelos teóricos que se pueden utilizar para simular los efectos de las fluctuaciones de campo magnético sobre las señales de RPE. Aquí se usa el modelo generalizado de las ecuaciones de Bloch, pero, a pesar de que no es muy difícil de entender, no se dará una explicación exhaustiva, puesto que excede la intención de este anexo. Solamente se explicarán de forma sucinta las diferentes situaciones que conlleva el proceso dinámico en aras de la comprensión del proceso.

Consideremos un radical que tiene dos entornos distintos, *a* y *b*. Supongamos que, por simplicidad, cada forma tiene una única línea de RPE. Una resuena a un campo magnético B_a y la otra a B_b y su separación será $\Delta B_0 = B_b - B_a$.

En la Figura 3 *a*, el sistema se encuentra en el límite de velocidad de interconversión lenta. La velocidad de interconversión es inferior al tiempo de respuesta del equipo, o lo que es lo mismo, el tiempo de vida medio de cada uno de los estados, *a* o *b* es muy alto, $\tau \rightarrow \infty$, por lo que aparece para cada especie una señal estrecha cuya anchura, Γ, denominaremos como inicial, Γ_0, como la que tiene el radical sin sufrir ningún proceso dinámico.

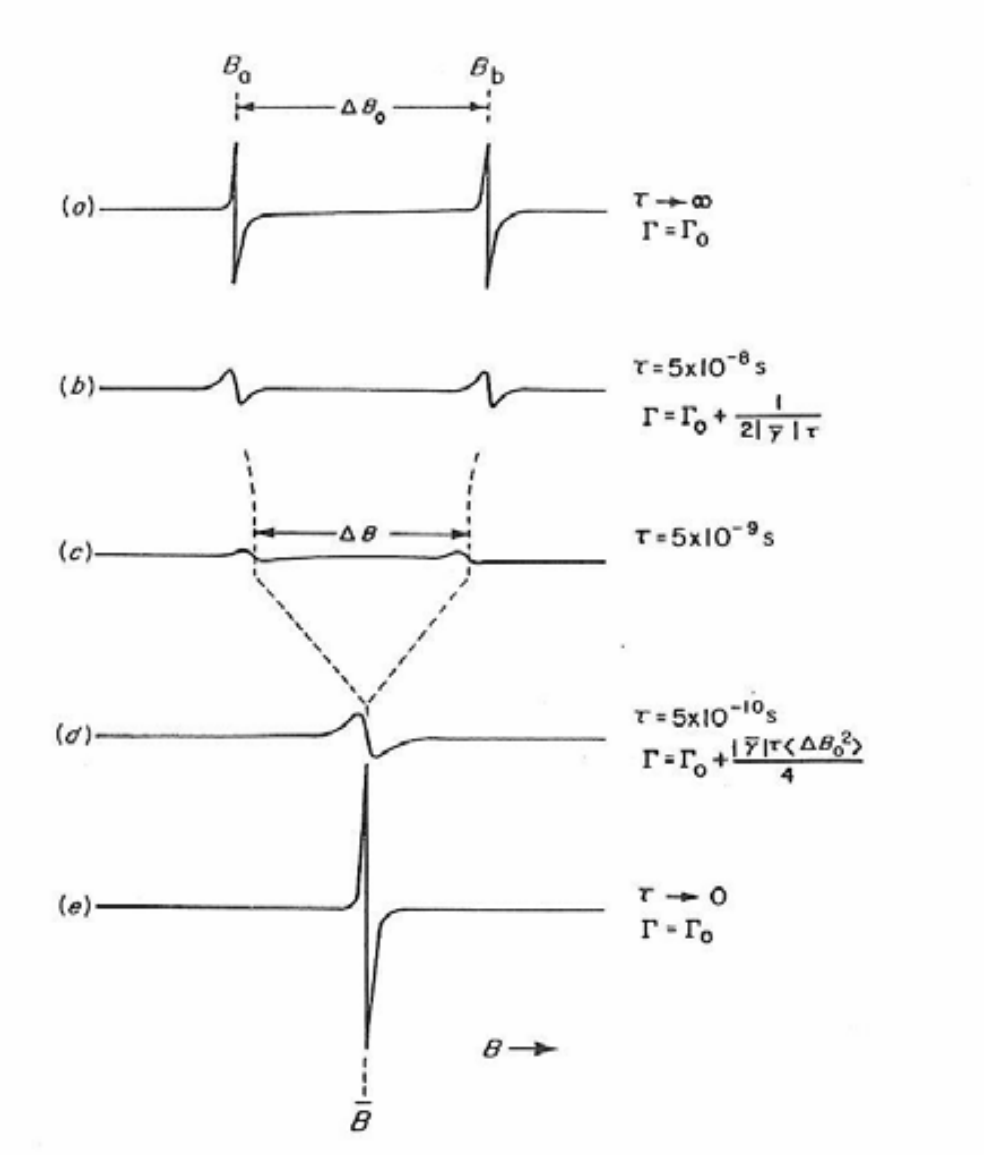

Figura 3 *Simulación de un espectro de RPE mostrando el efecto dinámico que ocasiona el aumento de la velocidad de interconversión entre dos especies a y b correspondientes a un mismo radical.*

En la Figura 3*b*, La velocidad de interconversión es moderada y está más próxima al tiempo de respuesta del equipo, el tiempo de vida medio de cada uno de los estados, *a* o *b* es menor, $\tau = 5 \times 10^{-8}$ s, y la anchura de línea comienza a aumentar.

En la Figura 3*c*, $\tau = 5 \times 10^{-9}$ s. La velocidad es tan rápida que la influencia se extiende no solo al ensanchamiento de las líneas sino que comienzan a desplazarse siendo ΔB_0 cada vez más pequeño.

La Figura 3*d*, $\tau = 5 \times 10^{-10}$ s es el punto de coalescencia. $\Delta B_0 \rightarrow 0$ y la línea ancha todavía, se centra en el punto medio, $(B_b + B_a)/2$.

Finalmente, en la Figura 3*e*, es el límite de velocidad de interconversión rápida. La velocidad de interconversión es claramente superior al tiempo de respuesta del equipo, o lo que es lo mismo, el tiempo de vida medio de cada uno de los estados, *a* o *b* es muy bajo, $\tau \rightarrow 0$, por lo que aparece una única señal cuya anchura vuelve a ser estrecha, $\Gamma = \Gamma_0$.

Una vez que se entiende el fenómeno general de ensanchamiento y cambio de posición de líneas que implica un proceso dinámico, se puede explicar lo que ocurre en el caso concreto de que, en un radical, tenga lugar una Transferencia Electrónica Intramolecular. En este caso particular la variación en la anchura de línea viene provocado por cambios en el acoplamiento hiperfino debidos a la diferente ubicación del electrón desapareado del radical por efecto de la transferencia, y se puede relacionar con el momento angular de espín nuclear, M_I, de los núcleos con que acopla.

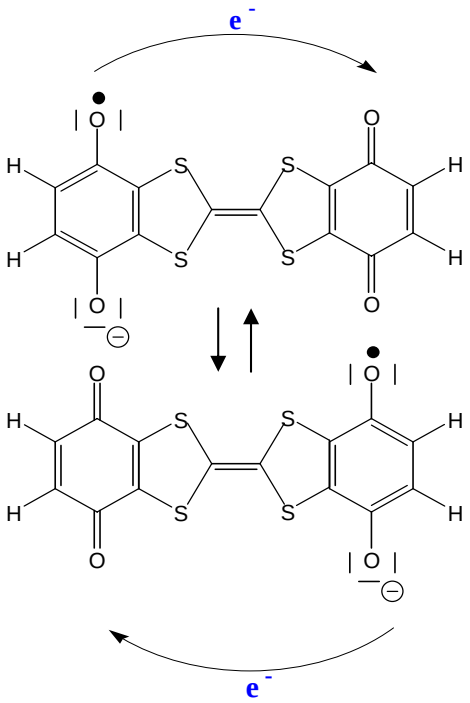

Esquema 1

Explicaremos el caso del compuesto de valencia mixta, $\mathbf{1}^{\bullet-}$. En el Esquema 1, se puede ver como cada centro electroactivo del radical posee dos protones equivalentes y se quiere ilustrar la forma en que el electrón desapareado va de un centro al otro, debido a la transferencia electrónica.

Imaginemos primero que no hay transferencia electrónica. En este caso el electrón está localizado en uno de los dos centros activos y acopla fundamentalmente con los dos protones equivalentes que tiene el mismo anillo sobre el que está localizado. Con los otros dos hidrógenos, el acoplamiento es tan débil que no llega a resolverse debido a su lejanía con respecto a la zona sobre la que se ubica mayoritariamente el electrón desapareado. La descripción de un sistema similar se muestra en la Figura 4.

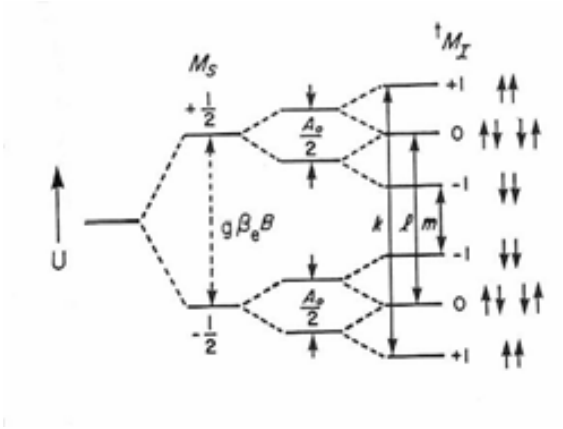

Figura 4 *Niveles de energía y transiciones para un sistema con un electrón desapareado y dos núcleos equivalentes con I = 1/2.*

Efectivamente, en la Figura 4, se muestran los niveles de energía y las transiciones para un sistema con un electrón desapareado y dos núcleos equivalentes con espín nuclear I = 1/2. Se pueden ver los dos niveles de energía debidos al electrón ($M_S = \pm 1/2$) y los desdoblamientos correspondientes primero a un protón equivalente y luego al otro, definiendo un sistema con un número cuántico de espín nuclear total de $^tM_I = \sum M_I = \pm 1$. A la derecha se muestran todas las configuraciones posibles de los dos espines nucleares definiendo tres transiciones, es decir, tres líneas con una intensidad 1:2:1.

Consideremos ahora los efectos dinámicos. En realidad tenemos dos grupos de protones equivalentes entre sí, Esquema 1, los de la izquierda, que denominaremos H_a y los dos de la derecha, H_b.

Consideremos primero los protones de uno de estos grupos, los izquierdos o los derechos. En cada grupo, la modulación dinámica es en fase, es decir, en cada pareja de protones el desdoblamiento hiperfino aumenta o disminuye al unísono, por lo tanto, son equivalentes en cualquier instante, es decir, son *completamente equivalentes*. Si esto es así, la posición de sus líneas espectrales puede describirse siempre por el número cuántico de espín nuclear total de ${}^tM_I = \sum_i M_{I(i)}$ que en este caso, con dos protones, es ${}^tM_I = \sum M_I = \pm 1$, de manera que se comportan como si fuesen un único núcleo.

En el caso del comportamiento de una pareja de protones con respecto a la otra, la modulación de los dos desdoblamientos hiperfinos es exactamente fuera de fase, es decir, cuando una aumenta la otra disminuye. Puesto que el promedio de desdoblamientos hiperfinos para los dos grupos de protones tiene siempre el mismo valor, se dice que son *dinámicamente equivalentes*. El hecho de que no sean los protones izquierdos para con los derechos, instantáneamente equivalentes, conlleva la aparición de lo que se denomina el **efecto de línea alternante**.

En la Figura 5, se muestra la representación del espectro de un radical conteniendo dos grupos de protones similar al que tiene el compuesto de valencia mixta, $\mathbf{1}^{\bullet-}$. En cada pareja de protones, éstos son completamente equivalentes con ${}^tM_I = \sum M_I = \pm 1$, mientras que las parejas entre sí, están sujetas a una modulación fuera de fase. ${}^tM_I = {}^tM_{Ia} + {}^tM_{Ib}$.

A la temperatura a la que la velocidad de interconversión, en nuestro caso de transferencia electrónica, es muy lenta, la velocidad de interconversión es inferior al tiempo de respuesta del equipo y el espectro que se observa es el que se muestra en la Figura 5*a*. En muestro caso corresponde a tres grupos de tres señales con una intensidad 1:2:1 y una constante de acoplamiento grande, entre protones de la misma pareja, de a_{2H} = 2,49 G. Como la constante de acoplamiento entre parejas, la pequeña, no se llega a resolver, el espectro que se observa en realidad es de tres líneas. Figura 6 a 260 K.

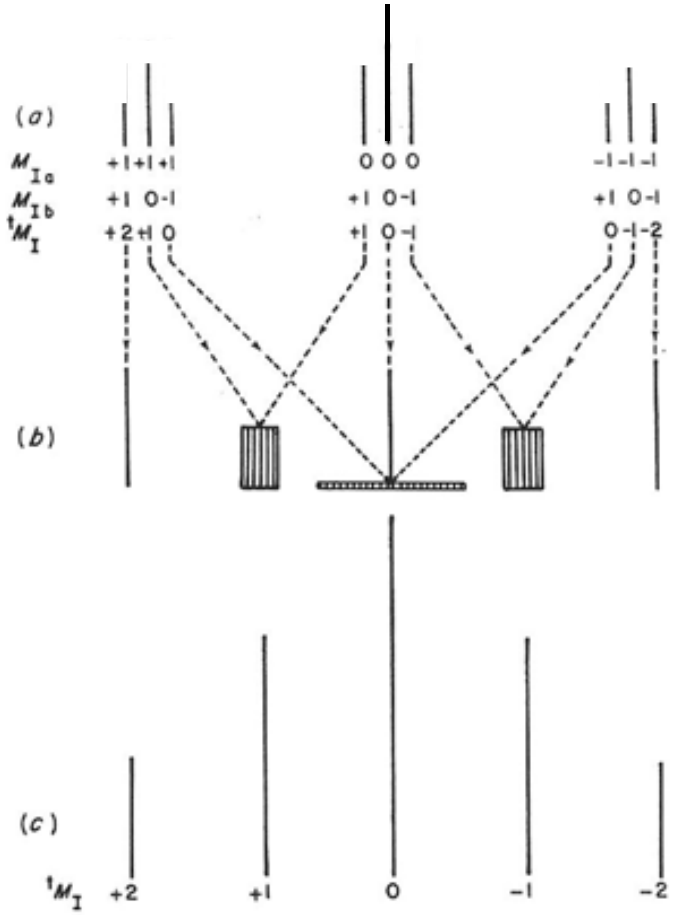

Figura 5 *Representación del efecto de línea alternante en el espectro de un radical con dos grupos de protones.*

A medida que la velocidad de interconversión crece, la velocidad de transferencia se acerca el tiempo de respuesta del equipo y las líneas coalescen como se muestra en la Figura 5*b* (la anchura y altura de los bloques rayados muestran la anchura y la amplitud de línea a una velocidad de transferencia dada). Entre la Figura 5*a y* Figura 5*b*, están indicados los números cuánticos de espín nuclear total de cada pareja de protones, $^tM_{Ia}$ y $^tM_{Ib}$ y el número cuántico de espín nuclear total de l sistema, $^tM_I = {}^tM_{Ia} + {}^tM_{Ib}$. El efecto de línea alternante consiste en que, tanto la anchura como la amplitud de la línea resultante del proceso dinámico, depende del mayor o menor desplazamiento de campo magnético de la nueva línea resultante. Así, si tenemos en cuenta el número cuántico de espín nuclear total del sistema, ^tM_I, las líneas correspondientes a los valores de +2, -2 y 0 central, al pasar de *a* a *b* no cambian de posición por lo que su anchura y amplitud no varía. En el caso de los valores +1 y -1, hay un cierto desplazamiento, por lo que las líneas resultantes serán

más anchas y de menor amplitud. Finalmente para los valores de 0 lateral, el desplazamiento magnético es grande y la línea resultante es tan ancha y de una amplitud tan pequeña, que prácticamente no se ve, observándose solamente en esta posición la contribución del valor 0 central, que no presenta desplazamiento como hemos dicho antes. El efecto de ensanchamiento alternante real se puede apreciar en los espectros a temperaturas intermedias de la Figura 6.

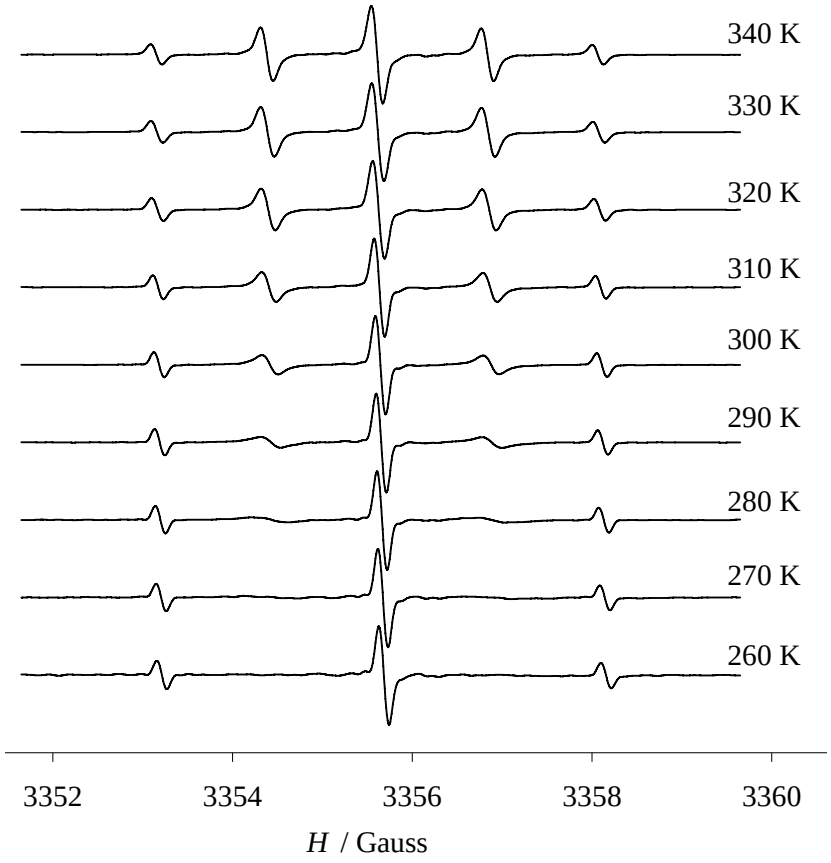

Figura 6 *Espectros de RPE a distintas temperaturas de una solución del compuesto* $Q^{\cdot-}$-*TTF-Q en acetato de etilo/terc-butanol 10:1 y* $P(C_6H_5)_4Br$.

A la temperatura a la que la velocidad de interconversión, en nuestro caso de transferencia electrónica, es muy rápida, la velocidad de interconversión es superior al tiempo de respuesta del equipo y el espectro que se observa es el que se muestra en la Figura 5*c*. Los acoplamientos hiperfinos están completamente promediados y se observan las cinco líneas con intensidad 1:4:6:4:1 característico de cuatro núcleos con espín nuclear 1/2, equivalentes entre sí, con una constante de desdoblamiento

hiperfino de a_{4H} = 1,24 G. El espectro real es el que se observa en la Figura 6 a 340 K.

5. ESPECTROS EN CONDICIONES ANISÓTROPAS. DISOLUCIONES DILUIDAS SÓLIDAS.

A medida que disminuimos la temperatura, la disolución comienza a hacerse mas viscosa y aparecen efectos como los ensanchamientos de línea homogéneos o heterogéneos. En el caso extremo de que tengamos una disolución congelada o un polvo microcristalino, los cristales o las moléculas están fijos y orientados al azar, y tanto el factor *g* como las constantes de acoplamiento hiperfino reflejan su anisotropía con respecto al campo magnético manifestando su naturaleza tensorial. El factor *g* es un tensor de rango dos caracterizado por nueve componentes que se descomponen en sus partes simétrica y asimétrica. Puesto que la parte asimétrica no suele ser detectada, la parte simétrica es diagonalizable en su sistema de tres ejes principales. Lo mismo le ocurre al tensor hiperfino, que refleja la anisotropía de la distribución del electrón desapareado alrededor del núcleo magnéticamente activo. Con este tipo de espectros obtenemos información sobre la simetría local del sistema paramagnético.

Por ejemplo, para una muestra que presente simetría axial, dos de los tres elementos de la diagonal de la matriz del tensor *g* son iguales y el espectro presentará señales de absorción entre dos valores de campo magnético, denominados $B_\perp$ y $B_\parallel$. La mayor intensidad del espectro a valores próximos a $B_\perp$ es debido a la mayor probabilidad estadística de encontrar especies paramagnéticas orientadas perpendicularmente y no paralelamente al campo magnético exterior. La Figura 7 muestra un espectro simulado de una muestra rígida amorfa de una especie con un tensor *g* axial junto con la matriz que lo define. Las señales a $B_{//}$ y $B_\perp$del espectro corresponden a las dos orientaciones canónicas y a los ejes principales del tensor *g*.

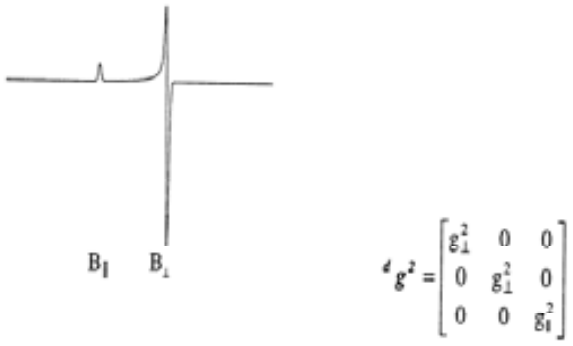

Figura 7 *Espectro correspondiente a un tensor $^d g_2$ axial.*

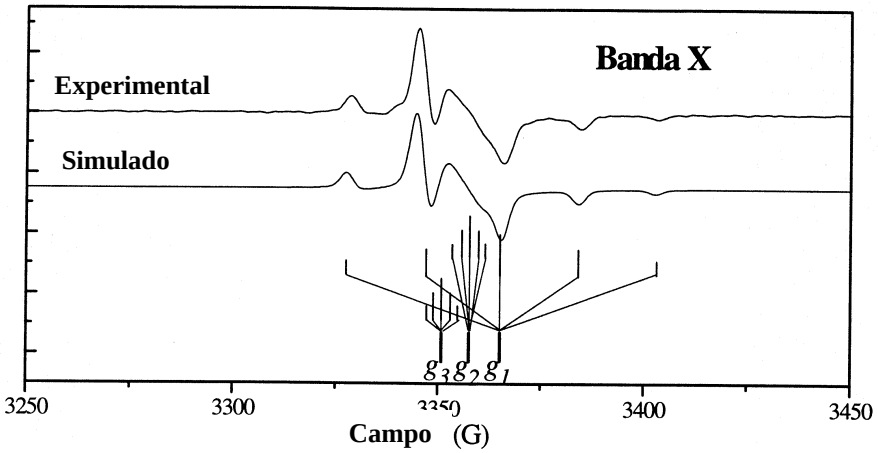

Dirección prin. de g	Tensor hiperfino A (G)	Tensor g
1	18,75	2,002
2	1,45	2,007
3	1,45	2,011

Figura 8 *Espectro experimental, simulado y parámetros de la simulación de una disolución de fenil α-nitronil nitróxido congelada.*

En la Figura 8 se muestra el espectro de la misma disolución de fenil α-nitronil nitróxido de la Figura 2, pero congelada. Se puede observar como la manifestación de la naturaleza tensorial del factor g y del acoplamiento hiperfino afecta a la forma del espectro.

6. DESDOBLAMIENTOS A CAMPO CERO. ESTRUCTURA FINA.

Cuando en una molécula hay más de un electrón desapareado, birradicales, trirradicales, etc., puede ocurrir que los electrones estén tan alejados entre sí que se comporten, en la practica, como un monoradical, o que manifiesten lo que se denominan desdoblamientos a campo cero. Estas contribuciones pueden aparecer en sistemas con S >1/2 y dan cuenta de los desdoblamientos en energía entre los distintos niveles que tienen lugar en ausencia de campo magnético aplicado, como un efecto combinado, en ordenes de perturbación superiores, de la interacción espín-órbita y electrostática, de la interacción espín-espín etc. En general pueden expresarse como formas multilineales, de orden par, de los operadores de espín. El más simple corresponde a una forma bilineal, y puede aparecer en sistemas con S >1/2.

Cuando un sistema posee dos electrones desapareados que interaccionan entre sí, aparecen dos estados de distinta energía: uno simétrico (estado triplete, S = 1) y otro antisimétrico (estado singlete, S = 0) con respecto al intercambio de electrones. Estos dos estados presentarán unas energías relativas y una separación energética entre ellos que dependerá del signo y la magnitud de la integral de canje **J**. Las tres configuraciones distintas o subniveles del estado triplete presentan energías diferentes incluso en ausencia del campo magnético externo debido al campo magnético que genera cada electrón sobre el otro (desdoblamiento a campo cero). Ver un ejemplo en la Figura 9**.**

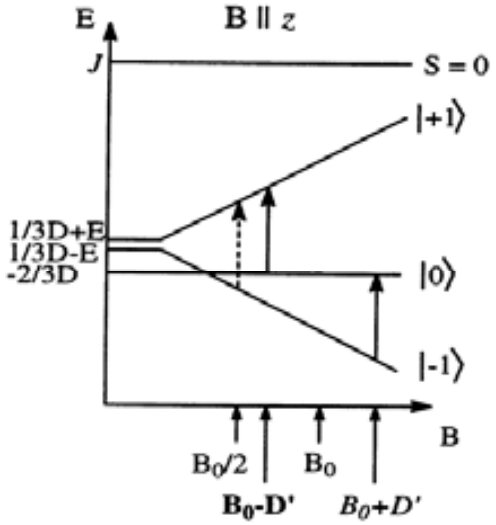

Figura 9 *Estados de energías y transiciones electrónicas permitidas correspondientes a $\Delta M_s = 1$, para un sistema S = 1 con J >0 y D >3E en la orientación canónica B//z.*

Podemos decir que, en el caso más sencillo de un estado S=1, la componente de desdoblamiento a campo cero del hamiltoniano de espín será:

$$H_{zfs} = \overline{S}\,\overline{D}\,\overline{S}$$

Donde $\overline{D}$ es un tensor simétrico de traza nula. La resolución del determinante secular correspondiente demuestra que se puede escribir la solución en función de dos únicos parámetros, **D** y **E** que definen totalmente el sistema. Es importante destacar que el parámetro **D** depende de la distancia promedio que hay entre los dos electrones que interaccionan, mientras que el parámetro **E** sólo depende de la simetría de la función de onda. Otro lado importante a destacar es que, debido a que la traza de $\overline{D}$ es nula, una especie triplete en condiciones isótropas (cuando la molécula gira a gran velocidad) la interacción dipolar está promediada y aparecerá como una sola línea.

Como se puede observar en la Figura 9, el espectro de RPE de un sistema birradicalario presenta dos líneas (flechas sólidas) correspondientes a las transiciones $\Delta M_s = 1$, cuya posición es función de la orientación individual de cada molécula o microcristal con respecto al campo aplicado. Además también es diferente la posición en las otras dos orientaciones canónicas del estado triplete (no representadas en la Figura 9), por lo que la forma de los espectros de RPE de

soluciones amorfas rígidas o de muestras policristalinas resulta una envolvente de los espectros de todas las orientaciones posibles respecto el campo aplicado B. Así, el espectro de RPE consistirá en una zona ancha de absorción centrada en la región de g = 2. Los puntos singulares que presenten estos espectros corresponden a las orientaciones canónicas del birradical respecto al tensor D.

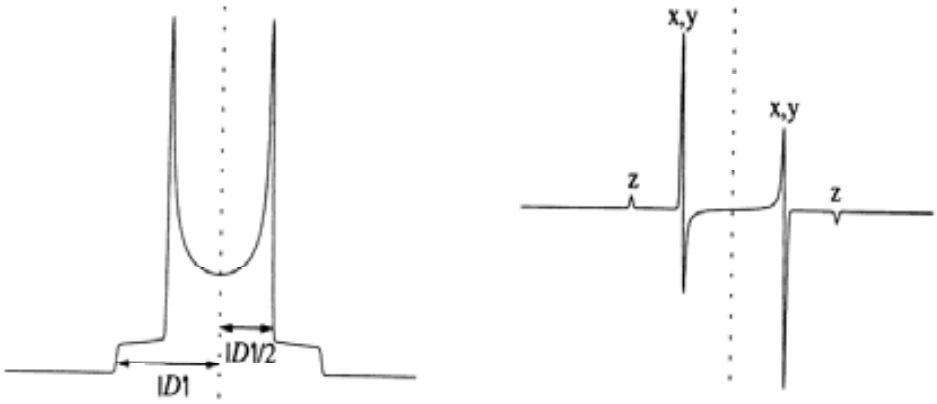

Figura 10 *Forma típica de un espectro correspondiente a una especie triplete con simetría axial. A la izquierda se muestra el espectro de absorción calculado y a la derecha la primera derivada.*

También se puede apreciar una transición a un valor de campo magnético aproximado de B/2 (flecha de puntos), que corresponde a una transición semi-prohibida que implica un cambio del número cuántico magnético total $\Delta M_s = 2$. Esta transición se denomina *transición a campo mitad*, es una señal que aparece en la zona de g = 4 y que será idéntica para todas las moléculas independientemente de sus orientaciones.

En la Figura 10 se muestra el espectro típico de una especie triplete con simetría axial (E = 0), en el que se puede ver que identificando los puntos singulares y midiendo los valores de campo magnético que los separan se pueden determinar los valores absolutos de los parámetros **D** y **E**.

A partir del valor de D se puede calcular la distancia promedio que separa los dos electrones desapareados del birradical mientras que de E se obtendrá información sobre la geometría del sistema.

7. BIBLIOGRAFÍA

1. A. Abragan, The Principles of Nuclear Magnetism. Oxford University Press. Oxford, **1961**.
2. J. A. Weil, J. R. Bolton, J. E. Wertz, Electron Paramagnetic Resonance, Jonh Wiley & Sons, New York, **1994**.
3. N. M. Atherton, Principles of Electron Resonance, Ellis Horwood Limited, London, **1993**.

Publicaciones.

- N. Gautier, F. Dumur, V. Lloveras, J. Vidal-Gancedo, J. Veciana, C. Rovira, P. Hudhomme. "*Intramolecular Electron Transfer Mediated by a Tetrathiafulvalene Bridge in a Purely Organic Mixed-Valence System*".

  Angew. Chem. Int. Ed. **2003**, *42*, 2765-2768.

- F. Dumur, N. Gautier, N. Gallego-Planas, Y. Sahin, E. Levillain, N. Mercier, P. Hudhomme, M. Masino, A. Girlando, V. Lloveras, J. Vidal-Gancedo, J. Veciana, C. Rovira. "*Novel Fused D-A Dyad and A-D-A Triad Incorporating Tetrathiafulvalene and p-Benzoquinone*".

  J. Org. Chem. **2004**, *69*, 2164-2177.

- J. L. López, A. Tárraga, A. Espinosa, M. Desamparados Velasco, P. Molina, V. Lloveras, J. Vidal-Gancedo, C. Rovira, J. Veciana, D. J. Evans, K. Wurst. *"A New Multifunctional Ferrocenyl-Substituted Ferrocenophane Derivative: Optical and Electronic properties and Selective Recognition of* Mg^{2+} *Cation"*.

  Chem. Eur. J. **2004**, *10*, 1815-1826.

- P. Hudhomme, F. Dumur, N. Gautier, A. Gorgues, V. Lloveras, J. Vidal-Gancedo, J. Veciana, C. Rovira. "*Intramolecular Electron Transfer Mediated by a Tetrathiafulvalene (TTF) Bridge*".

  J. Phys. IV France **2004**, *114*, 509-510.

- A. Caballero, V. Lloveras, A. Tárraga, A. Espinosa, M. D. Velasco, J. Vidal-Gancedo, C. Rovira, P. Molina, J. Veciana. *"An Electroactive Nitrogen-rich [4.4]Ferrocenophane Displaying a Redox Switchable Behaviour. Selective Sensing, Complexation and Decomplexation of* Mg^{2+} *ions*".

  Angew. Chem. Int. Ed. **2005**, *44*, 1977-1981.

- V. Lloveras, A. Caballero, A. Tárraga, M. Desamparados Velasco, A. Espinosa, K. Wurst, D. J. Evans, J. Vidal-Gancedo, C. Rovira, P. Molina, J. Veciana. *"Synthesis and Characterization of Radical Cations Derived from Mono- and Biferrocenyl-Substituted 2-aza-1,3-butadienes: A Study of the Influence of an Asymmetric and Oxidizable Bridge on Intramolecular Electron Transfer"*.

  Eur. J. Inorg. Chem. **2005**, 2436-2450.

- A. Caballero, R. Martínez, V. Lloveras, I. Ratera, J. Vidal-Gancedo, K. Wurst, A. Tárraga, P. Molina, J. Veciana. "*Highly selective chromogenic and redox or fluorescent sensors of Hg^{2+} in aqueous environment based on 1,4-disubstituted azines*".

  J. Am. Chem. Soc. **2005**, *127*, 45, 15666-15667.

- V. Lloveras, J. Vidal-Gancedo, D. Ruiz-Molina, T. M. Figueira-Duarte, J.-F. Nierengarten, J. Veciana, C. Rovira. "*Influence of Bridge Topology and Torsion on the Intramolecular Electron Transfer*".

  Faraday Discussions, **2006**, *131*, 291-305.

Organosulfur Conducting Bridges

Intramolecular Electron Transfer Mediated by a Tetrathiafulvalene Bridge in a Purely Organic Mixed-Valence System**

Nicolas Gautier, Frédéric Dumur, Vega Lloveras, José Vidal-Gancedo, Jaume Veciana, Concepció Rovira, and Piétrick Hudhomme**

Tetrathiafulvalene (TTF) and its derivatives have been successfully used as building blocks of low-dimensional organic conductors and superconductors where intermolecular electron-transfer phenomena play a key role in the electronic transport properties.[1] Important results have been also achieved using TTFs as versatile strong π-donor systems in materials chemistry,[2] particularly in intramolecular charge-transfer materials for donor–acceptor molecules[3] or in photoinduced electron transfer when linked to [60]fullerene.[4] However, TTF has never been used as a bridge to promote electron conduction between two groups. Nowadays, unimolecular electronic devices are at the forefront of research in nanotechnology because of the anticipated limits to the further miniaturization of microelectronics.[5] Moreover, direct electronic conduction through single molecules has recently been demonstrated[6] showing the potential use of integrated molecular-sized devices. As a consequence, there is great interest in studying the role of various parameters that govern the intramolecular electron-transfer (IET) rates. Mixed-valence compounds are the prototypes of molecules able to undergo fast electron transfer through a bridge. Such systems have been widely used to study IET between redox centers of both inorganic[7] and organic nature,[8] with the aim of understanding electron-transfer processes to aid the design of molecular wires.[9]

One way to test the electron conduction through TTF is to use it as a bridge between two redox moieties in a mixed-valence system. Consequently, our target molecule was the TTF-diquinone **1**, Q-TTF-Q, since the *p*-benzoquinone groups are particularly useful organic redox centers to generate mixed-valence systems[10] that form persistent radical anions upon reduction.[11] The behavior of **1** has been studied by electrochemistry and ESR spectroscopy, and we have also performed the synthesis of the TTF-monoquinone **2**, TTF-Q, as a model compound.

Syntheses of **1** and **2** were achieved using the same key intermediate 2-oxo-1,3-dithiole derivative **7** (Scheme 1). The iminium salt **4** was prepared according to a previously described procedure.[12] After quantitative conversion to the 2-thioxo-1,3-dithiole **5**, the hydroquinone functionalities were protected using acetyl or silyl groups by well-established reactions. Further transchalcogenation of **6a** and **6b** furnished the 2-oxo-1,3-dithiole derivatives **7** in excellent yields. The triethylphosphite coupling methodology was applied to **7a** and the resulting TTF derivative **8** was transformed into the bis(1,4-hydroquinone)-TTF derivative by subsequent methanolysis in a methoxide solution and subsequent treatment with *p*-toluenesulfonic acid (PTSA). Without isolating the later intermediate, the fused Q-TTF-Q system **1** was obtained as green-blue crystals by selective oxidation using 2,3-dichloro-5,6-dicyano-1,2-benzoquinone (DDQ).To obtain the TTF-Q assembly **2**, the Horner–Wadsworth–Emmons olefination approach was applied to create the TTF core,[13] which involved the 2-oxo-1,3-dithiole functionality and the anion of phosphonate **9**.[14] After deprotection of the silyl groups of compound **10**, subsequent oxidation with *p*-benzoquinone afforded compound **2** as green crystals.

The cyclic voltammogram of **1** showed two one-electron reversible oxidation waves at $E^0_{ox1} = +0.99$ and $E^0_{ox2} = +1.36$ V (versus a Ag/AgCl electrode), which are characteristic for the TTF moiety, and two distinguishable reversible waves at $E^1_{red} = -0.20$ and -0.28 V, which correspond to the stepwise one-electron reduction of each *p*-quinone moiety. The potential difference of $\Delta E = 0.08$ V between the two waves indicates that the reduction of the second *p*-quinone group is somewhat affected by the presence of the first $Q^{-\bullet}$ center, and suggests that an effective electronic coupling exists between both Q centers, which is mediated by the TTF bridge.

We have studied the intramolecular electron-transfer process in the Q-TTF-$Q^{-\bullet}$ mixed-valence system by temperature-dependent ESR spectroscopy. Electrochemical or chemical reduction[15] of model compound **2** gives the TTF-$Q^{-\bullet}$, which gives an ESR spectrum that is characterized by three lines with 1:2:1 intensities that result from coupling with two equivalent aromatic protons ($a_H = 2.50$ G). This ESR spectrum was singularly invariant over a wide temperature range (270–360 K) and also with concentration, which shows that there is no intermolecular electron transfer in this system. In contrast, the ESR spectrum of the TTF-bridged mixed-valence anion radical Q-TTF-$Q^{-\bullet}$ changes upon cooling from 340 to 260 K (Figure 1). While the spectrum at 260 K was essentially identical to that of model compound TTF-$Q^{-\bullet}$ (three lines in 1:2:1 intensity, $a_H = 2.47$ G), the spectrum at temperatures higher than 340 K is characterized by the coupling of four equivalent aromatic protons (five lines in 1:4:6:4:1 intensity, $a_H = 1.23$ G; Figure 1a).[16] As the temperature is gradually lowered from 340 to 260 K, the alternate lines broaden and disappear because of extensive dynamic electron exchange between both of the Q electrophores through the TTF bridge (Scheme 2).[17] The lowest temper-

[*] Dr. C. Rovira, V. Lloveras, Dr. J. Vidal-Gancedo, Prof. J. Veciana
Institut de Ciència de Materials de Barcelona (CSIC)
Campus Universitari de Bellaterra, 08193 Cerdanyola (Spain)
Fax: (+34) 93-5805-729
E-mail: cun@icmab.es
Prof. P. Hudhomme, Dr. N. Gautier, Dr. F. Dumur
Ingénierie Moléculaire et Matériaux Organiques
UMR 6501, 2 Bd Lavoisier, Université d'Angers
49045 Angers (France)
Fax: (+33) 2-4173-5405
E-mail: pietrick.hudhomme@univ-angers.fr

[**] This work was partially supported by grants from the MENRT (for N.G.), the "Ville d'Angers" (for F.D.), DGI-Spain BQU2000-1157, and DURSI-Catalunya 2001SGR-00362. This research was undertaken as part of the European collaborative COST Program (Action D14/0004/99).

 DOI: 10.1002/anie.200250587

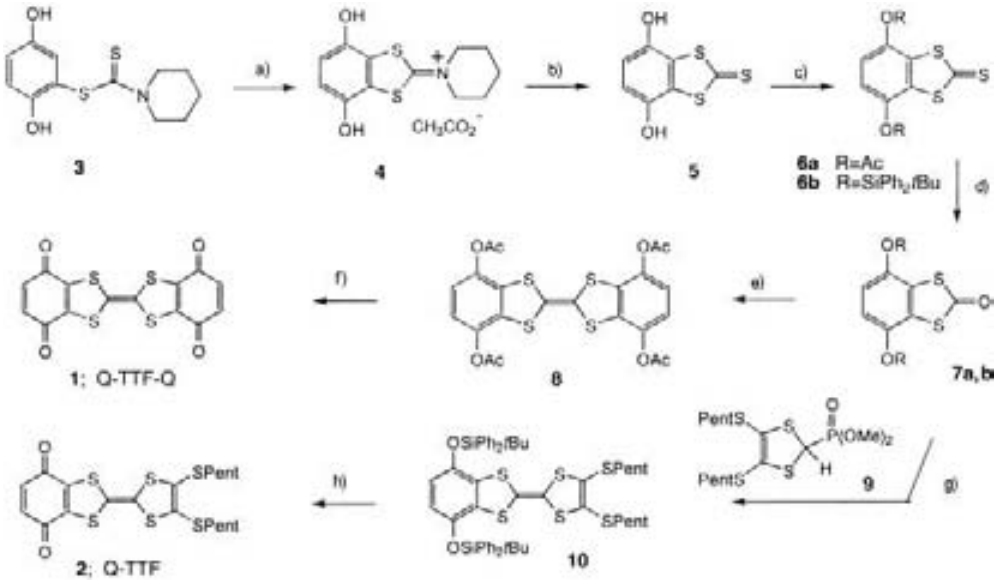

Scheme 1. Syntheses of **1** and **2**. Reagents: a) *p*-benzoquinone then glacial AcOH, 80 °C, 96%; b) $Na_2S{\cdot}9H_2O$, MeOH, 98%; c) Ac_2O, Et_3N, 80% for **6a**; $Ph_2tBuSiCl$, DMF, imidazole, 86% for **6b**; d) $Hg(OAc)_2$, CH_2Cl_2/glacial AcOH, 88% for **7a**, 85% for **7b**; e) Δ, $P(OEt)_3$, 45%; f) MeONa/MeOH, then PTSA and H_2O, then DDQ, 57%; g) phosphonate **9**, *n*BuLi, THF, −78 °C to 20 °C, 90%; h) nBu_4NF/THF then *p*-benzoquinone, 75%.

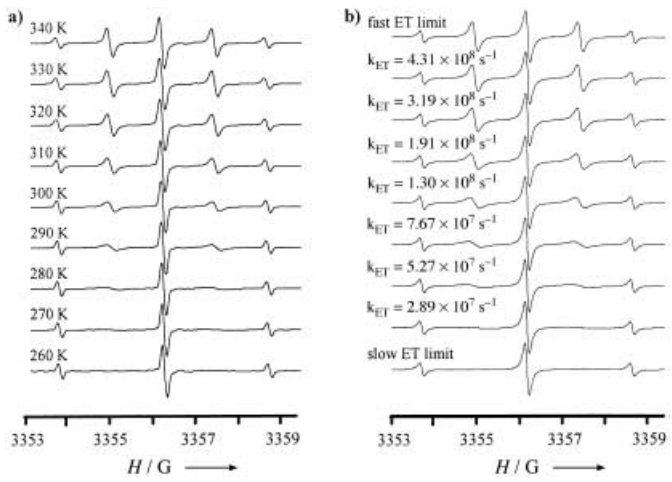

Figure 1. Experimental (a) and simulated (b) ESR spectra of $\mathbf{1}^{-\cdot}$ at different temperatures in ethyl acetate/*tert*-butanol (10:1) with PPh_4Br.

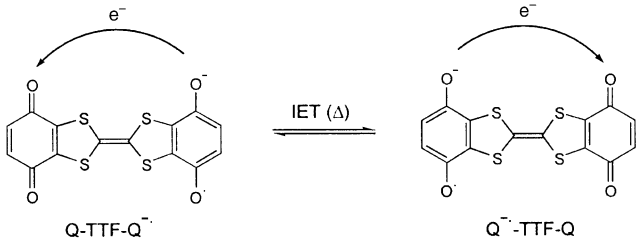

Scheme 2. Electron exchange through the TTF bridge.

ature spectrum unequivocally demonstrates that the odd electron of Q-TTF-$Q^{-\cdot}$ is localized on one particular Q unit on the ESR time scale, and as the temperature is raised the activation energy barrier is overcome, which promotes a faster IET process between the two Q moieties.

The dynamics of the intramolecular exchange process was theoretically simulated[18] (Figure 1b) and first-order rate constants for the thermally activated IET process were extracted by fitting the experimental ESR spectra. The simulation leads to a linear Arrhenius plot over the 330–270 K temperature range, which gives the activation parameters: $E_{act} = 7.96\ kcal\,mol^{-1}$; $\log A = 13.9$ ($\Delta G^{\ddagger}_{298K} = 6.4\ kcal\,mol^{-1}$; $\Delta H^{\ddagger} = 7.4\ kcal\,mol^{-1}$; $\Delta S^{\ddagger} = 3.1$ e.u.). The activation parameters for compound **1** are close to those previously reported for the anthracene-diquinone anion radical.[10e] This is one of the very few cases of an intervalence system for which the IET process can be followed by ESR spectroscopy,[8a,b,d,l,10e] which allows an accurately determination of the rate constant for thermally activated electron transfer. Figure 1 shows the results obtained in a 10:1 mixture of ethyl acetate/*tert*-butanol. However, the rate constants of the electron-transfer (ET) process have been determined in different solvents, which gives rise to different rate constants because of energy variations resulting from solvent reorganization. For example, the rate constants at 300 K are very similar in dichloromethane and ethyl acetate ($k_{ET} = 2.58 \times 10^8\ s^{-1}$ and $2.10 \times 10^8\ s^{-1}$, respectively) and of the same order in the 10:1 mixture of ethyl acetate/*tert*-butanol ($k_{ET} = 1.30 \times 10^8\ s^{-1}$), whereas in *tert*-butanol the ET process is slower ($k_{ET} = 2.89 \times 10^7\ s^{-1}$). It is important to indicate that the thermally activated IET process can only be fully studied using the 10:1 ethyl acetate/*tert*-butanol mixture, since other solvent systems exhibit interfering precipitation processes. As a result of the high insolubility of the monoanion radical species in any solvent, we have not been able to generate the corresponding dianion by chemical reduction or electrochemical reduction at −0.5 V.

The high insolubility of the Q-TTF-$Q^{-\cdot}$ mixed-valence species also prevents the quantitative study of the IET process by Vis/NIR spectroelectrochemical methods, since the com-

pound starts to precipitate after passing a very small quantity of charge. Nevertheless, by deconvoluting the Vis/NIR spectra at different reduction steps, a broad charge-transfer band centered around 1300 nm is clearly observed for the generated Q-TTF-$Q^{-\bullet}$ mixed-valence species. Moreover, this band is completely absent for both the neutral species and in the TTF-$Q^{-\bullet}$ model compound.

The Q-TTF-$Q^{-\bullet}$ species is, therefore, a prototypical class II mixed-valence system involving moderately coupled redox centers.[19]

In summary, we have obtained a new, purely organic mixed-valence compound in which the existence of a temperature-dependent intramolecular electron transfer has not only been undoubtedly established but for which the rate constant for the thermally activated IET process has been accurately determined. In addition, this is the first time that a bridge exhibiting a strong electron-donating character, such as TTF, has been used in a mixed-valence system. The results here demonstrate that TTF is a suitable molecular bridge for the promotion of intramolecular electron transfer between two redox centers and constitutes a natural route towards the measurement of an electrical current through metal-TTF-metal nanojunctions. In that sense, TTF can be considered as the prototype of a huge family of electron donors in which the ionization potential (I_D) is small and can be tuned by changing the substituents and the conjugated extension. These characteristics are very important since one of the criteria for a good donor molecular wire is that the I_D value must be small, and must closely match the work function of the metal layer that acts as an electrode.[6c] We are currently working on the introduction of conjugated spacers between the 1,3-dithiole moieties of compound **1** to elongate the TTF bridge, and also on the utilization of other redox centers to replace *p*-benzoquinone groups.

Received: November 20, 2002
Revised: March 3, 2003 [Z50587]

Keywords: electron transfer · mixed-valent compounds · molecular electronics · quinones · tetrathiafulvalene

[1] a) J. M. Williams, J. R. Ferraro, R. J. Thorn, K. D. Carlson, U. Geiser, H. H. Wang, A. M. Kini, M. H. Whangbo, *Organic Superconductors (including fullerenes)*, Prentice Hall, Englewood Cliffs, NJ, **1992**; b) *Organic conductors. Fundamentals and applications* (Ed.: J. P. Farges), Marcel Dekker, New York, **1994**.

[2] a) M. R. Bryce, *J. Mater. Chem.* **2000**, *10*, 589 – 598; b) J. L. Segura, N. Martín, *Angew. Chem.* **2001**, *113*, 1416 – 1455; *Angew. Chem. Int. Ed.* **2001**, *40*, 1372 – 1409.

[3] M. R. Bryce, *Adv. Mater.* **1999**, *11*, 11 – 23.

[4] N. Martín, L. Sánchez, B. Illescas, I. Pérez, *Chem. Rev.* **1998**, *98*, 2527 – 2547.

[5] Molecular electronics is a field of study that proposes the miniaturization and the use of a single molecule to function as the key component in future devices. See J. M. Tour, A. M. Rawlett, M. Kozaki, Y. Yao, R. C. Jagessar, S. M. Dirk, D. W. Price, M. A. Reed, C.-W. Zhou, J. Chen, W. Wang, I. Campbell, *Chem. Eur. J.* **2001**, *7*, 5118 – 5134, and references therein.

[6] a) L. A. Bumm, J. Arnold, M. T. Cygan, T. D. Dunbar, T. P. Burgin, L. Jones II, D. L. Allara, J. M. Tour, P. S. Weiss, *Science*, **1996** *271*, 1705 – 1707; b) M. A. Reed, C. Zhou, C. J. Muller, T. P. Burgin, J. M. Tour, *Science* **1997**, *278*, 252 – 254; c) R. M. Metzger, *Acc. Chem. Res.* **1999**, *32*, 950 – 957; d) C. P. Collier, E. W. Wong, M. Belohradsky, F. M. Raymo, J. F. Stoddart, P. J. Kuekes, R. S. Williams, J. R. Heath, *Science* **1999**, *285*, 391 – 394; e) C. Joachim, J. K. Gimzewski, A. Aviram, *Nature* **2000**, *408,* 541 – 548; f) J. M. Tour, *Acc. Chem. Res.* **2000**, *33*, 791 – 804; g) *Electron Transfer in Chemistry, Vol. 3* (Eds.: F. Scandola, C. Chiorboli, M. T. Indelli, M. A. Rampi), Wiley-VCH, New York, **2001**.

[7] a) R. J. Crutchley, *Adv. Inorg. Chem.*, **1994**, *41*, 273 – 325; b) "Molecular-level Electronics": A. P. de Silva in *Electron Transfer in Chemistry, Vol. 5* (Ed.: V. Balzani), Wiley, New York, **2001**.

[8] a) F. S. Nelsen, J. A. Thomson-Colon, M. J. Katfory, *J. Am. Chem. Soc.* **1994**, *116*, 1589; b) J. Bonvoisin, J.-P. Launay, C. Rovira, J. Veciana, *Angew. Chem.* **1994**, *106*, 2190 – 2193; *Angew. Chem. Int. Ed. Engl.* **1994**, *33*, 2106 – 2109; c) K. Lahlil, A. Moradpour, C. Bowlas, F. Menou, P. Cassoux, J. Bonvoisin, J.-P. Launay, G. Dive, D. Dehareng, *J. Am. Chem. Soc.* **1995**, *117*, 9995 – 10002; d) F. S. Nelsen, R. F. Ismagilov, D. A. Trieber, *Science* **1997**, *278,* 846 – 849; e) C. Lambert, G. Nöll, *Angew. Chem.* **1998**, *110*, 2239 – 2242; *Angew. Chem. Int. Ed.* **1998**, *37*, 2107 – 2110; f) C. Lambert, G. Nöll, *J. Am. Chem. Soc.* **1999**, *121*, 8434 – 8442; g) D. Ruiz-Molina, J. Sedó, C. Rovira, J. Veciana in *Handbook of Advanced Electronic and Photonic Materials and Devices, Vol. 3* (Ed.: H. S. Nalwa), Academic Press, San Diego, **2001**, pp. 303 – 327; h) J.-P. Launay, *Chem. Soc. Rev.* **2001**, *30*, 386 – 397; i) C. Rovira, D. Ruiz-Molina, O. Elsner, J. Vidal-Gancedo, J. Bonvoisin, J.-P. Launay, J. Veciana, *Chem. Eur. J.* **2001**, *7*, 240 – 250; j) M. Mayor, M. Büschel, K. M. Fromm, J.-M. Lehn, J. Daub, *Chem. Eur. J.* **2001**, *7*, 1266 – 1272; k) C. Lambert, G. Nöll, J. Schelter, *Nat. Mater.* **2002**, *1*, 69 – 73; l) S. V. Lindeman, S. V. Rosokha, D. Sun, J. K. Kochi, *J. Am. Chem. Soc.* **2002**, *124*, 842 – 855.

[9] S. Creager, C. J. Yu, C. Bamdad, S. O'Connor, T. MacLean, E. Lam, Y. Chong, G. T. Olsen, J. Luo, M. Gozin, J. F. Kayyem, *J. Am. Chem. Soc.* **1999**, *121*, 1059 – 1064.

[10] Polycondensed aryl rings were previously used as a bridge for the intramolecular electron transfer between two *p*-benzoquinones in mixed-valence compounds; a) T. H. Jozefiak, L. L. Miller, *J. Am. Chem. Soc.* **1987**, *109*, 6560 – 6561; b) T. H. Jozefiak, J. E. Almlöf, M. W. Feyereisen, L. L. Miller, *J. Am. Chem. Soc.* **1989**, *111*, 4105 – 4106; c) J. E. Almlöf, M. W. Feyereisen, T. H. Jozefiak, L. L. Miller, *J. Am. Chem. Soc.* **1990**, *112*, 1206 – 1214; d) L. L. Miller, C. A. Liberko, *Chem. Mater.* **1990**, *2*, 339 – 340; e) S. F. Rak, L. L. Miller, *J. Am. Chem. Soc.* **1992**, *114*, 1388 – 1394.

[11] Landolt-Börnstein, New series, *Vol. 11/17e* **1986**, p. 206, and references therein.

[12] Yields were improved by the use of piperidine instead of pyrrolidine. D. Sun, M. Krawiec, W. H. Watson, *J. Chem. Crystallogr.* **1997**, *27*, 515 – 526.

[13] C. Boulle, O. Desmars, N. Gautier, P. Hudhomme, M. Cariou, A. Gorgues, *Chem. Commun.* **1998**, 2197 – 2198.

[14] Phosphonate **9** was synthesized according to an established procedure; A. J. Moore, M. R. Bryce, *Synthesis* **1991**, 26 – 28.

[15] Chemical reduction of Q-TTF and Q-TTF-Q was performed with Cu metal in CH_2Cl_2 or ethyl acetate/*tert*-butanol (10:1) solutions containing tetraphenylphosphonium bromide. Electrochemical reduction was carried out using a solution of nBu$_4$NPF$_6$ (0.2 M in CH_2Cl_2).

[16] As the coupling constant a_H is dependent on the spin density, the delocalization of the electron over both quinone groups means that this constant is half as large for compound **1** as for **2**.

[17] A. Hudson, G. R. Luckhurst, *Chem. Rev.* **1969**, *69,* 1961.

[18] J. Heinzer, *Mol. Phys.* **1971**, *22*, 167; *Quantum Chemistry Program Exchange* **1972**, No. 209. We thank Prof. A. Lund for a copy of this program.
[19] M. B. Robin, P. Day, *Adv. Inorg. Chem. Radiochem.* **1967**, *10*, 247. Mixed-valence compounds are classified in three categories. Class I: the redox centers are completely localized and behave as separated entities; Class II: intermediate coupling between the mixed-valence centers exists; Class III: the system is completely delocalized and the redox centers show intermediate valence states.

JOC*Article*

Novel Fused D−A Dyad and A−D−A Triad Incorporating Tetrathiafulvalene and *p*-Benzoquinone

Frédéric Dumur, Nicolas Gautier, Nuria Gallego-Planas, Yücel Şahin,† Eric Levillain, Nicolas Mercier, and Piétrick Hudhomme*

Ingénierie Moléculaire et Matériaux Organiques, UMR 6501, Boulevard Lavoisier, Université d'Angers, F-49045 Angers, France

Matteo Masino and Alberto Girlando

Dipartimento Chimica Generale ed Inorganica, Chimica Analitica, Chimica Fisica, Università di Parma, Parco Area delle Scienze, I-43100, Parma, Italy

Vega Lloveras, José Vidal-Gancedo, Jaume Veciana, and Concepció Rovira

Institut de Ciència de Materials de Barcelona (C.S.I.C), Campus de la U.A.B, 08193 Bellaterra, Spain

pietrick.hudhomme@univ-angers.fr

Received November 17, 2003

Novel fused donor−acceptor dyad (TTF−Q or D−A) and acceptor−donor−acceptor triad (Q−TTF−Q or A−D−A) incorporating the donor tetrathiafulvalene (TTF) and the acceptor *p*-benzoquinone (Q) have been synthesized. The solution UV−vis spectra of these molecules display a low-energy absorption band that is attributed to an intramolecular charge transfer between both antagonistic units. The presence of reversible oxidation and reduction waves for the donor and acceptor moieties was shown by cyclic voltammetry, in agreement with the ratio TTF/quinone(s) units. The successive generation from these compounds of the cation radical and anion radical obtained upon (electro)-chemical oxidation and reduction, respectively, was monitored by optical and ESR spectroscopies. The anion radical $Q-TTF-Q^{-\bullet}$ triad was demonstrated to be a class II mixed-valence system with the existence of a temperature-dependent intramolecular electron transfer. The crystallographic tendency of these fused systems to overlap in mixed stacks of alternating A−D−A units is also discussed.

Introduction

Much attention is still devoted to the investigation of D−A dyads and D−A−D and A−D−A triads in order to control the stoichiometry of both donor (D) and acceptor (A) partners, as well as the degree of charge transfer, which are crucial parameters in the design of organic metals. This considerable research effort is justified by the potential applications of these molecular systems, which are the basis for artificial photosynthetic systems,[1] materials presenting semiconducting or nonlinear optical properties,[2] molecular electronic,[3] and photovoltaic[4] devices. Development of new donor−acceptor architectures affording highly polarizable molecules is particularly important in order to progress in these fields. These compounds are characterized by low excitation energies leading to interesting optical properties. These could also be candidates for single one-component conductors showing intrinsic conductivities when relative donating and accepting abilities are controlled.[5] Moreover, the challenge of verifying experimentally the Aviram−Ratner concept of unimolecular electrical rectification on D−σ−A system,[6] in which the donor tetrathiafulvalene (TTF) and the acceptor tetracyanoquinodimethane (TCNQ) are connected via a saturated link, was recently achieved on the D−π−A hexadecylquinolinium tricyanoquinodimethanide molecule: the excited neutral state was found to be relatively accessible from the zwitterionic ground state $D^{+}-\pi-A^{-}$.[7] Tetrathiafulvalene has attracted much interest for its high electron-donating ability in this field of intramolecular charge-transfer materials.[8] But, to avoid the major problem in the synthesis of TTF−spacer−acceptor compounds resulting in the formation of the

* Corresponding author. Fax: +33 2 41 73 54 05.
† Permananent address: Department of Chemistry, Anadolu University, T-26470 Eskişehir, Turkey.

(1) (a) Fox, M. A., Chanon, M., Eds.; *Photoinduced Electron Transfer*; Elsevier: Amsterdam, 1988. (b) Kurreck, H.; Huber M. *Angew. Chem., Int. Ed. Engl.* **1995**, *34*, 849.

(2) (a) Prasad, P. N.; Williams, D. J. *Introduction to Nonlinear Optical Effects in Molecules and Polymers*; Wiley: New York, 1991. (b) Nalwa, H. S. *Adv. Mater.* **1993**, *5*, 341. (c) Long, N. J. *Angew. Chem., Int. Ed. Engl.* **1995**, *34*, 21. (d) Wong, M. S.; Bosshard, C.; Pan, F.; Günter, P. *Adv. Mater.* **1996**, *8*, 677.

(3) (a) Metzger, R. M.; Panetta, C. *New. J. Chem.* **1991**, *15*, 209. (b) Launay J. P. *Molecular Electronics. In Granular Nanoelectronics*; Ferry, D. K., Ed.; Plenum Press: New York, 1991. (c) Petty, M. C., Bryce, M. R., Bloor, D., Eds.; *Introduction to Molecular Electronics*; Oxford University Press: New York, 1995.

(4) Martín, N.; Sánchez, L.; Illescas, B.; Pérez I. *Chem. Rev.* **1998**, *98*, 2527.

(5) Yamashita, Y.; Tomura, M. *J. Mater. Chem.* **1998**, *8*, 1933.

(6) Aviram, A.; Ratner M. *Chem. Phys. Lett.* **1974**, *29*, 277.

10.1021/jo035689f CCC: $27.50
Published on Web 02/21/2004

CHART 1

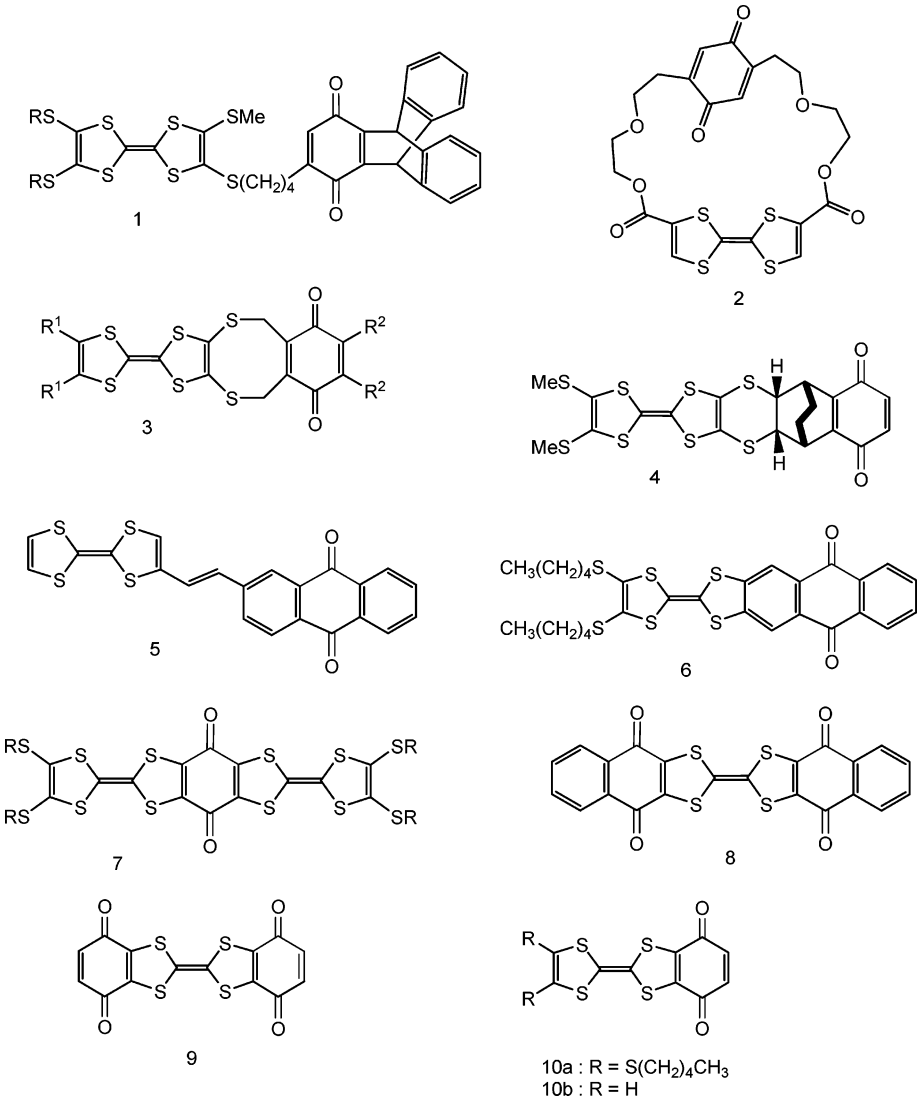

stable and insoluble intermolecular charge-transfer complex between both counterparts prior to their covalent linking, an alternative route was developed considering the linkage of the TTF derivatives to a weak electron acceptor such as quinone. The subsequent conversion into the strong TCNQ acceptor was investigated, but despite several attempts, there appears to be no example of a TTF−quinone being converted into the corresponding TTF−TCNQ derivative.

Several TTF−σ−quinone dyads were previously studied, but no intramolecular charge-transfer band was discernible in the UV−visible spectrum for molecules **1**,[9] **2**,[10] and **3**[11] (Chart 1). Molecule **4**, with a design having a fixed distance and orientation between the TTF and the quinone moieties, showed a weak intramolecular charge-transfer interaction.[12] The molecular type of conjugated **5**[13] or fused **6**[14] D−A dyads with anthraquinone as the acceptor, as well as fused D−A−D **7**[15] and A−D−A **8**[16] triads, were also introduced. In this latter case, the poor solubility of triad **8** prevented a further functionalization and also the structural study of this A−D−A system. Additionally and very surprisingly, the

(7) (a) Metzger, R. M.; Chen, B.; Höpfner, U.; Lakshmikantham, M. V.; Vuillaume, D.; Kawai, T.; Wu, X.; Tachibanan, H.; Hughes, T. V.; Sakurai, H.; Hosch, C.; Cava, M. P.; Brehmer, L.; Ashwell, G. J. *J. Am. Chem. Soc.* **1997**, *119*, 10455. (b) Metzger, R. M. *J. Mater. Chem.* **1999**, *9*, 2027. (c) Metzger, R. M. *Acc. Chem. Res.* **1999**, *32*, 950. (d) Roth, S.; Blumentritt, S.; Burghard, M.; Cammi, E.; Carroll, D.; Curran, S.; Düsberg, G.; Liu, K.; Muster, J.; Philipp, G.; Rabenau, T. *Synth. Met.* **1998**, *94*, 105. (e) Metzger, R. M. *Chem. Rev.* **2003**, *103*, 3803.

(8) (a) Segura, J. L.; Martín, N. *Angew. Chem., Int. Ed.* **2001**, *40*, 1372. (b) Bryce, M. R. *J. Mater. Chem.* **2000**, *10*, 589. (c) Bryce, J. M. *Adv. Mater.* **1999**, *11*, 11.

(9) Scheib, S.; Cava, M. P.; Baldwin, J. W.; Metzger, R. M. *J. Org. Chem.* **1998**, *63*, 1198.

(10) Moriarty, R. M.; Tao, A.; Gilardi, R.; Song, Z.; Tuladhar, S. M. *Chem. Commun.* **1998**, 157.

(11) (a) Segura, J. L.; Martín, N.; Seoane, C.; Hanack, M. *Tetrahedron. Lett.* **1996**, *37*, 2503. (b) Gonzales, M.; Illescas, B.; Martín, N.; Segura, J. L.; Seoane, C.; Hanack, M. *Tetrahedron* **1998**, *54*, 2853.

(12) Tsiperman, E.; Regev, T.; Becker, J. Y.; Bernstein, J.; Ellern, A.; Khodorkovsky, V.; Shames, A.; Shapiro, L. *Chem. Commun.* **1999**, 1125.

(13) Pérez, I.; Liu, S.-G.; Martín, N.; Echegoyen, L. *J. Org. Chem.* **2000**, *65*, 3796.

(14) Gautier, N.; Mercier, N.; Riou, A.; Gorgues, A.; Hudhomme, P. *Tetrahedron Lett.* **1999**, *40*, 5997.

(15) (a) Adam, M.; Müllen, K. *Adv. Mater.* **1994**, *6*, 439. (b) Frenzel, S.; Müllen, K. *Synth. Met.* **1996**, 175.

(16) (a) Watson, W. H.; Eduok, E. E.; Kashyap, R. P.; Krawiec, M. *Tetrahedron* **1993**, *49*, 3035. (b) The bis(1,4-naphthoquinone)TTF exhibited a reduction wave at $E°_{1/2} = -0.32$ V (NHE), but at both negative and positive potentials, the current increases sharply with increasing voltage, giving no distinct oxidation−reduction couples.

SCHEME 1[a]

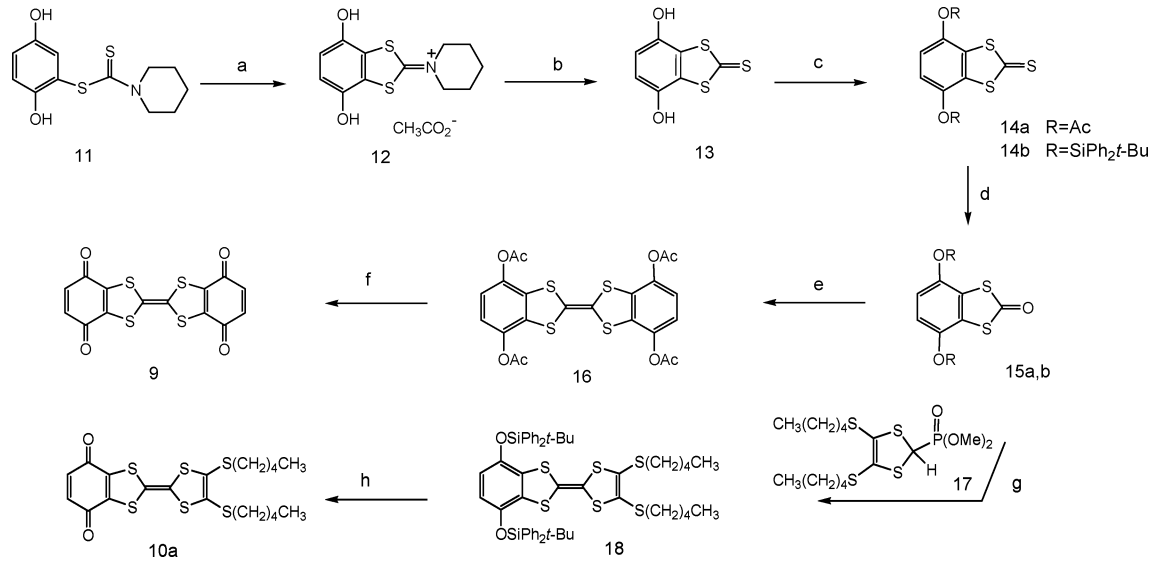

[a] Reagents: (a) *p*-benzoquinone then glacial AcOH, 80 °C, 96% (lit.[19a] 63%). (b) $Na_2S{\cdot}9H_2O$, MeOH, 98% (lit.[19a] 71%). (c) Ac_2O, Et_3N, 80% for **14a**; $Ph_2tBuSiCl$, DMF, imidazole, 86% for **14b**. (d) $Hg(OAc)_2$, CH_2Cl_2/glacial AcOH, 88% for **15a**, 85% for **15b**. (e) Δ $P(OEt)_3$, 45% (lit.[19a] 47% using $P(OEt)_3$/toluene). (f) (i) MeONa/MeOH; (ii) PTSA, H_2O; (iii) DDQ, 57%. (g) phosphonate **17**, *n*-BuLi, THF, −78 to 20 °C, 90%. (h) (i) *n*-Bu_4NF/THF; (ii) *p*-benzoquinone, 75%.

cyclic voltammetry study did not exhibit the oxidation waves corresponding to the TTF donor fragment.[16] On the other hand, the cyclic voltammetry of compound **7** revealed the presence of two two-electron oxidation waves corresponding to both TTF moieties, but no data were reported on the electrochemical behavior of the *p*-benzoquinone fragment.[15]

In this work we report the synthesis, theoretical calculations, spectroscopic and electrochemical properties of A−D−A triad **9** (Q−TTF−Q) and D−A (TTF−Q) dyad **10** corresponding to fused TTF−quinone(s) assemblies, also considered to be potential precursors for fused donor−acceptor oligomers or TTF−TCNQ systems. The study of the derived oxidized and reduced species is also presented in which previous results demonstrated that intramolecular electron transfer (IET) process occurred in the mixed-valence $Q-TTF-Q^{-\bullet}$ system.[17] Moreover, we present the study of the crystallographic arrangement of the fused Q−TTF−Q **9** to check if the previously proposed concept of designing organic metals with A−D−A type molecules, where the donors and acceptors are covalently linked via a saturated methylene spacer or a sulfur atom,[18] can be extended to fused systems.

Results and Discussion

Synthesis. The synthesis of triad A−D−A **9** and dyad D−A **10** was performed using the same key intermediate 2-oxo-1,3-dithiole derivative **15** (Scheme 1). *p*-Benzoquinone was reacted with the dithiocarbamate salt (isolated from the addition of piperidine to carbon disulfide) in the presence of glacial acetic acid in a mixture of DMF/DMSO as solvents. The corresponding Michael addition followed by the aromatization produced compound **11** in 97% yield. The latter was further oxidized using *p*-benzoquinone, and the following cyclization upon treatment with glacial acetic acid led to the iminium salt **12** in 96% yield for the two steps.[19] After quantitative conversion to the corresponding 2-thioxo-1,3-dithiole **13** using sodium sulfide, the hydroquinone functionalities were protected using the acetyl or silyl groups. Well-established procedures afforded compounds **14a** and **14b** in 80 and 86% yields, respectively. The transchalcogenation upon treatment with mercuric acetate furnished the 2-oxo-1,3-dithiole derivatives **15** in excellent yields.

The triethyl phosphite coupling methodology was applied to **15a**, and the resulting tetrathiafulvalene **16** was isolated as yellow crystals in 45% yield. Subsequent methanolysis using a methoxide solution in THF/MeOH afforded TTF−bis(1,4-hydroquinone) after treatment with *p*-toluenesulfonic acid (PTSA).[20] Without isolating the fused TTF−bis(1,4-hydroquinone) intermediate, the oxidation was carried out using DDQ to yield the fused A−D−A system **9** as green-blue crystals after classical workup and chromatography on florisil using CH_2Cl_2/EtOAc (99/1) as the mixture of eluents.

To reach the fused D−A assembly **10a**, we applied a nonclassical Horner−Wadsworth−Emmons olefination to create the TTF core involving the 2-oxo-1,3-dithiole functionality.[21] After reaction of **15b** with the anion of phosphonate **17**[22] in THF and silicagel column chroma-

(17) Some parts of this work have been previously reported: Gautier, N., Dumur, F.; Lloveras, V.; Vidal-Gancedo, J.; Veciana, J.; Rovira, C.; Hudhomme, P. *Angew. Chem., Int. Ed.* **2003**, *42*, 2765.

(18) Khodorkovsky, V.; Becker J. Y. *Organic Conductors, Fundamentals and Applications*; Farges, J. P., Ed.; New York, 1994.

(19) (a) Synthesis of this compound was carried out according to a previously described methodology, several yields being improved by small modifications of experimental procedures: Sun, D.; Krawiec, M.; Watson, W. H. *J. Chem. Crystallogr.* **1997**, *27*, 515. (b) Yields were particularly improved by using piperidine instead of pyrrolidine: Gautier, N.; Gallego-Planas, N.; Mercier, N.; Levillain, E.; Hudhomme, P. *Org. Lett.* **2002**, *4*, 961.

(20) We should note that an identical reaction using inorganic acids such as hydrochloric acid or sulfuric acid solutions was unsuccessful. In these cases, the resulting precipitate could be the result of concomitant protonation of the TTF core.

(21) Boulle, C.; Desmars, O.; Gautier, N.; Hudhomme, P.; Cariou, M.; Gorgues, A. *Chem. Commun.* **1998**, 2197.

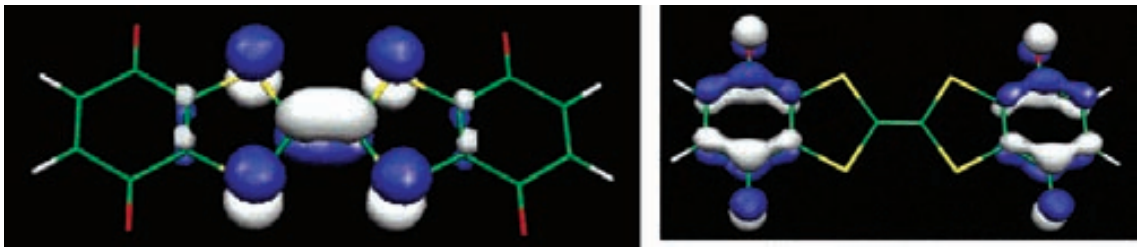

FIGURE 1. HOMO orbital (left) and LUMO orbital (right) of triad **9** obtained by DFT calculations.

tography (CH_2Cl_2/petroleum ether (1/4) as the mixture of eluents), we could isolate compound **18** as yellow crystals in 90% yield. The deprotection of the silyl group was carried out using tetrabutylammonium fluoride, and then subsequent oxidation using *p*-benzoquinone afforded compound **10a** as green crystals in 75% yield after column chromatography on florisil using CH_2Cl_2/petroleum ether (1/1) as the mixture of eluents.

Theoretical Calculations and Spectroscopic Properties of 9 and 10. Density Functional Theory (DFT) calculations were performed using Gaussian 98[23] at the B3LYP/6-31G* level of theory for a full geometry optimization, with no symmetry contraints, of the fused D−A and A−D−A systems. Even if no symmetry was imposed, the optimized geometry obtained confirmed the high symmetry of this A−D−A molecule (D_{2h} symmetry). For the A−D−A assembly **9**, the molecular orbital analysis of both compounds showed that the largest coefficients in the HOMO orbital are mainly located on the central TTF core (the $S_2C{=}CS_2$ fragment) and the calculated energy value for this HOMO orbital was −5.35 eV (Figure 1). As expected, the coefficients in the LUMO orbital were centered on the quinone moieties, showing an alternation of π-bond signs in these rings, but this LUMO orbital was characterized by two quasi-degenerated orbitals: the LUMO (−3.89 eV) and the LUMO +1 (−3.84 eV). Consequently, the calculated HOMO−LUMO gap was estimated to be 1.46 eV. The degenerated LUMO orbital is due to alternating signs of the wave function coefficients in the π-molecular orbitals, as shown in Figure 1. A perpendicular plane reflects the same coefficients and signs of the wave function of each quinone unit.

Geometry optimization was also performed on the D−A system **10a** and **10b**, and the same conclusions were reached in terms of the localization of the HOMO and LUMO coefficients and energies (for **10a**, HOMO = −5.04 eV, LUMO = −3.67 eV; for **10b**, HOMO = −4.90 eV, LUMO= −3.69 eV) with an estimated gap of 1.37 eV for **10a** and 1.21 eV for **10b**.

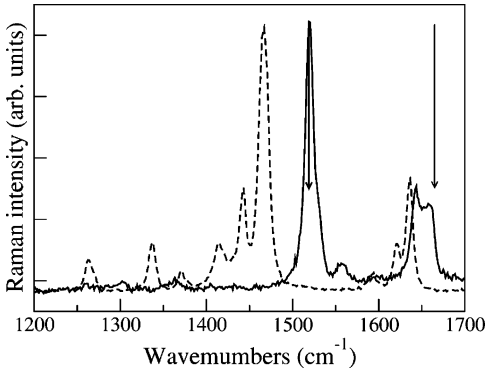

FIGURE 2. Raman spectra of **9** (continuous line) and **10a** (dashed line), 568 nm excitation. The arrows indicate the position of the C=O and C=C stretchings in the Raman spectra of neutral *p*-benzoquinone and TTF crystals, respectively.

All spectroscopic data (^1H and ^{13}C NMR, MS, IR, Raman) were in agreement with the described structures of **9** and **10a**. Particularly, these compounds appeared to be especially stable. As suggested first by the presence of the molecular peak as the base peak in mass spectrometry, this stability was confirmed by the thermal gravimetric analysis (TGA) study, which showed the beginning of the decomposition at 240 and 290 °C for **9** and **10a**, respectively. The Raman spectrum of D−A **10a** (Figure 2) showed a clear downward shift of both carbonyl (∼1630 cm^{-1}) and central C=C (1446 cm^{-1}) stretching of the quinone and TTF units, respectively, with respect to the corresponding values (∼1665 and 1518 cm^{-1}) of neutral *p*-benzoquinone[24] and neutral TTF.[25] A less pronounced downward shift was observed for the C=O stretching of A−D−A **9**, whereas the TTF C=C stretching is practically unshifted in this case (Figure 2; the frequencies are at ∼1655[24] and 1522 cm^{-1}). The same trend was found in the IR spectra, where the carbonyl antisymmetric stretch is located at 1650 and at 1648 cm^{-1} for **9** and **10a**, respectively, to be compared to about 1665 cm^{-1} for *p*-benzoquinone.[24] This behavior indicated a partial charge transfer from the TTF core to the carbonyl groups of the quinone moiety. The charge transfer was rather small for **9** but increased in the asymmetric unit **10a** and, in the solid state, could have both intra- and intermolecular character (see below).

(22) Phosphonate **17** was synthesized according to well-established procedures from corresponding substituted 1,3-dithiole-2-thione: Moore, A. J.; Bryce, M. R. *Synthesis* **1991**, 26.

(23) Frisch, M. J.; Trucks, G. W.; Schlegel, H. B.; Scuseria, G. E.; Robb, M. A.; Cheeseman, J. R.; Zakrzewski, V. G.; Montgomery, J. A., Jr.; Stratmann, R. E.; Burant, J. C.; Dapprich, S.; Millam, J. M.; Daniels, A. D.; Kudin, K. N.; Strain, M. C.; Farkas, O.; Tomasi, J.; Barone, V.; Cossi, M.; Cammi, R.; Mennucci, B.; Pomelli, C.; Adamo, C.; Clifford, S.; Ochterski, J.; Petersson, G. A.; Ayala, P. Y.; Cui, Q.; Morokuma, K.; Malick, D. K.; Rabuck, A. D.; Raghavachari, K.; Foresman, J. B.; Cioslowski, J.; Ortiz, J. V.; Stefanov, B. B.; Liu, G.; Liashenko, A.; Piskorz, P.; Komaromi, I.; Gomperts, R.; Martin, R. L.; Fox, D. J.; Keith, T.; Al-Laham, M. A.; Peng, C. Y.; Nanayakkara, A.; Gonzalez, C.; Challacombe, M.; Gill, P. M. W.; Johnson, B. G.; Chen, W.; Wong, M. W.; Andres, J. L.; Head-Gordon, M.; Replogle, E. S.; Pople, J. A. *Gaussian 98*, revision A.9; Gaussian, Inc.: Pittsburgh, PA, 1998.

(24) Liu, R.; Zhou, X.; Pulay, P. *J. Phys. Chem.* **1993**, *96*, 4255 and references therein. Notice that in both Raman and IR, the carbonyl stretching bands are affected by Fermi resonance. We believe that the doublet structure seen in the Raman spectra of **9** and **10a** (Figure 2) share the same origin. Accordingly, in the text we report as an approximate frequency the corresponding average.

(25) Bozio, R.; Zanon, I.; Girlando, A.; Pecile, C. *J. Chem. Phys.* **1979**, *71*, 2282.

SCHEME 2. Polarization of the S−C═C−C═O Conjugated System of Triad 9 Supported by the Charge Distribution Obtained by Theoretical Calculations and in Agreement with the Polarization Suggested for Compound 19[26]

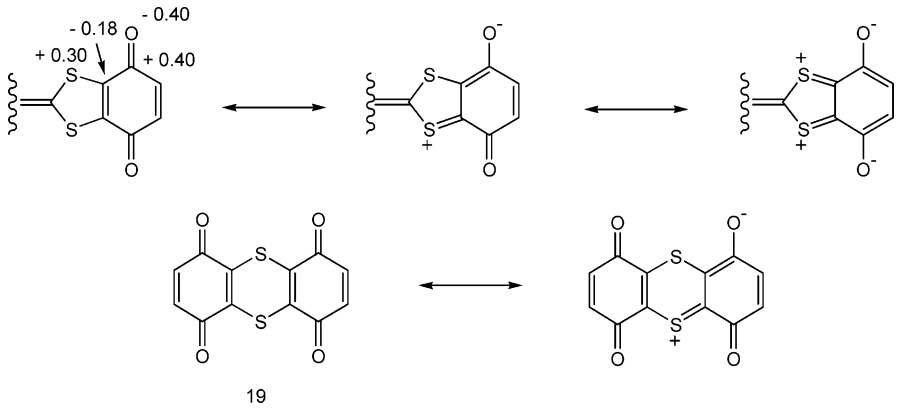

19

On the other hand, this influence of TTF on the benzoquinone moiety was shown in solution by comparing the ^{13}C spectra of **9** and **10a** with that of *p*-benzoquinone itself. Although the ^{13}C chemical shift of the carbonyl functionality appeared at 187.1 ppm ($CDCl_3$ as the reference) for *p*-benzoquinone, the upfield shift to 177.9 and 177.7 ppm for the corresponding carbon of **9** and **10a**, respectively, should result from the displacement of the electron density caused by the push−pull S−C═C−C═O system, suggesting the mesomeric form shown in Scheme 2. This resonance form was previously proposed for the bis(*p*-benzoquinone) **19**, which showed a maximum absorption at 508 nm in acetonitrile.[26] The charge distribution calculated by DFT methods on the neutral compound **9** was in complete agreement with a strong polarization of the S−C═C−C═O conjugated system and strongly supported the partial zwitterionic nature of the ground state (Scheme 2).

The electronic absorption spectrum of **9** confirmed the existence of the electronic interaction between both D and A moieties, and comparatively, the effect of the strong donor tetrathiafulvalene became evident. The UV−visible spectra of **9** showed the presence of a broad absorption band in the 500−1100 nm region, with the strongest absorption evidenced in CS_2 and centered at ca. 808 nm, which clearly indicates a weak charge-transfer interaction resulting from the conjugation involving both donor and acceptor moieties (Figure 3).

The measurement at different concentrations proved the intramolecular nature of this charge transfer from donor to acceptor moiety. A red-shift effect was observed for **10a**, which presented a broad absorption band between 600 and 1300 nm centered at ca. 892 nm in CS_2. For both **9** and **10a**, the position of the band just corresponds to the HOMO−LUMO gap calculated as described above. These D−A and A−D−A compounds exhibited strong solvatochromism of the charge-transfer band depending on the polarity of solvents (Table 1).

Electrochemical Properties of Fused TTF−Quinone(s) 9 and 10a. The cyclic voltammogram of D−A **10a** (*n*-Bu_4NPF_6 0.1 M in CH_2Cl_2/acetonitrile 9/1) showed two one-electron reversible oxidation waves at $E_{ox1}^0 = +0.74$ V and $E_{ox2}^0 = +1.11$ V (vs Ag/AgCl) corresponding to the successive generation of the cation radical and dication of the TTF moiety. Two reduction processes were shown for the *p*-benzoquinone moiety, including the first one-electron reversible reduction wave at $E_{red1}^0 = -0.21$ V (Figure 4) and the second reduction wave E^0_{red2} at approximately −1.20 V, which was not reversible in these experimental conditions. Concerning the A−D−A compound **9**, the oxidation potentials were clearly shifted to more positive values ($E_{ox1}^0 = +0.99$ and $E_{ox2}^0 = +1.36$ V, vs Ag/AgCl), the electron-withdrawing effect of the quinone group being responsible for this phenomenon. The *p*-benzoquinone moiety was characterized by a two-electron reversible reduction wave E_{red1}^0 approximately at −0.25 V. In fact, a splitting of this first reduction wave ($E_{red1}^0 = -0.20$ V and $E_{red1'}^0 = -0.28$ V) was observed by

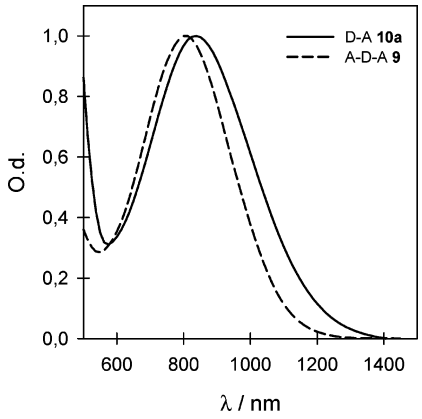

FIGURE 3. Electronic absorption spectra of **9** and **10a** in CS_2.

TABLE 1. Wavelength of the Charge Transfer UV−vis Absorption Maxima of A−D−A 9 and D−A 10a in Solvents of Varying Polarity[a]

solvent	A−D−A **9** (λ nm)	D−A **10a** (λ nm)
DMSO	670	762
DMF	735	758
acetonitrile	738	776
toluene	773	820
dichloromethane	782	847
CCl_4	804	863
CS_2	808	892

[a] Extinction molar coefficient of this charge transfer band was determined for **9** and **10a** in toluene to be 780 and 425 M^{-1} cm^{-1}, respectively.

(26) Hünig, S.; Siunzger, K.; Bau, R.; Metzenthin, T.; Salbeck, J. *Chem. Ber.* **1993**, *126*, 465.

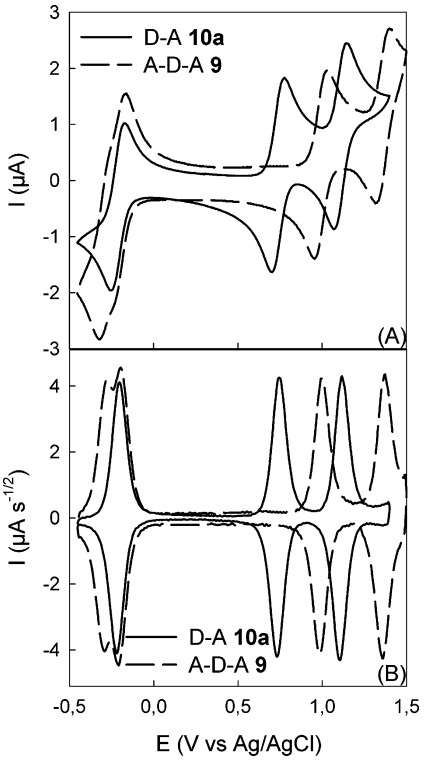

FIGURE 4. Cyclic voltammograms (top) and their corresponding deconvolution (bottom) of D−A **10a** and triad **9**; Pt electrode vs Ag/AgCl, nBu$_4$NPF$_6$ 0.1 M in CH_2Cl_2/CH_3CN 9/1, 10^{-3} M, v = 500 mV/s. The second reduction waves are not presented on this figure.

using a slowest scan rate or cyclic voltammogram deconvolution. Thus, the successive generation of Q−TTF−Q$^{-\bullet}$ and Q$^{-\bullet}$−TTF−Q$^{-\bullet}$ species was observed. This phenomenon of splitting showed that the electrochemical behavior of both *p*-benzoquinone moieties is resulting from modifications on the electronic interaction between TTF and *p*-benzoquinone moieties at the Q−TTF−Q$^{-\bullet}$ stage and from Coulombic repulsion between reduced species at the Q$^{-\bullet}$−TTF−Q$^{-\bullet}$ stage. The values corresponding to the difference between the oxidation potential and the electron affinity were experimentally determined to be 1.19 eV for triad A−D−A **9** and 0.95 eV for dyad D−A **10a**, by calculating the difference between the first oxidation peak of TTF (Ep_a) and the first reduction peak of *p*-benzoquinone (Ep_c).

To clearly observe the second two-electron reduction waves of the *p*-benzoquinone moiety, we performed experiments using *o*-dichlorobenzene/acetonitrile (19/1) as the mixture of solvents. The cyclic voltammogram of triad **9** exhibited two reversible one-electron oxidation processes with redox potentials $E_{ox1}{}^0$ and $E_{ox2}{}^0$ at +0.97 and +1.34 V (vs Ag/AgCl), respectively, and two independent reduction processes. After deconvolution, the first reversible system was shown as two successive reductive steps corresponding to the generation of Q−TTF−Q$^{-\bullet}$ and Q$^{-\bullet}$−TTF−Q$^{-\bullet}$ species with redox potentials $E_{red1}{}^0$ and $E_{red1'}{}^0$ at −0.33 and −0.40 V, respectively. The second quasi-reversible system showed one broad wave corresponding to the reduction into Q^{2-}−TTF−Q$^{-\bullet}$ and Q^{2-}−TTF−Q^{2-} species at −1.16 V (Figure 5).

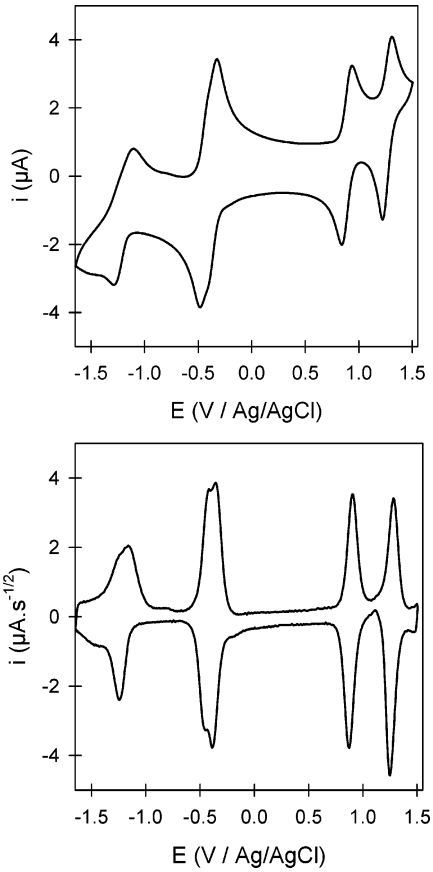

FIGURE 5. Cyclic voltammogram (top) and its deconvolution (bottom) of triad **9**; Pt electrode vs Ag/AgCl, nBu$_4$NPF$_6$ 0.1 M in *o*-dichlorobenzene/CH_3CN 19/1, 5 × 10^{-4} M, v = 200 mV/s.

As the bis(1,4-benzoquinone)TTF **9** was clearly characterized in terms of cyclic voltammetry, we were interested in the problem resulting from the bis(1,4-naphthoquinone)TTF **8** and the absence of electroactive species of this compound upon oxidation as noted by W. H. Watson et al.[16] We therefore applied our synthetic methodology to synthesize the bis(1,4-naphthoquinone)-TTF (Scheme 3). Thus, the reaction of 2,3-dichloronaphthoquinone with potassium sulfide and carbon disulfide in DMF, followed by treatment with sodium dithionite, afforded the 2-thioxo-1,3-dithiole derivative **20** as described.[16] Precursor **22** was obtained by acetylation using acetic anhydride in the presence of triethylamine in 79% yield and transchalcogenation by treatment with mercuric acetate in glacial acetic acid in 96% yield. Triethyl phosphite coupling reaction was performed, affording the tetrathiafulvalene derivative **23** in 53% yield. The conversion into quinone functionality described herein was successfully carried out using DDQ, affording in 68% yield the bis(1,4-naphthoquinone)TTF **8** as a light green powder, this characteristic being in agreement with the compound previously reported.[16]

Despite its very low solubility, this compound **8** was studied by cyclic voltammetry using n-Bu$_4$NPF$_6$ 0.1 M as a supporting electrolyte and *o*-dichlorobenzene/acetonitrile (19/1) as the mixture of solvents (2 × 10^{-4} M, v = 200 mV/s). In contradiction with previous observation,[16] compound **8** was characterized by two reversible oxidation and two reduction waves attributed to the TTF and naphthoquinone moieties, respectively, this cyclic voltam-

SCHEME 3[a]

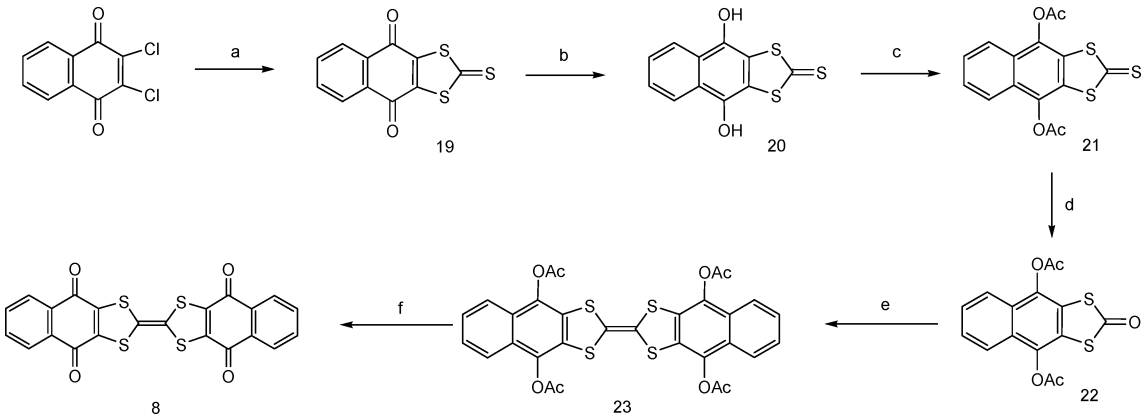

[a] Reagents: (a) K_2S, CS_2, DMF, 65% (lit.[16a] 63%). (b) $Na_2S_2O_4$, 75% (lit.[16a] 97%). (c) Ac_2O, Et_3N, 79%. (d) $Hg(OAc)_2$, CH_2Cl_2/glacial AcOH, 96%. (e) Δ $P(OEt)_3$, 53%. (f) (i) MeONa/MeOH; (ii) PTSA, H_2O; (iii) DDQ, 68%

mogram being similar to that obtained for **9** (Figure 5). Thus, the two oxidation waves corresponding to the formation of the cation radical and dication of the TTF were shown at +0.96 and +1.35 V (vs Ag/AgCl), respectively. The first reduction process appeared as a split system with two different waves at −0.56 and −0.61 V and the second reduction process as a broad wave at −1.20 V.

Properties of Oxidized and Reduced Species from Triad 9 and Dyad 10a. The optical properties of the cation radical and dication of bis(1,4-benzoquinone)-TTF **9** were investigated by in situ UV−vis−NIR spectroscopy, by addition of increasing amounts of $NOBF_4$. Chemical oxidation led to the rapid disappearance of bands attributed to the neutral TTF derivative (broad band from 600 to 1100 nm centered at 782 nm) and to the development of new bands characteristic for the cation radical (434, 580 nm) and the dication (566 nm) (Figure 6).[27] The values of the HOMO−LUMO difference calculated by DFT methods followed the same trend as the UV−visible data and were estimated to be 1.50 eV for $\mathbf{9}^{+\bullet}$ (HOMO = −9.65 eV, LUMO = −8.15 eV) and 1.82 eV for $\mathbf{9}^{2+}$ (HOMO = −14.46 eV, LUMO = −12.54 eV). As for the neutral molecule **9**, the optimized geometry found for the cation radical $\mathbf{9}^{+\bullet}$ was almost planar, while the dication $\mathbf{9}^{2+}$ presented distortion from planarity of 14°.[28] This torsion angle in the geometry of $\mathbf{9}^{2+}$ may be related to increasing *σ*-character in the C−C central bond between the two 1,3-dithiolium moieties. This is supported by the optimized central bond lengths, computed as 1.35 Å for the neutral molecule **9**, 1.40 Å for the cation radical $\mathbf{9}^{+\bullet}$, and 1.44 Å for the dication $\mathbf{9}^{2+}$.

The cation radical $\mathbf{9}^{+\bullet}\cdot\mathbf{CF_3SO_3}^-$ was also chemically prepared as a pure solid by oxidation of the triad **9** by using as an oxidizing agent iodobenzene diacetate in the presence of triflic acid according to a synthetic approach recently reported for the efficient stoichiometric control of TTF-derived cation radicals.[29] The IR spectrum of $\mathbf{9}^{+\bullet}\cdot\mathbf{CF_3SO_3}^-$ clearly showed the appearance of strong bands at 1255, 1027, and 636 cm^{-1} characteristic of the SO_3^- anion.[29] The most evident change in the Raman spectrum is the downward shift of the TTF central double-band stretch from 1519 to 1399 cm^{-1}. The ESR signal of an acetone solution of the cation radical salt $\mathbf{9}^{+\bullet}\cdot\mathbf{CF_3SO_3}^-$ exhibited the expected quintet (g = 2.0071), showing a small coupling of the electronic spin with the four equivalent hydrogen atoms of the quinone moieties (a_H = 0.36 G). Moreover, the ^{33}S hyperfine coupling constant was also observed upon amplification of the spectrum (a_S = 4.1 G).

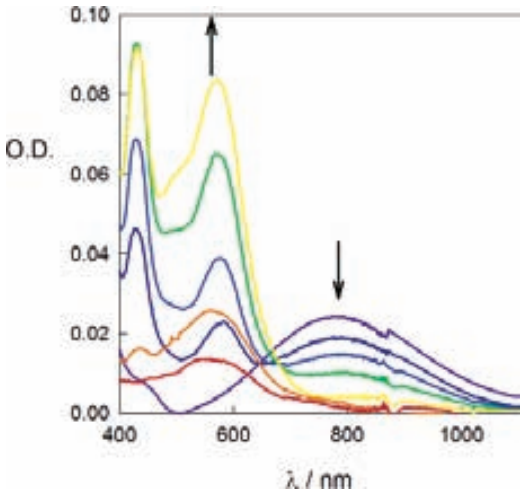

FIGURE 6. Evolution of the optical spectrum for the neutral triad **9** (3×10^{-4} M in CH_2Cl_2) upon oxidation using $NOBF_4$ in CH_3CN solution.

The anion radical $\mathbf{9}^{-\bullet}\cdot\mathbf{P(C_6H_5)_4}^+$, as well as a pure solid, was prepared by chemical reduction with Cu metal in CH_2Cl_2 containing tetraphenylphosphonium bromide. This compound is highly insoluble, and a very fine precipitate is formed almost at the beginning of the

(27) For references on calculated and experimental UV−visible absorption of cation radical and dication of TTF derivatives, see: (a) Khodorkovsky, V.; Shapiro, L.; Krief, P.; Shames, A.; Mabon, G.; Gorgues, A.; Giffard, M. *Chem. Commun.* **2001**, 2736. (b) Andreu, R.; Garín, J.; Orduna, J. *Tetrahedron* **2001**, *57*, 7883.

(28) This distortion from planarity between the two dithiolium rings was previously observed on the crystal structure of the dication from the unsymmetrical outer S-position isomer of BEDT-TTF. Hudhomme, P.; Le Moustarder, S.; Durand, C.; Gallego-Planas, N.; Mercier, N.; Blanchard, P.; Levillain, E.; Allain, M.; Gorgues, A.; Riou, A. *Chem. Eur. J.* **2001**, *7*, 5070.

(29) Giffard, M.; Mabon, G.; Leclair, E.; Mercier, N.; Allain, M.; Gorgues, A.; Molinié, P.; Neilands, O.; Krief, P.; Khodorkovsky, V. *J. Am. Chem. Soc.* **2001**, *123*, 3852.

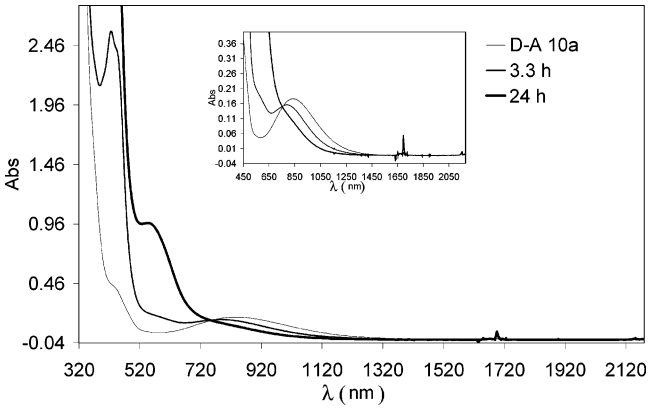

FIGURE 7. Evolution of the UV−vis−NIR spectrum during the course of the reduction of D−A **10a**, at different times of reaction. The inset is the enlargement of the vis−NIR part.

reduction process. The IR spectrum of $\mathbf{9}^{-\bullet}\cdot\mathbf{P(C_6H_5)_4}^{+}$ showed important modifications on the band corresponding to carbonyl groups and the appearance of characteristic P−C bands at 650−750 cm^{-1}. Isolated pure solid $\mathbf{9}^{-\bullet}\cdot\mathbf{P(C_6H_5)_4}^{+}$ is insoluble in most of the common organic solvents. A much diluted solution can only be prepared in ethyl acetate and presents a very weak ESR signal consisting of five lines. The high degree of insolubility of $\mathbf{9}^{-\bullet}\cdot\mathbf{P(C_6H_5)_4}^{+}$ prevents the quantitative study of the UV−vis−NIR spectra of the compound as well as the generation of the dianionic derivative $\mathbf{9}^{2-}$. An ESR study of the anion radical species $\mathbf{9}^{-\bullet}\cdot\mathbf{P(C_6H_5)_4}^{+}$ generated "in situ" is presented below.

DFT calculations were performed for a full geometry optimization of the anion radical Q−TTF−$Q^{-\bullet}$ system. The optimized geometry found for the anion radical $\mathbf{9}^{-\bullet}$ was perfectly planar. The calculation performed was unrestricted, and then each orbital obtained was a spin−orbital with single occupancy. The molecular orbital analysis showed that the HOMO orbital (singly occupied spin−orbital), with a calculated energy of −1.40 eV, presented the same shape (and coefficients) as the LUMO orbital of the neutral triad Q−TTF−Q **9**. The calculated energy value for the corresponding LUMO of the anion radical was −1.02 eV. We observed that the overall character for the single occupied HOMO and the corresponding LUMO was very similar to the LUMO of the neutral molecule: the only contributions on the HOMO and LUMO were located on the outer quinone part of the molecule.

Chemical reduction of the dyad **10a** with Cu metal in CH_2Cl_2 containing tetraphenylphosphonium bromide led to a decrease in the characteristic charge-transfer broad band of the neutral derivative and to the appearance and increase with reaction time of the bands due to the anion radical (425 and 550 nm)[30] (Figure 7). The ESR spectrum of this solution consists of a well-defined triplet (g = 2.0046) arising from the coupling of the unpaired electron with the two equivalent hydrogen atoms of the quinone (a_H = 2.50 G).

The presence on the same molecule of electron donor and acceptor(s) moieties allows the successive generation

(30) Zhao, X.; Imahori, H.; Zhan, C.-G.; Sakata, Y.; Iwata, S.; Kitagawa, T. *J. Phys. Chem.* **1997**, *101*, 622.

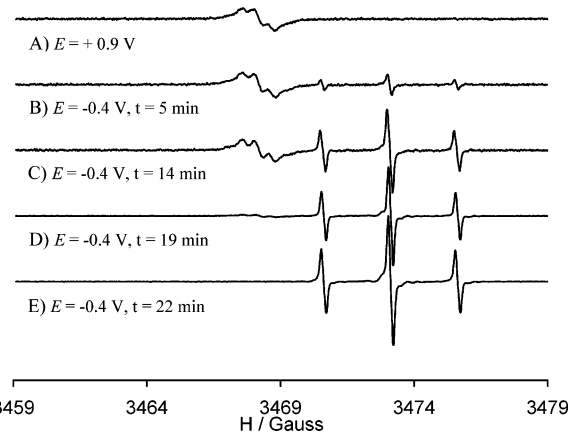

FIGURE 8. Evolution of the ESR spectra of dyad **10a** upon in situ electrooxidation (A) and subsequent electroreduction (B−E) (see text).

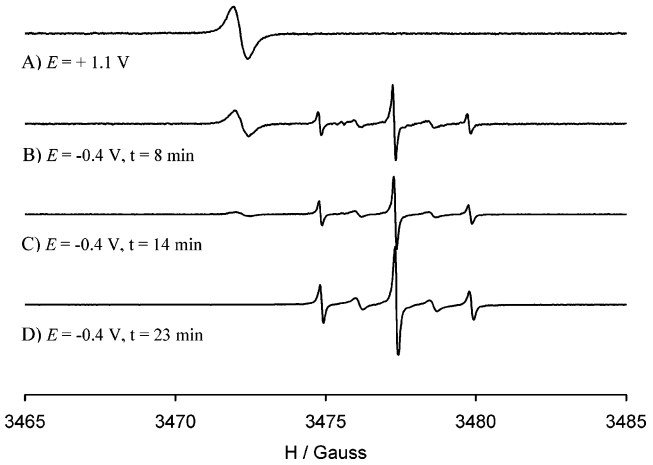

FIGURE 9. Evolution of the ESR spectra of triad **9** upon in situ electrooxidation (A) and subsequent electroreduction (B−D) (see text).

of their cation radical and anion radical derivatives upon oxidation or reduction, respectively. Thus, the cation radical $\mathbf{10a}^{+\bullet}$ was generated by electrochemical oxidation performed in an electrochemical cell adapted to the ESR spectrometer at +0.9 V (vs Ag/AgCl) in CH_2Cl_2 using n-Bu_4NPF_6 as an electrolyte and monitored by ESR spectroscopy (Figure 8).

The corresponding spectrum consisted of an overlapped triplet with the typical pattern of a coupling with the two equivalent quinonic protons (g = 2.0075, a_H = 0.46 G). By imposing a reduction potential at −0.40 V (vs Ag/AgCl), we could observe the slow disappearance of the signal corresponding to the cation radical and the appearance of the signal due to the anion radical $\mathbf{10a}^{-\bullet}$. The corresponding signal was the same as the species obtained by chemical reduction, which is a well-resolved triplet (g = 2.0047, a_H = 2.51 G). Using the same experimental procedure for triad **9** (Figure 9), we observed that the ESR spectrum for the cation radical $\mathbf{9}^{+\bullet}$ consisted of a poorly resolved quintet (g = 2.0074) and, for the anion radical $\mathbf{9}^{-\bullet}$, of a quintet having the second and fourth lines considerably broader than the other three. The ESR signal of the anion radical was very

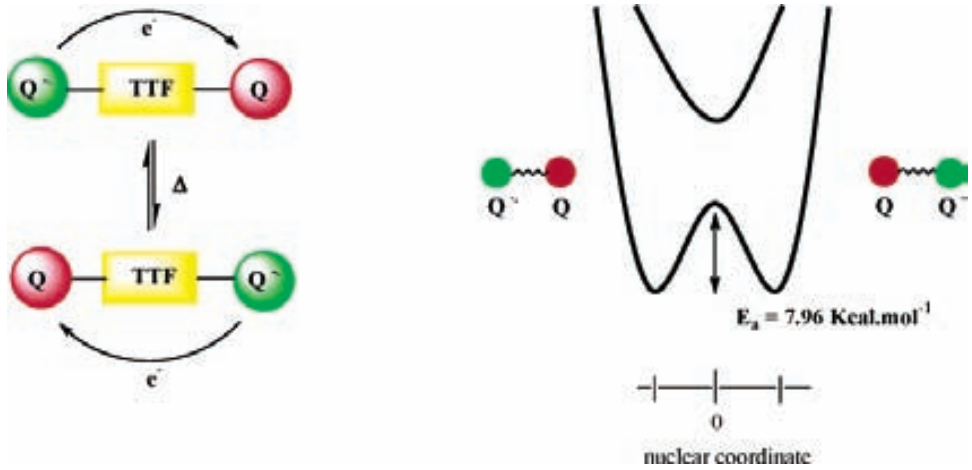

FIGURE 10. Intramolecular electron transfer proccess using the TTF as a bridge in the purely class II mixed-valence Q−TTF−Q$^{-\bullet}$ system.

SCHEME 4. Electron Exchange through the TTF Bridge between the Two Quinonic Centers

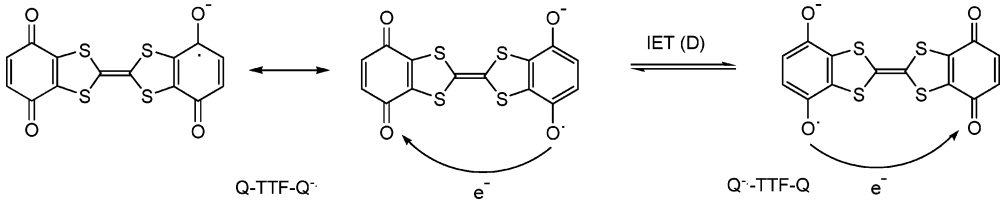

similar (although much more intense) to the one obtained from the ethyl acetate solution of solid **9**$^{-\bullet}$·**P(C$_6$H$_5$)$_4$**$^+$.

The specific features observed in the ESR spectrum for the anion radical **9**$^{-\bullet}$ can be considered as the signature of a dynamic process observed in the ESR time scale.[31] Taking into account that the cyclic voltammogram of the Q−TTF−Q triad **9** suggested an effective electronic coupling between both quinone centers by the presence of two distinguishable reduction processes (ΔE = 80 mV), the dynamic process can be attributed to the electron transfer between both quinones. To characterize this process, we performed the temperature dependence study of the ESR spectra of the mixed-valence species **9**$^{-\bullet}$. For comparison purposes, the anion radical of dyad **10a** was also investigated in the same way. Both species were generated by chemical reduction with Cu metal in different solvents containing tetraphenylphosphonium bromide.

The characteristic ESR spectrum of the anion radical TTF−Q$^{-\bullet}$ **10a**$^{-\bullet}$ that consists of three lines with 1:2:1 intensities was singularly invariant over a wide temperature range between 270 and 325 K in CH_2Cl_2 and between 260 and 340 K in a 10:1 mixture of ethyl acetate/*tert*-butyl alcohol. On the contrary, the ESR spectrum of the anion radical Q−TTF−Q$^{-\bullet}$, prepared under the same conditions, changed upon cooling from 340 to 260 K.[32] Thus, whereas the spectrum at 260 K was essentially identical with that of the analogue TTF−Q$^{-\bullet}$ (three 1:2:1 lines, a_H = 2.47 G (2H)), at higher temperatures (from 330 to 340 K), the spectra were characterized by couplings with two more equivalent protons (five lines 1:4:6:4:1, a_H = 1.23 G (4H)).[33] As the temperature was gradually decreased from 340 to 260 K, alternant lines broadened due to the dynamic electron exchange between both quinone electrophores through the TTF bridge (Scheme 4).[34] The low-temperature spectra of Q−TTF−Q$^{-\bullet}$ unequivocally demonstrated that the odd electron was localized on one quinone unit at the ESR time scale and the activation energy barrier was overcome by thermal stimulus to promote an intramolecular electron transfer (IET) process.[17] It is important to indicate that this IET process can only be studied in all its extension using a 10:1 mixture of ethyl acetate/*tert*-butyl alcohol. Due to the high insolubility of the Q−TTF−Q$^{-\bullet}$ mixed-valence species, it was not possible to perform a quantitative study of the IET process by vis−NIR spectroscopy.

We have clearly demonstrated for the first time that TTF can be used as a bridge promoting electron conduction between two redox centers and that the triad **9** is therefore the prototype of mixed-valence compound able to undergo fast intramolecular electron transfer through this bridge (Figure 10).[35]

With the aim of developing devices using the direct electronic conduction through single molecules,[36] our interest was then focused on the study of the role of various parameters governing the IET rates. The dynam-

(31) Weil, J. A.; Bolton, J. R.; Wertz, J. E. *Electron Paramagnetic Resonance*; John Wiley & Sons: New York, 1994.

(32) Spectra were recorded at the very beginning of the reduction process. At this stage, the major species present in the solution is the ESR silent neutral compound **9**. The observed ESR signal is due to the anion radical, since for statistical reasons dianion radical must have a negligible concentration.

(33) As the coupling constant a_H is dependent on the spin density, the delocalization of the electron over both quinones requires that this coupling constant is two times less for compound **9** than for **10a**: $a_H = (8\pi g_e/3g_o)\gamma_H\beta_H\rho_H(r_H)$. g_e/g_o is the ratio of the isotropic g value for the radical to that of the free electron; γ_H and β_H are the gyromagnetic nuclear ratio and the nuclear magneton, respectively, and $\rho_S(r_H)$ is the spin density on the nucleus of the hydrogen atom.

(34) Hudson, A.; Luckhurst, G. R. *Chem. Rev.* **1969**, *69*, 1961.

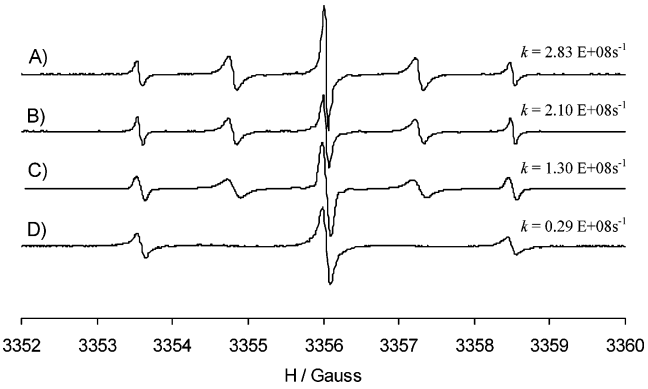

FIGURE 11. ESR spectra of Q−TTF−Q$^{-\bullet}$P$(C_6H_5)_4^+$ at 300 K, generated "in situ" in different solvents. (A) Dichloromethane, (B) ethyl acetate, (C) ethyl acetate/ *tert*-butyl alcohol 10:1, and (D) *tert*-butyl alcohol.

ics of the intramolecular exchange process was simulated using the Heinzer program,[37] and first-order rate constants were extracted by fitting the experimental spectra. The values obtained by simulation of all spectra obtained in a 10:1 mixture of ethyl acetate/*tert*-butyl alcohol led to a linear Arrhenius plot over the range 340−260 K, giving the following activation parameters: $E_{act} = 7.96$ kcal/mol; log $A = 13.9$ ($\Delta G^{\ddagger}_{298K} = 6.4$ kcal/mol, $\Delta H^{\ddagger} = 7.4$ kcal/mol, and $\Delta S^{\ddagger} = 3.1$ eu). As expected, the rate constant of the IET process varied with the solvent used due to the energy variation resulting from solvent reorganization.[32] In Figure 11, the differences in the rate constant at 300 K in dichloromethane, ethyl acetate, *tert*-butyl alcohol, and a 10:1 mixture of ethyl acetate/*tert*-butyl alcohol were clearly observed by the variation of the ESR spectra.

The Q−TTF−Q$^{-\bullet}$ species is therefore a prototypical class II mixed-valence system[38] involving moderately coupled redox centers as indicated by cyclic voltammetry results. This system can be compared with polyacene diquinones **24**−**26** as fused weak donors and acceptors previously reported (Scheme 5). It was also demonstrated that the odd electron of the anion radical of **24** was delocalized,[39] and on the contrary, the anion radicals derived from **25** and **26** were not delocalized and could then formally be considered as mixed-valence species.[40] Indeed, the optical spectra suggested that the unpaired electron on these anion radicals were localized on each subunit and was hopping from one side to another. Such an interpretation was confirmed by temperature-variable ESR spectra, and it would be interesting to note that the activation parameters previously reported for the anion radical of anthracene-diquinone **26**[41] were close to those determined for the anion radical Q−TTF−Q$^{-\bullet}$.

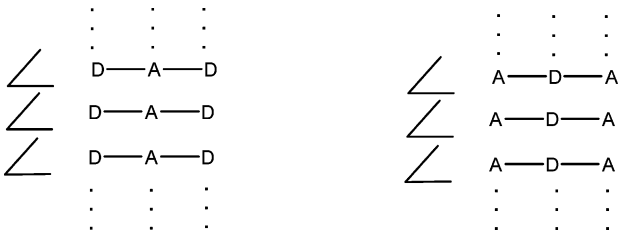

FIGURE 12. Segregated stacks of D−A−D or A−D−A systems.

SCHEME 5. Crystallographic and Single-Crystal IR Studies

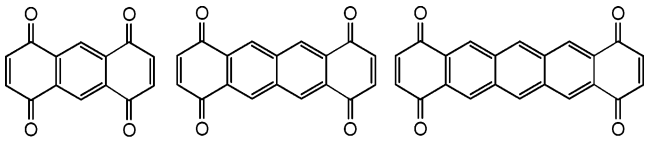

Crystallographic and Single-Crystal IR Studies. The packing mode in the crystals of these materials is a crucial parameter of their potential ability to reach conductivity.[18] To obtain such conducting-linked donor−acceptor complexes, the most important architectural requirement was the aggregation in the solid state of both donors (D) and acceptors (A) in segregated stacks, as extended in the approach of D−A−D[42] and A−D−A[43] systems for which the tendency to produce the corresponding stacking motifs was observed (Figure 12).

Although the weak donor and acceptor character of both moieties usually implies mixed stacks, diquinone derivatives can serve as an example of the A−D−A motif characterized by segregated stacking, showing an almost ideal one-dimensional array of quinone and phenyl

(35) Other organic systems presenting IET between redox centers have been previously reported: (a) Nelsen, F. S.; Thomson-Colon, J. A.; Katfory, M. *J. Am. Chem. Soc.* **1994**, *116*, 1589. (b) Bonvoisin, J.; Launay, J.-P.; Rovira, C.; Veciana, J. *Angew. Chem., Int. Ed. Engl.* **1994**, *33*, 2106. (c) Lahlil, K.; Moradpour, A.; Bowlas, C.; Menou, F.; Cassoux, P.; Bonvoisin, J.; Launay, J.-P.; Dive, G.; Dehareng, D. *J. Am. Chem. Soc.* **1995**, *117*, 9995. (d) Nelsen, F. S.; Ismagilov, R. F.; Trieber, D. A. *Science* **1997**, *278*, 846. (e) Lambert, C.; Nöll, G. *Angew. Chem., Int. Ed.* **1998**, *37*, 2107. (f) Lambert, C.; Nöll, G. *J. Am. Chem. Soc.* **1999**, *121*, 8434. (g) Ruiz-Molina, D.; Sedó, J.; Rovira, C.; Veciana, J. In *Handbook of Advanced Electronic and Photonic Materials and Devices*; Nalwa, H. S., Ed.: Academic Press: San Diego, 2001; Vol. 3, p 303. (h) Launay, J. P. *Chem. Soc. Rev.* **2001**, *30*, 386. (i) Rovira, C.; Ruiz-Molina, D.; Elsner, O.; Vidal-Gancedo, J.; Bonvoisin, J.; Launay, J.-P.; Veciana, J. *Chem.—Eur. J.* **2001**, *7*, 240. (j) Mayor, M.; Büschel, M.; Fromm, K. M.; Lehn, J.-M.; Daub, J. *Chem. Eur. J.* **2001**, *7*, 1266. (k) Lambert, C.; Nöll, G.; Schelter, J. *Nat. Mater.* **2002**, *1*, 69. (l) Lindeman, S. V.; Rosokha, S. V.; Sun, D.; Kochi, J. K. *J. Am. Chem. Soc.* **2002**, *124*, 842.

(36) (a) Bumm, L. A.; Arnold, J.; Cygan, M. T.; Dunbar, T. D.; Burgin, T. P.; Jones, L. II; Allara, D. L.; Tour, J. M.; Weiss, P. S. *Science* **1996** *271*, 1705. (b) Reed, M. A.; Zhou, C.; Muller, C. J.; Burgin, T. P.; Tour, J. M. *Science* **1997**, *278*, 252. (c) Metzger, R. M. *Acc. Chem. Res.* **1999**, *32*, 950. (d) Collier, C. P. Wong, E. W.; Belohradsky, M.; Raymo, F. M.; Stoddart, J. F.; Kuekes, P. J.; Williams, R. S.; Heath, J. R. *Science* **1999**, *285*, 391. (e) Joachim, C.; Gimzewski, J. K.; Aviram, A. *Nature* **2000**, *408*, 541. (f) Tour, J. M. *Acc. Chem. Res.* **2000**, *33*, 791. (g) Batchtold, A.; Hadley, P.; Nakanishi, T.; Dekker, C. *Science* **2001**, *294*, 1317. (h) Scandola, F., Chiorboli, C., Indelli, M. T., Rampi, M. A., Eds.; *Electron Transfer in Chemistry*; Wiley-VCH: New York, 2001; Vol. 3.

(37) Heinzer, J. *Mol. Phys.* **1971**, *22*, 167; *Quantum Chemistry Program Exchange* **1972**, No. 209. We thank Prof. A. Lund for a copy of this program.

(38) Robin, M. B.; Day, P. *Adv. Inorg. Chem. Radiochem.* **1967**, *10*, 247. Mixed-valence compounds are classified in three categories: (a) the redox centers are completely localized and behave as separated entities (class I), (b) intermediate coupling between the mixed-valence centers exists (class II), or (c) the system is completely delocalized and the intermediate redox states are attributed to the redox centers (class III).

(39) Jozefiak, T. H.; Miller L. L. *J. Am. Chem. Soc.* **1987**, *109*, 6560.

(40) Jozefiak, T. H.; Almlöf, J. E.; Feyereisen, M. W.; Miller, L. L. *J. Am. Chem. Soc.* **1989**, *111*, 4105.

(41) Rak, S. F.; Miller, L. L. *J. Am. Chem. Soc.* **1992**, *114*, 1388.

(42) Becker, J. Y.; Bernstein, J.; Bittner, S.; Levi, N.; Shaik, S. S.; Zer-Zion, N. *J. Org. Chem.* **1988**, *53*, 1689 and references therein.

(43) Le Paillard, M. P.; Robert, A.; Garrigou-Lagrange, C.; Delhaes, P.; Le Maguerès, P.; Ouahab, L.; Toupet, L. *Synth. Met.* **1993**, *58*, 233.

SCHEME 6

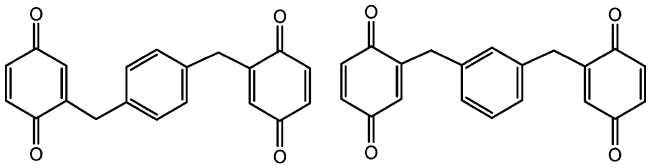

27 28

TABLE 2. Bond Lengths and Intramolecular Interactions in the Triad 9 Determined by the X-ray Crystallographic Structure and DFT Calculations

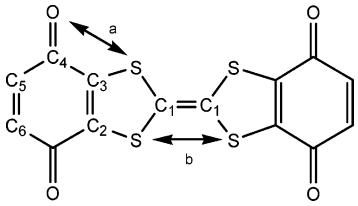

	a	*b*	C_1-C_1	C_1-S	$S-C_3$
crystallographic distance (Å)	3.01(2)	3.22(3)	1.340(9)	1.769(4)	1.739(5)
calculated distance (Å)	3.030	3.277	1.349	1.792	1.751

	C_3-C_2	C_3-C_4	C_4-O	C_4-C_5	C_5-C_6
crystallographic distance (Å)	1.349(6)	1.471(6)	1.227(6)	1.462(7)	1.342(7)
calculated distance (Å)	1.356	1.480	1.224	1.489	1.342

moieties for **27** and two-dimensional stacking for **28** (Scheme 6).[44]

Fine blue needles were obtained by slow evaporation of a solution containing the fused A−D−A system **9** in CH_2Cl_2/petroleum ether as a mixture of solvents. The X-ray crystallographic analysis revealed that the molecule is nearly planar, and only the carbonyl groups protruded from the molecular plane by 4°. This could be compared with the repulsion of the sulfur and oxygen lone pairs suggested in the case of **19**, for which the crystal structure showed that the carbonyl group protruded from the molecule plane by 2−10°.[26] Intramolecular S...O interactions were also shown [3.01(2) Å] between the oxygen atom of the quinone and the sulfur atom of TTF, this distance being shorter than the sum of the van der Waals radii of both atoms (d = 3.25 Å).[45] Moreover, calculated bond lengths and intramolecular interactions were in good agreement with the corresponding distances determined from the crystallographic structure (Table 2).[46]

The packing arrangement of A−D−A molecules, involving a strong donor (TTF) and a weak acceptor (benzoquinone), was characterized by regular stacks along the *a* axis (Figure 13), as encountered in the vast majority of weak charge transfer complexes.

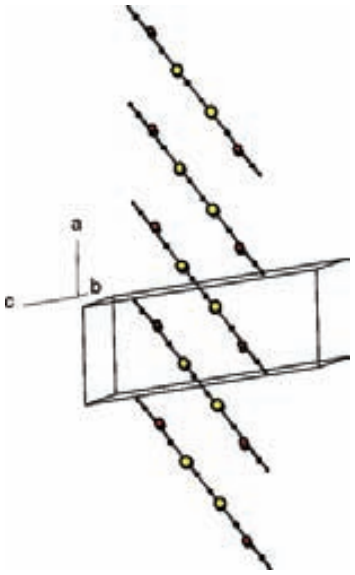

FIGURE 13. Regular stacking mode of TTF−diquinone molecules in the structure of **9**·CH_2Cl_2.

In fact, two consecutive molecules in stacks were shifted one from each other along the main molecular axis leading to a bond over cycle-type overlap between the central C=C bond of the TTF core and the benzene cycle of the acceptor (Figure 14a). Moreover, the bis(1,4-benzoquinone)TTF intermolecular distance between the face-to-face planes of the donor and acceptor moieties (d = 3.60 Å) showed a significant overlap and may be compared to the plane-to-plane distances between donor and acceptor molecules in crystal packings of mixed-stack intermolecular charge transfer complexes.[47] For example, the interplanar distance between donor and acceptor molecules in the charge-transfer complex octamethylene-TTF−TCNQ is 3.53 Å. However, compared to the D...A interactions, compound **9** did not exhibit the infinite mixed stacking ...A..D..A..D.. motif: as a consequence of the shift mode of molecules, only [A...D...A]-type "triplets" were encountered in stacks along the direction perpendicular to the molecular plane (Figure 14b).

It must be noted that in the prototypical D−A−D system previously reported,[40,48] i.e., the dibenzylTCNQ compound involving a strong acceptor (TCNQ) and weak donors (benzyl), isolated triplets D...A...D formed by the central TCNQ ring of a molecule and two phenyl rings of two neighboring molecules were clearly observed. However, in this last structure, X-ray analysis also revealed a segregated mode of stacking for TCNQ parts,[17] which differed from the observed situation in **9** where TTF moieties did not form segregated stacks. The interstack CH(benzene cycle)...O(quinone) hydrogen bond interactions were of particular interest and seemed to strongly influence the crystal packing of triad **9**, leading to cyclic $R_2^2(8)$ motifs, according to Etter's representation,[49] and cavities in which disordered solvent molecules (CH_2Cl_2) were inserted (Figure 15).

(44) (a) Becker, J. Y.; Bernstein, J.; Bittner, S.; Shaik, S. S. *Pure Appl. Chem*. **1990**, *62*, 467. (b) Becker, J. Y.; Bernstein, J.; Bittner, S.; Giron, Y.; Harlev, E.; Kaufman-Orenstein, L.; Peleg, D.; Shahal, L.; Shaik, S. S. *Synth. Met*. **1991**, *41*−*42*, 2523.

(45) Bondi, A. *J. Phys. Chem*. **1964**, *68*, 441.

(46) Bond distances suggest a weak intramolecular charge transfer from TTF to benzoquinone moiety; see: Guionneau, P.; Kepert, C. J.; Bravic, D.; Chasseau, D.; Truter, M. R.; Kurmoo, M., Day, *P. Synth. Met*. **1997**, *86*, 1973.

(47) Chasseau, D.; Gaultier, J.; Fabre, J. M.; Giral, L. *Acta Crystallogr*. **1982**, *B38*, 1632.

(48) Becker, J. Y.; Bernstein, J.; Bittner, S.; Levi, N.; Shaik, S. S. *J. Am. Chem. Soc*. **1983**, *105*, 4468.

(49) Etter, M. C.; MacDonald, J. C. *Acta Crystallogr*. **1990**, *B46*, 256.

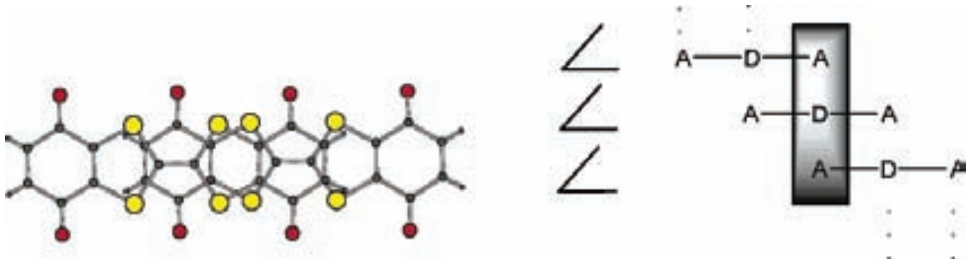

FIGURE 14. (left) Bond over cycle overlap type between two consecutive molecules in stacks and (right) schematic representation of the packing arrangement showing the A..D..A triplets.

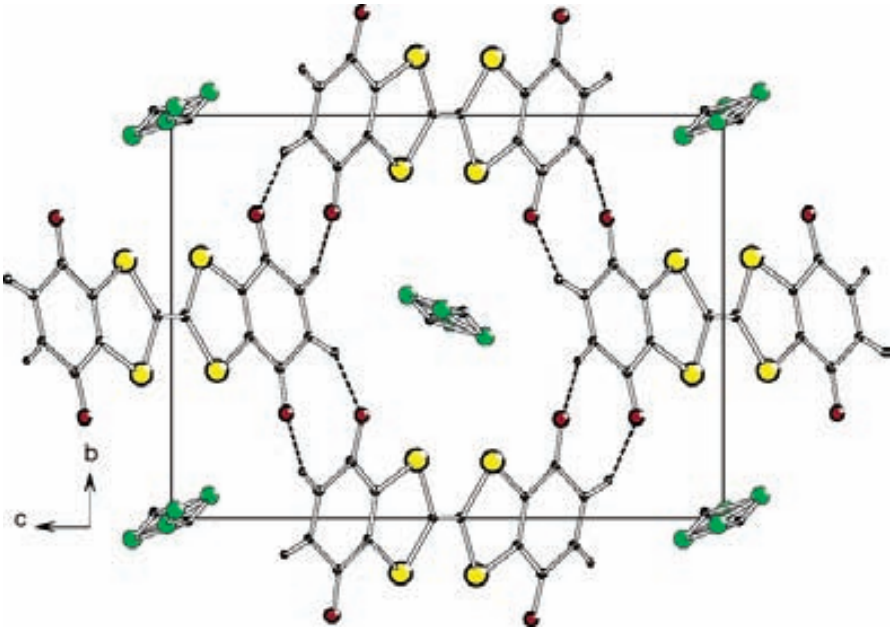

FIGURE 15. View of the crystal structure of **9**·CH_2Cl_2 along the stack axis showing intermolecular hydrogen bonding (dashed lines) and disordered CH_2Cl_2 molecules.

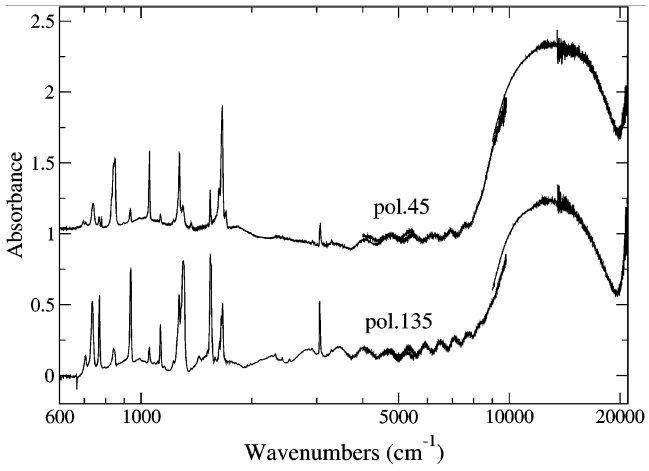

FIGURE 16. Polarized absorption spectra of A−D−A **9** from 600 to 21 000 cm^{-1}. Notice the logarithmic wavenumber scale. Beyond 4000 cm^{-1}, different beam splitters and polarizers have been used. No cosmetic changes have been made to reduce the noise or join the different spectral regions.

We have also obtained polarized IR and NIR−visible (from 600 to 21 000 cm^{-1}) absorption spectra of A−D−A crystal, as shown in Figure 16. The crystal plane was not identified, but it is likely *ac* (Figure 13). We have chosen the light polarizations to maximize the differences between the intensities of the IR bands. The electric vector of the radiation made an angle of approximately 45 and 135 degrees with respect to the needle axis. In addition to the IR features, the spectra displayed an electronic broad absorption centered around 13 000 cm^{-1} (1.6 eV, 770 nm). The band was clearly associated with the intramolecular charge transfer transition identified above in the solution spectra. However, the band was not polarized, and a closer inspection of the spectra revealed a slightly different position of the band maxima in the two polarizations (the difference was about 500 cm^{-1}; notice the logarithmic scale in the wavenumber axis). Given the mixed stack motif of the crystal structure, we speculated that we observed *two* overlapping charge transfer transitions, one intra- and the other intermolecular. The two were orthogonal each other. If the above supposition was correct, A−D−A would represent a good example of a two-dimensional, "intra−inter" charge transfer crystal.

In any case, we have clearly shown that this fused and perfectly planar A−D−A assembly involving a strong donor (TTF) and a weak acceptor (quinone) had a high propensity to crystallize in the crystallographic arrangement characterized by the nonideal packing to reach conductivity, in contrast to nonfused A−D−A or D−A−D

systems **27** and **28**, respectively. In fact, the electrical conductivity measured on pellets using the four-probe technique was estimated to be 10^{-9} and 2×10^{-9} S/cm for fused D−A **10** and A−D−A **9** systems, respectively, confirming the low degree of charge transfer in the undoped state.

Conclusion

To control the stoichiometry between D and A, we have developed an interesting approach consisting of synthesizing TTF fused to acceptors such as *p*-benzoquinone. The quinone moiety of **9** and **10** can be used as a precursor for stronger acceptor moieties, e.g., DCNQI or TCNQ.[50] Consequently, work is in progress to improve this acceptor ability of the quinone moiety in order to reach unprecedented fused TTF−TCNQ (D−A) derivatives and TCNQ−TTF−TCNQ (A−D−A). Quinone- or TCNQ-based intramolecular donor−acceptor systems constitute a promising field of applications due to the interesting optoelectronic properties they can exhibit. Moreover, with the aim of controlling the stacking of the D−A system, the preparation of LB films[51] of bisdodecyl-substituted derivative, as well as their possible rectifying behavior, is also under study.

In addition, we have obtained a purely mixed-valence compound $\mathbf{9}^{-\bullet}$ in which the existence of a temperature-dependent intramolecular electron transfer has clearly been established. The results we have just presented unambiguously show that TTF is a suitable bridge for promoting intramolecular electron transfer between two redox centers. Such a system is of particular interest for understanding electron-transfer processes for the design of molecular wires.[52]

Experimental Section

The general procedure is listed in Supporting Information. The melting points are uncorrected. ^{1}H NMR (200 or 500 MHz) spectra were measured with Me_4Si as an internal standard; the δ and J values are given in parts per million and hertz, respectively. The IR spectra are recorded in units of cm^{-1}.

2,5-Dihydroxyphenyl-1-piperidinedithioate 11. To a solution of *p*-benzoquinone (5.40 g, 50 mmol) in a solution of glacial acetic acid (24 mL) and DMF (24 mL) was added rapidly at 0 °C a solution of the dithiocarbamate salt (12.2 g, 50 mmol) in a mixture of DMSO (12 mL) and DMF (24 mL). The mixture was stirred for 1 h before dilution with 500 mL of water. Filtration of the precipitate yielded 13 g (yield = 97%) of white crystals. Mp = 94−96 °C.

4,7-Dihydroxy-1,3-benzodithioyliden-2-*N*-piperidinium Acetate 12. *p*-Benzoquinone (5.22 g, 48 mmol) was added to a solution of compound **11** (13 g, 48 mmol) dissolved in 250 mL of methanol, immediately yielding a red precipitate. The mixture was stirred for an additional 30 min and then filtered. The precipitate was washed with methanol and then dissolved in 20 mL of glacial acetic acid, and the solution was heated for 10 min at 80 °C. After the mixture was cooled, the addition of 150 mL of acetone afforded after filtration 15.16 g (yield = 96%) of pale gray crystals. Mp = 152−154 °C.

4,7-Dihydroxy-1,3-benzodithiole-2-thione 13. To a suspension of the iminium salt **12** (9.80 g, 31 mmol) in 130 mL of methanol was added by fractions sodium sulfide nonahydrate (59.3 g, 0.246 mol) with vigorous stirring. After stirring at room temperature for 3 h, the red solution was poured into a mixture of glacial acetic acid (80 mL) and water (2 L). The solution was stored in a refridgerator for 48 h, and then filtration yielded 6.67 g (yield = 98%) of pale yellow crystals. Mp = 239 °C (AcOH/MeOH) (lit.[19a] 238 °C).

4,7-Diacetyloxy-1,3-benzodithiole-2-thione 14a. To a suspension of hydroquinone **13** (7.12 g, 33 mmol) in 30 mL of CH_2Cl_2 were successively added 37 mL of triethylamine (0.263 mol) and 12.4 mL (0.132 mol) of acetic anhydride. After stirring for 1 h, the mixture was partially concentrated. After addition of 50 mL of petroleum ether, the precipitate was filtered and washed with methanol, affording 7.9 g (yield = 80%) of yellow crystals. Mp = 154 °C (CH_2Cl_2) (lit.[19a] 148−149 °C).

4,7-Bis(*tert*-butyldiphenylsilyloxy)-1,3-benzodithiole-2-thione 14b. To a solution of hydroquinone **13** (6.48 g, 30 mmol) in 120 mL of DMF were successively added *tert*-butyldiphenylchlorosilane (20.4 mL, 78 mmol) and imidazole (10.2 g, 150 mmol). The mixture was stirred overnight at room temperature. After addition of methanol (300 mL), the precipitate was filtered, and recrystallization furnished 17.68 g (yield = 86%) of yellow crystals. Mp = 176 °C (CH_2Cl_2/petroleum ether). Anal. Calcd for $C_{39}H_{40}O_2S_3Si_2$ (693.10): C, 67.58; H, 5.82; S, 13.88. Found: C, 67.52; H, 5.84; S, 13.99.

4,7-Diacetyloxy-1,3-benzodithiole-2-one 15a. To a solution of compound **14a** (4.95 g, 16.5 mmol) in CH_2Cl_2 (150 mL) and glacial acetic acid (110 mL) was added mercuric acetate (13.09 g, 41.1 mmol). After stirring at room temperature for 15 min, the solution was filtered on Celite. The solution was successively washed with water (3 × 150 mL), a saturated solution of $NaHCO_3$ (4 × 50 mL), and water (50 mL). The organic layer was dried ($MgSO_4$) and concentrated. The residue was purified by chromatography on silica gel (CH_2Cl_2). Recrystallization using CH_2Cl_2/petroleum ether afforded 4.10 g of white crystals (yield = 88%). Mp = 164 °C (lit.[19a] 163−164 °C).

4,7-Bis(*tert*-butyldiphenylsilyloxy)-1,3-benzodithiole-2-one 15b. The same experimental procedure that afforded **15a** was followed, starting from 2.68 g (8.9 mmol) of compound **14b**. The residue was purified by chromatography on silica gel (CH_2Cl_2/petroleum ether = 1/4). Recrystallization using CH_2Cl_2/petroleum afforded 2.16 g of white crystals (yield = 85%). Mp = 180 °C. Anal. Calcd for $C_{39}H_{40}O_3S_2Si_2$ (676.20): C, 69.19; H, 5.96; S, 9.47. Found: C, 69.08; H, 5.98; S, 9.77.

Bis(1,4-diacetyloxy)dibenzotetrathiafulvalene 16. A solution of 9.94 g of compound **15a** (35 mmol) in freshly distilled triethyl phosphite (75 mL) was refluxed for 3 h and 30 min. After the solution was cooled, the precipitate was filtered and the yellow crystals were washed with methanol (4.20 g; yield = 45%); mp > 280 °C (lit.[19a] > 280 °C).

2,3-Bis(pentylsulfanyl)-6,7-[3,6-bis(*tert*-butyldiphenylsilyloxy)benzo]tetrathiafulvalene 18. To a solution of 0.62 g (1.5 mmol) of phosphonate **17** in 15 mL of anhydrous THF was added, under an inert atmosphere at −78 °C, 1.0 mL (1.6 mmol) of *n*-BuLi (1.6 M in hexane). After the solution was stirred for 10 min, a solution of dithiolone **15b** (0.51 g, 0.75 mmol, 1 equiv) in 15 mL of anhydrous THF was added dropwise. After stirring for 3 h at room temperature, the reaction mixture was concentrated and purified by chromatography on silica gel (CH_2Cl_2/petroleum ether 1/9 to eliminate impurities and then 1/4 for the elution of compound **18**) affording 0.65 g of yellow crystals (yield = 90%); mp = 104 °C (CH_2Cl_2/petroleum ether); MS *m*/*z* (I%) 966 ($M^{+\bullet}$, 100), 864 (8), 534 (9), 457 (26), 135 (15).

(2,3)-(6,7)-Bis(1,4-dioxo-1,4-dihydrobenzo)tetrathiafulvalene 9. To a solution of 106 mg (0.224 mmol) of TTF derivative **16** in 15 mL on anhydrous THF was added a sodium methanolate solution prepared by treatment of 50 mg (2.24 mmol) of sodium in 3 mL of anhydrous methanol. The green

(50) For a review on TCNQ and DCNQI electron acceptors, see: Martín, N.; Segura, J. L.; Seoane, C. *J. Mater. Chem.* **1997**, *7*, 1661.
(51) Nadizadeh, H.; Mattern, D. L.; Singleton, J.; Wu, X.; Metzger, R. M. *Chem. Mater.* **1994**, *6*, 268.
(52) (a) Creager, S.; Yu, C. J.; Bamdad, C.; O'Connor, S.; MacLean, T.; Lam, E.; Chong, Y.; Olsen, G. T.; Luo, J.; Gozin, M.; Kayyem, J. F. *J. Am. Chem. Soc.* **1999**, *121*, 1059. (b) Caroll, R. L.; Gorman, C. B. *Angew. Chem., Int. Ed.* **2003**, *41*, 4378.

solution was stirred for 1 h at 60 °C, and then acidified by addition of 426 mg (2.24 mmol) of *p*-toluenesulfonic acid monohydrate. After the solution was stirred for 5 min, 107 mg of DDQ (0.471 mmol) was added and the solution was stirred for 2 h at room temperature. After dilution with CH_2Cl_2, the organic layer was washed with brine, dried ($MgSO_4$), and concentrated in vacuo. The purification on florisil (100−200 mesh) column chromatography using CH_2Cl_2/EtOAc (99/1) as a mixture of eluents followed by a recystallization in CH_2Cl_2/petroleum ether afforded 46 mg of blue crystals (yield = 57%): thermal gravimetric analysis (TGA) 240 °C (dec.); IR(KBr) cm^{-1} 1656 (C═O), 1544 (C═C); MS *m*/*z* (I%) 364 ($M^{+\bullet}$, 100), 226 (67), 88 (44).

Crystallographic Data of Compound 9. Single crystals of (0.5 × 0.13 × 0.05 mm) were grown at 293 K by slow evaporation of a CH_2Cl_2/petroleum ether solution containing **9**: $C_{15}H_6Cl_2O_4S_4$, M = 449.34 g/mol; monoclinic, *P*21/*c*; a = 5.829(1), b = 10.355(2), c = 14.429(3) Å, β = 98.19(2)°, V = 862.0(3) $Å^3$, Z = 2, ρ_{calcd} = 1.731 g/cm^3, λ(Mo Kα) = 0.71073 Å, 6445 reflections ($2 < \theta < 25°$) were collected at 293 K, 1626 unique reflections and 842 reflections with $I > 2\sigma(I)$ used in refinements, 129 parameters, R = 0.0537, wR = 0.0885. **Cation Radical $9^{+\bullet}\cdot CF_3SO_3^-$.** To a solution of 46.7 mg (0.128 mmol) of Q−TTF−Q **9** in 1.5 mL of CH_3CN was added 20.61 mg (0.064 mmol) of iodobenzene diacetate $PhI(OAc)_2$ and then 22.4 μL (0.256 mmol) of trifluoromethanesulfonic acid. After the mixture was stirred for 1 h, the resultant black precipitate was filtered and washed with diethyl ether (10 mL), toluene (10 mL), and CH_2Cl_2 (10 mL) successively. The black precipitate (36 mg) was isolated in 55% yield: IR (KBr) cm^{-1} 1658 (C═O), 1255, 1027, 636 (SO_3^-). Anal. Calcd for $C_{15}H_4F_3O_7S_5$ (514.52): C, 35.02; H, 0.98; S, 31.16. Found: C, 34.88; H, 1.08; S, 31.39.

Anion Radical $9^{-\bullet}\cdot P(C_6H_5)_4^+$. Q−TTF−Q **9** (5 mg) was dissolved in 2 mL of a 0.2 M solution of tetraphenylphosphonium bromide in anhydrous CH_2Cl_2. A Cu wire was introduced and led to react at room temperature for 24 h. After removal of Cu wire, the reaction mixture was centrifuged and the precipitate washed with CH_2Cl_2 several times, giving 6 mg of greenish powder (62% yield): IR (KBr) cm^{-1}; 1633, 1615 (C═O), 760, 723, 691 (P−C). UV−vis (ethyl acetate) λ (nm) 421, 516. Anal. Calcd for $C_{38}H_{24}O_4PS_6$ (703.84): C, 64.85; H, 3.44; S, 18.22. Found: C, 65.11; H, 3.00; S, 17.72.

2,3-Bis(pentylsulfanyl)-6,7-(1,4-dioxo-1,4-dihydrobenzo)tetrathiafulvalene 10a. To a solution of 100 mg (0.1 mmol) of TTF **18** in 8 mL of anhydrous THF was added 0.26 mL (0.26 mmol) of *n*-Bu_4NF (1 M in THF). After the solution was stirred for 30 min at room temperature, 112 mg (0.14 mmol) of *p*-benzoquinone was added, and stirring was continued for an additional 5 min. The purification on florisil (100−200 mesh) column chromatography using CH_2Cl_2/petroleum ether (1/1) followed by a recystallization in CH_2Cl_2/petroleum ether afforded 38 mg of green crystals (yield = 75%): thermal gravimetric analysis (TGA) 290 °C dec.; IR (KBr) cm^{-1} 1650; MS *m*/*z* (I%) 488 ($M^{+\bullet}$, 100), 384 (13), 347 (12), 259 (10), 226 (22). Anal. Calcd for $C_{20}H_{24}O_2S_6$ (488.77): C, 49.15; H, 4.95; S, 39.36. Found: C, 49.11; H, 5.00; S, 37.92.

4,9-Dioxo-4,9-dihydronaphtho[2,3-*d*]-1,3-dithiole-2-one 19. To a suspension of 16.75 g of finely powdered K_2S (152 mmol) in 40 mL of DMF was added 7.5 mL (125 mmol) of CS_2. After the mixture was stirred for 2 h at room temperature, 14.2 g (62.5 mmol) of 2,3-dichloronaphthoquinone was added. After stirring for 30 min, the reaction mixture was diluted with dichloromethane, washed with water, and dried ($MgSO_4$), and the solvents were partially concentrated. The product was precipitated by addition of methanol, and 10.7 g of red crystals was isolated (yield = 65%): mp = 164 °C (CH_2Cl_2) (lit.[16a] 160−162 °C); MS *m*/*z* (I%) 264 ($M^{+\bullet}$, 100), 188 (38), 160 (12), 132 (10), 104 (43), 76 (30).

4,9-Dihydroxynaphtho[2,3-*d*]-1,3-dithiole-2-one 20. A solution of 5 g (18.9 mmol) of compound **19** was shaken in a separating funnel in 200 mL of an aqueous solution of sodium dithionite ($Na_2S_2O_4$) (4% w/w). The initial red solution became yellow, and the organic layer was washed with water, dried ($MgSO_4$), and then concentrated to afford 3.80 g of yellow powder (yield = 75%); mp = 222−224 °C (CH_2Cl_2) (lit.[16a] 222−224 °C).

4,9-Diacetyloxynaphtho[2,3-*d*]-1,3-dithiole-2-thione 21. To a suspension of 3.8 g (14.3 mmol) of compound **20** in 40 mL CH_2Cl_2 were successively added 17 mL of triethylamine (121 mmol) and 6 mL (60.5 mmol) of acetic anhydride. After the mixture was stirred for 1 h, the yellow precipitate was filtered and 3.92 g of yellow crystals was obtained (yield = 79%); mp = 240 °C (CH_2Cl_2).

4,9-Diacetyloxynaphtho[2,3-*d*]-1,3-dithiole-2-one 22. To a solution of 3.92 g (11.2 mmol) of compound **21** in 100 mL of CH_2Cl_2 and 80 mL of glacial acetic acid was added 9.08 g (28.5 mmol) of mercuric acetate. After stirring for 15 min at room temperature, the reaction mixture was filtered on Celite. The filtrate was successively washed with water (2 × 100 mL), a saturated aqueous $NaHCO_3$ solution (2 × 100 mL), and then water (50 mL). The organic layer was dried ($MgSO_4$), and the solvent was concentrated to afford 3.6 g of white crystals (yield = 96%).

Bis(1,4-diacetyloxynaphtho)tetrathiafulvalene 23. A solution of 3.6 g (10.8 mmol) of compound **4** in 25 mL of freshly distilled triethyl phosphite was refluxed for 1 h. After the solution was cooled, the precipitate was filtered and washed with methanol to afford 2 g of yellow crystals (yield = 53%): mp > 300 °C; MS *m*/*z* (I%) 636 ($M^{+\bullet}$, 100), 622 (17), 600 (30), 558 (15), 506 (25).

(2,3)-(6,7)-Bis(1,4-naphthoquinone)tetrathiafulvalene 8. To a suspension of 200 mg (0.31 mmol) of compound **23** in 25 mL of anhydrous THF was added a solution of 170 mg (3.14 mmol) of sodium methoxide in 5 mL of anhydrous methanol. The green suspension was heated for 4 h at 80 °C. After the suspension was cooled at 0 °C, 597 mg of *p*-toluenesulfonic acid monohydrate (3.14 mmol) and 148 mg (0.65 mmol) of DDQ were added. After the mixture was stirred for an additional 2 h at room temperature, the precipitate was filtered, washed with THF to afford 100 mg of green crystals (yield = 68%): mp > 300 °C; MS *m*/*z* (I%) MALDI 464 ($M^{+\bullet}$); IR (KBr) cm^{-1} 1654 (C═O).

Acknowledgment. This work was partially supported by grants from the MENRT for Nicolas Gautier, the "Ville d'Angers" for Frédéric Dumur, DGI-Spain BQU2000-1157, and DURSI-Catalunya 2001SGR-00362. This research was undertaken as part of the European collaborative COST Program (Action D14/0004/99).

Supporting Information Available: ^1H and ^{13}C NMR and IR data with assignment of all signals; ^1H and ^{13}C NMR spectra of dyad **10a**; IR spectra of triad **9** and cation radical $9^{+\bullet}\cdot CF_3SO_3^-$ in KBr pellets; ESR spectrum of cation radical $9^{+\bullet}\cdot CF_3SO_3^-$ in acetone solution; IR spectrum of anion radical $9^{-\bullet}\cdot P(C_6H_5)_4^+$ in KBr pellets; ESR spectrum of the solid $9^{-\bullet}\cdot P(C_6H_5)_4^+$ in ethyl acetate at 300 K; evolution of the UV−vis−NIR spectrum at the beginning of the reduction of A−D−A **9**; and crystallographic data for triad **9**. This material is available free of charge via the Internet at http://pubs.acs.org.

JO035689F

A New Multifunctional Ferrocenyl-Substituted Ferrocenophane Derivative: Optical and Electronic Properties and Selective Recognition of Mg^{2+} Ions

Juan Luis Lopez,[a] Alberto Tárraga,[a] Arturo Espinosa,[a] M. Desamparados Velasco,[a] Pedro Molina,*[a] Vega Lloveras,[b] José Vidal-Gancedo,[b] Concepció Rovira,[b] Jaume Veciana,*[b] David J. Evans,[c] and K. Wurst[d]

Abstract: The synthesis, characterisation, and X-ray structure of a new strained asymmetric diferrocene derivative (**2**) is reported. Compound **2** acts as a highly specific electrochemical and optical Mg^{2+} ion sensor, as revealed by spectroscopic and electrochemical techniques. Thus, in the presence of Mg^{2+}, a new redox peak appears in the cyclic voltammogram (CV) that is anodically shifted compared to the $E_{1/2}$ of the free receptor ($\Delta E_{1/2} = 340$ mV). Diferrocene derivative **2** also gives a highly visual response upon addition of Mg^{2+}, namely a change of colour from orange to deep purple. In addition, compound **2** does not show any significant sensing activity in the presence of Ca^{2+} or alkaline ions. On protonation, it is converted into the stable diferrocenylcarbenium salt **4**, in which two different modes of stabilisation of the α-carbocationic centre are clearly demonstrated by a combination of ^{1}H NMR and ^{57}Fe Mössbauer spectroscopic measurements. Finally, by a partial (chemical or electrochemical) oxidation, compound **2** forms the asymmetric mixed-valence species $\mathbf{2}^{+}$, which can be isolated as the solid salt **6** by using $CF_3SO_3^-$ as a counterion. This mixed-valence species shows a fast intramolecular electron-transfer process, as ascertained by several spectroscopic techniques.

Keywords: electrochemistry · electron transfer · metallocenes · molecular recognition · Mössbauer spectroscopy

Introduction

The chemistry of ferrocene-based structures has been receiving increasing attention because of their importance in many fields such as electrochemistry, molecular recognition, material science and catalysis.[1] We have focussed our attention on two important aspects of the chemistry of these materials, namely molecular recognition and intramolecular electron transfer in mixed-valence diferrocene derivatives.

Design of redox-active receptors in which a change in electrochemical behaviour can be used to monitor complexation of guest species is an increasingly important area of molecular recognition.[2] In this context, ferrocene derivatives, mostly those which are substituted with macrocyclic ligands, are prototype molecules which have proved to be especially versatile as ion sensors.[3] Cation binding at an adjacent receptor site of a ferrocene-based host induces a positive shift in the redox potential of the ferrocene/ferrocenium couple, either by through-bond and/or through-space electrostatic interactions, interference or conformational change,[4] and the complexing ability of the ligand can be reversibly switched on or off by varying the applied electrochemical potential. The efficiency of these kinds of redox-active ligands crucially depends on the electronic communication between the metal centre involved. It has been shown that this communication is very favourable when donor atoms of a chelating ligand are directly attached to the ferrocene units.[3e,5] In particular, it has been suggested that an added degree of recognition is conferred by appearance of a new set of redox waves (two-wave behaviour) as-

[a] J. L. Lopez, Dr. A. Tárraga, Dr. A. Espinosa, Dr. M. D. Velasco, Prof. P. Molina
Universidad de Murcia
Departamento de Química Orgánica
Facultad de Química, Campus de Espinardo
30100 Murcia (Spain)
Fax: (+34) 968-364-149
E-mail: pmolina@um.es

[b] V. Lloveras, Dr. J. Vidal-Gancedo, Prof. C. Rovira, Prof. J. Veciana
Institut de Ciencia de Materials de Barcelona (CSIC)
Campus Universitari de Bellaterra, 08193 Cerdanyola (Spain)
Fax: (+34) 93-580-5729
E-mail: vecianaj@icmab.es

[c] Dr. D. J. Evans
Department of Biological Chemistry, John Innes Centre
Norwich Research Park, Colney, Norwich, NR4 7UH (UK)

[d] Dr. K. Wurst
Institut für Allgemeine Anorganische und Theoretische Chemie
Universität Innsbrück, 6020, Innarain 52a, Innsbrück (Austria)

Supporting information for this article is available on the WWW under http://www.chemeurj.org/ or from the author.

 DOI: 10.1002/chem.200305394

sociated with the oxidation of the ferrocene unit in the host–guest complex, compared with a single gradual shift in the potential of the original ferrocene redox couple.[6]

Since the advent of mixed-valence chemistry in 1967,[7] the study of electronic interactions in systems containing multiple, identical metal-centred fragments that individually display fast, reversible, one-electron exchange has been a topic of particular interest.[8] Mixed-valence compounds, which have at least two redox sites in different oxidation states linked by a bridge that mediates the transfer of electrons from one site to the other, are excellent benchmarks for the study of intramolecular electron-transfer phenomena.[9] In this context, many complexes containing two ferrocenyl moieties, which are linked together with a wide variety of structural motifs, have been synthesised to investigate the effectiveness of the bridging groups for electron transfer between the redox nuclei. Variation of the nature of the molecular framework of the bridge enables the extent of communication between the metal centres to be modulated, as reflected by the electrochemical response. Full characterisation of this kind of interaction between two iron atoms is provided by the electronic coupling parameter (V_{ab}), which has the units of energy and can be obtained from the position, intensity and width of the intervalence transition band, which generally occurs in the near infrared region.[10,11] Although metal–metal interactions of differing extents have been revealed for homobimetallic complexes in which the two ferrocene units are coupled intimately by π-unsaturated bridges,[12] heterocycles[13] or metallocycles,[14] examples that show electronic coupling between ferrocenyl units either through a carbenium ion[15] or hydroxyl-substituted sp^3 carbon atoms[16] are rare.

As shown in Figure 1, the structural features required for the properties of particular interest to us in ferrocene chemistry are very different: an effective spacer is needed to observe the intramolecular electron-transfer phenomena in diferrocene compounds, whereas the presence of an heteromacrocycle is the structural motif that is almost mandatory for molecular recognition processes.

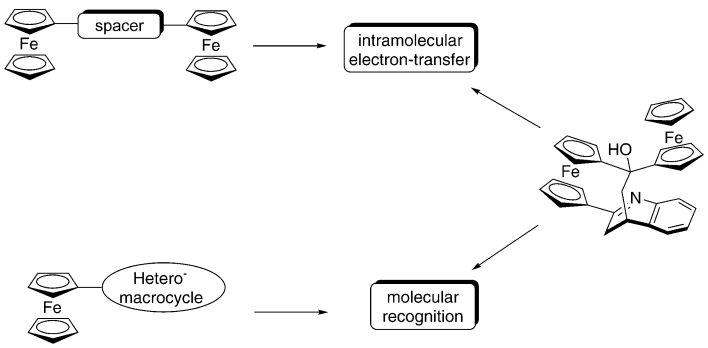

Figure 1. Schematic diagram of the structural features required for intramolecular electron-transfer phenomena and molecular recognition processes.

This paper is devoted to the preparation, structural determination and study of the physicochemical properties of the new diferrocene derivative **2**. This compound exhibits a defined topology with a ferrocenophane architecture and also incorporates an aza-substituted bridge. The combined effects of both structural characteristics suggest that: 1) it might experience an electron-cloud perturbation upon coordination or protonation and may thus function as a chemosensor for metal ions or protons; and 2) it could be converted by partial oxidation (chemical or electrochemical) into the corresponding mixed-valence compound $\mathbf{2}^+$, which would display interesting intramolecular electron-transfer phenomena and show coordination properties that should differ from those of the neutral derivative. Consequently, the combination of these two properties in diferrocene **2** could lead to interesting properties, such as electrochemically switchable chemosensing behaviour.

Results and Discussion

Diferrocenylcarbinol 2

Synthesis: This compound was prepared from the ferrocenophane **1**,[17] which can be viewed either as a [5]ferrocenophane bearing a 2,4-bridged dihydroquinoline ring or as a [4](2,4)-dihydroquinolinophane containing a 1,1′-disubstituted ferrocene bridge. Reaction of ferrocenophane **1** with ferrocenyllithium[18] in dry THF at room temperature under N_2 provided, after chromatographic purification, the diferrocenylcarbinol **2** as an orange solid, in 80% yield. (Scheme 1).

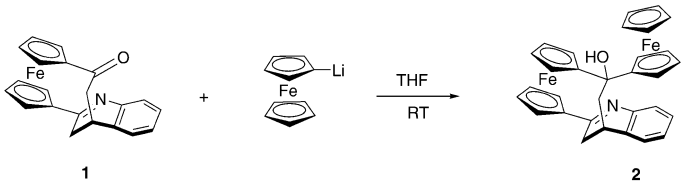

Scheme 1. Reaction scheme for the formation of compound **2**.

X-ray structure determination: Single crystals of **2** suitable for X-ray structure determination were grown from CH_2Cl_2/hexane. The molecular structure is shown in Figure 2 together with the numbering scheme. Compound **2** crystallises in the monoclinic space group $P2_1/n$ with four molecules in the unit cell. The molecular structure of **2** reveals almost eclipsed cyclopentadienyl rings for both ferrocenes. The differences between both ferrocenes are observed in the Fe–C(cyclopentadienyl) distances. Thus, whereas in the monosubstituted ferrocene the Fe–C distances are between 2.025 and 2.051 Å, in the disubstituted ferrocene the distances range between 2.024 and 2.084 Å. This generates a deformation angle between the two ring centroids and the iron atom of 176.5° for the monosubstituted and 175.6° for the disubstituted ferrocene, and tilt angles between the planes of the Cp rings of 3.5° and 5.8°, respectively. The deformation angle of the unstrained monosubstituted ferrocene can accrue from crystal packing effects. More evidence for the conformational strain is the bending of the single bonds C(20)–C(21) and C(10)–C(21) with respect to the Cp rings. Atom C(21) lies 0.021 Å and 0.277 Å out of the Cp planes

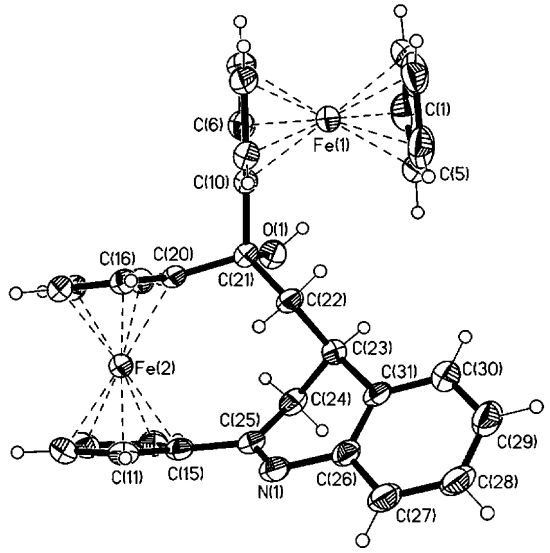

Figure 2. ORTEP view of the molecular structure of compound **2** showing the atom labelling in the asymmetric unit. Thermal ellipsoids are drawn at 50% probability level.

of the mono- and disubstituted ferrocene, respectively. The single bonds C(10)–C(21) and C(20)–C(21) have bending angles of 0.8° and 10.5°, respectively, in the opposite direction of the iron atoms. Interestingly, the bending angle of the single bond C(15)–C(25) is 5.6° in the direction of the iron atom of the disubstituted ferrocene. This bending in the direction of the iron atom can often be found in monosubsituted ferrocenes with aldehyde groups or vinyl groups with electron-withdrawing substituents, which can conjugate with the Cp ring. In these compounds the bending angles are in a range between 2° and 4°. The strain observed in the disubstituted ferrocene is, as expected, much smaller than that found in a related 2-aza[3]ferrocenophane compound, which has the nitrogen atom linked to both bridge carbons of the ferrocene, thus enforcing a rigid bridge geometry.[17b] In contrast to that compound, which has a short Fe–N distance, in **2** the nitrogen atom is far from the Fe atom of the disubstituted ferrocene, as it is situated in the external part of the molecule and, therefore, close interaction of the nitrogen atom with the iron atoms of each ferrocene unit is prevented. The monosubstituted ferrocene unit has a short Fe–HO interaction (d_{Fe-HO} 2.989 Å) reminiscent of agostic type bonding. The two ferrocene units are almost orthogonal, forming an angle of 106.93° between the closest Cp rings. On the other hand, only a small torsion angle is observed between the Cp ring of the disubstituted ferrocene and the aromatic ring connected to the nitrogen atom, thus promoting an available resonance pathway.

Table 1. ^{1}H NMR data for the three substituted Cp rings in compounds **2** and **4**.

	Compound	δH_2	δH_3	δH_4	δH_5	$\Delta\delta H_{2,3}$	$\Delta\delta H_{5,4}$
2	Cp_1	3.88	3.99	4.07	3.96	0.11	−0.11
	Cp_2	4.72	4.53	4.45	4.99	−0.19	−0.46
	Cp_3	4.41	4.14	4.14	3.80	−0.27	0.34
4	Cp_1	5.05	4.91	5.27	6.10	−0.14	−0.83
	Cp_2	5.86	5.51	5.12	5.66	−0.35	−0.54
	Cp_3	5.53	6.63	6.67	5.88	1.10	0.79

^{1}H NMR studies: An in-depth study of the ^{1}H NMR spectrum of the diferrocenylcarbinol **2** has been carried out. The room temperature 400 MHz ^{1}H NMR spectra of **2** was completely assigned (with the exception of the aromatic protons) by ^{1}H,^{1}H COSY, NOESY and spin-decoupled experiments. The analysis of its ^{1}H NMR spectrum presents the following characteristic features: 1) the diastereotopism of all the protons within the three substituted Cp rings, which appear as twelve multiplets in contrast to the singlet corresponding to the five equivalent protons within the unsubstituted Cp_4 ring (Table 1); 2) the diastereotopism shown by the two protons within each of the two methylene groups of the bridge, which appear at $\delta = 1.99$ ppm (t) and 2.41 ppm (dd), in the case of the CH_2 group placed at the 2-position of the bridge, and at $\delta = 2.52$ ppm (dd) and 3.70 ppm (dd), in the case of the CH_2 group placed in the dihydroquinoline moiety; 3) the methine group which appears as a multiplet at $\delta = 3.38$ ppm and iv) the OH group, which appears as a singlet at $\delta = 2.57$ ppm.

The results obtained from NOE experiments are illustrated in Figure 3. It is important to emphasise that while a NOE effect is detected between the OH group and the hydrogen atom H2 present in Cp_3, no effect is observed between the OH group and the hydrogen atom H5 within the same Cp_3 ring. This indicates that, although in principle a free rotation around the C_{OH}–C_{Cp3} bond could be assumed, giving rise to two possible extreme rotamers, from the NOE experiments only the rotamer shown in Figure 3 is detected. Moreover, inspection of the X-ray structure of alcohol **2** reveals the occurrence of an Fe···HO interaction ($d_{Fe\cdots H}$: 2.989 Å), reminiscent of the agostic type bonding reported for the protonation product of ferrocene and its proton exchange in highly acidic media,[19] and the intermediates in electrophilic substitution reactions on ferrocenes.[20] The interaction could account, to some extent, for a hampered rotation of the monosubstituted ferrocene unit.

Electrochemical study: An electrochemical study in CH_2Cl_2 was carried out at room temperature, with $[NnBu_4]ClO_4$ (0.1 M) as supporting electrolyte, a Pt disk as a working electrode and SCE as the reference electrode. The cyclic voltammetric (CV) response of **2** shows two closely spaced reversible oxidation processes at +0.510 V and +0.740 V (vs SCE electrode in CH_2Cl_2) (Table 2 and Figure 4). Likewise the differential pulse voltammogram (DPV) also exhibits two well-resolved oxidation waves of the same area.[21] The first reversible oxidation process arises from the oxidation of the monosubstituted ferrocene unit, while the second reversible oxidation process is associated with the oxidation of the 1,1′-disubstituted ferrocene unit. One might speculate

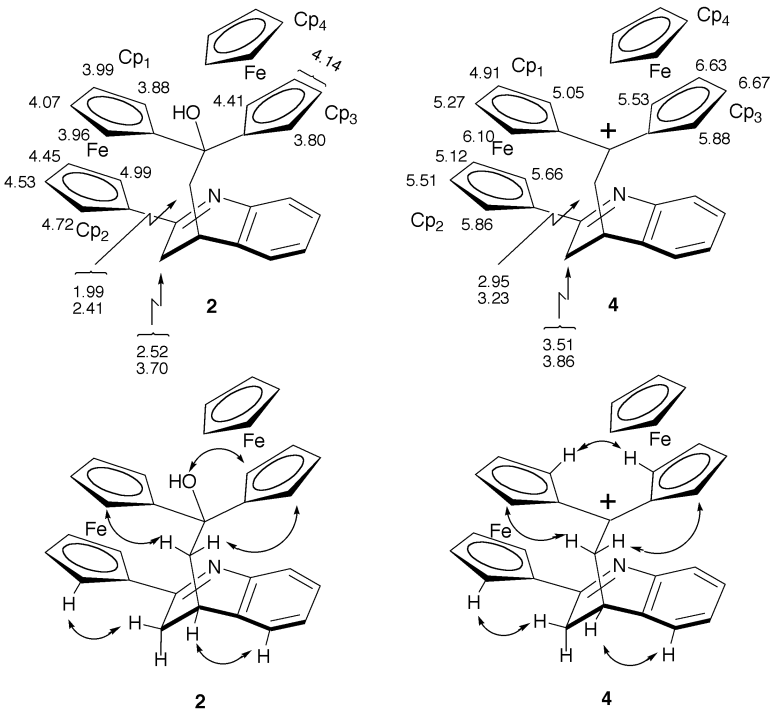

Figure 3. Chemical shifts and NOEs observed for compounds **2** and **4**.

Table 2. Cyclic voltammetry data.

	$E_{1/2}$ (1)[a] ($E_{pa}-E_{pc}$)		$E_{1/2}$ (2)[a] ($E_{pa}-E_{pc}$)		$E_{1/2}$ (3)[a] ($E_{pa}-E_{pc}$)	E_{pc} (irrev) (1)		E_{pc} (irrev) (2)	
	CH_3CN	CH_2Cl_2	CH_3CN	CH_2Cl_2	CH_3CN	CH_3CN	CH_2Cl_2	CH_3CN	CH_2Cl_2
2	0.450 (0.070)	0.510 (0.070)	0.670 (0.080)	0.740 (0.080)					
2·Mg^{2+}[b]	0.570 (0.080)		0.760 (0.070)		1.100 (0.070)	−0.430			
3	0.480 (0.060)	0.540 (0.080)	1.020 (0.070)	1.060 (0.140)		broad wave	−0.560		
4			0.985 (0.095)	1.160 (0.140)		−0.130	−0.070	−0.310	−0.260
6	0.470 (0.070)		1.010 (0.080)			−0.450			

[a] $E_{1/2}=(E_{pa}+E_{pc})/2$ versus SCE in volts. Electrolyte: [N*n*Bu$_4$]ClO_4; working and counter electrodes: Pt; reference electrode: SCE. [b] $E_{1/2}=(E_{pa}+E_{pc})/2$ versus decamethylferrocene (internal reference), in volts. Data obtained from measurements in CH_3CN/CH_2Cl_2 (3:2) as solvent. Under these conditions the redox potentials of compound **2** were: $E_{1/2}(1)=+0.540$ V and $E_{1/2}(2)=+0.760$ V versus DMFc.

that the difference between the oxidation waves ($\Delta E_{1/2}=$ 230 mV) in compound **2**, as well as the fact that the second oxidation process appears at a higher potential than those observed for closely related ferrocenophanes[17b] (0.740 V vs 0.580 V), is direct evidence for the presence of electronic communication between the two ferrocene units. However, we hesitate to invoke this explanation, because, even in the absence of communication, the difference between the potentials will increase simply because of the electrostatic effect.[22] In addition, the two ferrocenyl groups are intrinsically inequivalent and this also contributes to the difference in the oxidation potentials of the two ferrocene moieties. At this time, with only the electrochemical data, it is not possible to separate the combined effects of, or to determine the relative contribution of, chemical inequivalence and electronic communication through the carbon chain.

Metal-ion sensing properties of **2**: One of the most interesting attributes of compound **2** is the presence of two ferrocene redox-active moieties in proximity to the cation-binding dihydroquinoline site. The metal-recognition properties of proligand **2** were therefore evaluated by CV.[23] Whereas no perturbation of the CV was observed upon addition of Ca^{2+} ion, significant modification could be observed upon addition of Mg^{2+} ion. Thus, on addition of $Mg(ClO_4)_2$, a clear evolution of the second wave from $E_{1/2}=0.760$ V to 1.100 V ($\Delta E_{1/2}=340$ mV) was observed, whereas there was almost no effect on the first wave (a change from $E_{1/2}=0.540$ V to 0.570 V ($\Delta E_{1/2}=30$ mV)). More interesting is the observation of an extra irreversible reduction wave at $E_{1/2}=-0.430$ V, which is absent for the proligand. The current intensity of the anodic peak of the newly appearing reversible wave increases, while that of the disappearing reversible wave diminishes, with a linear dependence on the number of equivalents of the salt added; maximum perturbation of the CV was obtained with one equivalent of added Mg^{2+} ion (Table 2 and Figure 4). This "two-wave" behaviour is diagnostic of a large value for the equilibrium constant for cation binding by the neutral receptor.[6] The binding enhancement factor (BEF) is 1.8×10^{-6} and the reaction coupling efficiency[2d,e] (RCE) is 5.5×10^{5}. Remarkably, the presence of alkaline metal ions in solution ($LiClO_4$, $NaClO_4$ and $KClO_4$) had no effect on the CV, even when present in large excess. The major challenge in the design of Mg^{2+} sensors lie, for many applications, in the discrimination of Mg^{2+} ions from Ca^{2+}, Na^+ and K^+, as they play important roles as intracellular messengers in the regulation of cell function.[24] In this context, a number of redox-active ferrocene-based receptors such as imine-,[25] oxazoline-,[26] imidazoline-,[27] and pyridine-functionalised[28] ferrocene ligands have been described, which, in organic solvents, selectively respond to, but do not clearly

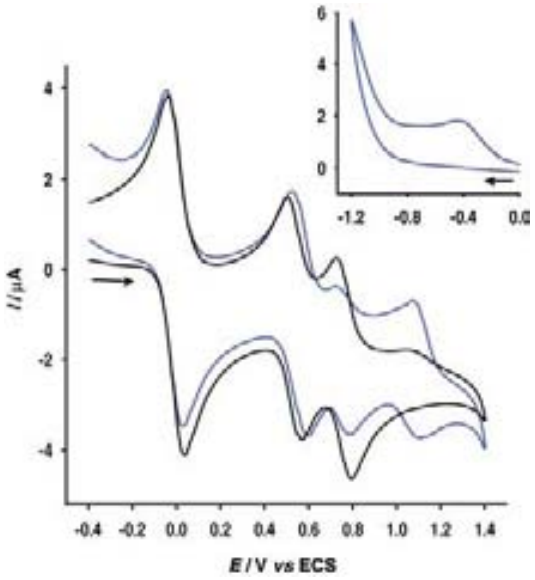

Figure 4. Cyclic voltammogram of compound **2** before (black) and after addition of 1 equivalent of $Mg(ClO_4)_2$ (blue); 1 mM **2** and 0.1 M $[NnBu_4]ClO_4$ in CH_3CN/CH_2Cl_2 also containing 1 mM DMFc, scan rate: 0.2 Vs^{-1}. The average of anodic and cathodic peak potentials $(E_{pa}+E_{pc})/2$ for DMFc was set at 0 V in each voltammogram.

differentiate between, Mg^{2+} and Ca^{2+} ions, with no interference from large excesses of Li^+, Na^+ and K^+.

We have discounted the possibility that the electrochemical response we observed upon addition of Mg^{2+} ion is due to adventitious protonation or hydration of the ligand. Addition of water to the resultant electrochemical solution elicited a further redox response, with the evolution of a new redox wave that corresponds to that assigned to the proligand. Therefore it can be concluded that metal-ion coordination occurs. The proligand **2** can be recovered unchanged in almost quantitative yield by aqueous workup.

The large positive shift in the ferrocene redox potential, upon coordination of Mg^{2+} ions by **2**, prompted us to investigate whether the coordination has an effect on the UV/Vis spectrum, as previous studies on ferrocene-based ligands have shown that their characteristic low-energy bands (LE) are perturbed by complexation.[29]

The UV-visible spectrum of **2** is consistent with most ferrocenyl chromophores in that they exhibit two charge-transfer bands in the visible region.[30] The prominent band at 319 nm ($\varepsilon = 8240\,M^{-1}cm^{-1}$; high energy (HE)), is assigned to a ligand-centred π–π* electronic transition (L–π*), and the less energetic and weaker band at 464 nm ($\varepsilon = 1195\,M^{-1}cm^{-1}$) (LE), responsible for the bright orange colour of this compound, is attributed to a metal-to-ligand charge-transfer (MLCT) process (d_π–π*) (Table 3). This assignment is in accordance with the latest theoretical treatment (model III) reported by Barlow et al.[31] The bands associated with the d–d transitions are masked by the MLCT band.[32]

Addition of anhydrous $Mg(ClO_4)_2$ into a solution of **2** in dichloromethane caused a progressive appearance of a new, more intense, absorption band located at $\lambda = 530$ nm ($\varepsilon = 4580\,M^{-1}cm^{-1}$) and the complete disappearance of the initial

Table 3. UV-visible/near-IR data in CH_2Cl_2.

Compound	λ_{max} [nm] (10^3 ε [$M^{-1}cm^{-1}$])
2	319 (8.2), 464 (1.2)
2·Mg^{2+}	530 (4.6)
3	342 (10.2), 530 (3.5), 731 (0.2)
4	325 (14.7), 375 (h), 465 (3.9), 641 (3.1)
6	329 (10.0), 507 (1.4), 625 (sh), 1230 (0.03)
$\mathbf{2}^{+1}$[a]	330 (10.5), 520[b] (1.8), 630 (sh), 1240 (0.03)
$\mathbf{2}^{+2}$[a]	339 (12.8), 524 (2.8), 630 (sh).

[a] Oxidised species obtained electrochemically in CH_2Cl_2 with 0.15 M nBu_4NPF_6. [b] Value obtained by deconvolution of the experimental spectrum.

LE band (Figure 5). The new band, which is 76 nm red-shifted, is assigned to MLCT (d_π–π*) transitions in the complexed ligand and is responsible for a change of colour from

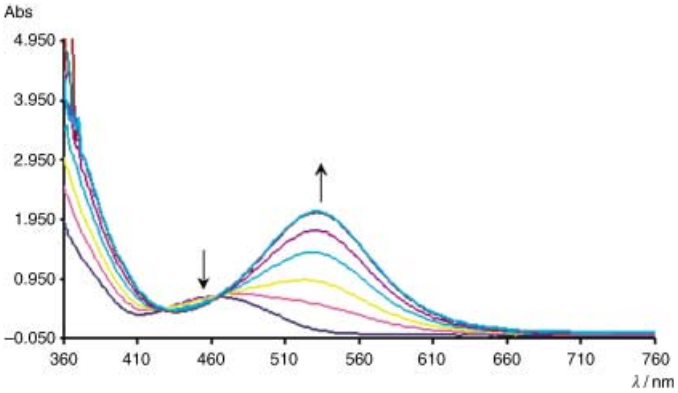

Figure 5. UV-visible spectra of the titration of alcohol **2** with 1 equivalent of $Mg(ClO_4)_2$ in CH_2Cl_2 ($c = 5\times10^{-4}\,mol\,dm^{-3}$). The initial spectrum is that of alcohol **2** and the final spectrum corresponds to the complexed form. Arrows indicate the absorptions that increased (up) and decreased (down) during the experiment.

orange (neutral proligand) to deep purple (complexed ligand). This colour change can be used for "naked-eye" detection of Mg^{2+}, even in the presence of Ca^{2+}. The HE band is also red-shifted, although only very little.

The bathochromic shift of the LE band and the remarkable increase in its molar absorptivity are consistent with an increase in the electronic interaction in the resulting complex, as the complexation process through the C=N−C group implies a lowering of the energy gap between the d_π orbitals of the iron atom (HOMO) and the π* orbital of the acceptor group (LUMO). This observation agrees with the appearance of an irreversible reduction wave in the CV of the complexed form of **2**, which is not observed for the proligand, and might be attributed to the reduction of the now highly polarised endocyclic C=N double bond. The complexation process in which the binding site (C=N−C) interacts with the cation gives rise to a more stabilised π* orbital in the C=N group, which acts as acceptor in the MLCT process. Consequently, the oxidant character of this group is enhanced and the charge-transfer process from the ferrocenyl (which acts as the donor group) to the acceptor unit, is then favoured upon cation binding.

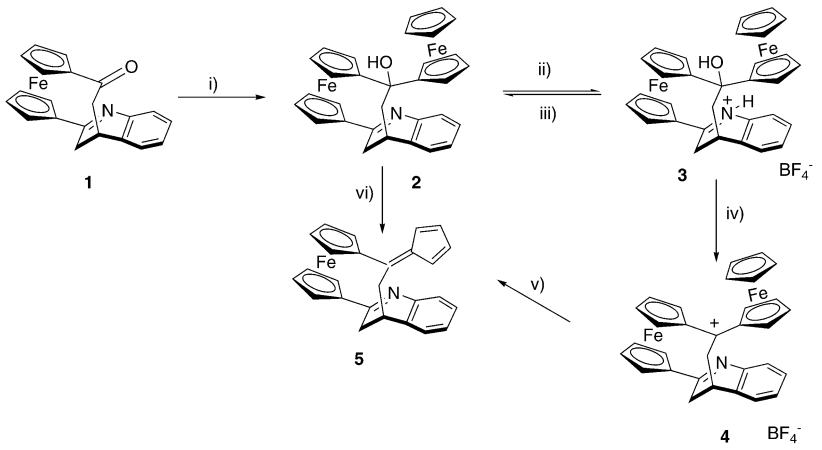

Scheme 2. Reagents and conditions: i) Fec-Li/THF, RT, 30 min, 80%; ii) 0.1 M HBF_4/CH_3CN (1 equiv); iii) K_2CO_3/MeOH, CH_3CN; iv) 0.1 M HBF_4/CH_2Cl_2 (1 equiv), 90%; v) a) 0.1 M HBF_4/CH_2Cl_2 (1 equiv) 90%; b) SiO_2, 10% Et_3N/*n*-hexane; vi) a) HCl (g)/CH_2Cl_2/$NH_4^+PF_6^-$; b) SiO_2 10% Et_3N/*n*-hexane, 90%.

The electrochemical and spectrophotometric data therefore indicate that the complexation process takes place only through the C=N−C group, with no complementary participation of the OH, a result which is consistent with the relative spatial orientation found for both groups in the solid state (X-ray structure of **2**) and in solution (NOE experiments of **2**). The association constant of the **2**·Mg^{2+} complex ($K_a = 1.8\times10^8\,M^{-2}$) could be evaluated by means of a UV-visible spectrophotometric titration.[33] Two well-defined isosbestic points were found at 428 and 464 nm (Figure 5), indicating that a neat interconversion between complexed and uncomplexed species occurs. A Job's method experiment carried out between **2** and $Mg(ClO_4)_2$ in dichloromethane at 25 °C revealed a ML_2 stoichiometry.[34] It is important to note that the association constant determined by UV-visible spectrophotometry corresponds to the complexation of the Mg^{2+} ion by neutral **2**, whereas the voltammetric shift reflects the interaction of the guest cation with the oxidised ligand.

Protonation of **2**: When **2** was treated with one equivalent of HBF_4 in acetonitrile, the N-protonated salt **3** was isolated as a deep purple solid. This, in turn, can be deprotonated by potassium carbonate in methanol to give the starting alcohol **2**. Treatment of the salt **3** with one equivalent of HBF_4 in dichloromethane afforded the diferrocenylcarbenium salt **4**, a green solid, in 90% yield. Complex **4** is highly persistent and thermally stable in the solid state and in dichloromethane, even when exposed to air. Direct conversion of alcohol **2** into **4** was achieved by addition of two equivalents of HBF_4 in dichloromethane at room temperature. However, when this treatment was carried out in acetonitrile, a complex mixture was obtained in which neither the N-protonated salt **3** nor the diferrocenylcarbenium salt **4** could be detected.

Further addition of one equivalent of HBF_4 to a solution of **4** in dichloromethane yielded the ferrocenylfulvene derivative **5** in 90% yield. This compound can also be prepared directly from **2**, in almost quantitative yield, by the action of an excess of dry hydrogen chloride. When this conversion was carried out in the presence of ammonium hexafluorophosphate, the reaction rate was increased. We have also found that compound **4** is slowly transformed into **5**, although in moderate yield, in acetonitrile at room temperature (Scheme 2).

In order to gain an insight of the stepwise protonation of **2**, spectrophotometric and electrochemical studies were performed. A solution of the compound **2** in dichloromethane was titrated with HBF_4 in dichloromethane and the absorption spectra were taken after each addition. The evolution of the UV-visible spectra is shown in the Supporting Information (Figure II). Upon addition of sub-stoichiometric quantities of HBF_4, the two characteristic charge-transfer absorption bands of ferrocenyl derivatives underwent a red-shift with an intensity increase, as predicted by the theoretical model III, developed by Marder et al.,[32] since both transitions involve charge transfer to the same empty acceptor-based orbital. As expected from its higher energy, the HE band ($\varepsilon = 10244\,M^{-1}cm^{-1}$) experienced a smaller red-shift (23 nm) than the LE band ($\varepsilon = 3549\,M^{-1}cm^{-1}$) (66 nm). These changes are observed until one equivalent of acid is added. After addition of the second equivalent of acid, the spectrum of the resulting diferrocenylcarbenium salt **4** is very different from its precursor. The resulting HE band and the first LE band are almost identical to those found in the neutral alcohol **2**. This addition also induces the appearance and development of a new broad band in the visible region at 641 nm ($\varepsilon = 3084\,M^{-1}cm^{-1}$). This explains the dark green colour of **4** and might be ascribed to a relevant transition to the iron-centred orbitals with the empty p orbital of the α-carbocationic centre.[35] The observation of some well-resolved isosbestic points during the protonation of **2** (at 320, 428 and 464 nm) and of **3** (at 245, 507, and 565 nm) indicates that there is no decomposition.

The electrochemical behaviour of compound **2** in the presence of variable concentrations of HBF_4·Et_2O was also investigated by CV in order to obtain further details about the protonation process. Thus, upon addition of sub-stoichiometric amounts of HBF_4 to a solution of **2** in dichloromethane, clear evolution of the second wave from $E_{1/2} = 0.740$ V to $E_{1/2} = 1.060$ V ($\Delta E_{1/2} = 320$ mV), and the appearance of a new irreversible reduction wave at $E_{1/2} = -0.560$ V, were observed (Figure 6). Maximum perturbation of the CV was obtained with two equivalents of added acid and, at this point, the second wave disappears. Interestingly, the new anodic wave has a typical diffusional shape, while, in contrast, a sharp cathodic stripping peak was observed. This indicates the precipitation of the oxidised protonated salt onto the electrode upon oxidation; on the reverse scan it redis-

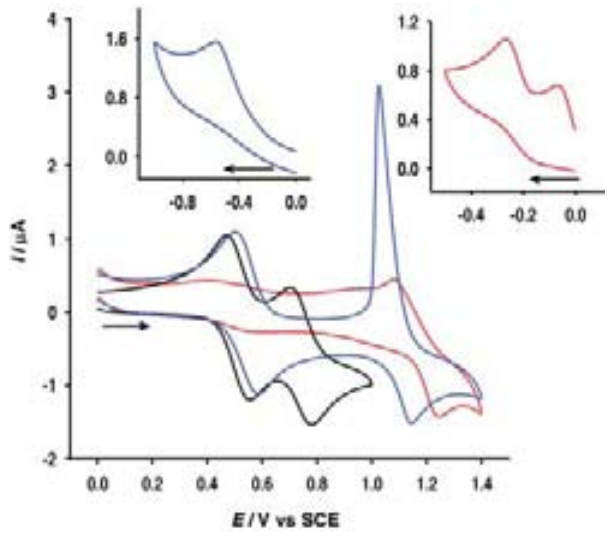

Figure 6. Voltammetric response of compound **2** (1 mM) in CH_2Cl_2 before (black) and after addition of 2 equivalents of HBF_4 (blue), and after addition of 4 equivalents of HBF_4 (red). Scan rate: 0.2 V s^{-1}. Upper inset reductive scan (0.2 V s^{-1}): left for **3** and right for **4**.

solves as it is reduced. If a small amount of acetonitrile is added to the dichloromethane electrolyte medium, the cathodic stripping peak disappears. The value of the redox potential shift on protonation ($\Delta E_{1/2} = 320$ mV) deviates by 64.6 mV from the theoretical value (255.4 mV) obtained from Plenio's relationship ($y = (-2.7 + 2.1x) \times 10^2$) between the inverse iron–nitrogen separation (x; 399.4 pm for **2**) and the shifts of the potential (y) found on protonation of several types of aza-substituted ferrocenes.[5] This deviation indicates that, apart from the electrostatic interaction between the complexed Mg^{+2} ion and the disubstituted ferrocene unit, an additional interaction between the ferrocene moieties should exist.

Further addition of two equivalents of acid produced dramatic changes in the CV. The first wave vanishes and a quasi-reversible wave at $E_{1/2} = 1.160$ V ($\Delta E_p = 140$ mV) appears. Remarkably, two well-defined irreversible reduction waves appear at -0.070 and -0.260 V versus SCE. These are attributed to the two-electron reduction of the carbenium centre. That this CV corresponds to the diferrocenylcarbenium salt **4** was confirmed by comparison with the CV of a pure sample of **4** recorded under the same conditions.

Spectroscopic characterisation of **4**: The structure of **4**, which is both a carbenium ion and a [5]ferrocenophane, has been elucidated from spectroscopic data. The high stability of carbenium ion **4** permits its accurate mass detection by high-resolution positive FAB-MS. The mass spectrum displayed an intense isotopic cluster, peaking at $m/z = 524$, assignable to the molecular ion. The relative abundance of the isotopic cluster was in good agreement with the simulated spectrum of $[M]^+$.

The room temperature 400 MHz ^{1}H NMR spectrum[36] of **4** was completely assigned (with the exception of the aromatic protons) by ^{1}H,^{1}H COSY, NOESY and spin-decoupled experiments. The diastereotopism of all the protons of the three substituted Cp rings is immediately apparent from the ^{1}H NMR spectrum of **4** (Table 1). The assignment of the protons corresponding to the different Cp rings present in the molecule, as well as the four diastereotopic protons present in the two methylene groups of this structure, were achieved by inspection of the ^{1}H,^{1}H COSY and two-dimensional NOESY spectra (Figure 3). In addition to full characterisation of these protons, some differences observed among the chemical shifts of the protons in the Cp_1, Cp_2 and Cp_3 rings are noted. In the Cp_3 ring a large deshielding for the β and β′ protons, with respect to that of the α and α′ protons, is observed ($\Delta\delta_{2'',3''} = 1.10$ and $\Delta\delta_{5'',4''} = 0.79$ ppm). This fits in with this cation having an important resonance contribution from a η^6-fulvene-η^5-cyclopentadienyliron(II) unit, with additional π-bonding of the metal with the exocyclic double bond. In this context it is also important to underline that the δ values for the β protons (H3″and H4″) are the largest observed for these type of protons in α-ferrocenylcarbenium ions.[37]

Direct metal participation in the stabilisation of the positive charge promotes significant bending of the exocyclic carbenium atom out of the Cp ring plane towards the central iron atom (Fe2). Consequently, the electronic density on the 2″- and 5″-positions have been found to be significantly increased, giving rise to a shielding of those protons with respect to H3″ and H4″, for which the opposite effect has been found.[38] These last two protons, H3″ and H4″, can be considered as fulvene-like protons. Interestingly, in the ^{1}H NMR spectrum of ferrocenylfulvene derivative **5**, the fulvene protons appear in the same region (6.4–6.7 ppm). On the other hand, the chemical shifts corresponding to the protons of the Cp_1 moiety clearly indicate that the iron atom in this ferrocene unit does not take part in stabilisation of the positive charge. The expected δ values for the β and β′ protons should thus be larger than those for the α and α′ protons.[34a] However, the observed situation is that the α and α′ protons are unshielded, with respect to the β and β′ protons ($\Delta\delta_{2,3} = -0.14$ and $\Delta\delta_{5,4} = -0.83$), following the typical pattern of a ferrocene unit linked to an electron-withdrawing group.[39]

Finally, the pattern observed for the δ values of the protons in the Cp_2 ring are in accordance with those observed in ferrocene rings monosubstitued with an electron withdrawing group: $\delta H2' > \delta H5' > \delta H3' > \delta H4'$ ($\Delta\delta_{5',4'} = -0.54$ and $\Delta\delta_{2',3'} = -0.35$). This parallels the observed pattern in the structurally related Cp_2 in alcohol **2**.

^{57}Fe Mössbauer spectroscopy has been employed to probe the iron environments in the prepared compounds (Table 4). At 77 K the neutral alcohol **2** shows one quadrupole split doublet of narrow linewidth with an isomer shift (IS) and quadrupole splitting (QS) in the normal range for ferrocenes.[40] There is no differentiation of the iron atoms, as shown by Mössbauer. The N-protonated salt **3** exhibits two nested quadrupole split doublets of equal relative intensity. The smallest of the QS values is lower than that for the parent alcohol **2**. This is expected as protonation increases the electron-withdrawing character of the C=N double bond and now favours backbonding from the ε_2 ($d_{x^2-y^2}$, d_{xy}) iron-

Table 4. ^{57}Fe Mössbauer parameters.

Compound	T [K]	IS	QS	HWHM[a]
2	77	0.52	2.33	0.13
3	77	0.50	2.41	0.13
		0.50	2.09	0.15
4	77	0.50	2.51	0.13
		0.51	2.11	0.14
	300	0.43	2.50	0.11
		0.44	2.14	0.13
6	77	0.51	2.22	0.17
	300	0.44	2.20	0.14

HWHM = half width at half maximum.

based orbitals to the ring, with a consequent decrease in QS values.[41]

The diferrocenylcarbenium **4** exhibits, at both 77 K and 300 K, two overlapping quadrupole split doublets of equal relative intensity. The i.s. moves with temperature as expected and the q.s. values are independent of temperature. The i.s. is also typical of ferrocene derivatives.[43] The smaller of the q.s. values of **4** is similar to that reported for diferrocenylmethylium tetrafluoroborate (2.10 mm s^{-1} at 298 K)[42] and is lower than that for the parent alcohol **2**. The other doublet of **4** has a QS that is higher than that of **2** and is similar to those found for a series of α-ferrocenylcarbenium ions.[43] It has been postulated that high QS values (greater than that of ferrocene itself) in α-ferrocenylcarbenium systems are due mainly to the interactions between the empty p orbital on C_{exo} with several occupied metal orbitals, probably most efficiently with one lobe of the $d_{x^2-y^2}$, the central belt of d_{z^2}, or one lobe of d_{zx}. Such an interaction would disrupt the normal binding of the ferrocene system,[44] giving rise to a ring tilt angle on the ferrocene moiety and causing the d_{z^2} to take part in the bonding.[45] As a consequence, this would promote bending towards the iron centre. Values of about 2.6–2.7 mm s^{-1} represent maximal iron participation for such systems, whereas lower QS values are due to electron withdrawal through ring-based orbitals ε_1.[43]

The reported parameters are consistent with the two iron atoms having different partial charges. However, **4** can not be described as mixed-valence as, in this case, a larger difference between QS values would be expected (e.g., in mixed-valence biferrocenium derivatives, the difference between the QS values of Fe^{II} and Fe^{III} is more than 0.66 mm s^{-1}).[46]

The useful combination of ^{1}H NMR and ^{57}Fe Mössbauer spectroscopic data of the diferrocenylcarbenium ion **4** strongly suggests two different processes for stabilisation of the α-carbocationic centre. The monosubstituted ferrocene group can clearly be considered as η^6-fulvene-η^5-cyclopentadienyliron(II) (deshielding for β protons with respect to α protons) with iron participation (high QS value), whereas the disubstituted ferrocene group is acting only through cyclopentadienyl-based orbitals (deshielding for α protons with respect to β protons) without iron participation (low QS value). That the nature of diferrocenylcarbenium ion **4** as a pentafulvene complex is more than just formal is demonstrated by its easy conversion to **5**, either spontaneously or under acidic conditions. Compound **4** represents an attractive example in which two ferrocene groups linked to an α-carbocationic centre show different spectroscopic (both ^{1}H NMR and ^{57}Fe Mössbauer) characteristics.

Mixed-valence compound 6

Synthesis: Mixed-valence compound **6** was isolated in 60% yield, as a stable purple solid, by controlled oxidation of **2** with silver trifluoromethanesulfonate. When **6** was treated with an excess of 4-dimethylaminopyridine in toluene at room temperature, the alcohol **2** was obtained, in 70% yield, after chromatographic separation on a deactivated silica gel column (Scheme 3).

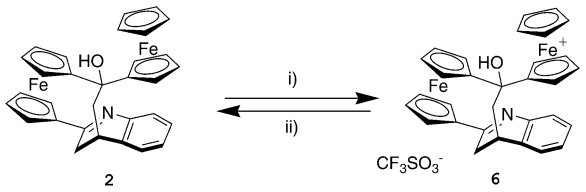

Scheme 3. Reagents and conditions: i) $AgCF_3SO_3$, toluene, RT, 1.5 h, 60%; ii) a) DMAP (excess); b) deactivated silica gel (10% ET_3N in *n*-hexane), 70%.

Physicochemical properties: A chronoamperometric study (see Figure IV in the Supporting Information) revealed the nature and purity of compound **6**. Plotting the sample current, at a fixed time of 800 ms versus the potential gave a sampled-current voltammogram, which displays two waves in the anodic and cathodic region, respectively, with the same wave height (Fe^{III}/Fe^{II} ratio 1:1). In contrast, the recorded sampled-current voltammogram for the neutral precursor **2** displayed two waves in the anodic region.

The CV of **6** in acetonitrile does not correspond to the expected one, that is, one with two reversible one-electron redox waves at +0.450 V and +0.670 V; however, it is almost identical to that obtained by complexation with $Mg(ClO_4)_2$. At the same time the CV of **6** is also very similar to the spectrum obtained by protonation of the neutral precursor **2** with one equivalent of acid, in that it displays an irreversible reduction wave at −0.450 V and two one-electron oxidation waves at +0.470 V and +1.010 V (See Figure V in the supporting information), respectively. These electrochemical results strongly suggest that, in acetonitrile, the asymmetric mixed-valence complex $\mathbf{2}^+$ exhibits an intramolecular complexation of the Fe^{III} atom by the nitrogen atom of the C=N double bond (Scheme 4). Support for this intra-

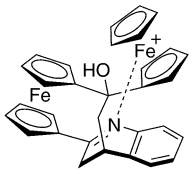

Scheme 4. Schematic representation of the intramolecular interaction in the mixed-valence complex $\mathbf{2}^+$.

molecular interaction is provided by the appearance of an absorption band at 520 nm (see Table 3) that resembles the HE band shown by $\mathbf{2}\cdot\mathbf{Mg}^{2+}$.

The mixed-valence compound **6** exhibits, both at 77 K and 300 K, a quadrupole split doublet with a QS of about 2.2 mm s^{-1}. The IS values move, as expected, with temperature and the QS values are independent of temperature. The observed quadrupole split doublet, even at 77 K, is associated with a mixed-valence state in which the intramolecular electron-transfer rate is greater than the Mössbauer timescale (10^7 s^{-1}) (Table 4). In **6** the QS is larger than those observed for other valence-delocalised biferrocenium cations. In general, ferrocenyl groups (electronic ground state $^1A_{1g}$) give spectra characterised by a large QS in the range 2.0–2.2 mm s^{-1}, while the spectra of ferrocenium cations (electronic ground state $^2E_{2g}$) are characterised by a small or vanishing QS. In localised mixed-valence biferrocenium cations, the value of the QS in the ferrocenyl moiety is slightly smaller than that expected for an Fe^{II} ferrocenyl unit and the Fe^{III} ferrocenium moiety has a slightly larger QS value. For asymmetric biferrocenophane mixed-valence compounds Mössbauer studies clearly indicate that the electronic ground state of the Fe^{III} unit is not pure $^2E_{2g}$ and larger QS values are observed. In these compounds, the Cp rings are tilted from the parallel geometry of ferrocenium. Bending back the Cp rings leads to an increase of $d_{x^2-y^2}$,d_{xy}-ring overlap and the metal nonbonding orbitals start to interact with the ligand π orbitals. Under these circumstances the iron ion loses some of its Fe^{III} character and there is consequently an increase in the QS value. In addition, an intramolecular interaction between the Fe^{III} atom and the nitrogen atom of the ferrocenophane framework (as evidenced by CV) also contributes to this increased QS.

IR spectroscopy has often been used to evaluate the rate of electron-transfer in mixed-valence compounds in the solid state when a suitable vibrator is available on one of the metallic termini. In these cases, when the electron-transfer is faster than the timescale (10^{13} s^{-1}), an averaging of this specific vibrational mode is observed for the mixed-valence compound **6** relative to the neutral compound **2** and the dioxidised $\mathbf{2}^{2+}$ species. A spectrum corresponding to the overlap of both spectra is obtained in the opposite case; that is, when a slow electron-transfer process takes place.[7,47]

Previous work on mixed-valence biferrocenes indicates that the perpendicular C–H bending band is the best indicator of the iron oxidation state. This band is seen at 815 cm^{-1} for neutral ferrocene and at 850 cm^{-1} for ferrocenium salts. A localised mixed-valence biferrocenium cation should exhibit one C–H bending band for the Fe^{II} ferrocenyl moiety and another one for the Fe^{III} ferrocenium moiety,[46d,48] while only one averaged band is expected for delocalised mixed-valence species. In our case, the IR spectrum of the neutral form **2** displays a C–H bending vibration band at 818 cm^{-1}, while in the diferrocenylcarbenium salt **4** this band appears at 843 cm^{-1}.

The IR spectra of the N-protonated salt **3** and the mixed-valence compound **6** only show one C–H bending vibration at 835 cm^{-1}. These findings are in agreement with the electrochemical results that indicate a partial positive polarisation of the C=N double bond induced by a through-space interaction with the Fe^{III} atom. They also point towards a fast electron-transfer process, in the solid state, for **6**.

The generation of the mixed-valence species from **2** was also performed electrochemically and monitored by UV-visible/near-IR spectroscopy. A stepwise Coulometric titration was performed on a solution of **2** in CH_2Cl_2 (3.5×10^{-3} mol L^{-1}), with $[N\mathit{n}Bu_4]PF_6$ (0.1 M) as supporting electrolyte. UV-visible/near-IR absorption spectra were regularly recorded by transferring a small aliquot of the solution contained in the electrochemical cell, for different average number of electrons (n) removed ($0\le n\le 2$), into a UV quartz cell . The UV-visible/near-IR data are collected in Table 3. Figure 7 shows the evolution of these spectra. The increase in the characteristics bands of ferrocenium ions at 520 and 630 nm is clearly observed, with a remarkable increase of the ε value for the 520 nm band when the second ferrocenium ion is formed, on transfer of more than one electron per mol.

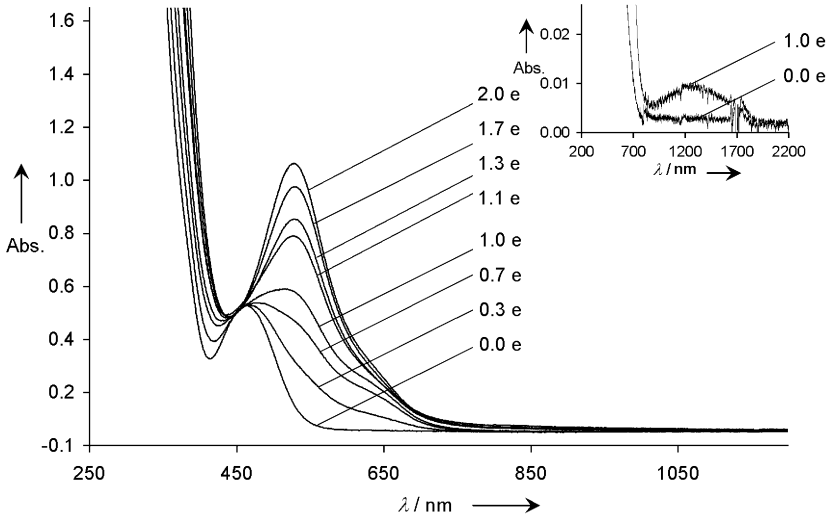

Figure 7. Evolution of the UV-Visible spectrum during the course of the oxidation of compound **2**. The average number of removed electrons is given on each spectrum. Inset: maximum of the intervalence charge-transfer band.

Interestingly, during the oxidation process of compound **2**, a new weak and broad band, centred at 1240 nm, appears. This band increases continuously until complete formation of $\mathbf{2}^{+}$ (see inset of Figure 7). The intensity of this band sub-

sequently decreases until it disappears when the dication $\mathbf{2}^{2+}$ is completely formed. This behaviour is typical of an intervalence charge-transfer (IVCT) band due to the presence of an intramolecular electron-transfer process in a class II mixed-valence compound.[7] From the characteristics of the IVCT band, the effective electronic coupling V_{ab} (in cm^{-1}) between both ferrocene redox centres can be determined, by using Equation (1) developed by Hush.[49]

$$V_{ab} = [2.05 \times 10^{-2} \sqrt{\varepsilon_{max} \nu_{max} \Delta\nu_{1/2}}] R^{-1} \quad (1)$$

In this equation $\Delta\nu_{1/2}$ (in cm^{-1}) is the half-height band width of the IVCT band, R (in Å) is the distance between the redox centres (in this case the intermetallic distance, as determined by the X-ray structure, has been used), ε_{max} (in $M^{-1}cm^{-1}$) is the maximum molar extinction coefficient, and ν_{max} (in cm^{-1}) is the wavenumber at the maximal absorbance. Equation (1) gives an effective electronic coupling (V_{ab}) for $\mathbf{2}^{+}$ of 90 cm^{-1} (0.0112 eV), which represents a weak coupling between the two ferrocene units, since it is only half the value observed in a diferrocene system linked by a long chain of six ethylene bonds.[50]

Unfortunately, the strong resemblance between the absorption spectra of $\mathbf{2{\cdot}Mg}^{2+}$ and the mixed-valence species $\mathbf{2}^{+}$ has prevented a detailed study of the electrochemically induced switchable chemosensor properties of **2**.

Conclusion

Diferrocene derivative **2**, which incorporates an aza-substituted bridge and has a ferrocenophane architecture with a ferrocenyl susbtituent, functions as a highly selective chemosensor for Mg^{2+} ions, while not showing any response to Ca^{2+} or alkaline ions. The response of **2** to Mg^{2+} can be detected either by electrochemical or optical techniques, even in the presence of other metal ions. The presence of two redox moieties in compound **2** allows formation of the mixed-valence compound, which, interestingly, shows moderate electronic coupling between both ferrocene units. It is therefore a new class II mixed-valence system in which intramolecular electron transfer has been studied by different spectroscopic techniques.

The reported properties of this new multifunctional ion-sensing derivative demonstrate that, with proper design, more efficient switchable chemosensors could be developed in the future.

Experimental Section

General methods: All reactions were carried out under N_2 and with solvents that were dried by routine procedures. All melting points were determined on a Kofler hot-plate melting point apparatus and are uncorrected. IR spectra were determined as Nujol emulsions or films on a Nicolet Impact 400 spectrophotometer. ^1H and ^{13}C NMR spectra were recorded on a Bruker AC200, 300 or 400 MHz instrument, and chemical shifts are referenced to signals of tetramethylsilane. Mössbauer spectra, obtained on an ES-Technology MS-105 spectrometer with a 100 MBq ^{57}Co source in a rhodium matrix at ambient temperature, were referenced to natural iron at 298 K. Solid samples were prepared by grinding with boron nitride. Parameters were obtained by fitting the data with Lorentzian lines, errors $< \pm 0.01$ mm s^{-1}. The EI and FAB^+ mass spectra were recorded on a Fisons AUTOSPEC 500 VG spectrometer, with 3-nitrobenzyl alcohol as a matrix. Microanalyses were performed on a Perkin–Elmer 240C instrument. Electrochemical measurements were taken with a QUICELTRON potentiostat/galvanostat controlled by a personal computer and driven by dedicated software. Electrochemical experiments were conducted in a conventional three-electrode cell, under a nitrogen atmosphere, at 25 °C. The working electrode was a Pt disk (1 mm in diameter), polished before each recording. The auxiliary electrode was a platinum wire. The reference electrode was SCE. All potentials are quoted with respect to SCE, except where noted. The experiments were in acetonitrile or dichloromethane solutions containing 0.1 M $[NnBu_4]ClO_4$ (**WARNING**:**CAUTION**) as supporting electrolyte. Under these experimental conditions, the ferrocenium/ferrocene couple was observed at +0.405 V versus SCE in acetonitrile and at +0.535 V versus SCE in dichloromethane. Deoxygenation of the solutions was achieved by bubbling with nitrogen for at least 10 minutes. Cyclic voltammetry (CV) curves were recorded at scan rates of 0.050–1 V s^{-1} and the scan potential was obtained in both positive and negative directions. The differential pulse voltammtery (DPV) curves were recorded at a 4 mV s^{-1} scan rate with a pulse height of 10 mV and a step time of 50 ms.

1,1′-[(3,4-Dihydro-2,4-quinolinediyl)(2-ferrocenyl-2-hydroxy-1,2-ethanediyl)]ferrocene (2): A solution of ferrocenyllithium, preparared by reaction of ferrocene (0.5 g, 2.68 mmol) and *t*BuLi (1.33 mL of a 1.7 M pentane solution, 2.26 mmol) in dry THF (5 mL) at 0 °C for 1 h, was added dropwise to a solution of **1** (0.2 g, 0.56 mmol) in THF (10 mL). The solution was stirred at room temperature for 10 min, then H_2O (20 mL) was added. The reaction mixture was extracted with CH_2Cl_2 (3 × 50 mL). The combined organic layers were washed with a saturated solution of NaCl (3 × 50 mL), then dried over anhydrous Na_2SO_4 and evaporated under reduced pressure. The crude product was purified by chromatography on a previously deactivated silica gel column, with 1:1 EtOAc/*n*-hexane as eluent, to give **2** in 80 % yield as an orange solid. This was crystallised from CH_2Cl_2/*n*-hexane (1:3). M.p. 290–293 °C (decomp); elemental analysis calcd (%) for $C_{31}H_{27}Fe_2NO$ (541.3): C 68.79, H 5.03, N 2.59; found: C 68.55, H 4.88, N 2.70.

3,4-Dihydroquinolium salt 3: A stirred solution of the alcohol **2** (73 mg, 0.14 mmol), in dry CH_2Cl_2 (10 mL), was treated dropwise with 1 equiv of the appropriate acid (HBF_4 or CF_3SO_3H) (e.g., 1.4 mL of a 0.1 M solution of HBF_4 in CH_2Cl_2), during which the orange colour of the solution changed to a deep purple. The resulting mixture was stirred for 5 min at room temperature, then the solvent was removed under vacuum to give a deep purple residue which was triturated with diethyl ether (10 mL). The purple solid that formed was isolated in almost quantitative yield and recrystallised by slow diffusion of Et_2O into a dilute solution of the compound in CH_2Cl_2. **3a** (X = BF_4): M.p. 222–225 °C (decomp); **3b** (X = CF_3SO_3): M.p. 215–220 °C (decomp).

Diferrocenylcarbenium 4: A stirred solution of the alcohol **2** (73 mg, 0.14 mmol) in dry CH_2Cl_2 (10 mL) was treated dropwise with 2 equiv of HBF_4 (2 × 1.4 mL of a 0.1 M solution of HBF_4 in CH_2Cl_2). During the addition, the orange colour of the solution evolved to a deep purple colour and finally to the green colour of the carbenium species. After the addition, the solution was stirred for 5 min, then the solvent was removed in vacuo. The crude product was treated with acetone/CH_2Cl_2 (1:3) and the resulting powder was washed with CH_2Cl_2 (4 × 2 mL) to give a deep green product, in 90 % yield. This was crystallised by slow diffusion of CH_2Cl_2 into a dilute solution of the compound in acetone. M.p. > 300 °C; FAB^+-HRMS: calcd for $C_{31}H_{26}NFe_2$: 524.0760; found: *m*/*z* (%): 522.0809 (15), 524.0765 (100), 525.0801 (79).

1,1′-[(3,4-Dihydro-2,4-quinolinediyl)(2-cyclopentadienylidene-1,2-ethanediyl)]ferrocene (5):

Method A: A 0.1 M solution of $[NBu_4]PF_6$ in dry CH_2Cl_2 (10 mL) was treated with a solution of **2** (0.2 g, 0.37 mmol) in dry CH_2Cl_2 (5 mL), and the reaction mixture was stirred for 5 min at room temperature. A stream of dry HCl was bubbled through the mixture for 1 h, during which a clear evolution of the colour of the solution, from orange to purple to green to purple, was observed. When the deep purple colour was persistent, the reaction mixture was filtered through a deactivated

(10% Et_3N in *n*-hexane) silica gel layer. The filtrate was evaporated to dryness and purified by chromatography on a deactivated silica gel column, using EtOAc/*n*-hexane (9:1) as eluent, to give **5**, in almost quantitative yield, as a red solid. This was crystallised by slow diffusion of *n*-hexane into a diluted solution of the compound in CH_2Cl_2.

Method B: A solution of the diferrocenylcarbenium **4** (0.1 g, 0.16 mmol) in CH_2Cl_2 (10 mL) was treated with HBF_4 (1 equiv., 1.1 mL of a 0.1 M solution of HBF_4 in CH_2Cl_2) and the mixture was stirred at room temperature and under nitrogen for 30 min, during which the deep green colour of the solution changed to deep purple. A crystalline sample in 90% yield was obtained following the same procedure as described above.

Method C: A solution of the diferrocenylcarbenium **4** (0.1 g, 0.16 mmol) in CH_3CN (10 mL) was stirred at room temperature for 10 min to give a black precipitate, which was filtered off. The filtrate was evaporated to dryness and the product was isolated, as described above, in 90% yield. M.p. 167–170°C; elemental analysis calcd (%) for $C_{26}H_{21}FeN$ (403.3): C 77.43, H 5.25, N, 3.47; found: C 77.14, H 5.30, N 3.27.

Mixed-valence compound 6: A sample of this mixed-valence compound was prepared by adding a solution of $AgCF_3SO_3$ (0.024 g, 0.094 mmol) in dry toluene (10 mL) to a solution of the alcohol **2** (0.051 g, 0.094 mmol) in the same solvent (50 mL). The reaction mixture was stirred at room temperature and under nitrogen for 1.5 h. The dark brown microcrystals formed were collected by filtration and washed with three portions of toluene (3×10 mL). The solid was dissolved in $CHCl_3$ (25 mL) and stirred at room temperature and under nitrogen for 10 min to give a deep purple solution and a dark precipitate. The solution was filtered under nitrogen and the precipitate was washed with $CHCl_3$ (3×10 mL). The combined organic layers were evaporated to dryness under reduced pressure. The resulting residue was triturated with dry Et_2O to give **9** as a deep purple solid in 60% yield. This was crystallised from CH_2Cl_2/toluene (1:1). M.p: 227–230°C (decomp); IR (CH_2Cl_2): $\tilde{\nu}$=3468, 1642, 1618, 1574, 1287, 1263, 1169, 1038, 835, 758 cm^{-1}; MS (FAB$^+$): *m*/*z* (%): 691 (5) [M^++1], 542 (100) [M^++1−CF_3SO_3]; elemental analysis calcd (%) for $C_{32}H_{28}F_3Fe_2NO_4S$ (691.3): C 55.60, H 4.08, N2.03; found: C 55.42, H 4.28, N 1.95.

X-ray crystal structure analysis:

Data collection: A Nonius Kappa CCD with an area detector was used. 19153 reflections were measured by means of ϕ- and ω-scans and extracted from the frames (DENZO-SMN).

Structure solution and refinement: Non-hydrogen atoms were refined anisotropically on F^2 (SHELXL 97), hydrogen atoms of the carbon atoms were refined at calculated positions, the hydrogen atom of the hydroxyl group was refined with an isotropic displacement parameter; *R* values for 320 parameters and 2402 observed reflections [$I>2\sigma(I)$]: R_1=0.0418 and wR_2=0.0977.

Crystal data: $C_{31}H_{27}Fe_2NO$, monoclinic, space group $P2_1/n$, a=11.3545(4), b=10.8175(6), c=18.725(1) Å, β=92.667(3)°, V=2297.45(19) Å^3, Z=4, T=233(2) K, $\lambda(Mo_{K\alpha})$=0.71073 Å, $F(000)$=1120, μ=1.289 mm^{-1}, ρ_{calcd}=1.565 gcm^{-3}, yellow prism 0.4×0.1×0.05 mm. CCDC-215840 contains the supplementary crystallographic data for this paper. These data can be obtained free of charge via www.ccdc.cam.ac.uk/conts/retrieving.html (or from the Cambridge Crystallographic Data Centre, 12 Union Road, Cambridge CB2 1EZ, UK; fax: (+44) 1223–336–033; or e-mail: deposit@ccdc.cam.uk).

Acknowledgement

We gratefully acknowledge the financial support of the DGI (Ministerio de Ciencia y Tecnología, Spain) (Projects. BQU2001-0014 and MAT2000-1388-C03-01), Fundación Séneca (CARM) (Project. No. PB/72/FS/02) and DGR Catalunya (Project 2001 SGR00362). We also wish to thank Prof. P. Deyá, Dr. A. Frontera and C.Garau (UIB) for computational facilities and helpful suggestions. The Biotechnology and Biological Sciences Research Council (UK) are thanked for funding (D.J.E.). J.L.L. and V.L., who is enrolled in the Ph.D. programme of the UAB (Universitat Autónoma de Barcelona), thank the MCyT (Spain) for their studentships.

[1] *Ferrocenes, Homogeneous Catalysis, Organic Synthesis, Material Science* (Eds.: A. Togni, T. Hayashi), VCH, Weinheim **1995**.

[2] a) G. W. Gokel, *Chem. Soc. Rev.* **1992**, *21*, 39–46; b) P. D. Beer, *Adv. Inorg. Chem.* **1992**, *39*, 79–157; c) P. L. Boulas, M. Gomez-Kaifer, L. Echegoyen, *Angew. Chem.* **1998**, *110*, 226–258; *Angew. Chem. Int. Ed.* **1998**, *37*, 216–247; d) P. D. Beer, P. A. Gale, G. Z. Chen, *Coord. Chem. Rev.* **1999**, *185/186*, 3–36; e) P. D. Beer, P. A. Gale, *Adv. Phys. Org. Chem.* **1998**, *31*, 1–90; d) P. D. Beer, P. A. Gale, *Angew. Chem.* **2001**, *113*, 502–532; *Angew. Chem. Int. Ed.* **2001**, *40*, 486–516.

[3] a) J. C. Medina, T. T. Goodnow, M. T. Rojas, J. L. Atwood, B. C. Lynn, A. E. Kaifer, G. W. Gokel, *J. Am. Chem. Soc.* **1992**, *114*, 10583–10595; b) P. D. Beer, Z. Cheng, M. G. B. Drew, J. Kingston, M. Ogden, P. Spencer, *J. Chem. Soc. Chem. Commun.* **1993**, 1046–1048; c) H. Plenio, H. El-Desoky, J. Heinze, *Chem. Ber.* **1993**, *126*, 2403–2408; d) M. J. L. Tendero, A. Benito, R. Martínez-Mañez, J. Soto, J. Payá, A. J. Edward, P. R. Raithby, *J. Chem. Soc. Dalton Trans.* **1996**, 343–352; e) H. Plenio, C. Aberle, *Organometallics* **1997**, *16*, 5950–5957; f) H. Plenio, C. Aberle, *Angew. Chem.* **1998**, *110*, 1467–1470; *Angew. Chem. Int. Ed.* **1998**, *37*, 1397–1399; g) M. E. Padilla-Tosta, R. Martínez-Mañez, T. Pardo, J. Soto, M. J. L. Tendero, *Chem. Commun.* **1997**, 887–888; h) H. Plenio, C. Aberle, Y. Al-Shihaded, J. M. Lloris, R. Martínez-Mañez, T. Pardo, J. Soto, *Chem. Eur. J.* **2001**, *7*, 2848–2861.

[4] P. D. Beer, P. A. Gale, G. Z. Chen, *J. Chem. Soc. Dalton Trans.* **1999**, 1897–1909.

[5] H. Plenio, J. Yang, R. Diodone, J. Heinze, *Inorg. Chem.* **1994**, *33*, 4098–4104.

[6] S. R. Miller, D. A. Gustowski, Z. H. Chen, G. W. Gokel, L. Echegoyen, A. E. Kaifer, *Anal. Chem.* **1988**, *60*, 2021–2024.

[7] M. Robin, P. Day, *Adv. Inorg. Chem. Radiochem.* **1967**, *10*, 247–422.

[8] a) D. Astruc, *Electron Transfer and Radical Processes in Transition-Metal Chemistry*, VCH, New York, **1995**; b) "Electron Transfer in Inorganic, Organic and Biological Systems": *Adv. Chem. Ser.* **1991**, *228*, whole volume.

[9] For reviews see: a) S. Barlow, D. O'Hare, *Chem. Rev.* **1997**, *97*, 637–669; b) D. Astruc, *Acc. Chem. Res.* **1997**, *30*, 383–391; c) J. P. Launay, *Chem. Soc. Rev.* **2001**, *30*, 386–397; d) P. Nguyen, P. Gomez-Elipe, I. Manners, *Chem. Rev.* **1999**, *99*, 1515–1548; e) W. Kaim, A. Klein, M. Glöckle, *Acc. Chem. Res.* **2000**, *33*, 755–763; f) K. D. Demadis, C. M. Hartshorn, T. J. Meyer, *Chem. Rev.* **2001**, *101*, 2655–2685.

[10] a) R. J. Crutchley, *Prog. Inorg. Chem.* **1994**, *41*, 273–325; b) C. Creutz, *Prog. Inorg. Chem.* **1983**, *30*, 1–71.

[11] a) D. E. Richardson, H. Taube, *Coord. Chem. Rev.* **1984**, *60*, 107–129; b) D. E. Richardson, H. Taube, *Inorg. Chem.* **1981**, *20*, 1278–1285; c) J. E. Sutton, H. Taube, *Inorg. Chem.* **1981**, *20*, 3125–3134; d) R. de la Rosa, P. J. Chang, F. Salaymeh, J. C. Curtis, *Inorg. Chem.* **1985**, *24*, 4229–4231; e) Y. Dong, J. T. Hupp, *Inorg. Chem.* **1992**, *31*, 3170–3172.

[12] a) W. H. Morrison, Jr., D. N. Hendrickson, *Inorg. Chem.* **1975**, *14*, 2331–2346; b) R. J. Webb, P. M. Hagen, R. J. Wittebort, M. Sorai, *Inorg. Chem.* **1992**, *31*, 1791–1801; c) S. Rittinger, D. Buchholz, M. H. Delville-Desbois, J. Linares, F. Varret, R. Boese, L. Zsolnai, G. Huttner, D. Astruc, *Organometallics*, **1992**, *11*, 1454–1456; d) P. Hudeczeck, F. H. Köhler, *Organometallics* **1992**, *11*, 1773–1775; e) T.-Y. Dong, T.-Y. Lee, S.-H. Lee, G.-H. Lee, S.-M. Peng, *Organometallics* **1994**, *13*, 2337–2348; f) T.-Y. Dong, C.-H. Huang, C.-K. Chang, H.-C. Hsieh, S.-M. Peng, G.-H. Lee, *Organometallics* **1995**, *14*, 1776–1785; g) S. Barlow, V. J. Murphy, J. S. O. Evans, D. O'Hare, *Organometallics* **1995**, *14*, 3461–3474; h) T.-Y. Dong, C.-K. Chang, S.-H. Lee, L.-L. Lai, M. Y.-N. Chiang, K.-J. Lin, *Organometallics* **1997**, *16*, 5816–5825; i) H. Hilbig, P. Hudeczek, F. H. Köhler, X. Xie, P. Bergerat, O. Kahn, *Inorg. Chem.* **1998**, *37*, 4246–4257; j) R. W. Meo, F. B. Somoza, T. R. Lee, *J. Am. Chem. Soc.* **1998**, *120*, 1621–1622; k) O. M. Heilg, M. A. Herker, W. Hiller, F. H. Köhler, A. Schell, *J. Organomet. Chem.* **1999**, *574*, 94–98.

[13] a) K. R. J. Thomas, J. T. Lin, Y. S. Wen, *J. Organomet. Chem.* **1999**, *575*, 301–309; b) K. R. J. Thomas, J. T. Lin, K.-J. Lin, *Organometallics* **1999**, *18*, 5285–5291; c) K. R. J. Thomas, J. T. Lin, Y. S. Wen, *Organometallics* **2000**, *19*, 1008–1012; d) A. Tárraga, P. Molina, D. Curiel, M. D. Velasco, *Organometallics* **2001**, *20*, 2145–2152.

[14] a) A. Ohkubo, T. Fujita, S. Ohba, K. Aramaki, H. Nishihara, *J. Chem. Soc. Chem. Commun.* **1992**, 1553–1555; b) Y. Yamada, J. Mizutani, M. Kurihara, H. Nishihara, *J. Organomet. Chem.* **2001**, *637–639*, 80–83.
[15] L. M. Tolbert, X. Zao, Y. Ding, L. A. Bottomley, *J. Am. Chem. Soc.* **1995**, *117*, 12891–12892.
[16] a) G. Ferguson, C. Glidewell, G. Opromolla, C. M. Zakaria, P. Zanello, *J. Organomet. Chem.* **1996**, *506*, 129–137; b) G. Ferguson, C. Glidewell, G. Opromolla, C. M. Zakaria, P. Zanello, *J. Organomet. Chem.* **1996**, *517*, 183–190.
[17] a) A. Tárraga, P. Molina, J. L. López, *Tetrahedron Lett.* **2000**, *41*, 2479–2482; b) A. Tárraga, P. Molina, J. L. López, M. D. Velasco, D. Bautista, P. G. Jones, *Organometallics* **2002**, *21*, 2055–2065.
[18] See reference [12g].
[19] a) T. J. Curphey, J. O. Santer, M. Rosenblum, J. H. Richards, *J. Am. Chem. Soc.* **1960**, *82*, 5249–5250; b) T. E. Bitterwolf, A. C. Ling, *J. Organomet. Chem.* **1972**, *40*, 197–203.
[20] a) A. F. Cunningham, Jr., *J. Am. Chem. Soc.* **1991**, *113*, 4864–4870; b) A. F. Cunningham, Jr., *Organometallics* **1994**, *13*, 2480–2485; c) A. F. Cunningham, Jr., *Organometallics* **1997**, *16*, 1114–1122; d) M. J. Mayor-López, J. Weber, B. Mannfors, A. F. Cunningham, Jr., *Organometallics* **1998**, *17*, 4983–4991; e) A. Irigoras, J. M. Mercero, I. Silanes, J. M. Ugalde, *J. Am. Chem. Soc.* **2001**, *123*, 5040–5043.
[21] The process observed was reversible, according to the following criteria: 1) separation of 60 mV between cathodic and anodic peaks, 2) close-to-unity ratio of the intensities of the cathodic and anodic currents and 3) constancy of the peak potential on changing the sweep rate in the CV. The same halfwave potential values have been obtained from the DPV peaks and from an average of the cathodic and anodic cyclic voltammetric peak.
[22] F. A. Cotton, J. P. Donahue, C. Lin, C. A. Murillo, *Inorg. Chem.* **2001**, *40*, 1234–1244.
[23] Experiments used the ligand **2** (1 mM) in CH_3CN/CH_2Cl_2 (3:2) in the presence of $[NnBu_4]ClO_4$ (0.1 M) and decamethylferrocene (1 mM), used as an internal standard. The potential of the $DCMFc^+$/DCMFc redox couple is −0.05 V versus SCE under our experimental conditions and the halfwave redox potentials were referred to this. Sequential addition of aliquots of 0.1 equivalents of 10^{-2} M solutions of the appropriate salt in CH_3CN were monitored by CV.
[24] P. Bühlmann, E. Pretsch, E. Bakker, *Chem. Rev.* **1998**, *98*, 1593–1687.
[25] P. D. Beer, K. Y. Wild, *Polyhedron* **1996**, *15*, 775–780.
[26] a) A. Chesney, M. R. Bryce, A. S. Batsanov, J. A. K. Howard, L. M. Goldenberg, *Chem. Commun.* **1998**, 677–678; b) O. B. Sutcliffe, A. Chesney, M. R. Bryce, *J. Organomet. Chem.* **2001**, *637–639*, 134–138.
[27] O. B. Sutcliffe, M. R. Bryce, A. S. Batsanov, *J. Organomet. Chem.* **2002**, *656*, 211–216.
[28] U. Siemeling, B. Neumann, H.-G. Stammler, A. Salmon, *Z. Anorg. Allg. Chem.* **2002**, *628*, 2315–2320.
[29] J. D. Carr, S. J. Coles, W. W. Asan, M. B. Hursthouse, K. M. A. Malik, J. H. R. Tucker, *J. Chem. Soc. Dalton Trans.* **1999**, 57–62, and references therein.
[30] T. Farrel, T. Meyer-Friedrichsen, M. Malessa, D. Haase, W. Saak, I. Asselberghs, K. Wostyn, K. Clays, A. Persoons, J. Heck, A. R. Manning, *J. Chem. Soc. Dalton Trans.* **2001**, 29–36, and references therein.
[31] S. Barlow, H. E. Bunting, C. Ringham, J. C. Green, G. U. Bublitz, S. G. Boxer, J. W. Perry, S. R. Marder, *J. Am. Chem. Soc.* **1999**, *121*, 3715–3723.
[32] Y. S. Sohn, D. N. Hendrickson, M. B. Gray, *J. Am. Chem. Soc.* **1971**, *93*, 3603–3612.
[33] The titration experiment was conducted by adding increasing amounts of a 2×10^{-2} M solution of anhydrous $Mg(ClO_4)_2$ in dry acetonitrile to a solution of **2** in dry dichloromethane at a constant concentration of the receptor. The value of the association constant is the average of three independent titrations.
[34] We note here that the different techniques used to monitor the metal binding do not always suggest the same stoichiometry. This is a known phenomenon in related systems and arises from the different concentrations and timescales employed in the different techniques. See: a) P. D. Beer, H. Sikanyika, C. Blackburn, J. F. McAleer, *J. Organomet. Chem.* **1988**, *350*, C15–C19; b) P. D. Beer, A. D. Keefe, H. Sikayika, C. Blackburn, J. F. McAleer, *J. Chem. Soc. Dalton Trans.* **1990**, 3289–3294.
[35] M. Ausorge, K. Polborn, T. J. Müller, *Eur. J. Inorg. Chem.* **2000**, 2003–2009.
[36] Due to poor solubility, ^{13}C NMR data for compound **4** could not be obtained.
[37] a) M. Cais, J. J. Dannenberg, A. Eisenstadt, M. I. Levenberg, J. H. Richards, *Tetrahedron Lett.* **1966**, *7*, 1695–1701; b) S. Lupan, M. Kapon, M. Cais, F. H. Herbstein, *Angew. Chem.* **1972**, *84*, 1104–1106; *Angew. Chem. Int. Ed. Engl.* **1972**, *11*, 1025–1027; c) G. K. S. Prakash, H. Buchholz, V. P. Reddy, A. Meijere, G. A. Olah, *J. Am. Chem. Soc.* **1992**, *114*, 1097–1098; d) F. L. Hedberg, H. Rosenberg, *J. Am. Chem. Soc.* **1969**, *91*, 1258–1259.
[38] J. H. Richards, E. A. Hill, *J. Am. Chem. Soc.* **1959**, *81*, 3484–3485.
[39] T. E. Pickett, C. J. Richards, *Tetrahedron Lett.* **1999**, *40*, 5251–5254.
[40] R. V. Parish, in *The Organic Chemistry of Iron, Vol. 1*, (Eds.: E. A. Koerner von Gustorf, F. W. Grevels, I. Fischler), Academic Press, **1978**, pp. 175–211.
[41] a) R. M. G. Roberts, J. Silver, *J. Organomet. Chem.* **1984**, *263*, 235–241; b) L. Korecz, M. Abou, G. Ortaggi, M. Graziani, U. Belluco, K. Burger, *Inorg. Chim. Acta* **1974**, *9*, 209–211; c) J. Silver, G. R. Fern, J. R. Miller, E. Slade, M. Ahmet, A. Houlton, D. J. Evans, G. J. Leigh, *J. Organomet. Chem.* **2001**, *637–639*, 311–317; d) A. Houlton, J. R. Miller, M. R. G. Roberts, J. Silver, *J. Chem. Soc. Dalton Trans.* **1990**, 2181–2183.
[42] R. Gleiter, R. Seeger, H. Binder, E. Fluck, E. M. Cais, *Angew. Chem.* **1972**, *84*, 1107–1109; *Angew. Chem. Int. Ed. Engl.* **1972**, *11*, 1028–1030.
[43] G. Nevshvad, R. M. G. Roberts, J. Silver, *J. Organomet. Chem.* **1982**, *236*, 237–244.
[44] A. Houlton, J. R. Miller, R. M. G. Roberts, J. Silver, *J. Chem. Soc. Dalton Trans.* **1991**, 467–470.
[45] J. Silver, *J. Chem. Soc. Dalton Trans.* **1990**, 3513–3516.
[46] a) T.-Y. Dong, C.-H. Huang, C.-K. Chang, Y.-S. Wen, S.-L. Lee, J.-A. Chen, W.-Y. Yeh, A. Yeh, *J. Am. Chem. Soc.* **1993**, *115*, 6357–6368; see reference [12e]; c) T.-Y. Dong, S.-H. Lee, C.-K. Chang, H.-M. Lin, K.-J. Lin, *Organometallics* **1997**, *16*, 2773–2786; see reference [12h]; e) T.-Y. Dong, L.-S. Chang, G.-H. Lee, S.-M. Peng, *Organometallics* **2002**, *21*, 4192–4200; f) T.-Y. Dong, B.-R. Huang, S.-M. Peng, G.-H. Lee, M. Y.-N. Chiang, *J. Organomet. Chem.* **2002**, *659*, 125–132; g) T.-Y. Dong, L.-S. Chang, G.-H. Lee, S.-M. Peng, *Inorg. Chem. Commun.* **2002**, *5*, 107–111.
[47] N. S. Hush, *Prog. Inorg. Chem.* **1967**, *8*, 391–444
[48] T.-Y. Dong, D. N. Hendrickson, K. Iwai, M. J. Cohn, A. L. Rheingold, H. Sano, S. Motoyama, *J. Am. Chem. Soc.* **1985**, *107*, 7996–8008.
[49] N. S. Hush, *Coord. Chem. Rev.* **1985**, *64*, 135–157.
[50] A.-C. Ribou, J.-P. Launay, M. L. Sachtleben, H. Li, C. W. Spangler, *Inorg. Chem.* **1996**, *35*, 3735–3740.

Received: July 28, 2003
Revised: November 3, 2003 [F5394]

Synthesis and Characterization of Radical Cations Derived from Mono- and Biferrocenyl-Substituted 2-Aza-1,3-butadienes: A Study of the Influence of an Asymmetric and Oxidizable Bridge on Intramolecular Electron Transfer

Vega Lloveras,[a] Antonio Caballero,[b] Alberto Tárraga,[b] M. Desamparados Velasco,[b] Arturo Espinosa,[b] Klaus Wurst,[c] David J. Evans,[d] José Vidal-Gancedo,[a] Concepció Rovira,[a] Pedro Molina,*[b] and Jaume Veciana*[a]

Keywords: Charge transfer / Electrochemistry / Electron transfer / Metallocenes / Optical spectroscopy

The synthesis and study of structural and electronic properties of mono-ferrocenyl π-conjugated complexes **5a**–**d**, whose electronic characteristics have been systematically varied by introducing an electron-donating or electron-withdrawing substituent either at the 1-position or at the 4-position of the 2-aza-1,3-butadiene moiety linked to the ferrocenyl unit, are presented. The structural and electronic properties of the homobimetallic complex **5f**, with two ferrocene units linked through the asymmetric and oxidizable 2-aza-1,3-butadiene bridge, is also reported. The crystal structures of complexes **5b**, **5d**, and **5f** show a large degree of conjugation in this family of compounds. Complexes **5** show a rich electrochemical behavior due both to the oxidation of ferrocenyl units and the 2-aza-1,3-butadiene bridge, as revealed by cyclic voltammetry. Radical cations $\mathbf{5}^{+\cdot}$ were prepared from **5** by coulometric oxidations following their generation by absorption spectroscopy. The electronic properties of all reported neutral and oxidized π-conjugated complexes have been investigated by means of UV/Vis–near-IR, EPR and ^{57}Fe Mössbauer spectroscopy. The detailed study of mono-oxidized species $\mathbf{5a}^{+\cdot}$–$\mathbf{5f}^{+\cdot}$ has permitted the determination of the influence of an asymmetric bridge with an electroactive character on the intramolecular electron transfer (IET) phenomenon, thus demonstrating that the 2-aza-1,3-butadiene bridge promotes the IET between the two metallic units of $\mathbf{5f}^{+\cdot}$ through two different pathways. The experimental data and conclusions are supported by DFT computations (B3LYP/3-21G*) and time-dependent DFT methods.

Introduction

Currently, there is considerable interest in the study of the properties of compounds bearing multiple redox centers separated by an organic bridge and, in particular, those that are able to produce mixed-valence species.[1] Such species are interesting not only because of their importance in producing new valuable materials, such as molecular wires and switches, that show intramolecular electron transfer (IET) phenomena, but also to understand the role of biologically relevant mixed-valence compounds.[2] One of the richer areas of metallocene chemistry is the study of general strategies for assembling two or more such electroactive metal fragments in close proximity in order to determine the type of electronic interactions between the metal fragments.[3] Among the various possibilities to bridge two cyclopentadienyl-type (Cp) ligands, emphasis has been laid on the electronic and steric properties of organic bridges because both will influence the interaction between the metal fragments bound to the Cp's and, in many cases, these factors will not be independent.

It is worth noting that IET can be monitored by the study of optical transitions occurring in mixed-valence complexes,[4] and that intervalence charge-transfer (IV-CT) bands may be observed in both σ- and π-bridged systems. In the former case, a through-space mechanism is generally believed to be responsible, such that low-energy bands at the near-IR are usually only observed in species that are sufficiently flexible to allow the two metal centers to come into close proximity. In π-bridged systems, near-IR bands are much more widely observed, even when the metals are well separated by rigid bridges, thereby suggesting that through-bond mechanisms are involved. IET in such π-bridged systems may proceed either by a superexchange and/or a hopping mechanism.[5] In the superexchange

[a] Institut de Ciència de Materials de Barcelona (CSIC), Campus Universitari de Bellaterra,
08193, Cerdanyola, Spain
Fax: +34-93-580-5729
E-mail: vecianaj@icmab.es
[b] Universidad de Murcia, Departamento de Química Orgánica, Facultad de Química,
Campus de Espinardo, 30100 Murcia, Spain
Fax: +34-968-364149
E-mail: pmolina@um.es
[c] Institut für Allgemeine Anorganische und Theoretische Chemie, Universität Innsbrück,
6020, Innrain 52a, Innsbruck, Austria
[d] Department of Biological Chemistry, John Innes Centre, Norwich Research Park, Colney, Norwich, NR4 7UH, UK
Supporting information for this article is available on the WWW under http://www.eujic.org/ or from the author.

  DOI: 10.1002/ejic.200400992

mechanism the bridge serves solely to mediate the wavefunctions of the two electroactive centers that act as electron-donor and -acceptor groups; the electron (or hole) is never vibronically localized on the bridge. In contrast, in the hopping mechanism the electron (or hole) is located at the bridge for a short time (vibronically localized) during its journey from one redox center to the other. The former mechanism is generally the origin of many of the observed IV-CT bands in mixed-valence species, while the hopping one is much less common, probably because of the strict structural and electronic requirements that must be fulfilled by the bridge. Nowadays there is a great interest in the development of organic bridges that favor the hopping mechanism between the two electroactive centers since they could provide new molecular devices that act as electronic relays to promote IETs over large distances.

A large number of bis-metallocenes and metallocenes linked by saturated carbon bridges have been synthesized and studied with respect to metal–metal interactions. It has been demonstrated that, compared to bis-metallocenes, species linked by a single carbon bridge show substantially weaker metal–metal interactions.[6] In general, stronger electrochemical metal–metal interactions occur when two linkages are made between two metallocenes and the metals are brought into closer proximity. On the other hand, IV-CT absorptions are usually not observed in the mono-oxidized derivatives of ferrocenes with insulating hydrocarbon bridges.[7] Most bis-metallocenes linked by saturated carbon bridges belong to class I in the Robin–Day classification,[8] the only interaction detected being at the electrochemical level and which can be attributed only to electrostatic and inductive effects. In contrast, ferrocenyl groups linked by unsaturated bridges show slightly larger metal–metal interactions than those with analogous saturated bridges,[2c,9–13] and the corresponding mono-oxidized olefin-bridged species show IV-CT absorptions in the near-IR region. Thus, many such species belong to class II, in which there is a moderate coupling between the two electroactive centers mediated by the organic bridge through a superexchange mechanism. Intermetallic interactions of different magnitudes have been observed in diferrocene complexes in which the two metallocene units are linked through a symmetric spacer with two conjugated double bonds (e.g. butadiene,[14] 1,4-diaza-1,3-butadiene,[15] 2,3-diaza-1,3-butadiene,[16] and others[17]). However, no examples have been reported of metal–metal interactions between metallocene units linked by an asymmetric spacer like the 2-aza-1,3-butadiene bridge.

Here we wish to present the synthesis and study of structural and electronic properties of ferrocenyl (Fc) π-conjugated complexes **5a**–**d**, whose electronic properties have been systematically varied by introducing an electron-donating or electron-withdrawing substituent, either at the 1-position or at the 4-position of the 2-aza-1,3-butadiene moiety linked to the ferrocenyl unit. We also wish to present here a study of the homobimetallic complex **5f**, which contains two ferrocene units linked by the asymmetric 2-aza-1,3-butadiene bridge. The mono-oxidized species of this complex, **5f**$^{+\bullet}$, has permitted the study of the influence of an asymmetric bridge with an electroactive character on the intramolecular electron transfer (IET) phenomenon, demonstrating that the 2-aza-1,3-butadiene bridge favors the IET between the two metallic centers.

Results and Discussion

Synthesis and Characterization

Compounds **5** were all prepared from the readily available diethyl aminomethylphosphonate (**1**),[18] which was condensed with the appropriate aromatic or organometallic aldehyde **2** to give the corresponding *N*-substituted diethyl aminomethylphosphonate **3** in excellent yields (85–95%). Generation of the metalloenamine by treatment with *n*BuLi at –78 °C and subsequently with one equivalent of the aldehyde **4** provided the 1,4-disubstituted 2-aza-1,3-butadienes **5** in yields ranging from 40% to 90% (Scheme 1). While two individual operations are required in the latter synthesis, it is possible to execute the entire sequence of reactions in a single flask without isolation of the intermediates **3** without affecting the yield. However, in this case, isolation of compounds **5** proved to be more difficult. Compounds **5**, recrystallized from dichloromethane/diethyl ether (1:10), were characterized by mass spectroscopy and ^{1}H and ^{13}C NMR spectroscopy, as well as by elemental analyses.

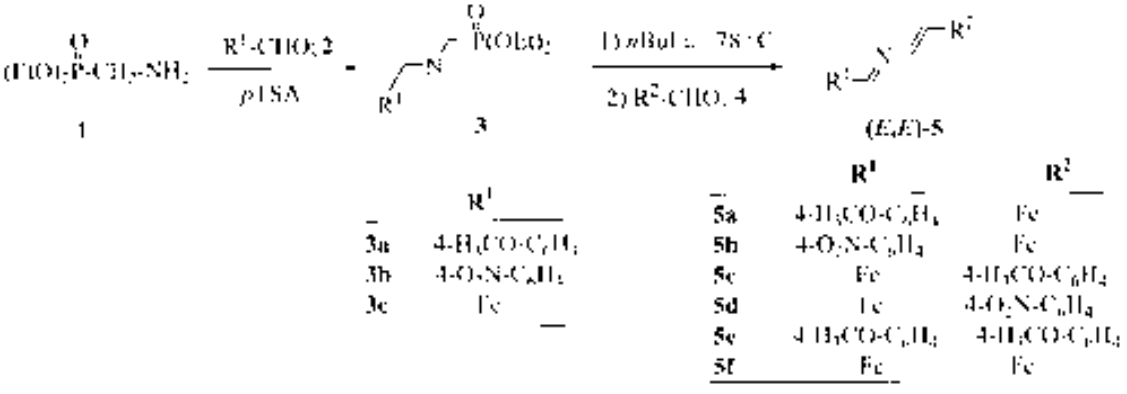

Scheme 1.

Assignment of the configuration of the double bonds present in the 1,4-disubstituted 2-aza-1,3-butadienes **5** was achieved by inspection of the ^{1}H NMR spectroscopic data. It is well established that the condensation reaction between a primary amine and an aldehyde is not stereoselective, hence both (*E*)- and (*Z*)-aldimine isomers are generally present in the reaction product. However, it must be emphasized that the condensation reaction between **1** and the appropriate aldehyde **2** takes place stereoselectively to give exclusively the (*E*)-isomer, as ascertained by ^{1}H NMR spectroscopy. Indeed, an NOE effect is observed to the methylene group on irradiation of the aldiminic proton of **3a**. On the other hand, *N*-substituted diethyl aminophosphonates **3**, after deprotonation with *n*BuLi, react smoothly in THF with the corresponding aldehyde **4** to give only the *trans* configured carbon-carbon double bond, as is expected in a Horner–Wadsworth–Emmons olefination process. This configuration was confirmed by the characteristic vicinal coupling constants (J = 14.0 Hz) in the ^{1}H NMR spectrum. In addition, NOE and two-dimensional NOESY experiments on a solution of compound **5f** in $CDCl_3$ confirmed not only the (*E*,*E*)-configuration of the double bonds present in the bridge, but also the *s-cis*-conformation in this solvent. Thus, on irradiation at δ = 7.04 ppm (H_4) an NOE effect is observed on the aldiminic H_1; no NOE effect is observed to H_1 when irradiation takes place at δ = 6.63 ppm (H_3).

X-ray Crystal Structures

Single crystals of compounds **5b**, **5d**, and **5f**, suitable for X-ray structure determination, were grown from diffusion of *n*-hexane into a solution of the compound in CH_2Cl_2. The crystal data and details of data collection and structure refinement are given as Supporting Information (Table S1). Attempts to grow good-quality single crystals of **5a** and **5c** for X-ray determination were unsuccessful.

Compound **5b** crystallizes in the triclinic space group $P\bar{1}$ with four molecules in the unit cell. Two independent molecules were found per asymmetric unit. Figure 1 (see a) shows the ORTEP drawing of the molecular structure of **5b** with the atomic numbering scheme. The molecular structure reveals that **5b** is present as the (*E*,*E*)-isomer, as is observed in solution by ^{1}H NMR spectroscopy, and has an *s-trans* configuration in the solid state. The interatomic distances and bond angles of **5b** are close to those previously observed for ferrocene[19] and other substituted ferrocene

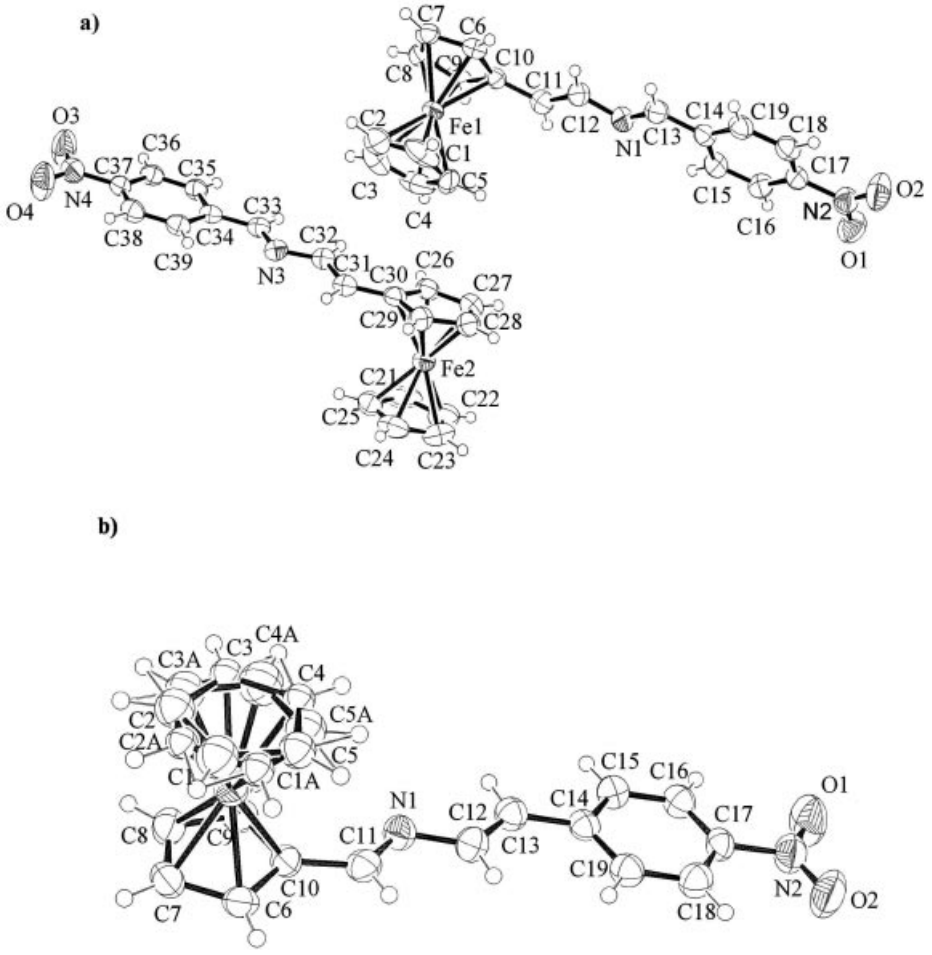

Figure 1. ORTEP views of the asymmetric unit of **5b** showing the atom numbering scheme (a) and of **5d** showing the atom numbering scheme (b). Thermal ellipsoids are drawn at the 50% probability level.

compounds.[20] The most interesting structural feature of **5b** is that all atoms of the 2-aza-1,3-butadiene bridge and the two attached rings are disposed in a planar configuration, thus indicating a large degree of π-conjugation and rigidity of this organic ligand.

Compound **5d** crystallizes in the monoclinic space group *P*21/*n* with four molecules in the unit cell. Figure 1 (see b) shows the ORTEP drawing with the atomic numbering scheme. Molecules of this compound are also present as the (*E*,*E*)-isomer, as observed in solution by ^{1}H NMR spectroscopy, and have an *s-trans* configuration in the solid state. The bond and dihedral angles reveal that all the atoms of the bridge and the two linked rings are disposed in a planar configuration, as in compound **5b**, thus indicating a large degree of conjugation in the π-system.

Compound **5f** crystallizes in the monoclinic space group *P*21/*c* with two molecules in the unit cell. Figure 2 shows the ORTEP drawing of **5f** with the atomic numbering scheme. The molecular structure of **5f** reveals a 1:1 disorder of the two atoms C12 and N1 at the same position. The crystallographic asymmetric unit is only one half of the molecule, since the other half is generated by a symmetry operation with a center of symmetry, as shown in Figure 2. Since the molecule does not really possess a symmetry center it must be disordered, therefore C12 and N1 were refined each with an occupancy of 0.5 with the same coordinates and temperature factors. Molecules of **5f** are also present as the (*E*,*E*)-isomer, as observed in solution by ^{1}H NMR spectroscopy, but in the solid state they adopt an *s-trans* conformation in contrast to the major conformation adopted in solution (vide supra). One of the two equivalent possibilities of the molecule is shown in Figure 2.

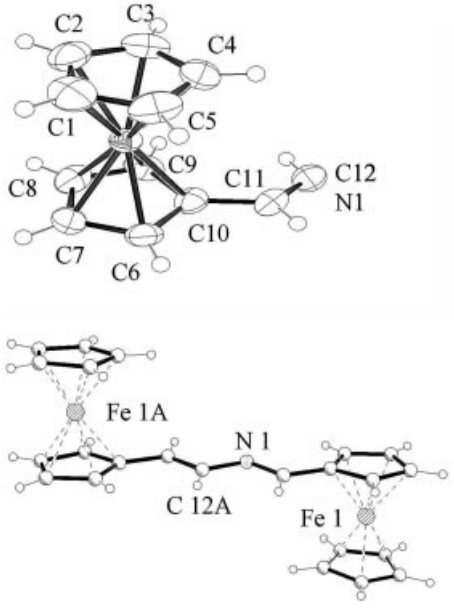

Figure 2. Top: ORTEP view of the asymmetric unit of **5f** showing the atom numbering scheme. Thermal ellipsoids are drawn at the 50% probability level. Bottom: drawing of a complete molecule of **5f**.

Theoretical Calculations

Geometry optimizations at the DFT level were carried out for neutral 2-aza-1,3-butadienes **5** as well as for the oxidized species **5**$^{\bullet+}$; the resulting geometrical parameters are gathered in Table 1. For those compounds whose X-ray structures are reported here, a high degree of coincidence is observed with the calculated values, as shown by the following critical geometrical parameters: the calculated N(bridge)···Fe distances for **5b**, **5d**, and **5f** are 5.309, 3.868, and 3.885 (Fe_1) and 5.380 Å (Fe_4), while the corresponding experimental distances are 5.242, 3.893, and 3.967 and 5.169 Å, respectively; the calculated Fe_1···Fe_4 distance in **5f** is 9.225 Å, while the experimental one is 9.107 Å. The other two calculated structures **5a** and **5c** display similar values (5.350 and 3.860 Å, respectively) for the N(bridge)···Fe distance. On the other hand, all calculated structures have a pure *s-trans* conformation (C1–N2–C3–C4 dihedral angles of 179.7°, 178.3°, 177.5°, 178.6°, and 179.2° for **5a**–**d** and **5f**, respectively), with the substituted phenyl rings almost parallel to the 2-aza-1,3-butadiene plane (angles between mean planes of 0.3°, 3.5°, 4.7°, and 1.4° for **5a**–**d**, respectively) and the bridge-attached Cp rings with small twisting angles (13.6°, 5.6°, 7.8°, 3.5°, 1.4°, and 12.1° for **5a**–**d** and Fc_1 and Fc_4 in **5f**, respectively). Where available, all experimental ring (Cp or substituted phenyl) twisting angles are systematically higher than the corresponding calculated values. From these calculations it is possible to conclude that both neutral 2-aza-1,3-butadienes **5** and oxidized species **5**$^{\bullet+}$ show planar structures exhibiting a large conjugation and a high structural rigidity (Table 1).

Electronic Spectroscopy

The UV/Visible data obtained in CH_2Cl_2 for **5a**–**d** and **5f** are collected in Table 2. These spectra are characterized by a very strong absorption with a maximum between 336 and 375 nm, which is assigned to a localized π-π* excitation mainly within the 2-aza-1,3-butadiene bridge. In addition to this band, another weaker absorption is visible between 469 and 535 nm, which is assigned to another localized excitation with a lower energy produced either by two nearly degenerate transitions, an Fe^{II} d-d transition[21] (e.g. HOMO–1 → LUMO+3 in **5a**), or by a metal-to-ligand charge transfer (MLCT) process (d_π-π*)[22] (e.g. HOMO–3 → LUMO+1 in **5a**). By comparison of the compounds with the ferrocenyl unit in the same position of the bridge it is easy to conclude that the presence of an electron-donating methoxy group (**5a** and **5c**) results in a significant decrease of the wavelength of the absorption maximum relative to the compounds with a nitro substituent (**5b** and **5d**). On the other hand, the compounds with the ferrocenyl group at the 4-position of the bridge show a shift of the absorption maxima to longer wavelengths relative to the compounds with the ferrocenyl group at the 1-position. Therefore, the calculated energy gap between HOMO and LUMO in the first position (3.6558 and 2.8194 eV for **5a** and **5b**, respectively) is slightly smaller than in the second position (3.6889 and

Table 1. Selected calculated[a] and geometrical parameters[b] for neutral 2-aza-1,3-butadienes **5** and oxidized species $\mathbf{5}^{+\cdot}$.

	R^1–C^1	C^1–N^1	N^2–N^3	C^3–C^4	C^4–R^4	$C^1N^2C^3$	$C^1N^2C^3C^4$	$R^{1\#}Azd^{\#}$	$Azd^{\#}R^{4\#}$	$Fe^1\cdots N^2$	$Fe^4\cdots N^2$	$Fe^1\cdots Fe^4$
5a	1.457	1.294	1.399	1.348	1.447	119.8	179.7	0.3	13.6		5.350	
5b	1.462	1.293	1.395	1.350	1.443	120.6	178.3	3.5	5.6		5.309	
	(1.454)	(1.280)	(1.387)	(1.335)	(1.447)	(117.7)	(176.7)	(5.2)	(9.6)		(5.242)	
5c	1.444	1.294	1.401	1.348	1.459	119.5	177.5	7.8	4.7	3.860		
5d	1.439	1.297	1.398	1.349	1.458	119.0	178.6	3.5	1.4	3.868		
	(1.442)	(1.282)	(1.394)	(1.320)	(1.460)	(117.1)	(179.2)	(3.9)	(4.2)	(3.893)		
5f	1.439	1.297	1.398	1.349	1.458	119.0	178.6	1.4	12.1	3.885	5.380	9.225
	(1.442)	(1.282)	(1.394)	(1.320)	(1.460)	(117.1)	(179.2)	(8.1)	(8.1)	(3.967)	(5.169)	(9.107)
$\mathbf{5a}^{+\cdot}$	1.431	1.313	1.370	1.366	1.424	119.5	177.5	1.0	7.4		5.445	
	(–0.026)	(+0.019)	(–0.029)	(+0.018)	(–0.023)	(–0.3)	(–2.2)	(+0.7)	(–6.2)		(+0.095)	
$\mathbf{5c}^{+\cdot}$	1.433	1.308	1.374	1.367	1.436	121.3	178.3	4.2	2.1	3.984		
	(–0.011)	(+0.014)	(–0.027)	(+0.019)	(–0.023)	(+1.8)	(+0.8)	(–3.6)	(–2.6)	(+0.124)		
$\mathbf{5d}^{+\cdot}$	1.446	1.296	1.392	1.354	1.455	121.0	179.9	7.6	1.0	3.900		
	(+0.007)	(–0.001)	(–0.006)	(+0.005)	(–0.003)	(+2.0)	(+1.3)	(+4.1)	(–0.4)	(+0.032)		
$\mathbf{5f}^{+\cdot}$	1.420	1.314	1.373	1.364	1.425	118.8	176.1	3.4	9.0	3.842	5.456	9.261
	(–0.024)	(+0.020)	(–0.028)	(+0.017)	(–0.022)	(–0.8)	(–3.1)	(+2.0)	(–1.6)	(–0.043)	(+0.076)	(+0.036)
$\mathbf{5f}^{2+}$	1.412	1.409	1.295	1.458	1.415	119.3	178.1	24.5[c]	35.7[c]	3.057	4.124	7.172
	(–0.008)	(+0.094)	(–0.078)	(+0.094)	(–0.010)	(+0.5)	(–0.2)	(+21.1)	(+26.7)	(–0.785)	(–1.332)	(–2.089)

[a] The experimental values for neutral compounds, where available, and, for oxidized species, the calculated absolute difference in relation to the precedent structure before one-electron oxidation, are given in parentheses. [b] Distances [Å] and bond and dihedral angles [°]; # stands for the azadiene skeleton (Azd), Cp or substituted-phenyl mean planes. [c] Unusually large angles between mean planes do not reflect a twisting rotation around a C_{Cp}–C_{Azd} bond, but a bending distortion of the exocyclic substituent towards Fe atom in order to alleviate the electron deficiency. See for instance ref.[49]

Table 2. Calculated and experimental electronic absorption bands of neutral compounds **5a**–**d** and **5f**.

Compound	R^1	R^2	Calculated λ_{max} [nm] (oscillator strength)	Experimental[a] λ_{max} [nm] (10^{-3} ε, $M^{-1}cm^{-1}$)
5a	4-$CH_3OC_6H_4$	Fc	343.6 (0.7961), 375.8 (0.1944), 469.7 (0.0052)	345 (24.5), 360 (sh), 470 (2.1)
5b	4-$NO_2C_6H_4$	Fc	378.7 (0.4862), 526.9 (0.0965)	375 (16.9), 535 (4.4)
5c	Fc	4-$CH_3OC_6H_4$	341.3 (1.2479), 369.2 (0.0132), 470.3 (0.0033)	342 (20.7), 356 (sh), 469 (1.9)
5d	Fc	4-$NO_2C_6H_4$	366.1 (0.5466), 522.6 (0.0690)	371 (18.7), 504 (4.5)
5f	Fc	Fc	336.2 (0.0415), 339.9 (0.1006), 476.2 (0.0033)	336 (25.5), 346 (sh), 478 (3.6)

[a] In CH_2Cl_2.

2.9889 eV for **5c** and **5d**, respectively) and this gap is greatly increased by the presence of an electron-donating substituent at the aromatic ring. Finally, the homobimetallic complex **5f** shows an absorption spectrum that is very similar to those of complexes **5a** and **5c**, as expected from the similar electron-donor abilities of ferrocenyl and *p*-methoxyphenyl groups (calculated HOMO–LUMO gap of 3.7785 eV for **5f**).

At this point, it is useful to consider the electronic transitions in terms of the molecular orbitals involved. Analysis of the electronic transitions by time-dependent DFT methods (TDDFT) gave essentially identical results for each studied compound between experimental and calculated transitions (summarized in Table 2). The agreement between calculated optical transitions and the experimentally observed results lends credence to the used theoretical level as well as to the attained geometries and the molecular-orbital model developed to explain such optical transitions. In addition, such an agreement confirms the assignation previously made to each optical transition.

Electrochemistry

Compounds **5** are all expected to show electroactivity due both to the Fe^{II}/Fe^{III} couple and the oxidation of the 2-aza-1,3-butadiene bridge. Indeed, monoferrocenyl derivatives **5a**–**d** show two oxidation waves in the range 0–1.5 V vs. SCE; their potentials are collected in Table 3. The first oxidation wave for all compounds is reversible and occurs at potentials close to that of the Fe^{II}/Fe^{III} couple in ferrocene (0.460 V vs. SCE, or 0.530 V vs. decamethylferrocene, DMFc).[23] Therefore, this wave is assigned to the Fe^{II}/Fe^{III} redox couple. The oxidation potentials of the ferrocenyl units of these compounds show a dependence on the position of the 2-aza-1,3-butadiene bridge to which they are attached and also on the electron-donating ability of the aromatic group linked to the bridge. Thus, higher potentials are observed when the ferrocenyl is attached at the 1-position of the bridge and when the substituent of the aromatic ring is a nitro group. In contrast to the first oxidation wave, the second wave is clearly not reversible for **5a**–**c** under the conditions of our experiments, since only the anionic peak appears in the cyclic voltammogram. Taking into account that the *p*-methoxyphenyl moiety is the most "ferrocene-like" group in terms of its electron-donating capability, as demonstrated experimentally by the similarity of the UV/Vis spectra of **5a**, **5c**, and **5f** (vide supra), and also by independent non-linear optical measurements,[24] the 1,4-bis(*p*-methoxyphenyl)-2-aza-1,3-butadiene **5e** was also studied for comparison purposes. The CV of this compound shows two

irreversible oxidation waves at 1.084 and 1.440 V vs. DMFc that may be assigned to the oxidation of the N atom of the bridge and the *p*-methoxyphenyl group, respectively. This assignment is based on the fact that when the N atom of **5e** is protonated under acidic conditions the first oxidation peak disappears while the second remains unchanged. On the basis of these observations, the second wave observed in the CVs of compounds **5a**–**c** is also assigned to the oxidation of the 2-aza-1,3-butadiene group, the potential of which varies from 1.090 V to 1.416 V vs. DMFc and also shows a dependence on the substituents of the aromatic ring and on the relative position of the ferrocenyl and aromatic groups. Such an irreversible oxidation wave is not observed for compound **5d**, probably because it appears at a potential more positive than +1.5 V vs. DMFc due to the strong electron-withdrawing character of the nitro group.

Table 3. Cyclic voltammogram data for compounds **5a**–**f** in CH_2Cl_2.

Compound	R^1	R^2	$^1E_{1/2}$ (Fc^+/Fc)[a]	$^2E_{ap}$ (irrev)[a]
5a	4-$CH_3OC_6H_4$	Fc	0.530	1.090
5b	4-$NO_2C_6H_4$	Fc	0.590	1.190
5c	Fc	4-$CH_3OC_6H_4$	0.698	1.416
5d	Fc	4-$NO_2C_6H_4$	0.704	–
5e	4-$CH_3OC_6H_4$	4-$CH_3OC_6H_4$	–	1.084, 1.440
5f	Fc	Fc	0.560 0.770	1.116

[a] $E_{1/2}$ [V] vs. decamethylferrocene.

To gain further insight into the nature of the irreversible oxidation wave, the electrochemical behavior of compounds **5a**–**d** was investigated in the presence of HBF_4. Upon protonation, the potential shift of the ferrocenyl unit present in these compounds was found to be strongly dependent on its position in the 2-aza-1,3-butadiene bridge. When it is placed at the 4-position a $\Delta E_{1/2}$ (L – LH^+) of 70 mV (**5a**) and 80 mV (**5b**) was observed, while when it is placed at the 1-position the corresponding shifts are 300 mV (**5c**) and 320 mV (**5d**). Additionally, in all these cases, the irreversible wave associated with the oxidation of the bridge disappeared upon protonation, except for **5c**, which seems to be due to the oxidation of the methoxy group present in the ring.

The species formed during the irreversible oxidation waves of **5a**–**c** are probably the radical cations centered mainly at the N atom of the 2-aza-1,3-butadiene bridge, species which must be relatively unstable under the experimental conditions used. Although no electrochemical oxidation study of the 2-aza-1,3-butadiene fragment has been reported, this description is based on the fact that the anodic oxidation of the closely related *N*-benzylidene-*p*-anisidine Schiff bases show two irreversible anodic peaks at 1.08–1.25 and 1.41–1.61 V vs. SCE. The peak potentials of the first wave, which show good linearity against the σ^+ values of the substituent in the benzylidene ring, are ascribed to the formation of a radical cation centered at the nitrogen atom, whereas the second peak is attributed to the oxidation of the substituent in the aromatic ring.[25] In this sense, the electrochemical behaviors of compound **5e** and *N*-*p*-methoxybenzylidene-*p*-anisidine are almost identical, since the CV displays two irreversible oxidation peaks at 1.08 and 1.52 V vs. SCE.

The CV of **5f**, which contains two ferrocenyl groups, was recorded in two different experiments. Firstly, the CV (see a in Figure 3) scanned from 0–1 V shows two closely spaced reversible one-electron oxidations corresponding to the oxidation of the ferrocenyl units present in the molecule. Secondly, when the CV was run from 0.0–1.6 V, after the first scan, three oxidation waves were observed: two for the ferrocenyl units and one for the oxidation of the bridge. The cathodic return wave is, in general, higher and thinner than the anodic forward wave, which can be attributed to some adsorption of the oxidized compound onto the electrode surface in the ferrocenium form. The difference between the anodic and cathodic peak potentials (ΔE_p) is lower than the 58 mV value expected for a reversible single-electron wave of an electroactive species in solution at 20 °C (the fully adsorbed redox species would ideally have a ΔE_p value of zero). However, it is important to emphasize that the results obtained in the latter experiment could only be reproduced when the electrode was cleaned before subsequent scans were run. Otherwise, the wave corresponding to the oxidation of the bridge disappears, indicating that the electrode behaves as an insulator in the region in which the azadiene moiety is oxidized. The protonation process of **5f** was also followed by cyclic voltammetry. Upon protonation, the three waves present in the neutral ligand evolve into two waves in the protonated derivative, the latter wave appearing at almost the same potential region as that corresponding to the bridge in the neutral ligand. In order to understand the nature of the unit causing that wave, Osteryoung square-wave voltammetry (OSWV) experiments were carried out by protonation of **5f** (see b in Figure 3). While the neutral ligand exhibits only two oxidation waves at 0.560 and 0.770 V vs. DMFc, stepwise addition of HBF_4 resulted in a clear evolution of the first oxidation wave from 0.560 V to 0.630 V and the disappearance of the second oxidation wave, accompanied by concomitant appearance of a new oxidation wave at 1.060 V. The peak intensity of the new oxidation wave increases with the concentration of the acid added up to until two equivalents. At this point, the original oxidation waves disappear and the new ones reach full development. The resulting two oxidation waves, with a 1:1 ratio and a separation of 0.430 V, are due to the oxidation of the two ferrocenyl moieties in the protonated complex. Again, for reproducibility, it is very important to clean the electrode after each scan.

It is worth mentioning that the difference between the first two reversible oxidation waves in compound **5f** ($\Delta E_{1/2}$ = 210 mV) is much larger than those observed for most bis-ferrocenyl compounds with four-membered π-conjugated bridges, such as 1,4-bis(ferrocenyl)butadiene (129 mV),[14] 1,4-bis(ferrocenyl)butadiyne (120 mV),[10] 1,4-bis(ferrocenyl)-1,4-diazabutadiene (60 mV),[15] and 1,4-bis(ferrocenyl)-2,3-diaza-1,4-dimethylbutadiene (90 mV).[16] The origin of this large $\Delta E_{1/2}$ value must be ascribed to the asym-

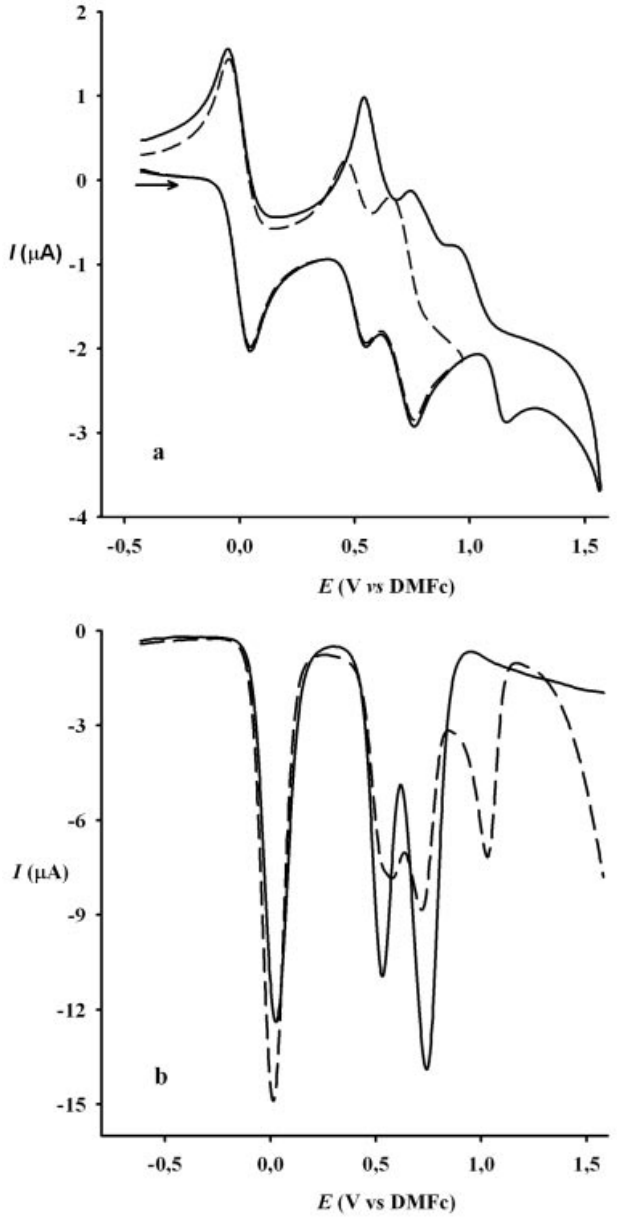

Figure 3. a) Cyclic voltammogram of compound **5f** (1 mM) in $CH_2Cl_2/[(nBu)_4N]ClO_4$ scanned at 0.1 $V s^{-1}$ from –0.5 V to 0.9 V (dash) and from –0.5 V to 1.6 V (solid). b) OSWV of compound **5f** (1 mM) in $CH_2Cl_2/[(nBu)_4N]ClO_4$ recorded at 0.1 $mV s^{-1}$ before (solid) and after (dash) addition of 1 equiv. of HBF_4. Decamethylferrocene (DMFc) was used as an internal standard.

metry of the bridge linking the two ferrocenyl groups. Thus, the distinct position of the N atom with respect to the two ferrocenyl groups should perturb the two ferrocenyl moieties to a different extent.

Optically Induced Intramolecular Electron Transfer in $5a^{\cdot+}$–$d^{\cdot+}$

It has been demonstrated that in electrochemically active ferrocenylthiophene derivatives, in which the gap between the metal and the organic bridge oxidation potentials is relatively small, it is possible, upon oxidation of the ferrocenyl group, to induce optically an electron transfer from the thienyl group to the Fe^{III} center.[26] This IET has an associated low-energy ligand-to-metal charge transfer (LMCT) band in the near-IR, which is very similar to those observed in symmetrical mixed-valence complexes. Moreover, it has been reported recently that the electrochemical oxidation of Fe^{II} centers of mono- or bis(ferrocenylethynyl)oligothiophenes, in which the potential difference between the reversible oxidation of the ferrocenyl group and the irreversible oxidation of the thienyl ring varies from 0.38 V to 1.12 V, yields the corresponding radical cations, which also exhibit oligothiophene-to-Fe^{III} charge-transfer LMCT bands in the near-IR region.[27] Taking into account that in compounds **5a**–**d** the potential differences between the two successive oxidation waves are in the range of 0.3–0.7 V (Table 3), and that these values are comparable to those of oligothiophene-substituted ferrocenes, the oxidized ferrocenyl derivatives $\mathbf{5a}^{\cdot+}$–$\mathbf{d}^{\cdot+}$ were considered suitable candidates to study the optically induced IET from the 2-aza-1,3-butadiene bridge to the Fe^{III} center. In favor of such an expectation is the recently reported fact that ferrocenyl derivatives containing a $-CH_2-N(R)-CH_2-$ bridge undergo intramolecular electron transfer between the Fe^{III} center and the nitrogen atom in the electrochemically oxidized state to give an intermediate containing an Fe^{II} center and a nitrogen with a radical cation character.[28]

The generation of the oxidized species derived from **5a**–**d** was performed electrochemically and monitored by absorption spectroscopy. Stepwise coulometric titrations were performed on ca. 2×10^{-3} M solutions of complexes **5a**–**d** in CH_2Cl_2, with $[(nBu)_4N]PF_6$ (0.15 M) as supporting electrolyte, and the absorption spectra were regularly recorded for different average number ($0 \le n \le 1$) of removed electrons. The UV/Vis–near-IR spectroscopic data of $\mathbf{5a}^{\cdot+}$–$\mathbf{d}^{\cdot+}$ are collected in Table 4. The spectra of $\mathbf{5a}^{\cdot+}$–$\mathbf{d}^{\cdot+}$ show three absorption bands, one in the UV region in the range of 371–418 nm of strong intensity, another in the visible region between 518 and 685 nm, with a weaker intensity, and an even weaker additional band in the near-IR region between 973–1219 nm. The latter band is not observed for $\mathbf{5d}^{\cdot+}$. The high-energy absorptions in the UV appear at similar wavelengths and have comparable intensities to those shown by the corresponding neutral complexes **5a**–**d** and, therefore, they are assigned to localized π-π* transitions at the 2-aza-1,3-butadiene group. The absorptions appearing in the visible region are similar to the bands shown by other oxidized ferrocenyl derivatives and, consequently, are assigned to Cp → Fe^{III} ligand-to-metal charge transfer (LMCT) transitions.[21] Finally, the absorption band in the near-IR, which is not observed in the neutral complexes and is likely to take place after the creation of an electronic vacancy in the HOMO, is assigned to a 2-aza-1,3-butadiene → Fe^{III} LMCT transition. This assignment is based on the following considerations: (i) during the course of the oxidations of **5a**–**c** these low-energy bands increase continuously in intensity, achieving a maximum when the oxidation process is complete (see

Figure 4); (ii) defined isosbestic points at 385 and 487 nm are maintained during the course of the oxidations (see Figure 4); and (iii) similar low-energy transitions have been observed in the near-IR region in other Fe^{III} and Ru^{III} complexes with conjugated oligothiophene ligands[26,27] and with a -CH_2-N(*R*)-CH_2- bridge.[28] Therefore, the absorption bands in the near-IR shown by **5a**$^{\cdot+}$–**c**$^{+}$ correspond to an optically induced electron transfer from the 2-aza-1,3-butadiene to the Fe^{III} center, as schematically shown in Figure 5 using the Marcus–Hush model.[4] We have assumed that during this optical transition one electron from the localized pair of nonbonding electrons on the N atom of the 2-aza-1,3-butadiene bridge is transferred to the Fe^{III} d_π orbital of the ferrocene moiety. This assumption is supported by the presence of a high-energy filled orbital in oxidized complexes **5a**$^{\cdot+}$–**d**$^{+}$ (e.g. HOMO–2 in **5a**$^{\cdot+}$ and HOMO–3 in **5c**$^{\cdot+}$) that is mainly localized on this N atom, as pointed out by theoretical calculations. Such calculations also show an absolute energetic minimum on the potential energy hypersurface essentially corresponding to the respective neutral top after the appropriate geometrical reorganization to redistribute the electronic density. Only a rough correlation with the experimental absorption values was claimed from time-dependent DFT calculations performed on some of these structures (see Table 4), due to the reported inaccuracy of these types of methods in particular cases.[29] Although there is only a rough correlation between the experimental and calculated values of absorption bands for oxidized complexes **5a**$^{\cdot+}$–**d**$^{\cdot+}$, the results of the time-dependent DFT calculations confirmed the assignations of optical transitions previously given for **5a**$^{\cdot+}$–**d**$^{\cdot+}$, based on experimental facts.

Table 4. Calculated and experimental electronic absorptions of oxidized species **5a**$^{+\cdot}$–**d**$^{+\cdot}$ and **5f**$^{+\cdot}$.

Compound	Calculated λ_{max} [nm] (oscillator strength)		Experimental[a] λ_{max} [nm] (10^{-3} ε, $M^{-1}cm^{-1}$)	
5a$^{+\cdot}$	418.8 (0.1538), 421.1 (0.1415), 486.6 (0.0560), 527.7 (0.0002), 566.0 (0.0014), 618.0 (0.3043)	947.5 (0.0210)	418 (8.5), 481 (3.8), 519 (2.8), 575 (1.9), 618 (0.9)	975 (1.0)
5b$^{+\cdot}$	–	–	259 (16.7), 330 (10.24), 390(sh), 518 (2.29), 685 (0.70)	1219 (0.30)
5c$^{+\cdot}$	269.6 (0.3447), 286.9 (0.1123), 360.0 (0.3045), 414.9 (0.2880), 556.8 (0.2648)	974.5 (0.0275)	259 (9.8), 293 (7.3), 383(7.2), 536 (2.2)	973 (0.13)
5d$^{+\cdot}$	–	–	263 (19.7), 286 (sh), 371(25.2), 549 (4.2)	–
5f$^{+\cdot}$	349.3 (0.1272), 374.2 (0.0753), 425.8 (0.0428), 549.5 (0.0101)	846.0 (0.0027), 1249.4 (0.0017)	327 (12.8), 369 (sh), 429 (sh), 547 (4.9)	764 (0.33), band A; 1250 (0.64) band B
5f^{2+}	–	–	297 (sh), 365 (11.4), 558 (3.7)	764 (0.60), band A; 971 (0.36); band C

[a] In CH_2Cl_2.

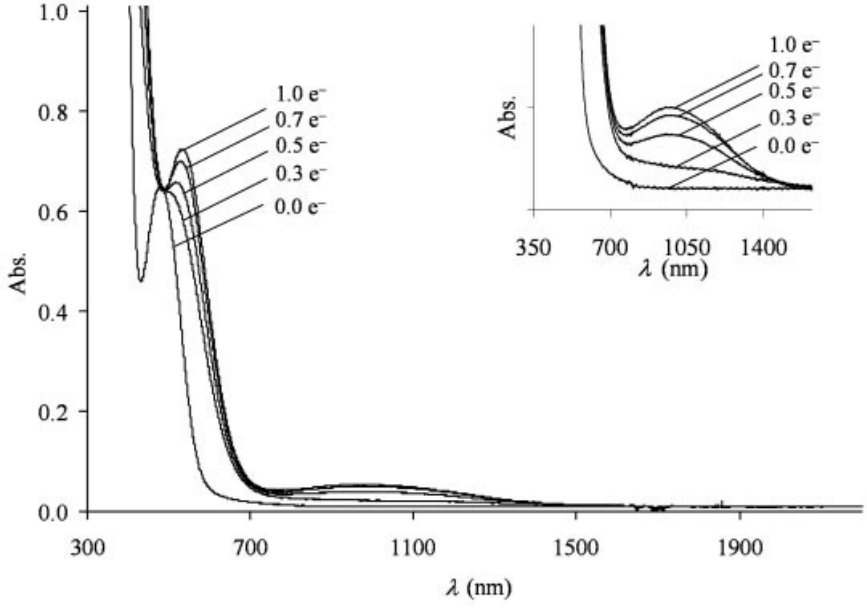

Figure 4. Evolution of Vis-near-IR spectra during the course of the oxidation of compound **5c**. The average number of removed electrons is given on each spectrum. Inset: NIR region enlargement.

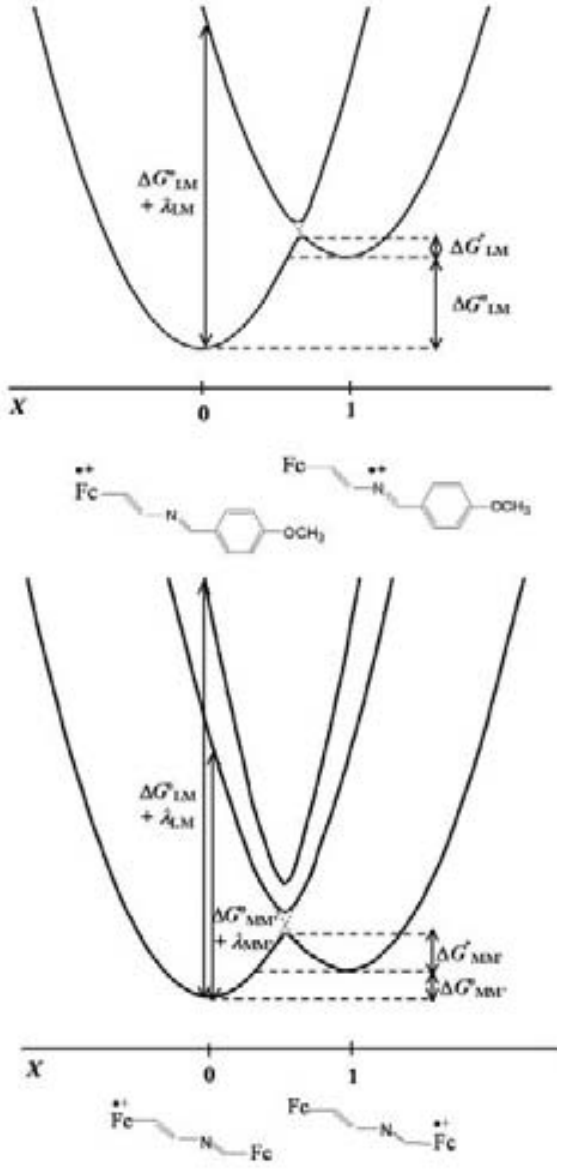

Figure 5. Marcus–Hush model used to describe IET in asymmetric oxidized complexes **5a**$^{\cdot+}$–**d**$^{\cdot+}$ (top) and in oxidized homobimetallic complex **5f**$^{\cdot+}$ (bottom).

The Marcus–Hush model can be used to describe the classical intramolecular electron-transfer process when the electron is coupled between a donor and an acceptor group via a single oscillator having the same frequency in both initial and final states.[4] Originally developed for the interpretation of intervalence charge transfer (IV-CT) bands in extended solids, the Marcus–Hush model has been extended and applied to IV-CT in mixed-valence organometallic[30,31] and organic compounds,[1g,32] as well as to LMCT and metal-to-ligand charge transfer (MLCT) processes in charge-localized asymmetric complexes.[33,34] In accordance with such precedents we have also used the Marcus–Hush model to study the IET of asymmetric complexes **5a**$^{\cdot+}$–**d**$^{\cdot+}$. As schematized in Figure 5, such species exist in two states having the charge/hole localized either on the metal (M) or a particular region of the organic ligand (L), which are separated by the relative free enthalpy $\Delta G°_{LM}$. The electronic coupling between the two electroactive centers (M and L) is measured by the V_{LM} term and the optical transition energy of the LMCT band at its maximum ($h\nu_{max}$; in cm^{-1}), corresponds to the sum of $\Delta G°_{LM}$ and the vertical reorganization energy λ_{LM} (i.e. $h\nu_{max} = \Delta G°_{LM} + \lambda_{LM}$).

The spectral data of LMCT bands of **5a**$^{\cdot+}$–**d**$^{\cdot+}$, summarized in Table 5, can be used to determine the electronic coupling parameter, V_{LM}, and the reorganization energy, λ_{LM}, for each oxidized compound. This was accomplished by deconvoluting the LMCT bands[35] using the classical procedure (see Figure S2 in the Supporting Information) assuming that the effective electron-transfer distance is the distance between the Fe and N atoms. Such distances can be determined from the crystal structures of **5b**, **5d**, and **5f** (5.2 and 3.9 Å for the complexes with the ferrocenyl groups attached to the 4- and 1-positions, respectively). The relative free enthalpies of the two vibronically localized electronic states for compounds **5a**–**c** can be estimated, in a first approximation, from the difference of electrochemical potentials corresponding to the oxidation of the 2-aza-1,3-butadiene center (L) and to the ferrocenyl center (M) of neutral complexes. Due to the experimental impossibility of measuring the L^0/L^{+1} couple of the 2-aza-1,3-butadiene when it is linked to a neutral ferrocenyl group, the corresponding oxidation potential was assumed to be 40 mV less positive than the anionic peak of compound **5e**, observed at +1.084 V, since the *p*-methoxyphenyl and ferrocenyl groups have similar electron-donor capabilities but the first group is not electrochemically active at potentials lower than +1.4 V (vide supra). An inspection of the resulting V_{LM} val-

Table 5. LMCT and IV-CT band parameters, obtained from the spectral deconvolution, and calculated IET parameters for radical cations **5a**$^{+\cdot}$–**d**$^{+\cdot}$and **5f**$^{+\cdot}$.

	R^1	R^2	ΔG^0_{LM} [cm^{-1}]	$h\nu_{max}$ [cm^{-1}]	λ_{LM} [cm^{-1}]	ε_{max} [M^{-1} cm^{-1}]	$\Delta\nu_{1/2}$ [cm^{-1}]	f[a]·10^3	d [Å]	V_{LM} [cm^{-1}]
5a$^{+\cdot}$	4-$CH_3OC_6H_4$	Fc	4150	10260	6110	1000	2640	12.1	5.2	650
5b$^{+\cdot}$	4-$NO_2C_6H_4$	Fc	3660	8200	4540	300	2090	2.9	5.2	280
5c$^{+\cdot}$	Fc	4-$CH_3OC_6H_4$	2790	10280	7490	130	3800	2.3	3.9	380
5d$^{+\cdot}$	Fc	4-$NO_2C_6H_4$	2740	–	–	–	–	–	–	–
5f$^{+\cdot}$	Fc	Fc	3900	13090[b] (band A)	9190[b]	330[b]	3450[b]	5.2[b]	5.2	480[b]
			1110	8000[c] (band B)	6890[c]	640[c]	2500[c]	7.4[c]	9.1	260[c]

[a] Total oscillator strength obtained by $f = 4.6\times10^{-9}\ \varepsilon_{max}\cdot\Delta\nu_{1/2}$. [b] LMCT band corresponding to an electron transfer between L and M units. [c] IV-CT band corresponding to an electron transfer between M and M′ units.

ues for complexes **5a**–**c** (Table 5) shows that electronic couplings between the ferrocenyl and the 2-aza-1,3-butadiene ligand are moderate, such that all these complexes belong to class II.[8] In addition, the electronic coupling of complexes **5a**–**c** is influenced by the position to which the ferrocenyl is attached, as well as on the electron-donor capability of the substituent on the phenyl group. It should be noted from the spectral analysis that the charge-transfer transition oscillator strengths clearly increase for complexes **5a**–**d**. Complex **5d** apparently does not show any LMCT band. This can be ascribed to the presence of a nitro group linked to the 4-position of the bridge, which drains some electron density from the 2-aza-1,3-butadiene chain, thus lowering the effective overlap between diabatic orbitals and decreasing the probability of the transition. This effect has indeed been predicted theoretically for other electron-withdrawing groups, such as the cyano group.[36]

Intramolecular Electron Transfer in the Mixed-Valence Compound $5f^{+\cdot}$

Oxidized species derived from **5f** were generated electrochemically and their formation followed by absorption spectroscopy. Thus, a stepwise coulometric titration was performed on a 2×10^{-3} M solution of **5f** in CH_2Cl_2, with $[(n\text{Bu})_4\text{N}]PF_6$ (0.15 M) as supporting electrolyte, and absorption spectra were regularly recorded for a different average number ($0 \le n \le 2$) of removed electrons. Figure 6a shows the evolution of the spectra during the oxidation of **5f** in the $0 \le n \le 1$ range, with an increase of the Cp → Fe^{III} LMCT band appearing at 547 nm, characteristic of a ferrocenium ion, and a decrease of the band that corresponds to a localized excitation of a ferrocene group at 478 nm. Along with the changes of these bands, the appearance and maintenance of two well-defined isosbestic points at 425 and 501 nm was observed. Nevertheless, the most interesting feature is that during the oxidation of **5f** two new weak and broad bands centered at 764 nm (band A) and at 1250 nm (band B) appear, and these increase continuously in intensity until one electron has been removed (i.e. when the formation of $\mathbf{5f}^{+\cdot}$ is complete). As also shown in Figure 6, on removing more electrons ($1 \le n \le 2$) the intensity of band A continues to increase until its intensity has doubled, while band B decreases until it disappears (when the dication $\mathbf{5f}^{2+}$ is completely formed). At the same time, another new weak and broad band at 971 nm (band C) increases until the fully oxidized species $\mathbf{5f}^{2+}$ is formed. Table 4 collects all the spectroscopic data for oxidized complexes $\mathbf{5f}^{+\cdot}$ and $\mathbf{5f}^{2+}$. The deconvolution of the experimental spectra of $\mathbf{5f}^{+\cdot}$, performed on spectral intensity times wavenumber vs. wavenumber, assuming Gaussian shapes (Figure 6c), allows an accurate determination of the position, width, and intensity of bands A and B, which are gathered in Table 5.[35,37] These spectral parameters are relevant for the characterization of intramolecular electron transfer in $\mathbf{5f}^{+\cdot}$

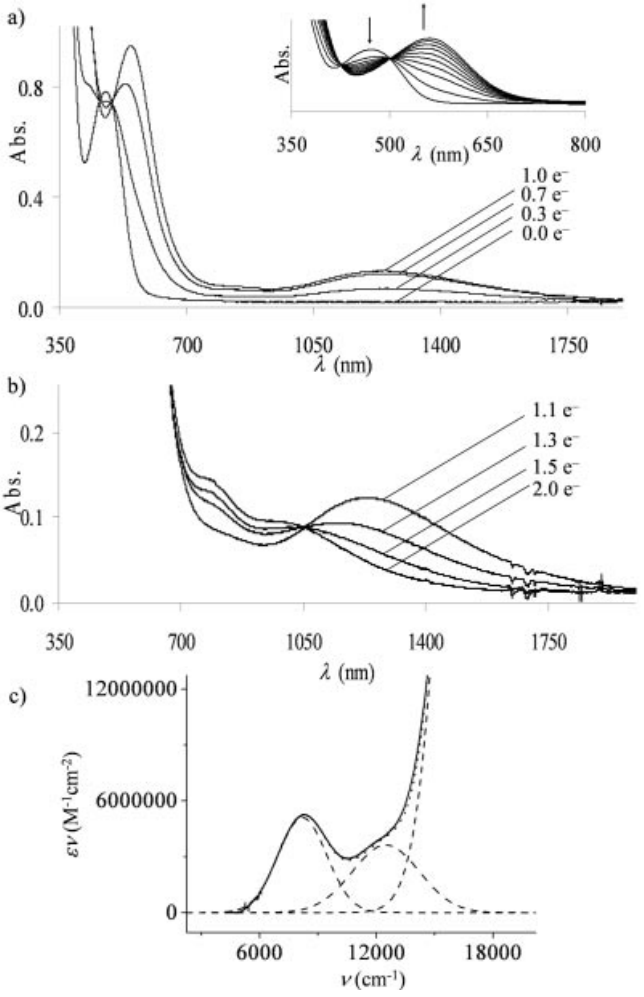

Figure 6. Evolution of Vis-near-IR spectra upon oxidation of **5f**: a) oxidation of **5f** until the maximum ($n = 1$) of the mixed-valence species $\mathbf{5f}^{+\cdot}$ is achieved. Inset: Expanded spectra of the visible region showing the two isosbestic points; b) oxidation until the maximum ($n = 2$) of the fully oxidized species $\mathbf{5f}^{2+}$ is achieved; c) deconvolution of the NIR spectrum of the $\mathbf{5f}^{+\cdot}PF_6^{-\cdot}$ salt. The experimental spectrum was deconvoluted by means of three Gaussian functions (dashed lines) using spectral intensity times wavenumber vs. wavenumber. The sum of the dashed lines (dotted line) closely matches the experimental spectrum (solid line).

The presence of several near-IR bands in the spectrum of a mixed-valence complex is not uncommon, and their occurrence is generally explained by one of three different possible causes.[38,39] One could be the presence of a strong spin-orbit coupling effect, which becomes important only for complexes containing third-row transition metals.[38] A second source could be the presence of a double-exchange mechanism,[39] a mechanism that becomes more probable as the bridge length and the level of π-orbitals increases. Finally, such multiple near-IR bands might be caused by the presence of a bridge with accessible redox state levels, as has been recently proposed to explain the rich absorption spectrum of certain mixed-valence compounds with redox-active bridges.[1g] Based on the behaviors of $\mathbf{5a}^{+\cdot}$–$\mathbf{c}^{+\cdot}$, the latter source seems to be the most probable origin for the

two near-IR bands of **5f**$^{+\cdot}$. Accordingly, and also based on the spectral evolution observed during the oxidation of **5f**, the band A is assigned to a 2-aza-1,3-butadiene → Fe^{III} LMCT transition, which implies an electron transfer from the N atom of the 2-aza-1,3-butadiene bridge to the Fe^{III} site linked at the 4-position of the bridge, whereas band B is attributed to the bridge-mediated superexchange between the two coupled iron sites (M and M′) − an IET between the two iron sites.

In order to estimate the effectiveness of both IET pathways we used the Marcus–Hush model, as schematized in Figure 5, where the reorganization energies of both transitions, λ_{LM} and $\lambda_{MM'}$, were determined from the absorption maxima of the bands A and B. For the free-energy difference between the two electronic states of **5f**$^{+\cdot}$ having the charge localized on each Fe site we used, in a first approximation, the value of $\Delta G°_{MM'}$ (1113 cm^{-1}) obtained from the difference of the first oxidation potentials of **5c** and **5f**. For $\Delta G°_{LM}$ we used a value of 3904 cm^{-1}, which was determined by employing the same approximations as for **5a**$^{+\cdot}$–**c**$^{+\cdot}$ (vide supra). The spectral parameters of bands A and B were also used to determine the effective electronic coupling parameters V_{LM} and $V_{MM'}$, taking as effective electron-transfer distances those measured between the N and the two Fe atoms in the crystal structure of **5f**. Both effective electronic couplings are moderate, indicating that the mixed-valence **5f**$^{+\cdot}$ also belongs to class II.[8] The relative values of V_{LM} and $V_{MM'}$ indicate that the IET may proceed through the two different pathways. The IET mediated by the bridge through a superexchange is apparently less effective than that in which the electron jumps into the bridge. It is also of interest to compare the effective electronic coupling between the two iron sites of **5f**$^{+\cdot}$ with that of the mixed-valence compound derived from 1,4-diferrocenyl-1,3-butadiene, i.e., $[Fc(CH=CH)_2Fc]^{+\cdot}$.[14] The latter compound has a $V_{MM'}$ of 430 cm^{-1}, which is larger than that of **5f**$^{+\cdot}$, suggesting that the replacement of an sp^2 C atom by an N atom in the 1,3-butadiene bridge results in a decrease of the interaction between both ferrocenes, probably because of a poorer overlap between the diabatic orbitals of the two ferrocenes with the orbital of the bridge involved in the superexchange mechanism. Indeed, in both types of systems the HOMO of the neutral molecule is the bridge-centered superexchange involved MO, which can be considered as being formed by a combination of the higher energy MO of π-type at the bridge and two $3e_2'$-based MOs of both ferrocene subunits (Figure 7). At the level of theory used, the latter is 0.953 eV higher in energy than the HOMO in 1,3-butadiene, but 1.587 eV higher than HOMO–1 in the 2-aza-1,3-butadiene, the HOMO being that containing the electron lone-pair at the N atom. (See Figure S3 in the Supporting Information). This leads to a poorer, although still significant, overlap between the diabatic orbitals of the two ferrocenes with the orbital of the bridge involved in the superexchange mechanism.

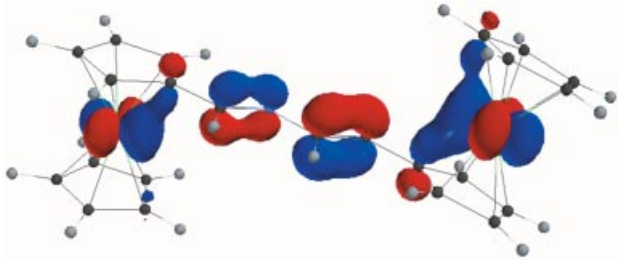

Figure 7. Superexchange-responsible MO (HOMO) in compound **5f** at a 0.050 isovalue.

For the mixed-valence **5f**$^{+\cdot}$ the free energy difference between the two electronic states having the charge localized on each Fe site is 3.2 kcal mol^{-1}. This relatively large value suggests that, at 300 K, the population of the state with the positive charge located on the iron attached to the 4-position of the 2-aza-1,3-butadiene bridge is dominant, with just a very small population (<0.1%) of the state with the charge on the other iron site. In addition, we can make a crude estimation of the thermal activation energy barrier for the interconversion of such two states, using the Marcus–Hush model.[40,41] The resulting thermal energy barrier of about 7.4 kcal mol^{-1} suggests a rate constant of about 10^8 s^{-1} at 300 K and hence any spectroscopic technique with a time scale faster than 10^9 s^{-1} should show the valence-localized mixed-valence complex **5f**$^{+\cdot}$, with the positive charge trapped on the Fe site attached at the 4-position of the bridge, at this temperature. This effect would be even more pronounced at temperatures below 100 K, so that with spectroscopic techniques such ^{57}Fe Mössbauer and EPR the valence should appear to be localized, as is indeed the case (see Supporting Information).

Conclusion and Perspectives

The presence of low-energy LMCT and IV-CT bands in the oxidized forms **5a**$^{+\cdot}$–**d**$^{+\cdot}$ and **5f**$^{+\cdot}$ of mono- and bis-ferrocenyl derivatives attached to a 2-aza-1,3-butadiene bridge indicates the existence of optically induced IETs between the metal units and the organic linkers. This important result demonstrates that the introduction of a heteroatom, like the N atom, in a conjugated organic bridge is an attractive strategy for promoting IET through an alternative pathway. This finding may have implications in the design of molecular electron-transfer materials and, in particular, in the development of new molecular devices that act as electronic relays which promote IET over large distances. Efforts in this direction are in progress in our laboratories using symmetrical compounds with two electroactive units attached to oxidizable, symmetrical, and conjugated organic bridges containing two heteroatoms.

Experimental Section

General Procedures: All reactions were carried out under N_2 and using solvents which were dried by routine procedures. All melting points were determined on a Kofler hot-plate melting point apparatus and are uncorrected. IR spectra were determined as Nujol emulsions or films on a Nicolet Impact 400 spectrophotometer. UV/Vis–near IR spectra were recorded on a Varian Cary 5 E spec-

trophotometer. ^{1}H and ^{13}C NMR spectra were recorded on a Bruker AC200, 300, or 400 spectrometer (200, 300, or 400 MHz for ^{1}H). Chemical shifts are referenced to signals of tetramethylsilane in the case of ^{1}H and ^{13}C NMR spectra and to 85% aqueous phosphoric acid in the case of ^{31}P NMR spectra. The EI and FAB$^+$ mass spectra were recorded on a Fisons AUTOSPEC 500 VG spectrometer, using 3-nitrobenzylalcohol as matrix. EPR spectra were obtained with an X-Band Bruker ESP 300E spectrometer equipped with a TE_{102} microwave cavity, a Bruker variable temperature unit, a field frequency lock system Bruker ER 033 M; line positions were determined with an NMR Gaussmeter Bruker ER 035 M. The modulation amplitude was kept well below the line width, and the microwave power was well below saturation. Crystallographic measurements were made at 233(2) K on a Bruker diffractometer equipped with an area detector positioned at the window of a rotating anode generator using Mo-K_α radiation (λ = 0.71073 Å). Mössbauer spectra were recorded on an ES-Technology MS-105 spectrometer, with a 100 MBq ^{57}Co source, in a rhodium matrix. Solid samples were prepared by grinding with boron nitride. Spectra were referenced to natural iron at 298 K. Parameters were obtained by fitting the data with Lorentzian lines; errors <0.01 mm s^{-1}. Microanalyses were performed on a Perkin–Elmer 240C instrument. The cyclic voltammetric measurements were performed on a QUICELTRON potentiostat/galvanostat controlled by a personal computer and driven by dedicated software. Cyclic voltammetry was performed with a conventional three-electrode configuration consisting of platinum working and auxiliary electrodes and an SCE reference electrode. The experiments were carried out with a 10^{-3} M solution of sample in dry CH_2Cl_2 containing 0.1 M $[N(nC_4H_9)_4]ClO_4$ as supporting electrolyte. Deoxygenation of the solutions was achieved by bubbling nitrogen for at least 10 min and the working electrode was cleaned after each run. The cyclic voltammograms were recorded with a scan rate increasing from 0.05 to 1.00 V s^{-1}. The square-wave voltammograms were recorded before and after addition of sequential additions of an aliquot of 0.1 equiv. of 2.5×10^{-2} M solutions of $HBF_4 \cdot Et_2O$ in CH_3CN. ΔE_s = 4 mV, ΔE_p = 25 mV, and f = 15 Hz. Decamethylferrocene (DMFe) (–0.07 V vs. SCE) was used as an internal reference both for potential calibration and for reversibility criteria. Oxidations were performed by electrolysis in a three-electrode cell under argon using dry CH_2Cl_2 as solvent and 0.15 M $[N(n\text{-}C_4H_9)_4]ClO_4$ as supporting electrolyte. The progress of the oxidation was followed coulometrically (or chronoamperometrically) by 263A of EG&PAR potentiostat-galvanostat. The reference electrode and the counter electrode were separately immersed in the solvent containing the supporting electrolyte and isolated from the bulk solution by a glass frit. The working electrode was a platinum grid. UV/Vis–near IR absorption spectra were regularly recorded by transferring a small aliquot of the solution contained in the electrochemical cell into a UV quartz cell for a different average number of removed electrons.

Theoretical Calculations: Geometry optimizations were performed with the Spartan'02 package (Spartan'02, build 119, Wavefunction Inc., Irvine, CA). For neutral compounds **5a**–**f** a preliminary optimization was done at the semi-empirical PM3(d) level and the obtained geometries were then refined at the DFT level of theory,[42] which has proved to be remarkably successful in reproducing experimental ground-state geometries and rotational barriers for ferrocenes.[43] The B3LYP functional[44] (Becke's three-parameter hybrid functional[45] with the Lee–Yang–Parr[46] correlation functional) and the 3-21G* basis set were used. Harmonic frequency calculations verified the nature of the stationary points as minima (all real frequencies).[47] The geometry of oxidized radical-cation species **5a**$^{+\cdot}$, **5c**$^{+\cdot}$, **5d**$^{+\cdot}$, and **5f**$^{+\cdot}$ were optimized starting from the corresponding neutral minimized structures with the appropriate charge and multiplicity constraints. Structure **5b**$^{+\cdot}$ was not calculated due to systematic failures in the SCF convergence. Similarly, **5f**$^{+\cdot}$ was used as the initial geometry for the fully oxidized **5f**$^{2+}$. Time-dependent DFT methods (TDDFT), as contained within the Gaussian 98 program suite,[48] performed as an SPE calculation at the same level as the minimized structures, were employed to study the excited states and model the UV/Vis–NIR electronic transitions in both neutral and oxidized species.

General Procedure for the Preparation of Diethyl *N*-Arylidene- and [(Ferrocenylmethylidene)aminomethyl]phosphonates 3: A mixture of diethyl aminomethylphosphonate (0.78 g, 4.64 mmol), an equimolar amount of the appropriate aldehyde **2**, and *p*-toluenesulfonic acid (0.01 g, 0.058 mmol) in dry benzene (50 mL) was stirred at room temperature for 4 h. Then, the flask was fitted with a Dean–Stark trap and a reflux condenser and heated overnight, atr reflux temperature, with constant removal of water. The reaction mixture was allowed to cool to room temperature and the solvent was removed under vacuum to give the corresponding diethyl phosphonates **3** as colored oils, which were used without further purification in the next step.

Diethyl [(*p*-Methoxybenzylidene)aminomethyl]phosphonate (3a): Yield: 95%. IR (Nujol): $\tilde{\nu}$ = 1641, 1609, 1577, 1524, 1444, 1422, 1396, 1316, 1252, 1166, 1102, 969 cm^{-1}. ^{1}H NMR ($CDCl_3$): δ = 1.34 (t, $^4J_{H,P}$ = 6.5 Hz, 6 H), 3.84 (s, 3 H), 4.07 (d, $^1J_{H,P}$ = 16.8 Hz, 2 H),4.19–4.09 (m, 4 H), 6.91 (d, J = 8.6 Hz, 2 H), 7.68 (d, J = 8.6 Hz, 2 H), 8.22 (d, $^4J_{H,P}$ = 4.7 Hz, 1 H) ppm. ^{13}C NMR ($CDCl_3$): δ = 16.5 (d, $^3J_{P,C}$ = 5.6 Hz, CH_3), 55.3 (CH_3O), 57.4 (d, $^1J_{P,C}$ = 152.6 Hz, NCH_2), 62.4 (d, $^2J_{P,C}$ = 6.7 Hz, OCH_2), 114.0 (CH_{Ar}), 128.7 (q), 130.0 (CH_{Ar}), 162.0 (q), 164.9 (d, $^3J_{P,C}$ = 16.0 Hz, CH=N) ppm. ^{31}P NMR ($CDCl_3$): δ = 22.68 ppm. EIMS: m/z (%) = 285 (100) [M$^+$], 152 (82), 148 (61), 125 (90), 121 (80), 97 (44), 91 (19), 78 (25).

Diethyl [(*p*-Nitrobenzylidene)aminomethyl]phosphonate (3b): Yield: 85%. IR (Nujol): $\tilde{\nu}$ = 1654, 1604, 1523, 1454, 1404, 1360, 1266, 1097, 1016, 966, 847 cm^{-1}. ^{1}H NMR ($CDCl_3$): δ = 1.34 (t, $^4J_{H,P}$ = 6.9 Hz, 6 H), 4.01–4.24 (m, 6 H), 7.91 (d, J = 8.0 Hz, 2 H), 8.26 (d, J = 8.0 Hz, 2 H), 8.40 (d, $^4J_{H,P}$ = 5.1 Hz, 1 H) ppm. ^{13}C NMR ($CDCl_3$): δ = 16.4 (d, $^3J_{P,C}$ = 5.7 Hz, CH_3), 57.7 (d, $^1J_{P,C}$ = 152.7 Hz, NCH_2), 62.7 (d, $^2J_{P,C}$ = 6.6 Hz, OCH_2), 123.8 (CH_{Ar}), 130.5 (CH_{Ar}), 140.9 (q), 149.2 (q), 163.2 (d, $^3J_{P,C}$ = 22.0 Hz, CH=N) ppm. ^{31}P NMR ($CDCl_3$): δ = 21.77 ppm. EIMS: m/z (%) = 300 (36) [M$^+$], 163 (60), 152 (96), 125 (82), 108 (100), 90 (95), 81 (42).

Diethyl [(Ferrocenylmethylidene)aminomethyl]phosphonate (3c): Yield: 94%. IR (Nujol): $\tilde{\nu}$ = 1642, 1473, 1448, 1398, 1241, 1166, 1035, 972, 828, 778 cm^{-1}. ^{1}H NMR ($CDCl_3$): δ = 1.38 (t, $^4J_{H,P}$ = 3.3 Hz, 6 H), 3.92 (d, 2 H, $^2J_{H,P}$ = 18 Hz), 4.08–4.25 (m, 4 H), 4.23 (s, 5 H), 4.36 (t, J = 1.8 Hz, 2 H), 4.64 (t, J = 1.8 Hz, 2 H), 8.19 (d, $^4J_{H,P}$ = 4.8 Hz, 1 H) ppm. ^{13}C NMR ($CDCl_3$): δ = 16.3 (d, $^3J_{P,C}$ = 5.7 Hz, CH_3), 57.2 (d, $^1J_{P,C}$ = 150.7 Hz, NCH_2), 62.4 (d, $^2J_{P,C}$ = 6.5 Hz, OCH_2), 68.5 (2 × CH, Cp), 69.1 (5 × CH, Cp), 70.6 (2 × CH, Cp), 79.7 (d, $^4J_{P,C}$ = 9 Hz, q, Cp), 166.2 (d, $^3J_{P,C}$ = 19.5 Hz, CH=N) ppm. ^{31}P NMR ($CDCl_3$): δ = 22.77 ppm. EIMS: m/z (%) = 363 (86) [M$^+$], 298 (100), 224 (39), 260 (48), 121 (63), 81 (25), 65 (9), 56 (24).

General Procedure for the Preparation of 1,4-Disubstituted-2-aza-1,3-butadienes 5: *n*-Butyllithium (1.6 M in hexane, 3 mL) was added dropwise to a solution of the appropriate diethyl phosphonate **3** (4.64 mmol) in dry THF (20 mL) at –78 °C under nitrogen. A solution of an equimolar amount of the appropriate aldehyde **4** (4.64 mmol) in dry THF (10 mL) was added dropwise to this stirred

solution and the mixture was stirred for 1.5 h. Then, the reaction mixture was allowed to reach room temperature and was heated at reflux temperature overnight. After the solution had cooled to room temperature, the solvent was evaporated under reduced pressure and the crude product was stirred with water (50 mL) and then extracted with dichloromethane (4 × 50 mL). The combined organic layers were dried with anhydrous Na_2SO_4 and, after filtration, the solution was concentrated to dryness to give a crude product which was crystallized from dichloromethane/diethyl ether (1:10).

4-Ferrocenyl-1-(*p*-methoxyphenyl)-2-aza-1,3-butadiene (5a): Yield: 90%; m.p. 175–176 °C. IR (Nujol): $\tilde{\nu}$ = 1605, 1511, 1456, 1395, 1240, 1162, 1107, 1074, 1046, 1024, 990, 985, 830, 741 cm^{-1}. ^1H NMR ($CDCl_3$): δ = 3.86 (s, 3 H), 4.15 (s, 5 H), 4.28 (t, J = 1.6 Hz, 2 H), 4.43 (t, J = 1.6 Hz, 2 H), 6.70 (d, J = 14.0 Hz, 1 H), 6.94 (d, J = 8.0 Hz, 2 H), 7.18 (d, J = 14.0 Hz, 1 H), 7.75 (d, J = 8.0 Hz, 2 H), 8.18 (s, 1 H) ppm. ^{13}C NMR ($CDCl_3$): δ = 55.3 (CH_3O), 67.0 (2 × CH, Cp), 69.0 (2 × CH, Cp), 69.3 (5 × CH, Cp), 81.5 (q, Cp), 114.2 (CH_{Ar}), 128.3 (CH=CH), 129.4 (q), 129.9 (CH_{Ar}), 139.7 (CH=CH), 158.0 (q), 161.5 (CH=N) ppm. EIMS: m/z (%) = 345 (100) [M^+], 280 (77), 278 (10), 121 (31), 56 (23). $C_{20}H_{19}FeNO$ (345.22): calcd. C 69.58, H 5.55, N 4.06; found C 69.35, H 5.40, N 4.15.

4-Ferrocenyl-1-(*p*-nitrophenyl)-2-aza-1,3-butadiene (5b): Yield: 50%; m.p. 223–224 °C. IR (Nujol): $\tilde{\nu}$ = 1600, 1514, 1454, 1335, 1182, 1109, 1030, 957, 745, 698 cm^{-1}. ^1H NMR ($CDCl_3$): δ = 4.12 (s, 5 H), 4.32 (t, J = 1.6 Hz, 2 H), 4.42 (t, J = 1.6 Hz, 2 H), 6.87 (d, J = 13.0 Hz, 1 H), 7.21 (d, J = 13.0 Hz, 1 H), 7.89 (d, J = 8.1 Hz, 1 H), 8.22 (s, 1 H), 8.23 (d, J = 8.1 Hz, 1 H) ppm. ^{13}C NMR ($CDCl_3$): δ = 67.5 (2 × CH, Cp), 69.6 (5 × CH, Cp), 69.9 (2 × CH, Cp), 80.4 (q), 124.2 (CH_{Ar}), 128.5 (CH_{Ar}), 134.0 (CH=CH), 138.6 (CH=CH), 142.3 (q), 148.5 (q), 154.7 (CH=N) ppm. EIMS: m/z (%) = 360 (100) [M^+], 330 (19), 295 (23), 265 (21), 192 (34), 165 (30), 121 (62). $C_{19}H_{16}FeN_2O_2$ (360.19): calcd. C 63.36, H 4.48, N 7.78; found C 63.54, H 4.35, N 7.69.

1-Ferrocenyl-4-(*p*-methoxyphenyl)-2-aza-1,3-butadiene (5c): Yield: 85%; m.p. 102–103 °C. IR (Nujol): $\tilde{\nu}$ = 1645, 1605, 1565, 1514, 1250, 1176, 1107, 1038, 969, 826 cm^{-1}. ^1H NMR ($CDCl_3$): δ = 3.82 (s, 3 H), 4.22 (s, 5 H), 4.47 (t, J = 1.6 Hz, 2 H), 4.73 (t, J = 1.6 Hz, 2 H), 7.34 (d, J = 14.0 Hz, 1 H), 7.40 (d, J = 8.0 Hz, 2 H), 7.82 (d, J = 14.0 Hz, 1 H), 7.88 (d, J = 8.0 Hz, 2 H), 8.21 (s, 1 H) ppm. ^{13}C NMR ($CDCl_3$): δ = 55.2 (CH_3O), 68.7 (2 × CH, Cp), 68.9 (5 × CH, Cp), 71.1 (2 × CH, Cp), 80.4 (q), 114.1 (CH_{Ar}), 127.5 (CH_{Ar}), 127.6 (CH=CH), 129.3 (q), 141.0 (CH=CH), 159.0 (q), 161.5 (CH=N) ppm. EIMS: m/z (%) = 345 (100) [M^+], 318 (40), 279 (24), 278 (14), 186 (43), 121 (66), 56 (39). $C_{20}H_{19}FeNO$ (345.22): calcd. C 69.58, H 5.55, N 4.06; found C 69.33, H 5.28, N 4.21.

1-Ferrocenyl-4-(*p*-nitrophenyl)-2-aza-1,3-butadiene (5d): Yield: 40%; m.p. 182–183 °C. IR (Nujol): $\tilde{\nu}$ = 1561, 1508, 1438, 1337, 1225, 1177, 1123, 1107, 1033, 750, 696 cm^{-1}. ^1H NMR ($CDCl_3$): δ = 4.24 (s, 5 H), 4.56 (t, J = 1.6 Hz, 2 H), 4.78 (t, J = 1.6 Hz, 2 H), 6.87 (d, J = 13.4 Hz, 1 H), 7.52 (d, J = 8.0 Hz, 2 H), 7.55 (d, J = 13.4 Hz, 1 H), 8.18 (d, J = 8.0 Hz, 2 H), 8.35 (s, 1 H) ppm. ^{13}C NMR ($CDCl_3$): δ = 69.4 (2 × CH, Cp), 69.6 (5 × CH, Cp), 72.1 (2 × CH, Cp), 79.6 (q), 124.2 (CH_{Ar}), 125.2 (CH=CH), 126.6 (CH_{Ar}), 143.7 (q), 146.4 (q), 146.5 (CH=CH), 165.9 (CH=N) ppm. EIMS: m/z (%) = 360 (100) [M^+], 333 (22), 192 (22), 186 (34), 165 (27), 120 (63), 56 (33). $C_{19}H_{16}FeN_2O_2$ (360.19): calcd. C 63.36, H 4.48, N 7.78; found C 63.19, H 4.29, N 7.62.

1,4-Bis(*p*-methoxyphenyl)-2-aza-1,3-butadiene (5e): Yield: 85%; m.p. 170–172 °C. IR (Nujol): $\tilde{\nu}$ = 1647, 1609, 1553, 1510, 1454, 1423, 1373, 1311, 1280, 1255, 1174, 1111, 1024, 986, 943, 875, 813 cm^{-1}. ^1H NMR ($CDCl_3$): δ = 3.80 (s, 3 H), 3.84 (s, 3 H), 6.86 (d, J = 8.0 Hz, 2 H), 6.91 (d, J = 14.1 Hz, 1 H), 6.94 (d, J = 8.0 Hz, 2 H), 7.40 (d, J = 8.0 Hz, 2 H), 7.44 (d, J = 14.1 Hz, 1 H), 7.76 (d, J = 8.0 Hz, 2 H), 8.25 (s, 1 H) ppm. ^{13}C NMR ($CDCl_3$): δ = 55.2, 55.3, 114.0, 114.1, 127.8, 129.2, 129.4, 130.0, 140.4, 159.2, 159.7, 161.8 ppm. EIMS: m/z (%) = 267 (100) [M^+], 252 (44), 236 (28), 160 (69), 121 (35), 91 (28). $C_{17}H_{17}NO_2$ (267.33): calcd. C 76.38, H 6.41, N 5.24; found C 76.20, H 6.67, N 5.12.

1,4-Bis(ferrocenyl)-2-aza-1,3-butadiene (5f): Yield: 87%; m.p. 253–255 °C. IR (Nujol): $\tilde{\nu}$ = 1649, 1580, 1102, 1023, 1041, 1003, 966, 829, 810 cm^{-1}. ^1H NMR ($CDCl_3$): δ = 4.15 (s, 5 H), 4.22 (s, 5 H), 4.27 (s, 2 H), 4.40 (s, 2 H), 4.45 (s, 2 H), 4.72 (s, 2 H), 6.60 (d, J = 13.2 Hz, 1 H), 7.05 (d, J = 13.2 Hz, 1 H), 8.11 (s, 1 H) ppm. ^{13}C NMR ($CDCl_3$): δ = 66.80 (2 × CH, Cp), 68.61 (2 × CH, Cp), 69.00 (2 × CH, Cp), 69.20 (10 × CH, Cp), 71.00 (2 × CH, Cp), 80.81 (q, Cp), 82.11 (q, Cp), 126.32 (CH=), 140.32 (=CH-N), 159.82 (CH=N) ppm. EIMS: m/z (%) = 423 (100) [M^+], 358 (60), 212 (32), 186 (28), 121 (64), 56 (25). $C_{23}H_{21}Fe_2N$ (423.12): calcd. C 65.29, H 5.00, N 3.31; found C 65.40, H 4.88, N 3.50.

Preparation of the Mixed-Valence Compound $5f^+I_3^-$: A sample of this mixed-valence compound was prepared by adding a solution of iodine (0.030 g, 0.12 mmol) in dry benzene (5 mL) to a solution of 1,4-diferrocenyl-2-aza-1,3-butadiene (0.1 g, 0.24 mmol) in the same solvent (50 mL). The reaction mixture was stirred at room temperature under nitrogen for 1 h and the dark-purple microcrystals formed were collected by filtration and washed with three portions of benzene and one portion of diethyl ether. The solid obtained was dried in a dessicator overnight. FAB MS: m/z (%) = 424 (100) [M^+ + 1]. $C_{23}H_{21}Fe_2I_3N$ (803.82): calcd. C 34.33, H 2.61, N 1.74; found C 34.23, H 2.38, N 1.58.

Supporting Information: Crystal data of **5b**, **5d**, and **5f**, optical absorption data of oxidized species and the procedure for their analysis with the Marcus–Hush model, and ^{57}Fe Mössbauer and EPR spectra are provided.

Acknowledgments

We gratefully acknowledge the financial support of the DGI, Ministerio de Ciencia y Tecnología, Spain (projects MAT2003-04699 and CTQ2004-02201), the Fundación Séneca (CARM) (project no. PB/72/FS/02), and DGR, Catalunya (2001 SGR00362). The Biotechnology and Biological Sciences Research Council, UK, is also thanked for funding (D.J.E.).

[1] a) D. Segal, A. Nitzan, W. B. Davis, M. R. Wasielewski, M. A. Ratner, *J. Phys. Chem. B.* **2000**, *104*, 3817–3829; b) M. N. Paddow-Row, in *Electron Transfer in Chemistry* (Ed.: V. Balzani), Wiley-VCH, Weinheim, **2001**, pp. 179–271; c) L. DeCola, P. Belser, in *Electron Transfer in Chemistry* (Ed.: V. Balzani), Wiley-VCH, Weinheim, **2001**, pp. 97–136; d) K. Kilsa, J. Kajanus, A. N. Macpherson, J. Martensson, B. Albinsson, *J. Am. Chem. Soc.* **2001**, *123*, 3069–3080; e) J.-P. Launay, *Chem. Soc. Rev.* **2001**, *30*, 386–397; f) M. D. Newton, *Chem. Rev.* **1991**, *91*, 767–792; g) S. F. Nelsen, R. F. Ismagilov, D. F. Powell, *J. Am. Chem. Soc.* **1998**, *120*, 1924–1925; h) W. B. Davis, W. A. Svec, M. A. Ratner, M. R. Wasielewski, *Nature* **1998**, *396*, 60–53; i) D. S. Weiss, J. R. Cowdery, R. H. Young, in *Electron Transfer in Chemistry* (Ed.: V. Balzani), Wiley-VCH, Weinheim, **2001**, pp. 379–471; j) H. Bassler, in *Semiconducting Polymers* (Eds.: G. Hadziioannou, P. F. van Hutten), Wiley-VCH, Weinheim, **2000**, pp. 365–410.

[2] a) U. T. Müller-Westerhoff, *Angew. Chem. Int. Ed. Engl.* **1986**, *25*, 702–717; b) E. E. Bunel, P. Campos, J. Ruz, L. Valle, I. Chadwick, M. Santa Ana, G. Gonzalez, J. M. Manriquez, *Organometallics* **1988**, *7*, 474–476; c) E. E. Bunel, L. Valle, N. L. Jones, P. J. Carroll, M. Gonzalez, N. Muñoz, J. M. Manriquez, *Organometallics* **1988**, *7*, 789–791; d) H. Atzkern, B. Huber, F. H. Köhler, G. Müller, R. Müller, *Organometallics* **1991**, *10*, 238–244; e) J. Hiermeier, F. H. Köhler, G. Müller, *Organometallics* **1991**, *10*, 1787–1793.

[3] a) A. C. Benniston, V. Goulle, A. Harriman, J. M. Lehn, B. Marczinke, *J. Phys. Chem.* **1994**, *98*, 7798–7804; b) M. Haga, M. M. Ali, S. Koseki, K. Fujimoto, A. Yoshimura, K. Nozaki, T. Ohno, K. Nakajima, D. J. Stufkens, *Inorg. Chem.* **1996**, *35*, 3335–3347; c) M. E. Elliot, D. L. Derr, S. Ferrere, M. D. Newton, Y. P. Liu, *J. Am. Chem. Soc.* **1996**, *118*, 5221–5228; d) C. Pataoux, C. Coudret, J. P. Launay, C. Joachim, A. Gourdon, *Inorg. Chem.* **1997**, *36*, 5037–5049; e) J.-P. Sauvage, J.-P. Collin, J.-C. Chambron, S. Guillerez, C. Coudret, *Chem. Rev.* **1994**, *94*, 993–1019; f) N. S. Hush, *Coord. Chem. Rev.* **1985**, *64*, 135–157; g) A. C. Ribou, J. P. Launay, K. Takhashi, T. Nihira, S. Tarutani, C. W. Spangler, *Inorg. Chem.* **1994**, *33*, 1325–1329.

[4] a) C. Creutz, *Prog. Inorg. Chem.* **1983**, *30*, 1–73; b) R. J. Crutchley, *Adv. Inorg. Chem.* **1994**, *41*, 273–325; c) S. Barlow, D. O'Hare, *Chem. Rev.* **1997**, *97*, 637–669; d) N. S. Hush, *Prog. Inorg. Chem.* **1967**, *8*, 391–444.

[5] a) C. Lambert, G. Nöll, J. Schelter, *Nat. Mater.* **2002**, *1*, 69–73; b) P. J. Low, M. A. J. Paterson, H. Puchmann, A. E. Goeta, J. A. K. Howard, C. Lambert, J. C. Cherryman, D. R. Tackley, S. Leeming, B. Brown, *Chem. Eur. J.* **2004**, *10*, 83–91.

[6] W. H. Morrison, S. Krogsrud, D. N. Hendrickson, *Inorg. Chem.* **1973**, *12*, 1998–2004.

[7] a) F. Delgado-Pena, D. R. Talham, D. O. Cowan, *J. Organomet. Chem.* **1983**, *253*, C43–C46; b) M. F. Moore, S. R. Wilson, D. N. Hendrickson, U. T. Mueller-Westerhoff, *Inorg. Chem.* **1984**, *23*, 2918–2920; c) M. F. Moore, S. R. Wilson, M. J. Cohn, T. Y. Dong, U. T. Mueller-Westerhoff, D. N. Hendrickson, *Inorg. Chem.* **1985**, *24*, 4559–4565.

[8] M. Robin, P. Day, *Adv. Inorg. Radiochem.* **1967**, *10*, 247–422.

[9] a) T. Y. Dong, T. J. Ke, S. M. Peng, S. K. Yeh, *Inorg. Chem.* **1989**, *28*, 2103–2106; b) B. Floris, P. Tagliatesta, *J. Chem. Res., Synop.* **1993**, 42–43.

[10] C. Le Vanda, K. Bechgaard, D. O. Covan, *J. Org. Chem.* **1976**, *41*, 2700–2704.

[11] I. Motoyama, M. Watanabe, H. Sano, *Chem. Lett.* **1978**, 513–516.

[12] C. Jutz, *Tetrahedron Lett.* **1959**, 1–4.

[13] a) J. Lukasser, H. Angleitner, H. Schottenberger, H. Kopacka, M. Schweiger, B. Bildstein, K. H. Ongania, K. Wurst, *Organometallics* **1995**, *14*, 5566–5578; b) A. Tárraga, P. Molina, J. L. López, A. Espinosa, D. J. Evans, *Tetrahedron Lett.* **2002**, *43*, 4717–4720.

[14] A. C. Ribou, J. P. Launay, M. L. Sachtleben, H. Li, C. W. Spangler, *Inorg. Chem.* **1996**, *35*, 3735–3740.

[15] B. Bildstein, M. Malaun, H. Kopacka, M. Fontani, P. Zanello, *Inorg. Chim. Acta* **2000**, *300–302*, 16–22.

[16] a) A. G. Osborne, M. W. da Silva, M. B. Hursthouse, K. M. A. Malik, G. Opromolla, P. J. Zanello, *J. Organomet. Chem.* **1996**, *516*, 167–176; b) V. A. Sauro, M. S. Worketin, *Can. J. Chem.* **2002**, *80*, 250–256.

[17] a) A. Tárraga, P. Molina, D. Curiel, M. D. Velasco, *Organometallics* **2001**, *20*, 2145–2152; b) A. Tárraga, P. Molina, D. Curiel, M. D. Velasco, *Tetrahedron Lett.* **2002**, *43*, 8453–8457.

[18] S. K. Davidsen, G. W. Phillips, S. F. Martin, *Org. Synth.* **1993**, *8*, 451–458.

[19] P. Séller, J. D. Dunitz, *Acta Crystallogr., Sect. B* **1982**, *38*, 1741.

[20] J. L. López, A. Tárraga, A. Espinosa, M. D. Velasco, P. Molina, V. Lloveras, J. Vidal-Gancedo, C. Rovira, J. Veciana, D. J. Evans, K. Wurst, *Chem. Eur. J.* **2004**, *10*, 1815–1826.

[21] a) G. L. Geoffroy, M. S. Wrighton, *Organometallic Photochemistry*, Academic Press, New York, **1979**; b) Y. S. Sohn, D. N. Hendrickson, H. B. Gray, *J. Am. Chem. Soc.* **1971**, *93*, 3603–3612.

[22] S. Barlow, H. E. Bunting, C. Ringham, J. C. Green, G. U. Bublitz, S. G. Boxer, J. W. Perry, S. R. Marder, *J. Am. Chem. Soc.* **1999**, *121*, 3715–3723.

[23] N. G. Connelly, W. E. Geiger, *Chem. Rev.* **1996**, *96*, 877–910.

[24] V. Alain, A. Fort, M. Barzoukas, T.-H. Chen, S. R. Blanchard-Desce, S. R. Marder, J. W. Perry, *Inorg. Chim. Acta* **1996**, *242*, 43–49.

[25] M. Masui, H. J. Ohmori, *J. Chem. Soc., Perkin Trans. 2* **1972**, 1882–1887.

[26] a) Y. B. Zu, M. O. Wolff, *Chem. Mater.* **1999**, *11*, 2995–3001; b) Y. B. Zu, D. B. Millet, M. O. Wolf, S. J. Rettig, *Organometallics* **1999**, *18*, 1930–1938.

[27] Y. B. Zu, M. O.Wolf, *J. Am. Chem. Soc.* **2000**, *122*, 10121–10125.

[28] a) I. Yamaguchi, T. Sakano, H. Ishii, K. Osakada, T. Yamamoto, *J. Organomet. Chem.* **1999**, *584*, 213–216; b) M. Horie, T. Sakano, K. Osakada, H. Nakao, *Organometallics* **2004**, *23*, 18–20; c) M. Horie, Y. Suzaki, K. Osakada, *J. Am. Chem. Soc.* **2004**, *126*, 3684–3685.

[29] M. Turki, C. Daniel, S. Zalis, A. Vicek, J. van Slageren, D. J. Stufkens, *J. Am. Chem. Soc.* **2001**, *123*, 11431–11440.

[30] M. C. B. Colbert, J. Lewis, N. J. Long, P. R. Raithby, M. Younus, A. J. P. White, D. J. Williams, N. N. Payne, L. Yellowlees, D. Beljonne, N. Chawdhury, R. H. Friend, *Organometallics* **1998**, *17*, 3034–3043.

[31] Y. Zhu, O. Clot, M. O. Wolf, G. P. A. Yap, *J. Am. Chem. Soc.* **1998**, *120*, 1812–1821.

[32] C. Lambert, G. Nöll, *J. Am. Chem. Soc.* **1999**, *121*, 8434–8442.

[33] a) P. Desjardins, G. P. A. Yap, R. J. Crutchley, *Inorg. Chem.* **1999**, *38*, 5901–5905; b) C. E. B. Evans, M. L. Naklicki, R. J. Crutchley, *Inorg. Chem.* **1995**, *34*, 1350–1354.

[34] T. Ito, N. Imai, T. Yamagushi, T. Hamaguchi, C. H. Londergan, C. P. Kubiak, *Angew. Chem. Int. Ed.* **2004**, *43*, 1376–1381 and references cited therein.

[35] I. R. Gould, D. Noukakis, L. Gómez-Jahn, R. H. Young, J. L. Goodman, S. Farid, *Chem. Phys.* **1993**, *176*, 439–456.

[36] C. Joachim, *Thesis*, Université Paul Sabatier, Tolouse, France, **1990**, pp. 146, 211, and 214.

[37] The proportion of mixed-valence species at half-oxidation (*P*), where $P = K_c^{1/2}/(2 + K_c^{1/2})$ is generally used to compute the intensity of corrected spectra. The comproportionation constant, K_c, which is related to the thermodynamic stability of the mixed-valence compound, of the equilibrium of comproportionation, $[Fe^{II}\text{-L-}F^{II}] + [Fe^{III}\text{-L-}F^{III}] \leftrightharpoons 2[Fe^{II}\text{-L-}F^{III}]$, was calculated for **5f** from the electrochemical data, giving a value of 3.6×10^3. With such a high value of K_c, *P* is almost 100% so that the dependency on K_c is very small and it is not necessary to correct the intensity of the spectrum.

[38] a) E. M. Kober, K. A. Goldsby, D. N. S. Narayane, T. J. Meyer, *J. Am. Chem. Soc.* **1983**, *105*, 4303–4309; b) P. A. Lay, R. H. Magnuson, H. Taube, *Inorg. Chem.* **1988**, *27*, 2364–2371; c) W. M. Laidlaw, R. G. Denning, *J. Chem. Soc., Dalton Trans.* **1994**, 1987–1994.

[39] a) D. E. Richardson, H. Taube, *J. Am. Chem. Soc.* **1983**, *105*, 40–51; b) J. Halpern, L. E. Orgel, *Discuss. Faraday Soc.* **1960**, *29*, 32–41.

[40] According to Hush and Marcus, for symmetrical weakly coupled class II mixed-valence complexes the activation barrier to electron transfer is given by $\Delta G_{MM'}^* = \lambda_{MM'}/4 - V_{MM'} + (V_{MM'}^2/\lambda_{MM'})$; see ref.[41]. With the parameters given in Table 5 for $\mathbf{5f}^{+\cdot}$, a value of $\Delta G_{MM'}^* + \Delta G^\circ_{MM'} = 7.4$ kcal mol^{-1} is obtained for the 4-Fe^{3+} + 1-Fe^{2+} → 4-Fe^{2+} + 1-Fe^{3+} process. The corresponding first-order rate constant (k_{th})can be calculated from $k_{th} = k \cdot \nu_n \cdot \exp(-\Delta G_{MM'}^*/RT)$ where $k = 1$, since the reaction is adiabatic, and the nuclear frequency factor, ν_n, is $2.00 \times 10^{+13}$ s^{-1}, as determined from $\nu_n = [2(V_{MM'})^2/h] \cdot [(\pi^3/\lambda_{MM'}RT)^{1/2}]$. This gives a value for k_{th} of $8.8 \times 10^{+7}$ s^{-1} at 300 K.

[41] a) R. A. Marcus, *J. Chem. Phys.* **1956**, *24*, 966–978; b) R. A. Marcus, *J. Chem. Phys.* **1965**, *43*, 679; c) R. A. Marcus, N. Sutin, *Inorg. Chem.* **1975**, *14*, 213–216; d) C. Creutz, M. D. Newton, N. Sutin, *J. Photochem. Photobiol. Sect. A* **1994**, *82*, 47–59.
[42] a) E. J. Baerends, D. E. Ellis, P. Ros, *Chem. Phys.* **1973**, *2*, 41–51; b) W. Kohn, A. D. Becke, R. G. Parr, *J. Phys. Chem.* **1996**, *100*, 12974–12980.
[43] a) A. Berces, T. Ziegler, L. Fan, *J. Phys. Chem.* **1994**, *98*, 1584–1595; b) A. Berces, T. Ziegler, *Top. Curr. Chem.* **1996**, *182*, 41–85; c) U. Hohm, D. Goebel, S. Grimme, *Chem. Phys. Lett.* **1997**, *272*, 328–334; d) C. A. Morrison, S. F. Bone, D. W. H. Rankin, H. E. Robertson, F. Parsons, R. A. Coxall, S. Fraser, J. A. S. Howell, P. C. Yates, N. Fey, *Organometallics* **2001**, *20*, 2309–2320.
[44] L. J. Bartolotti, K. Fluchick, in *Reviews in Computational Chemistry* (Eds.: K. B. Lipkowitz, B. D. Boyd), VCH Publishers, New York, **1996**, vol. 7, pp. 187–216.
[45] A. D. Becke, *J. Chem. Phys.* **1993**, *98*, 5648–5652.
[46] C. Lee, W. Yang, R. G. Parr, *Phys. Rev. B* **1988**, *37*, 785–789.
[47] J. W. McIver, A. K. Komornicki, *J. Am. Chem. Soc.* **1972**, *94*, 2625–2633.
[48] Gaussian 98, Revision A.9, M. J. Frisch, G. W. Trucks, H. B. Schlegel, G. E. Scuseria, M. A. Robb, J. R. Cheeseman, V. G. Zakrzewski, J. A. Montgomery Jr., R. E. Stratmann, J. C. Burant, S. Dapprich, J. M. Millam, A. D. Daniels, K. N. Kudin, M. C. Strain, O. Farkas, J. Tomasi, V. Barone, M. Cossi, R. Cammi, B. Mennucci, C. Pomelli, C. Adamo, S. Clifford, J. Ochterski, G. A. Petersson, P. Y. Ayala, Q. Cui, K. Morokuma, D. K. Malick, A. D. Rabuck, K. Raghavachari, J. B. Foresman, J. Cioslowski, J. V. Ortiz, A. G. Baboul, B. B. Stefanov, G. Liu, A. Liashenko, P. Piskorz, I. Komaromi, R. Gomperts, R. L. Martin, D. J. Fox, T. Keith, M. A. Al-Laham, C. Y. Peng, A. Nanayakkara, M. Challacombe, P. M. W. Gill, B. Johnson, W. Chen, M. W. Wong, J. L. Andres, C. Gonzalez, M. Head-Gordon, E. S. Replogle, J. A. Pople, Gaussian, Inc., Pittsburgh PA, **1998**.
[49] R. Gleiter, R. Seeger, *Helv. Chim. Acta* **1971**, *54*, 1217–1220..
Received: November 30, 2004

Sensors

An Electroactive Nitrogen-Rich [4.4]Ferrocenophane Displaying Redox-Switchable Behavior: Selective Sensing, Complexation, and Decomplexation of Mg^{2+} ions**

Antonio Caballero, Vega Lloveras, Alberto Tárraga, Arturo Espinosa, María D. Velasco, José Vidal-Gancedo, Concepció Rovira, Klaus Wurst, Pedro Molina, and Jaume Veciana**

Redox-responsive ligands that contain a ferrocene unit as the redox-active group have been one of the most extensively studied groups among the numerous examples of these ligands.[1] These ferrocene-containing ligands have been widely investigated because of their electrochemical response upon complexation of a suitable guest molecule or ion. A positive shift of the Fe^{II}/Fe^{III} redox couple is observed on coordination of a metal ion because the proximity of the metal alters the ability of the ferrocene framework to be oxidized.[1,2] A further exciting challenge that has been less explored is the design of redox-switchable ligands that are not only able to monitor binding (namely, a shift in the $E_{1/2}$ value upon metal complexation is observed) but are also able to act as an actuator through the progressive electrochemical release of the metal cation (that is, the binding constant upon electrochemical oxidation is decreased). In this context, some electroactive tetrathiafulvalene (TTF) derivatives that exist in three different redox stages (as a neutral species, radical cation, and dication) have been described as tunable materials that can bind a metal cation when neutral (TTF) and then expel it upon oxidation (TTF^{2+}).[3] This is an

[*] A. Caballero, Prof. A. Tárraga, Dr. A. Espinosa, Dr. M. D. Velasco, Prof. P. Molina
Universidad de Murcia
Departamento de Química Orgánica, Facultad de Química
Campus de Espinardo, 30100 Murcia (Spain)
Fax: (+34) 968-364-149
E-mail: pmolina@um.es

V. Lloveras, Dr. J. Vidal-Gancedo, Prof. C. Rovira, Prof. J. Veciana
Institut de Ciencia de Materials de Barcelona (CSIC)
Campus Universitari de Bellaterra
08193 Cerdanyola (Spain)
Fax: (+34) 935-805-729
E-mail: vecianaj@icmab.es

Dr. K. Wurst
Institut für Allgemeine, Anorganische und Theoretische Chemie
Universität Innsbruck
Innrain 52a, A-6020 Innsbruck (Austria)

[**] This work was supported by the Dirección General de Investigación (Spain) (projects MAT2003-04699 and BQU 2001-0014), Generalitat de Catalunya (2001SGR00362 and CERMAE), and Fundación Séneca CARM (PB/72/FS/02). We also thank Acción Integrada Hispano-Austríaca HU20020046, and V.L. is grateful to the Ministerio de Educación y Ciencia for a predoctoral grant.

Supporting information for this article is available on the WWW under http://www.angewandte.org or from the author.

 DOI: 10.1002/ange.200462521

unfamiliar area in ferrocene-based ligands and it has been only described in a very few cases: first, in an early report about the abrupt decrease in the binding strength of Na^+ ions by electrochemical oxidation of a pentaoxa[13]ferrocenophane[4] and then, later on, in a few compounds that had only one ferrocenyl redox-active center.[5]

On the basis of this work, we designed a new highly preorganized molecular system that links two ferrocene subunits that have dissimilar electronic environments through a conjugated double bridge, which comprises a putative cation-binding site. This molecular system should show three different oxidation states with different binding abilities so that a metal cation can be bound in its neutral state and then released upon oxidation of the complexed species. Herein, we report the preparation of one such system, the redox-switchable, azaferrocenophane ligand **4**, that fulfils those electronic and structural characteristics. We also report the ability of **4** to selectively recognize Mg^{2+} ions and the unequivocal demonstration of electrochemical-mediated control of successive trapping and expulsion of Mg^{2+} ions. Furthermore, the ability of **4** to transport Mg^{2+} ions through a liquid membrane is described, in which the switchable activation/deactivation of the ligand is carried out electrochemically.

Compound **4** was prepared (Scheme 1) from the readily available diethyl aminomethylphosphonate (**1**),[6] which was

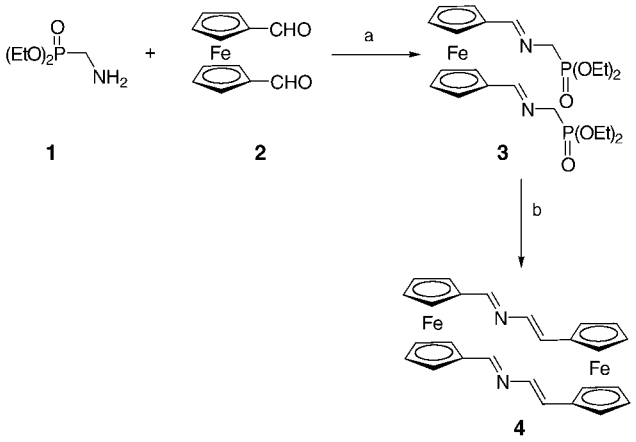

Scheme 1. Synthesis of 2,17-diaza[4,4]ferrocenophane **4**: a) anhydrous Na_2SO_4/CH_2Cl_2, RT, 4 h; b) *n*BuLi/THF, −78 °C, and then **2**, 12 h, RT.

condensed with 1,1′-diformylferrocene[7] (**2**) to give the corresponding *N*-substituted diethyl aminomethylphosphonate **3** in excellent yield (95%). Generation of the metalloenamine by reaction with *n*BuLi at −78 °C and subsequent reaction with one equivalent of 1,1′-diformylferrocene (**2**) provided 2,17-diaza[4,4]ferrocenophane **4** in 31% yield, which was recrystallized from THF and characterized by ^{1}H NMR and ^{13}C NMR spectroscopic, FAB mass-spectrometric, and elemental analysis.

The X-ray crystal structure reveals that the two bridges of compound **4** are in the *E*,*E* form in the solid state (and also in solution as observed by ^{1}H NMR spectroscopy) and that they have an *s-trans* configuration (Figure 1).[8] Consequently, ferrocenophane **4** has two nitrogen atoms that are arranged

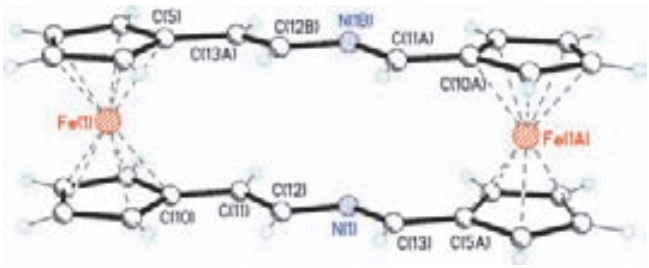

Figure 1. Crystal structure of the ferrocenophane **4**.

in such a way that they can act as a chelating agent for a metal cation: the nitrogen atoms are eclipsed at a distance of 3.48 Å and have their nonbonding pair of electrons on the same side of the molecule.

One of the most interesting attributes of ferrocenophane **4** is the presence of two differentiated redox-active ferrocene moieties close to the cation-binding bisaldimine site. The metal-recognition properties of **4** were evaluated by optical and electrochemical analysis. The cyclic voltammetric (CV) and Osteryoung square-wave voltammetric (OSWV) analyses of **4** (Figure 2) show two well-resolved quasi-reversible one-electron oxidations in a 1:1 ratio at formal potentials of +0.44 and +0.89 V versus decamethylferrocene (DMFc). The first reversible oxidation process arises from the oxidation of the ferrocene unit at the 4-position of the two bridges, while the second is associated with the oxidation of the ferrocene unit at

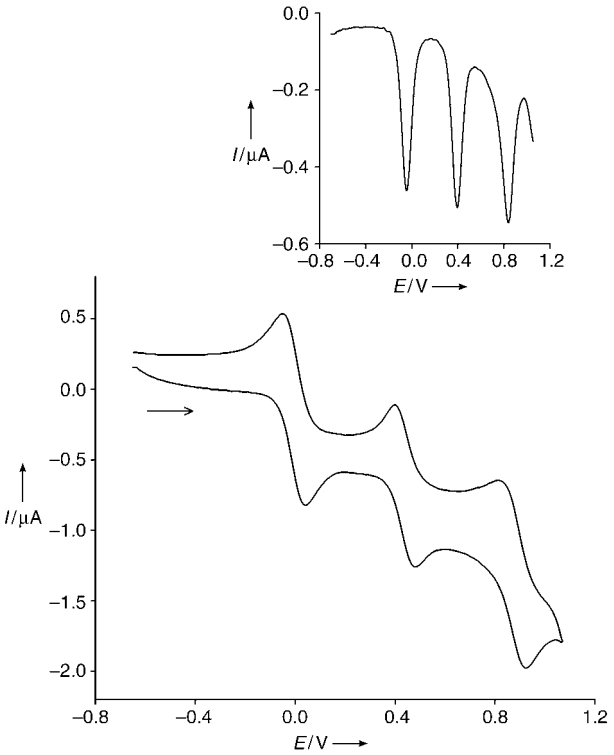

Figure 2. Cyclic voltammogram of **4** in CH_2Cl_2. Conditions: 1 mM of **4** and 0.1 M nBu_4NClO_4, a Pt-disk electrode, and a scan rate of 0.1 Vs^{-1} in the presence of DMFc as the internal standard. Upper inset: square-wave voltammogram of compound **4** (1 mM) in $CH_2Cl_2/(nBu)_4N^+ClO_4^-$ recorded at 0.1 Vs^{-1}.

the 1-position. Whereas, no perturbation of the voltammograms was observed upon addition of Ca^{2+}, Li^{+}, Na^{+}, and K^{+} ions, even in a large excess, a significant modification was observed for the first oxidation wave upon addition of Mg^{2+} ions (see the Supporting Information). In contrast, the second oxidation wave was apparently not perturbed on the addition of Mg^{2+} ions. This particular behavior is characteristic of a large equilibrium constant for the binding of Mg^{2+} ions by the neutral receptor.[9] The fact that the second oxidation process of complex $[Mg_2(\mathbf{4})]^{4+}$ practically occurs at the same potential as that observed for the free ligand **4** (that is, the $\mathbf{4}^{+}/\mathbf{4}^{2+}$ couple) suggests that the complex is disrupted after the first monoelectronic oxidation of complex $[Mg_2(\mathbf{4})]^{4+}$ and the second oxidation really takes place on the uncomplexed mono-oxidized species $\mathbf{4}^{+}$. Therefore, ligand **4** behaves as a switchable receptor that appears to be a very attractive carrier for the selective transport of Mg^{2+} ions.

The UV/Vis spectrum of the neutral ligand **4** is characterized by a very strong absorption band at 331 nm ($\varepsilon = 17200\,\text{M}^{-1}\text{cm}^{-1}$), which is assigned to a high-energy ligand-centred π–π* electronic transition, and a lower-energy weaker band at 500 nm ($\varepsilon = 1600\,\text{M}^{-1}\text{cm}^{-1}$), which is attributed to a metal-to-ligand charge-transfer (CT) process (d–π*).[10] Such spectral characteristics confer an orange color to the neutral ferrocenophane **4**. The mono-oxidized species $\mathbf{4}^{+}$ has a remarkable green–brown color and exhibits absorption bands at 355 nm ($\varepsilon = 17000\,\text{M}^{-1}\text{cm}^{-1}$) and 528 nm ($\varepsilon = 1900\,\text{M}^{-1}\text{cm}^{-1}$) along with a weak CT band at 1353 nm ($\varepsilon = 400\,\text{M}^{-1}\text{cm}^{-1}$). The presence of this weak CT band is a clear manifestation of the electronic coupling between the two redox-active ferrocene groups through the conjugated azadiene bridges. The dioxidized species $\mathbf{4}^{2+}$ exhibits a yellowish color and shows absorption bands at 334 nm ($\varepsilon = 17600\,\text{M}^{-1}\text{cm}^{-1}$) and 512 nm ($\varepsilon = 1400\,\text{M}^{-1}\text{cm}^{-1}$) along with one ligand-to-metal CT band at 1027 nm ($\varepsilon = 290\,\text{M}^{-1}\text{cm}^{-1}$).

The addition of increasing amounts of $Mg(ClO_4)_2$ to a solution of **4** in CH_2Cl_2 caused a progressive appearance of a band at 350 nm ($\varepsilon = 19900\,\text{M}^{-1}\text{cm}^{-1}$) and a new, more intense band located at $\lambda = 520$ nm ($\varepsilon = 3700\,\text{M}^{-1}\text{cm}^{-1}$) as well as the complete disappearance of the initial band at 500 nm. A well-defined isosbestic point at 339 nm indicates that a neat interconversion between the uncomplexed and complexed species occurs (Figure 3). The new band is red-shifted by 20 nm and is responsible for the change of color from orange (neutral ferrocenophane **4**) to deep purple (complexed ferrocenophane $[Mg_2(\mathbf{4})]^{4+}$). This color change can be used for a "naked-eye" detection of Mg^{2+} ions even in the presence of Ca^{2+} ions. The high-energy band of **4** is also red-shifted by 19 nm upon complexation of Mg^{2+} ions. It is important to note that the appearance of an Mg^{2+} ion induced sigmoidal curve in the titrations suggests that a 1:2 host-to-guest complex is formed via the corresponding 1:1 complex. In this case, the binding mode should be estimated on the basis of the following biphasic equilibria:

$$\mathbf{4} + Mg^{2+} \rightleftharpoons [Mg(\mathbf{4})]^{2+};\ K_{11} \quad (1)$$

$$[Mg(\mathbf{4})]^{2+} + Mg^{2+} \rightleftharpoons [Mg_2(\mathbf{4})]^{4+};\ K_{12} \quad (2)$$

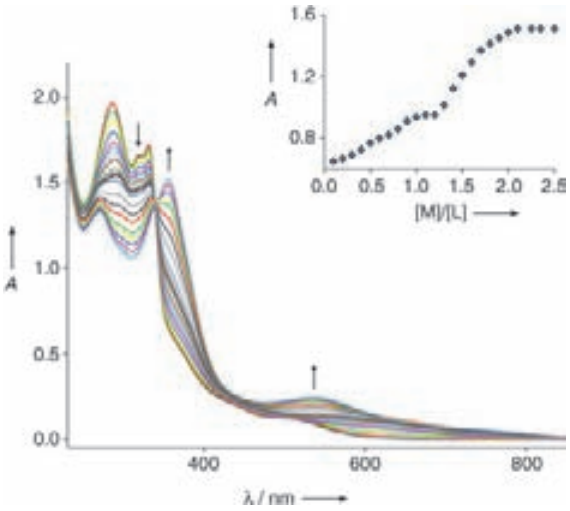

Figure 3. UV/Vis spectra obtained during the titration of **4** with $Mg(ClO_4)_2$ in CH_2Cl_2 ($c = 10^{-4}$ mol dm^{-3}). The initial spectrum is of the neutral species **4** and the final spectrum is of $[Mg_2(\mathbf{4})]^{4+}$. The arrows indicate the absorptions that increased (up) and decreased (down) during the titration experiments. Upper inset: change of absorbance at 537 nm upon addition of $Mg(ClO_4)_2$.

The two association constants, calculated by nonlinear least-squares analysis, were found to be $K_{11} = 9.8 \times 10^5$ and $K_{12} = 6.3 \times 10^5\,\text{M}^{-1}$, respectively.

A spectro–electrochemical study of the electrochemically induced, switchable chemosensor properties of complex $[Mg_2(\mathbf{4})]^{4+}$ was carried out. Thus, two equivalents of $Mg(ClO_4)_2$ were added to a solution of **4** in CH_2Cl_2 with $[n\text{Bu}_4\text{N}]PF_6$ (0.15 M) as the supporting electrolyte to obtain the complexed ferrocenophane $[Mg_2(\mathbf{4})]^{4+}$ species. The complex was oxidized at $+1.0$ V versus $Ag/AgNO_3$ until complete oxidation was reached and the color of the solution changed from deep purple to yellow (Figure 4). The optical spectrum of the resulting solution was the same as that obtained by the bielectronic oxidation of the free ligand **4** to $\mathbf{4}^{2+}$, thus suggesting that decomplexation of the two Mg^{2+} ions occurs during the electrochemical oxidation. The solution was completely reduced at $+0.35$ V versus $Ag/AgNO_3$, and the initial spectrum of the complex was fully recovered together with its purple color. Thus, the free dioxidized ligand $\mathbf{4}^{2+}$ is reduced to **4**, which has a large binding affinity for Mg^{2+} ions and nitites the formation of complex $[Mg_2(\mathbf{4})]^{4+}$. Oxidation of complex $[Mg_2(\mathbf{4})]^{4+}$ and its subsequent reduction were carried out over several cycles in a chronoamperometric experiment (Figure 4). The optical spectrum was recorded after each step and found to be fully recovered on completion of the step; thus, demonstrating the reversibility of the complexation/decomplexation process.

A preliminary study of the ability of the ferrocenophane **4** to transport Mg^{2+} ions across a CH_2Cl_2 liquid membrane was also undertaken. The CH_2Cl_2 membrane seperates two aqueous phases, the "source" and "receiving" phases, that are layered at the two branches of an H-type cell with a working electrode in one of the branches (see the Supporting Information). This study measures the time-dependence of the transportation of Mg^{2+} ions by the carrier **4** across the

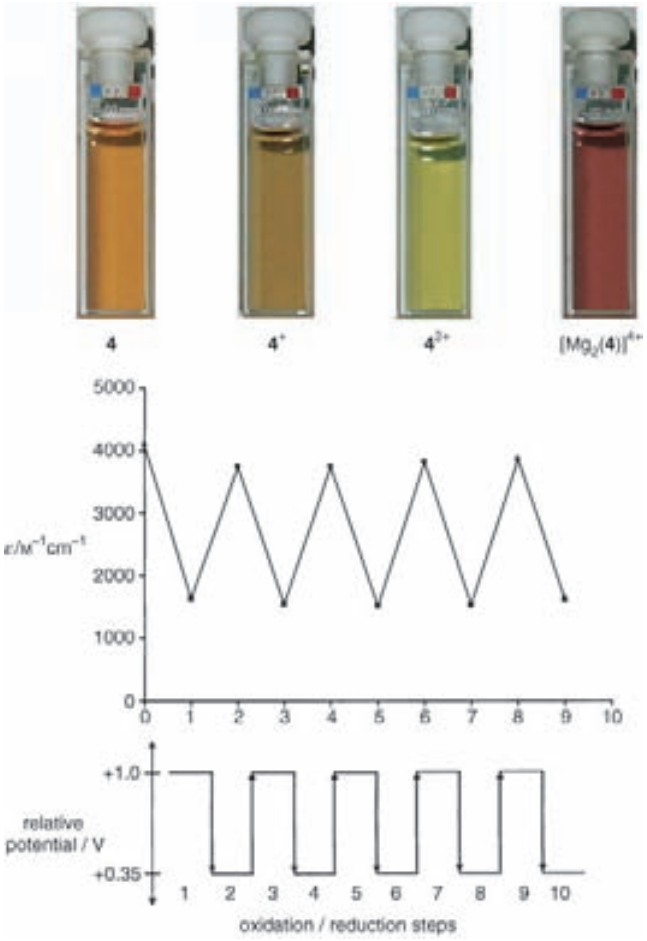

Figure 4. Top: colors shown by the studied species. Bottom: stepwise oxidation and reduction cycles carried out in CH_2Cl_2 by chronoamperometric analysis, which uses fixed potentials at +1.00 and +0.35 V and follows the changes observed by visible spectroscopy at 520 nm.

CH_2Cl_2 liquid membrane. The transport of Mg^{2+} ions was studied in the presence of **4** but in the absence of any applied potential at the working electrode of the H-type cell in a preliminary control experiment. Then, by oxidation of the carrier **4** a controlled potential electrolysis at the working electrode was performed while a constant potential of +0.95 V (versus $Ag/AgNO_3$) was maintained. The transport rate of the Mg^{2+} ions increased abruptly and the stationary state was achieved rapidly after starting the electrolysis (see the Supporting Information). These results are attributed to the decreased ion-binding ability of $\mathbf{4}^{2+}$ with respect to the neutral carrier **4**. A transport rate of Mg^{2+} ion of 3.2×10^{-6} mol h^{-1} was observed in the control experiment with no applied potential but it was increased to 2.1×10^{-5} mol h^{-1} when the controlled potential electrolysis was applied. Thus, electrochemical oxidation leads to a nearly sevenfold increase in the transport rate.

In conclusion, we have reported the first example of a redox-switchable receptor composed of two electronically coupled, electroactive ferrocene subunits that selectively recognizes Mg^{2+} ions through complexation. Transport and release of the Mg^{2+} ions by an external electrochemical stimulus is shown to be possible. The combination of two ferrocene subunits that have dissimilar electronic environments connected by two conjugated bridges with cation-binding sites is shown to be an attractive strategy for preparing new reversible redox-switchable ion carriers.

Received: November 5, 2004
Published online: February 21, 2005

Keywords: electrochemistry · ferrocene · ionophores · magnesium · UV/Vis spectroscopy

[1] a) P. D. Beer, *Adv. Inorg. Chem.* **1992**, *39*, 79–157; b) P. L. Boulas, M. Gomez-Kaifer, L. Echegoyen, *Angew. Chem.* **1998**, *110*, 226–258; *Angew. Chem. Int. Ed. Engl.* **1998**, *37*, 216–247; c) P. D. Beer, *Acc. Chem. Res.* **1998**, *31*, 71–80; d) P. D. Beer, P. A. Gale, *Adv. Phys. Org. Chem.* **1998**, *31*, 1–90; e) A. E. Kaifer, *Acc. Chem. Res.* **1999**, *32*, 62–71; f) P. D. Beer, J. Cadman, *Coord. Chem. Rev.* **2000**, *205*, 131–155; g) P. D. Beer, P. A. Gale, *Angew. Chem.* **2001**, *113*, 502–532; *Angew. Chem. Int. Ed.* **2001**, *40*, 486–516; h) I. E. Philip, A. E. Kaifer, *J. Am. Chem. Soc.* **2002**, *124*, 12678–12679; h) P. V. Bernhardt, E. G. Moore, *Aust. J. Chem.* **2003**, *56*, 239–258.

[2] For recent examples of ferrocene compounds that bind and electrochemically respond to metal cations, see: a) J. L. Lopez, A. Tarraga, A. Espinosa, M. D. Velasco, P. Molina, V. Lloveras, J. Vidal-Gancedo, C. Rovira, J. Veciana, D. J. Evans, K. Wurst, *Chem. Eur. J.* **2004**, *10*, 1815–1826; b) A. Tarraga, P. Molina, J. L. Lopez, M. D. Velasco, *Dalton Trans.* **2004**, 1159–1165; c) M. Li, P. Cai, C. Duan, F. Lu, J. Xie, Q. Meng, *Inorg. Chem.* **2004**, *43*, 5174–5176; d) A. Ion, M. Buda, J.-C. Moutet, E. Saint-Aman, G. Royal, I. Gautier-Luneau, M. Bonin, R. Ziessel, *Eur. J. Inorg. Chem.* **2002**, 1357–1366; e) O. B. Sutcliffe, R. M. Bryce, A. S. Batsanov, *J. Organomet. Chem.* **2002**, *656*, 211–216; f) H. Plenio, C. Aberle, Y. Al Shihaded, J. M. Lloris, R. Martinez-Mañez, T. Pardo, J. Soto, *Chem. Eur. J.* **2001**, *7*, 2848–2861.

[3] F. Le Derf, E. Levillain, G. Trippé, A. Gorgues, M. Sallé, R.-M Sebastian, A.-M. Caminade, J. P. Majoral, *Angew. Chem.* **2001**, *113*, 230–233; *Angew. Chem. Int. Ed.* **2001**, *40*, 224–227; b) F. Le Derf, M. Mazari, N. Mercier, E. Levillain, G. Trippé, A. Riou, P. Richomme, J. Becher, J. Garin, J. Orduna, N. Gallego-Planas, A. Gorgues, M. Sallé, *Chem. Eur. J.* **2001**, *7*, 447–455; c) J. L. Segura, N. Martín, *Angew. Chem.* **2001**, *113*, 1416–1455; *Angew. Chem. Int. Ed.* **2001**, *40*, 1372–1409; d) J. Lyskawa, F. Le Derf, E. Levillain, M. Mazari, M. Sallé, L. Dubois, P. Viel, C. Bureau, S. Palacin, *J. Am. Chem. Soc.* **2004**, *126*, 12194–12195.

[4] T. Saji, I. Kinoshita, *J. Chem. Soc. Chem. Commun.* **1986**, 716–717.

[5] a) A. C. Hall, C. Suarez, A. Hom-Choudhury, A. N. A. Manu, C. D. Hall, G. J. Kirkovits, I. Ghiriviga, *Org. Biomol. Chem.* **2003**, *1*, 2973–2982; b) J. C. Medina, T. T. Goodnow, M. T. Rojas, J. L. Atwood, B. C. Lynn, A. E. Kaifer, G. W. Gokel, *J. Am. Chem. Soc.* **1992**, *114*, 10583–10595.

[6] S. K. Davidsen, G. W. Phillips, S. F. Martin, *Org. Synth.* **1993**, *8*, 451–458.

[7] G. G. A. Balavoine, G. Doisneau, T. Fillebeen-Khan, *J. Organomet. Chem.* **1991**, *412*, 381–382.

[8] X-ray single-crystal diffraction data for **4** was collected on a Nonius KappaCCD diffractometer with an area detector and graphite-monochromized $Mo_{K\alpha}$ radiation ($\lambda = 0.71074$ Å). Crystal data: $C_{26}H_{22}Fe_2N_2$, $M_r = 474.16$, monoclinic, space group $C2/c$ with $a = 20.5134(3)$, $b = 9.9522(2)$, $c = 9.9596(4)$ Å, $\alpha = 90.00$, $\beta = 106.986(2)$, $\gamma = 90.00$, $V = 1944.59(9)$ Å^3, $Z = 4$, $T = 233$ K, $\mu = 15.08$ cm^{-}. Least-squares refinement based on measured reflections with $I > 2\sigma(I)$ led to convergence with a final $R1 =$

0.0240, *wR*2 = 0.0592, and GOF = 1.063. CCDC-262815 contains the supplementary crystallographic data for this paper. These data can be obtained free of charge from The Cambridge Crystallographic Data Centre via www.ccdc.cam.ac.uk/data_request/cif.

[9] S. R. Miller, D. A. Gustowski, Z. H. Chen, G. W. Gokel, L. Echegoyen, A. E. Kaifer, *Anal. Chem.* **1988**, *60*, 21021 – 21024.

[10] S. Barlow, H. E. Bunting, C. Ringham, J. C. Green, G. V. Bublitz, S. G. Boxer, J. W. Perry, S. R. Marder, *J. Am. Chem. Soc.* **1999**, *121*, 3715 – 3723.

J|A|C|S
COMMUNICATIONS

Published on Web 10/22/2005

Highly Selective Chromogenic and Redox or Fluorescent Sensors of Hg^{2+} in Aqueous Environment Based on 1,4-Disubstituted Azines

Antonio Caballero,[†] Rosario Martínez,[†] Vega Lloveras,[‡] Imma Ratera,[‡] José Vidal-Gancedo,[‡] Klaus Wurst,[§] Alberto Tárraga,[†] Pedro Molina,*[,†] and Jaume Veciana*[,‡]

Departamento de Química Orgánica, Facultad de Química, Universidad de Murcia, Campus de Espinardo, 30100 Murcia, Spain, Institut de Ciència dels Materials de Barcelona (CSIC), Campus UAB, 08193, Cerdanyola, Catalonia, Spain, and Institut für Allgemein und Anorganische Chemie, Universität Innsbruck, Innrain 52a, A-6020 Innsbruck, Austria

Received July 11, 2005; E-mail: pmolina@um.es

Mercury contamination occurs through a variety of natural and anthropogenic sources,[1] and it causes serious environmental and health problems because marine aquatic organisms convert inorganic mercury into neurotoxic methylmercury which bioaccumulates through the food chain.[2] A number of selective Hg^{2+} sensors have been devised using redox,[3] chromogenic,[4] or fluorogenic[5] changes. However, most of these molecules display shortcomings in practical use, such as cross-sensitivities toward other metal ions, delayed response to mercury ions, and/or low water solubility. Despite the development of individual single-signaling sensors, there are no multichannel signaling receptors on Hg^{2+} binding. As a result, developing new and practical multi-signaling sensors for Hg^{2+} in aqueous media is still a challenge.[6]

For the selective recognition of soft heavy metal ions, nitrogen binding sites might be a choice as it is well exemplified with classical azacrown ethers.[7] Previous studies on complexation of ferrocene with binding ligands have shown that not only the characteristic band between 400 and 500 nm, ascribed to the lowest energy metal-to-ligand transition, is perturbed by complexation but also a positive shift of the Fe^{II}/Fe^{III} redox couple is observed.[8] Pyrene has often been used as an effective fluorescence probe because of its high detection sensitivity.[9] Formation of a complex results in a change in the fluorescence emission intensities of pyrene excimer and monomer.[10] Two informative parameters associated with the pyrene excimer are the intensity ratio of the excimer to the monomer emission (I_E/I_M) and the wavelength corresponding to the maximum of the excimer emission (λ_E). While the I_E/I_M parameters are sensitive to the structure of the pyrene systems, the emission λ_E is less variable and locates at 475−485 nm. On the basis of such precedents, suitable designed aza-substituted ferrocene and pyrene derivatives might be good candidates as dual signaling sensors. This can be realized by combining the 2,3-diazabutadiene ligand[11] (azine) with the redox activity of the ferrocene and the photoactivity of the pyrene.

Herein we report the synthesis, characterization, and metal recognition properties of 1,4-disubstituted 2,3-diaza-1,3-butadienes bearing two redox ferrocene groups, **1**, and one photoactive pyrene and a *p*-methoxyphenyl group, **2**. These structural motifs would thus yield a combined optical and redox, or fluorescent-based sensors, in a single molecule. Symmetrical azine **1** (70% yield) was prepared by known procedures,[12] while the unsymmetrical azine **2** was obtained by a modification of the Zwierzak's method.[13] The X-ray structure of **1** reveals that the bridge is in the *E*,*E* form, and that the dihedral angles between the bridged Cp ring of both Fe and the C−C−N plane are −5.5 and 5.5°, bearing a good electronic conjugation along the bridge (see Supporting Information)

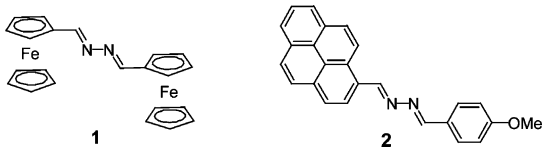

The metal recognition properties of **1** were evaluated by electrochemical and optical analysis. The cyclic voltammetric (CV) and differential pulse voltammetric (DPV) analyses in acetonitrile show two almost-overlapped one-electron oxidation processes for **1**, whereas in acetonitrile/water (7:3), only one oxidation peak around 0.65 V is observed, versus decamethylferrocene. Whereas no perturbation of the DPV voltammogram of **1** was observed upon addition of Mg^{2+}, Ca^{2+}, Ni^{2+}, Zn^{2+}, and Cd^{2+} metal ions,[14] a significant modification was observed upon addition of Hg^{2+}. In acetonitrile, the two oxidation peaks were converted into one and anodically shifted. Most remarkably is the fact that the selective response toward Hg^{2+} is preserved in the presence of water. Thus, the peak was also anodically shifted upon complexation in acetonitrile/water (7:3) ($\Delta E_{1/2} = 60$ mV) (Figure 1a). The UV/visible spectra of compound **1** are almost identical in dichloromethane, acetonitrile, and acetonitrile/water (7:3). These spectra are characterized by two maximum at 309 and 476 nm, which are assigned to a localized $\pi-\pi^*$ excitation within the diaza-bridge and a metal-to-ligand charge transfer, respectively.[15]

The addition of increasing amounts of $Hg(ClO_4)_2$ to a solution of **1** in acetonitrile/water (7:3) caused the appearance of a new band at $\lambda = 521$ nm and the disappearance of the initial band at 476 nm (Figure 1b). The three well-defined isosbestic points indicate that a neat interconversion between the uncomplexed and complexed species occurs. The new band is red-shifted by 45 nm and is responsible for the change of color from yellow (neutral azine **1**) to deep purple (complexed azine). This color change can be used for a "naked-eye" detection of Hg^{2+} ions in an aqueous environment (Figure 1c), with a detection limit of 5.2×10^{-5} M. The absorption spectral data indicate a 1:1 binding model and an association constant of 4.35

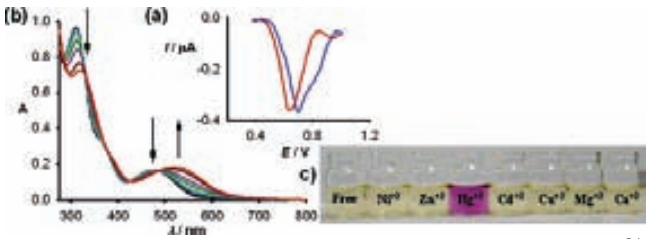

Figure 1. (a) DPV of free ligand **1** (red) and after formation of **1**·Hg^{2+} (blue) in CH_3CN/H_2O 7/3 with $[(n\text{-}Bu)_4N]\,ClO_4$ as supporting electrolyte. (b) Absorption spectra of **1** in CH_3CN/H_2O (7:3) upon addition of increasing amounts of $Hg(ClO_4)_2$. (c) Color change due to binding of **1** in CH_3CN/H_2O (7:3) ($c = 1 \times 10^{-4}$ M) with Hg^{2+} in comparison with other metal cations.

[†] Universidad de Murcia.
[‡] Institut de Ciència dels Materials de Barcelona.
[§] Universität Innsbruck.

10.1021/ja0545766 CCC: $30.25

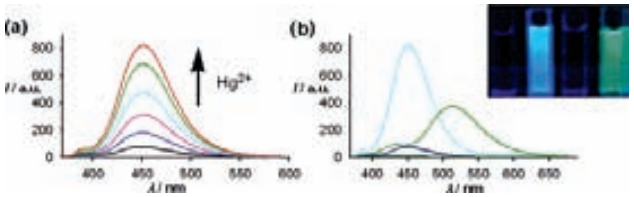

Figure 2. (a) Fluorescence emission spectra of **2** (excitation at 350 nm) in CH_3CN/H_2O (7:3) upon titration with $Hg(ClO_4)_2$. The final spectrum (red) corresponds to the complexed form $\mathbf{2}\cdot Hg^{2+}$ after addition of 1 equiv of Hg^{2+}. (b) Fluorescence spectra after the addition of 1 equiv of $Hg(ClO_4)_2$ to **2** in CH_3CN/H_2O (7:3) (blue) and in CH_3CN (green). Spectra for the free ligand **2** in CH_3CN/H_2O (7:3) (deep blue) and CH_3CN (deep green). (Inset) From left to right: **2** in CH_3CN/H_2O (7:3) and adding 1 equiv of $Hg(ClO_4)_2$, and **2** in CH_3CN and adding 1 equiv of $Hg(ClO_4)_2$.

$\times 10^5\ M^{-1}$ in acetonitrile (see Supporting Information). This result has also been confirmed by MALDI-TOF/MS, where a peak corresponding to the 1:1 complex is observed (see Supporting Information).

The ability of the azine bridge to complex Hg^{2+} selectively was checked with compound **2**, which has a fluorogenic instead of a redox signaling unit as **1**. The absorption spectra of ligand **2** in acetonitrile or acetonitrile/water (7:3) show the typical pyrene absorption bands[16] at 238, 285, and 313 nm, along with a low-energy band centered at 383 nm, attributed to the charge transfer between the donor and acceptor units of the molecule, which is responsible of its pale-yellow color. When Hg^{2+} metal ions are added, the low-energy band suffers a bathochromic shift (51 nm). Four well-defined isosbestic points indicated that a neat interconversion between the uncomplexed and complexed species occurs. The red-shift of the low-energy band is responsible for the change of color of the solution from pale-yellow to deep-orange. The resulting titration was fitted to a 1:1 binding model, and the association constant was $9.79 \times 10^7\ M^{-1}$ in acetonitrile (see Supporting Information). It is noticeable that only Hg^{2+} from Li^+, Na^+, K^+, Mg^{2+}, Ca^{2+}, Cu^{2+}, Zn^{2+}, Cd^{2+}, Ni^{2+}, Sm^{3+}, Eu^{3+}, Yb^{3+}, and Lu^{3+} metal ions is able to produce a bathochromic shift of this band, indicating that the color variation is highly specific for Hg^{2+} ions. The spectrum of the free ligand **2** in acetonitrile shows weak fluorescence with typical emission bands at 387 and 435 nm ($\lambda_{exc} = 350$ nm), which are attributed to the pyrene monomeric emission,[17] with rather low quantum yield ($\Phi_o = 0.0006$).[18] However, in acetonitrile/water (7:3), it also shows weak fluorescence with one emission band at 390 nm (monomer emission) but also a red-shifted structureless maximum at 450 nm, typical of pyrene excimer fluorescence,[9] with low quantum yield ($\Phi_o = 0.005$). The low quantum yield of the unbounded ligand **2** results from the quenching of the pyrene emission by the lone pair of the nitrogen atoms[19] in the free state. So, it could be expected that, upon complexation with a metal cation, the lone pairs no longer participate in the quenching process, causing the recovery of the fluorescence.

To evaluate the sensing behavior of **2**, we measured its fluorescence in acetonitrile as function of the Hg^{2+} concentration. Addition of only small amounts of Hg^{2+} to the solution dramatically increased the excimer emission band at 510 nm.

This band increased until addition of 1 equiv of Hg^{2+} was completed. The result obtained indicates the formation of a 1:1 complex. The final fluorescence enhancement factor (FEF) was 157, the ratio $I_{E(510)}/I_{M(387)}) = 17$, and the quantum yield was 67-fold ($\Phi = 0.04$). Upon addition of 1 molar equiv of Hg^{2+} ions to a solution of **2** in acetonitrile/water (7/3), a remarkable FEF = 11 of the excimer emission band at 450 nm was also clearly observed. A blue-shift upon increasing solvent polarity can visually and readily be discernible by the change of the blue fluorescence in acetonitrile/water to green fluorescence in acetonitrile (Figure 2b). Analysis of emission spectral data indicates a 1:1 binding model and an association constant of $1.65 \times 10^6\ M^{-1}$ in acetonitrile (see Supporting Information). Compound **2** was found to have high selectivity toward Hg^{2+} ions and a detection limit[20] of 4.6×10^{-6} M, which is sufficiently low to allow the fluorogenic detection of submillimolar concentrations of Hg^{2+}. The fluorescence quantum yield was 10-fold ($\Phi = 0.04$), and the ratio $I_{E(450)}/I_{M(390)} = 13$. Fluorescence spectra of **2** recorded in the presence of Li^+, Na^+, K^+, Mg^{2+}, Ca^{2+}, Cu^{2+}, Zn^{2+}, Cd^{2+}, Ni^{2+}, Sm^{3+}, Eu^{3+}, Yb^{3+}, and Lu^{3+} metal ions did not alter the shape or the intensity of the fluorescence spectra, indicating no interference.

In summary, we have reported for the first time two new sensors which operate through two different channels (**1**: optic/redox, and **2**: optic/fluorescent) exhibiting higher sensitivity and selectivity for Hg^{2+} in aqueous environment than other previously reported sensors, although they cannot operate in pure water as it does in the seminal example of Lippard et al.[6] Remarkable is sensor **2** since its optical change in sensing can be used for a naked-eye detection of Hg^{2+} ions, whereas its fluorescent response can be modulated by varying the solvent polarity.

Acknowledgment. We thank the DGI (Spain) (Projects CTQ 2004-0221 and MAT2003-04699), DGR, Catalunya (2001 SGR00362), and Fundación Séneca (CARM-Spain) PB/72/FS/02.

Supporting Information Available: Crystallographic and electrochemical data of **1**, synthesis, optical, fluorescence, selectivity, and detection limit data of **1** and **2**. This material is available free of charge via the Internet at http://pubs.acs.org.

References

(1) (a) Renzoni, A.; Zino, F.; Franchi, E. *Environ. Res.* **1998**, *77*, 68−72. (b) Benoit, J. M.; Fitzgerald, W. F.; Damman, A. W. *Environ. Res.* **1998**, *78*, 118−133.
(2) (a) Boening, D. W. *Chemosphere* **2000**, *40*, 1335−1351. (b) Harris, H. H.; Pickering, I. J.; George, G. N. *Science* **2003**, *301*, 1203−1203.
(3) (a) Lloris, J. M.; Martinez-Mañez, R.; Padilla-Tosta, M. E.; Pardo, T.; Soto, J.; Beer, P. D.; Cadman, L.; Smith, D. K. *J. Chem. Soc., Dalton Trans.* **1999**, 2359−2369. (b) Jimenez, D.; Martinez-Mañez, R.; Sancenon, F.; Soto, J. *Tetrahedron Lett.* **2004**, *45*, 1257−1259.
(4) (a) Sancenón, F.; Martinez-Mañez, R.; Soto, J. *Chem. Commun.* **2001**, 2262−2263. (b) Choi, M. J.; Kim, M. Y.; Chang, S.-K. *Chem. Commun.* **2001**, 1664−1665.
(5) (a) Youn, N. J.; Chang, S.-K. *Tetrahedron Lett.* **2005**, *46*, 125−129. (b) Moon, S.-Y.; Youn, N. J.; Park, S. M.; Chang, S.-K. *J. Org. Chem.* **2005**, *70*, 2394−2397. (c) Miyake, Y.; Ono, A. *Tetrahedron Lett.* **2005**, *46*, 2441−2443.
(6) (a) Nolan, E. M.; Lippard, S. J. *J. Am. Chem. Soc.* **2003**, *125*, 14270−14271. (b) Ono, A.; Togashi, H. *Angew. Chem., Int. Ed.* **2004**, *43*, 4300−4302.
(7) Lehn, J.-M.; Montavon, F. *Helv. Chim. Acta* **1978**, *61*, 67.
(8) Caballero, A.; Lloveras, V.; Tarraga, A.; Espinosa, A.; Velasco, M. D.; Vidal-Gancedo, J.; Rovira, C.; Wurst, K.; Molina, P.; Veciana, J. *Angew. Chem., Int. Ed.* **2005**, *44*, 1977−1981 and references therein.
(9) Winnick, F. M. *Chem. Rev.* **1993**, *93*, 587−614.
(10) (a) Sahoo, D.; Narayanaswami, V.; Kay, C. M.; Ryan, R. O. *Biochemistry* **2000**, *39*, 6594−6601.
(11) Son, S. U.; Park, K. H.; Jung, I. G.; Chung, Y. K. *Organometallics* **2002**, *21*, 5366−5362.
(12) (a) Casey, R. M. T.; Guinan, P.; Canavan, A.; McCann, M.; Cardin, C.; Kelly, N. B. *Polyhedron* **1991**, *10*, 483−489. (b) Osborne, A. G.; da Silva, M.W.; Hursthouse, M. H.; Malik, K. M. A.; Opromolla, G.; Zanello, P. *J. Organomet. Chem.* **1996**, *516*, 167−176. (c) Yamin, B. N.; Ali, N. M. *Acta Cryst.* **2003**, *E59*, 95−96.
(13) Koziara, A.; Turski, K.; Zwierzak, A. *Synthesis* **1986**, 298−300.
(14) Cu^{2+} ions in acetonitrile are not complexed by **1**, but an intermolecular redox reaction takes place between them (see the Supporting Information).
(15) Barlow, S.; Bunting, H. E.; Ringham, C.; Green, J. C.; Bublitz, G. U.; Boxer, S. G.; Perry, J. W.; Marder, S. R. *J. Am. Chem. Soc.* **1999**, *121*, 3715−3723.
(16) Förster, T.; Kasper, K. Z. *Elektrochem.* **1955**, *59*, 976−980.
(17) Bodenant, B.; Fages, F.; Delville, M. M. *J. Am. Chem. Soc.* **1998**, *120*, 7511−7519.
(18) The fluorescence quantum yields were measured with respect to anthracene as standard ($\Phi = 0.27 \pm 0.03$). Dawson, W. R.; Windsor, M. W. *J. Phys. Chem.* **1968**, *72*, 3251. For more information, see the Supporting Information.
(19) Davidson, S. R. *Adv. Phys. Org. Chem.* **1983**, *19*, 1.
(20) Shortreed, M.; Kopelman, R.; Kuhn, M.; Hoyland, B. *Anal. Chem.* **1996**, *68*, 1414−1418.

JA0545766

Influence of bridge topology and torsion on the intramolecular electron transfer

Vega Lloveras,[a] José Vidal-Gancedo,[a] Daniel Ruiz-Molina,[a] Teresa M. Figueira-Duarte,[b] Jean-François Nierengarten,[b] Jaume Veciana*[a] and Concepció Rovira*[a]

Received 11th May 2005, Accepted 8th June 2005
First published as an Advance Article on the web 12th October 2005
DOI: 10.1039/b506678f

To study molecules able to act as good "molecular wires", intramolecular electron transfer between two triphenylmethyl redox centers connected by bridges with different topologies and substituents have been studied in solution, both by UV-Vis-NIR and EPR spectroscopies. The synthetic methodology used allows a complete control of the geometry of polychlorotriphenylmethyl diradicals **1** and **2**, which have *para* and *meta* topologies, respectively, as well as of their *E*/*Z* isomerism. This fact is used to show the influence of the different topologies in the ease of electron transfer, which is larger for the *para* than for the *meta* isomer where a small or negligible electronic coupling is observed. The related diradical **3** that have the same topology as the *para* isomer **1** but bearing two substituents on the central phenyl ring shows similar ease of electron transfer, that the *para* isomer **1**.

1. Introduction

The enormous interest at present for molecular wires arises from the potential use of such systems on integrated molecular-sized devices, to scale down the size of the devices and integrate molecular switches with molecular-scale wires.[1] The interest and the foreseen technical advantages of such integrated molecular devices are significant.[2,3] First, the ever-increasing miniaturization of the architectural components of microchips reverts in the reduction size of computational systems. Second, the time it takes for an electron to travel through the circuit can be minimized using such molecular-scale electronic architectures.[3] On the other hand, the main drawbacks are: (i) the severe limitations existing for manipulating objects at the molecular level and for transferring the information from the macroscopic world to molecular electronic devices and (ii) the high conformational requirements that the molecule to be used must fulfil. For instance, an average interelectrode distance of 100 Å obtained using "top-down" techniques; *i.e.*, lithography, requires the synthesis of molecular systems that, in addition to a π-conjugated pathway, have similar dimensions to the interelectrode distance and restricted conformational geometries.

The first step to progress on this field is the understanding of rules for the prediction and control of the electron propagation in organic "molecular wires". Electron transfer in donor–bridge–acceptor (D–B–A) molecules has been actively investigated, in part to determine which aspects of the bridge structure control the intramolecular electron transfer (IET).[4] Mixed-valence compounds are excellent candidates for such studies since IET phenomena can be easily determined from the position, intensity and width of the so-called intervalence transition band that usually appears in the near-infrared region. In addition, in those systems that generate stable radical mixed valence species, the dynamics of the thermally activated IET process can also be studied from the thermal variation of the EPR spectrum of the mixed valence species.[5,6]

Even thought the conclusions from the solution studies do not necessarily correlates for the same molecules in other environment as is the solid state, in electrochemical experiments in which the donor or acceptor is replaced by a conducting solid also seek to reveal how the ET rate depends on

[a] *Institut de Ciència de Materials de Barcelona (CSIC), Campus Universitari de Bellaterra, 08193, Cerdanyola, Spain. E-mail: cun@icmab.es, vecianaj@icmab.es*
[b] *Laboratoire de Chimie de Coordination du CNRS, 205 route de Narbonne, 31077, Toulouse Cedex 4, France*

the "bridge" structures.[7] On the other hand, the values of the "decay factors" β obtained by measurements of current density through saturated and unsaturated molecules of different length, using junctions of the type Hg–SAM(1)/SAM(2)–Ag, are in good agreement with corresponding values obtained in solution.[8]

A prime objective of our research has been the synthesis and characterization of pure organic mixed valence systems using polychlorinated triphenylmethyl radical units as electroactive centers.[9] Such radicals are particularly interesting not only because they have a large persistency displaying high thermal and chemical stabilities but also because they are electroactive species giving rise, either chemically or electrochemically, to the corresponding anions and cations which are also quite stable species.[10] As a consequence, it seemed interesting to obtain and study symmetrical molecules consisting of two of these radicals linked with different types of bridges.

In order to maximize the electron transfer rates in mixed valence compounds, the bridge choice is crucial. Both its electronic structure and the effective distance between the redox centers are known to play a critical role in determining the ease of the electron transfer.[4] For these reasons, we have designed a series of structurally well defined diradicals that incorporate phenylene-vinylene units as a bridge since homo- and heteronuclear metallic complexes with phenylene and/or vinylene units promoting through-bond photoinduced energy or electron transfer over considerable distances (*i.e.* 20 Å) had already been described.[11]

We have studied both by UV-Vis-NIR and EPR spectroscopies the intramolecular electron transfer phenomena in the radical anions derived from the partial reduction of pure organic diradicals **1** and **2** that varies in the topological substitution of the bridge.

These diradicals, which exhibit a well defined topology and isomerism, consist of two polychlorinated triphenylmethyl radicals linked by divinylphenylene bridges. The difference with other previous work using these bridges relays in the bulk chlorine substituents in the two phenyl rings linked to the electroactive center (the radical central carbon) that can promote big changes in the angle of rotation due to steric hindrance. The synthetic methodology used allows a complete control of the *E*/*Z* isomerism of diradicals **1** and **2**, which have *para* and *meta* topologies, respectively. We will show that the topology clearly influences the ease of electron transfer. Indeed, small V_{ab} coupling are expected to appear when the triphenylmethyl radical units are connected in the *meta* position, in contrast to the case where the two units are in the *para* position.

By other hand, we also present the study of the intramolecular electron transfer phenomena in the radical anion derived from the partial reduction of diradical **3** with the same *para* topology as **1** but bearing substituents in two positions of the central phenyl ring of the bridge. We want to determine if the possible rotation around the σ bonds promoted by the steric hindrance between these substituents and the bulky chlorine atoms on the neighboring phenyl rings could originate a severe loss of coplanarity of the bridge and consequently, a decrease of the long-distance electronic coupling between the terminal sites.

2. Results and discussion

2.1. Synthesis

The synthetic route for preparing radicals **1–3** is based on two main steps. The first step is the synthesis of their triphenylmethane precursors by a Wittig reaction while the second step is the generation of the corresponding dicarbanions by an acid–base reaction followed by the subsequent oxidation of such carbanions to the corresponding diradicals (Scheme 1).

Reaction of the α-*H*-4-(bromomethyl)tetradecachlorotriphenylmethane derivative (**4**),[12] with triphenylphosphine yielded the starting substituted phosphonium bromide **5** which was coupled with the suitable bisaldehyde under Wittig conditions to give the corresponding polychlorinated bistriphenylmethanes **6**, **7** and **8**. This reaction is strongly stereoselective since it yields exclusively the *E*/*E*-isomers, as ascertained by NMR spectroscopy.[9c,13] Such stereoselectivity is justified if we consider that the ylide derived from the phosphonium bromide **5** is stabilized by the presence of the polychlorinated aromatic ring. In fact, the natural preference of ylides with electron withdrawing groups that stabilize the betaine form has been experimentally shown to give mainly the *E*-isomer.[14] In addition, the *Z*/*E*-isomer distribution of the Wittig products is also strongly influenced by the

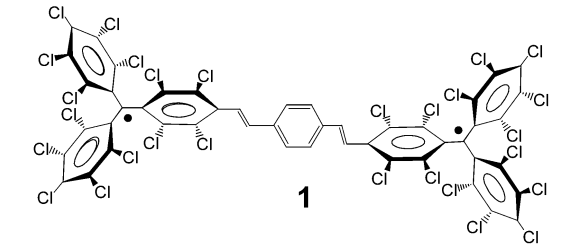

1

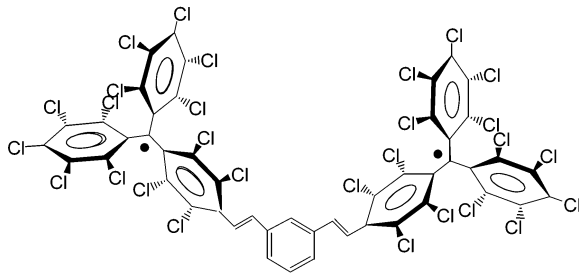

2

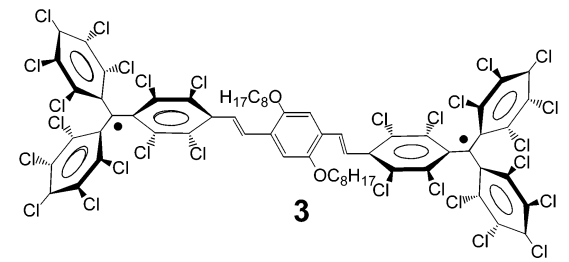

3

nature of the base used in the preparation of the ylide;[15] being the potassium *tert*-butoxide, used in this work, the base of choice for maximizing the yields of *E*-olefins.[16]

Afterwards, the synthesis of the diradical species **1**, **2** and **3** was undertaken by treatment of the corresponding triphenylmethane precursors **6**, **7** and **8** with an excess of n-$Bu_4N^+OH^-$ and the subsequent oxidation of the resulting dianions with *p*-chloranil in a "*one-pot reaction*". The complete synthesis can also be performed as a "*one-pot reaction*" without the isolation of the intermediate triphenylmethane derivatives **6–8** obtaining in this case better yields. Diradicals **1**, **2** and **3** were isolated as dark brown (75%), green (68%) and dark brown (64%) solids respectively. Characterization of all compounds was performed by elemental analysis and spectroscopic techniques.[17] As described for a related monoradical with *p*-bromovinylenephenylene substituent, bis(pentachlorophenyl)[4-(4-bromophenyl-β-styryl)-2,3,5,6-tetrachlorophenyl]-methyl radical (**9**),[9c] no isomerization of double bonds was noticed for diradicals **1–3** by spectroscopical techniques. Finally, it is worth noticing that the diradicals are highly persistent and thermally stable in the solid state and also in diluted solutions, even when exposed to air. No enhanced reactivities of the diradicals with respect to their monoradical counterparts were observed.

2.2 *Meta versus para* bridge topology

2.2.1 Study of diradicals 1 and 2. Electrochemical studies in CH_2Cl_2, with n-Bu_4NPF_6 (0.1 M) as supporting electrolyte (*vs*. SCE) and using a Pt wire as a working electrode, were done at room temperature. The CV of diradicals **1** and **2** show only one reversible reduction process at a constant potential of approximately −0.12 V (*vs*. Ag/AgCl), in spite of the presence of two electronically active triphenylmethyl units. This result suggests the presence of very weak or negligible electronic interactions between the triphenylmethyl units of diradicals **1** and **2**, since in the case of a strong or moderate electronic interaction between the two units, two electrochemical waves are anticipated.

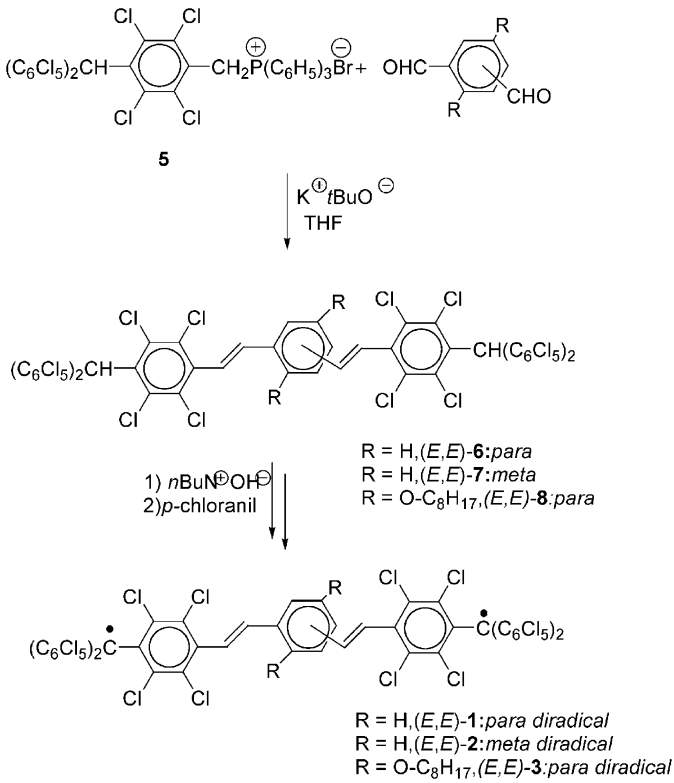

Scheme 1

Only if both units exhibit very weak or negligible electronic interactions, the two standard redox potentials must be very close and a single two-electron wave will be observed, with minor differences in shape with respect to a true two-electron process. Cyclic voltammetric peak separation of the reversible reduction waves for the diradicals **1** and **2** are 83 and 78 mV, respectively, which are similar to that observed for the related monoradical **9** (80 mV).[9c] Such separation serves as one criterion for electrochemical reversibility and those observed for radicals **1** and **2** are closed to the expected theoretical separation of 59 mV. The slightly higher peak separation may arise from the high resistance of the solutions used for the measurements.

The magnetic susceptibility of powder samples of biradicals **1** and **2** was measured in the temperature range of 4–300 K. Diradicals **1** and **2** follow the Curie–Weiss law, down to low temperatures, with $\theta = -4$ K and -0.4 K respectively, due to weak intra- and/or intermolecular antiferromagnetic interactions, being as expected larger for the *para* isomer **1**. The effective magnetic moments found at room temperature were 2.41 and 2.43 μ_B for diradicals **1** and **2**, respectively. These values are in excellent agreement with the theoretical effective magnetic moment expected for vanishing or non-interacting pair of doublets (2.45 μ_B).

UV-Visible spectra of diradicals **1** and **2** were recorded in dichloromethane and relevant data are shown in Table 1. Visible spectra of the polychlorotriphenylmethyl radicals usually show an intense absorption band around 386 nm and two weaker bands centered around 565–605 nm, all of which are assigned to the radical character of the triphenylmethyl units.[10] In the case of diradicals **1** and **2**, due to the presence of a certain degree of electronic delocalization, bathochromic shifts with enhanced absorptivities, compared to unsubstituted chlorinated triarylmethyl radicals, would be expected. This behaviour is indeed observed for diradical **2**. For diradical **1** substantially larger bathochromic shifts and enhanced absorptivities are observed as expected from the larger electronic delocalization present in this compound due to its *para* connectivity.

Table 1 Relevant UV-Vis and EPR data

Compound	EPR[ab] $\Delta H_{1/2}$	a_H	$a_{C,\alpha}$	$a_{C,arom}$	D/hc	E/hc	UV-Vis[e] λ/nm ($10^{-3}\varepsilon$)
1	0.95	0.95(2H)	14.0	5.9, 6.4	3.9×10^{-4}	[c]	600(3.2), 440(20.7), 386(57.4), 339(33.1)
$\mathbf{1}^{-\bullet}$	0.85	1.90(1H)	[d]	[d]	—	—	[f]
$\mathbf{1}^{-2}$	—	—	—	—	—	—	606(46.4), 522(49.3), 339(32.3)
2	0.98	0.90(2H)	13.9.0	5.5, 6.5	2.3×10^{-4}	[c]	573(3.1), 415(26.0), 385(33.7)
$\mathbf{2}^{-\bullet}$	0.58	1.80(2H) 0.60 (2H) 0.60 (2H)	[d]	[d]	—	—	[f]
$\mathbf{2}^{-2}$	—	—	—	—	—	—	570(49.4), 525.4(51.4), 293(39.2)
3	0.96	0.88(2H)	14.8	5.4, 6.5	3.9×10^{-4}	[c]	680(3.8), 503(11.6), 418(sh), 388(52.3) 321(15.7)
$\mathbf{3}^{-\bullet}$	0.88	1.80(1H)	[d]	[d]	—	—	1420 (0.26), 615 (36.5), 523 (38.9), 388 (49.6)
$\mathbf{3}^{2-}$	—	—	—	—	—	—	611(62.5), 525(60.3), 318(30.1)

[a] In CH_2Cl_2 solutions at rt; except for $\mathbf{1}^{-\bullet}$ and $\mathbf{2}^{-\bullet}$ and $\mathbf{3}^{-\bullet}$ that were taken at 200 K (see text). [b] Linewidths and hyperfine coupling constants (in Gauss) are computer simulated values; *g*-values found were similar, 2.0027(3), for all open-shell species. Zero-field splitting parameters (in cm^{-1}) observed in frozen solutions at 120 K. Principal components of *g*-tensors for $\mathbf{1}^{-\bullet}$ and $\mathbf{2}^{-\bullet}$ are, respectively, $g_x = 2.0033$, $g_y = 2.0033$, $g_z = 2.0010$ and $g_x = 2.0029$, $g_y = 2.0029$, $g_z = 2.0025$. These values were determined by simulation of frozen EPR spectra. [c] Negligible. [d] Not observed. [e] In CH_2Cl_2 solution at r.t. [f] See text.

X-band EPR spectra of radicals **1** and **2** were recorded in CH_2Cl_2 : toluene solution in the temperature range of 180–293 K. The isotropic EPR spectra at 300 K were fairly well simulated by using the parameters given in Table 1. The experimental and simulated spectra of diradical **1** is shown in Fig. 1 and is almost identical to the one of biradical **2**. At room temperature both spectra showed the lines corresponding to the coupling of the unpaired electrons with the different nuclei with nonzero magnetic moments; *i.e.*, with ^1H and the naturally abundant ^{13}C nuclei. Computer simulation gave the isotropic *g*-values (g_{iso}) and the isotropic hyperfine coupling constants (a_i). The obtained g_{iso}-values (2.0022 and 2.0024 for radicals **1**, **2** respectively) are very close to those observed for other polychlorotriphenylmethyl radicals.[10] More interesting is the analyses of the isotropic hyperfine coupling constant values with the hydrogen nuclei of the vinylene moieties and with some of the carbon nuclei of the triphenylmethyl unit. For instance, the EPR spectrum of diradicals **1** and **2** at 300 K display three main overlapping symmetrical lines originating from the hyperfine coupling with two hydrogen atoms of the ethylene moiety. The values of the coupling constants for diradicals **1** and **2** are approximately half than those found for the related monoradical **9**.[9c] It is then possible to conclude that the two electrons in diradicals **1** and **2** are magnetically interacting with a magnetic exchange coupling constant *J*, that fulfils the following condition, $J \gg a_i$.

Furthermore, the absolute values of zero-field splitting parameters, $|D/hc|$ and $|E/hc|$, for diradicals **1** and **2** were obtained from the simulated spectra of both diradicals in frozen solutions and are given in Table 1. These parameters arise from the dipolar magnetic interactions between the two unpaired electrons and can be used to calculate the average interspin separation in a given compound. Therefore, from the zero-field splitting parameter $|D/hc|$, given in cm^{-1}, and using eqn. (1),[18] an average interspin separation of 15.0 and 17.5 Å was found for diradicals **1** and **2**, respectively.

$$r = \left[\frac{3g^2\beta^2}{2hc}\frac{1}{|D/hc|}\right]^{1/3} \quad (1)$$

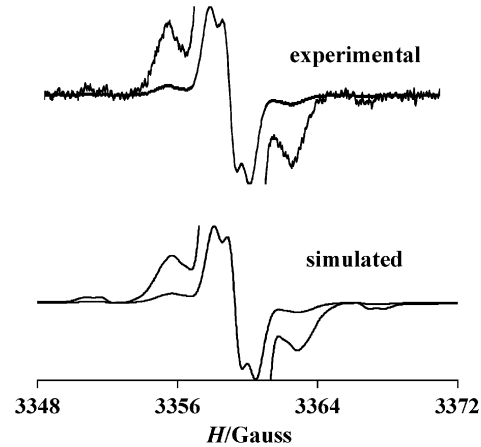

Fig. 1 Simulated and experimental isotropic solution EPR spectra of diradical **1** in CH_2Cl_2 : toluene (1 : 1) at 285 K.

The average interspin separation found for diradical **1** is smaller than the nominal separation between the two alpha carbon atoms, determined by semiempirical AM1 calculations,[19,20] where most of the spin density of polychlorinated triphenylmethyl radicals is localized.[10] Indeed, the through-bond distance between the two electron active sites; *i.e.*, the sum of bond lengths corresponding to the conjugated pathway is 24.1 Å and the through space distance is 19 Å. This result is in agreement with the existence of a certain degree of electronic delocalization due to the *para*-connectivity of the divinylphenylene bridge that reduces the effective separation of the two spins in **1**. As expected, the average interspin separation found for diradical **2** is closer to the nominal separation between the two α-carbon atoms (through bond, 22.7 Å and through space 17 Å) due to the lower degree of electronic conjugation in the *meta*-isomer in comparison with the isomer with *para*-connectivity. Finally, EPR measurements of frozen dilute solutions of both diradicals in the 4–100 K range revealed that there exists a very weak magnetic interaction between the two unpaired electrons since the signal intensity for both diradicals follows the Curie law. This result, along with the $J \gg a_i$ condition, permit to estimate the limits for the intramolecular exchange coupling constant for diradicals **1** and **2**; that are 15 $cm^{-1} \gg J/hc \gg 10^{-3}$ cm^{-1}.[21]

2.2.2 Intramolecular electron transfer process. Determination of the experimental electronic coupling parameter V_{ab} has been undertaken by spectroelectrochemistry using a previously described methodology.[22] Such a methodology is based on the reduction of diradicals **1** and **2** and the simultaneous observation of the corresponding electronic absorption spectra, regularly recorded during the reduction process for different values of the average number (n) of electrons added; where $0 \leq n \leq 2$. This situation allows us to control the evolution of the electrochemical reaction simply by monitoring the evolution of the characteristic radical and anion bands. The different reduced species that can be derived from both diradicals are depicted schematically in Scheme 2. As can be observed there, diradicals **1** and **2**, as well as the dianion $\mathbf{1}^{-2}$ and $\mathbf{2}^{-2}$, are homovalent species whereas the radical anions $\mathbf{1}^{-\bullet}$ and $\mathbf{2}^{-\bullet}$ should be regarded as a mixed-valence species. Accordingly, only the last species may show intervalence transition bands that usually appear at low energies; *i.e.*, at the near-infrared region.

During the reduction of diradical **1** the sharp band at 386 nm, characteristic of the radical chromophore, decreases until it completely disappears for $n = 2$, while the band at 339 nm does not change at all. At the same time, two new broad and intense bands at 522 and 606 nm grow in, which correspond to the continuous formation of the dianion $\mathbf{1}^{-2}$. Similar behavior was observed for diradical **2**. Fig. 2 shows the evolution of the UV-Vis spectra during the course of the reduction of diradical **1** until reaching the highest concentration of the mixed valence species $\mathbf{1}^{-\bullet}$. The observation of some well-defined isosbestic points during reduction of diradicals **1** and **2** indicate

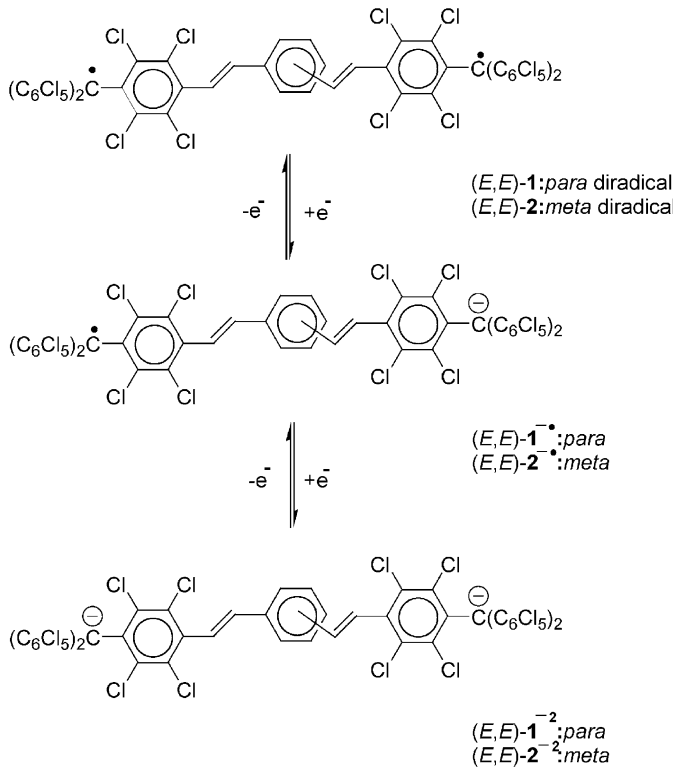

Scheme 2

that no by-products due to decomposition processes are originated during such electrochemical reductions.

The main difference in the stepwise coulometric titration of diradicals **1** and **2** is the observation of a new band centered around 1400 nm for the radical-anions $\mathbf{1}^{-\bullet}$, shown in Fig. 3. Indeed, during the reduction process of diradical **1**, a weak and broad band centered around 1400 nm appears and develops until the complete formation of $\mathbf{1}^{-\bullet}$. Afterwards, the intensity of this band decreases until

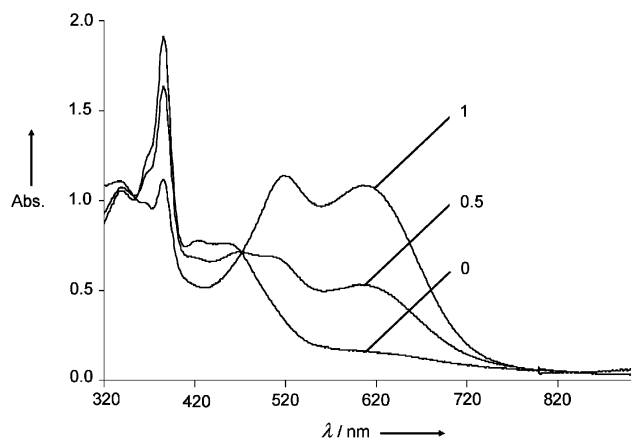

Fig. 2 Evolution of the UV-Vis spectrum during the course of the reduction of diradical **1**. The number of added electrons is given on each spectrum.

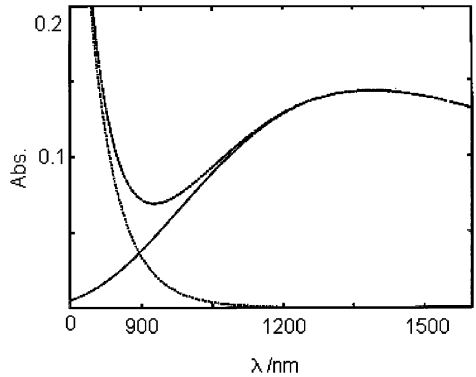

Fig. 3 Electronic spectrum of the mixed-valence species $\mathbf{1}^{-\bullet}$ (dashed line), sum of the intervalence transition band (dashed–dotted line) and the band corresponding to the radical and/or anion chromophore (dotted line).

it disappears when the dianion $\mathbf{1}^{-2}$ is completely formed. This is the typical behavior expected for an intervalence band originated by the presence of an intramolecular electron transfer phenomenon in the mixed-valence species $\mathbf{1}^{-\bullet}$. On the other side, no intervalence band was detected for the radical anion $\mathbf{2}^{-\bullet}$ formed during the reduction of diradical **2**.

The assignment of the band centered around 1400 nm in the spectra of $\mathbf{1}^{-\bullet}$ as an intervalence transition was confirmed by theoretical calculations following the method previously employed by Nelsen *et al.*[23] The energy of an intervalence transition, λ, comes from two different contributions, λ_{in} and λ_{out}, which correspond to the energy contributions produced by the arrangements of the internal part of the system (the molecule) and the outer medium (the solvating medium), respectively, when the electron is transferred. The inner shell, or internal Marcus, term, for polychlorinated triphenylmethyl radicals is $\lambda_{in} = 0.214$ eV and was obtained by quantum mechanical calculations at the AM1 level performed on the $(C_6Cl_5)_3C^{\bullet}$ fragment.[19] The outer shell term was estimated using the Marcus dielectric continuum model shown in eqn. (2),

$$\lambda_{out} = 14.41g\ (r,R)\gamma \tag{2}$$

where γ is the Marcus solvent parameter, which is 0.380 for CH_2Cl_2, $g(r,R)$ is the geometrical parameter of the electron active center and λ_{out} is given in eV. The $g(r,R)$ parameter is calculated using eqn. (3) from the effective radius, r, of the localized charge -represented as a sphere centered at the carbon atom- and R, the distance between the centers of the two electron active centers, R,[24]

$$g(r,R) = \frac{1}{r} - \frac{1}{R} \tag{3}$$

with $r = 5.4$ Å, as determined from the X-ray structure of the $(C_6Cl_5)_3C^{\bullet}$ radical,[10c] and $R = 19$ Å as the limit distance between the two electron active sites,[24] one obtains $\lambda_{out} = 0.726$ eV. Finally, the sum of both contributions yields $\lambda = 0.939$ eV; which is in fairly good agreement with the experimental value of 0.787 eV: *vide infra*, determined from the position of the intervalence band. Interestingly, λ_{in} provides a noteworthy contribution here to the total energy of the intervalence transition λ, whereas in the related case of partly oxidized tertiary aromatic amines this term was almost negligible relative to λ_{out}.[25]

In order to experimentally determine the effective electronic coupling V_{ab} (in cm^{-1}) between the redox sites of diradical **1** we can use eqn. (4), developed by Hush.

$$V_{ab} = [2.05 \times 10^{-2}\sqrt{\varepsilon_{max}\bar{\nu}_{max}\Delta\bar{\nu}_{1/2}}]R^{-1} \tag{4}$$

Here V_{ab} is given in cm^{-1}, R is the effective separation of the redox sites (in Å), ε_{max} is the maximum extinction coefficient (in $M^{-1}\ cm^{-1}$), $\bar{\nu}_{max}$ is the transition energy, and $\Delta\bar{\nu}_{1/2}$ is the full-width at half-height (both in cm^{-1}) of the intervalence absorption band. After correction for the comproportionation equilibrium between the different redox forms of **1**, $\mathbf{1}^{-\bullet}$ and $\mathbf{1}^{-2}$, and the deconvolution of

the experimental spectrum,[26] the following parameters for the intervalence absorption band were obtained: $\bar{\nu}_{max} = 6349\ cm^{-1}$ (*i.e.* $\lambda = E_{opt} = 0.787$ eV), $\Delta\bar{\nu}_{1/2} = 2940\ cm^{-1}$, and $\varepsilon_{max} = 677\ M^{-1}\ cm^{-1}$. Application of these parameters to eqn. (4) provides an effective electronic coupling for $\mathbf{1}^{-\bullet}$ of $V_{ab} = 121\ cm^{-1}$ (0.015 eV), when $R = 19$ Å is used.

We also studied the thermally activated electron transfer process in $\mathbf{1}^{-\bullet}$ by EPR spectroscopy. For this purpose, the electrochemical reduction of **1** was performed until an almost complete reduction to $\mathbf{1}^{-2}$ is achieved. The resulting solution contains, besides the desired mixed-valence $\mathbf{1}^{-\bullet}$ species, mainly the EPR-silent $\mathbf{1}^{-2}$ species and, therefore, the resolution of the spectra is good. The EPR spectrum of $\mathbf{1}^{-\bullet}$ at 200 K displays two symmetrical lines arising from the hyperfine coupling with one hydrogen atom of the ethylene moiety (Fig. 4) and the ^{1}H hyperfine coupling constant is very close to that of the related monoradical **9**.[9c] This result clearly demonstrates that at this temperature the unpaired electron of radical anion $\mathbf{1}^{-\bullet}$ is localized on the EPR timescale on only one-half of the molecule; *i.e.* on one stilbene-like moiety.

As depicted in Fig. 4, when the temperature is increased, a new central line gradually emerges between the two initial ones. This evolution is consistent with the increase of the electron jump rate on going from 200 K (the slow-exchange limit) to 300 K (the fast-exchange limit) due to a thermally activated electron transfer between the two equivalent sites, that lead to the coupling of the unpaired electron of $\mathbf{1}^{-\bullet}$ with two equivalent ^{1}H nuclei. The EPR spectra of $\mathbf{1}^{-\bullet}$ at various temperatures were fairly well simulated by using the rates given in Fig. 4 and the program of Heinzer.[27] The best fit was made by varying the rate constant k_{th} for the thermally activated electron transfer between the two equivalent sites. The experimental and simulated EPR spectra are compared in Fig. 4. The resulting k_{th} values were plotted using a linear Eyring plot [$\ln(k_{th}/T)$ *vs.* $1/T$] from where a value for the energy barrier to the thermal electron transfer, ΔH^*, of 0.117 eV was obtained.

According to Hush theory, E_{opt} corresponds to the energy for the vertical electron transfer between the sites. In the limit of a vanishingly small electronic interaction (*i.e.*, $V_{ab} \approx 0$), the thermal barrier to electron transfer is then predicted to be one-quarter of E_{opt}, because of the usual parabolic shape of the energy wells, according to the following relationship,

$$\Delta H^* = (E_{opt}/4) - V_{ab} \quad (5)$$

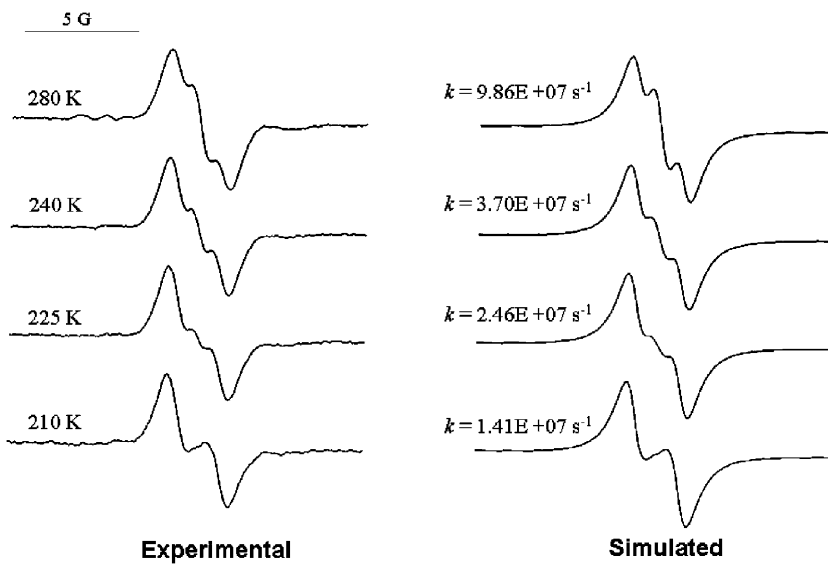

Fig. 4 Experimental (left) and simulated (right) EPR spectra of $\mathbf{1}^{-\bullet}$ at different temperatures in CH_2Cl_2 with 0.1 M of nBu$_4$NPF$_6$. Spectra recorded at the very end of the reduction process. At this stage, the major species present in the solution is the EPR-silent dianion $\mathbf{1}^{-2}$. Most of the observed EPR signal is due to $\mathbf{1}^{-\bullet}$, since for statistical reasons diradical **1** must have negligible concentration. See text for details on simulation.

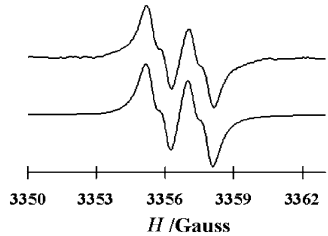

Fig. 5 Experimental (top) and simulated (bottom) EPR spectra of the mixed-valence species $\mathbf{2}^{-\bullet}$ in a frozen solution of toluene : CH_2Cl_2 (1 : 1) at 200 K.

In the present case, this relation is not fulfilled, because ΔH^* (0.117 eV) is appreciably lower than one-fourth of the optical energy (0.787/4 = 0.197 eV). A naïve argument would be to assign the difference to the presence of a significant electronic coupling. This would give $V_{ab} = 0.080$ eV, a value much higher than the one found experimentally from the intensity of the intervalence transition with eqn. (4); *i.e.*, 0.015 eV. Several hypotheses can be considered to explain the difference in V_{ab} values obtained by both methods: (i) The determination of V_{ab} by a difference between two terms of comparable magnitude from eqn. (5), is certainly highly inaccurate. (ii) Some processes such as nuclear tunneling could contribute to lower the effective thermal energy barrier. (iii) The use of eqn. (4) to calculate V_{ab}, may be not correct for organic compounds where there is a certain degree of electronic delocalization. Actually, the separation between the redox sites, R, which is employed in eqn. (4), is not perfectly defined because in the ground state the wavefunction of the electron is not fully localized on the alpha carbon atom, but has a non negligible extension on the adjacent phenyl rings. This fact has already been pointed out by Nelsen *et al.*[6c] and by Launay *et al.* for organic nitrogen compounds.[25]

The EPR spectrum of $\mathbf{2}^{-\bullet}$ at 200 K displays two symmetrical lines, each one with a shoulder, originated by the hyperfine coupling with the two hydrogen atoms of one of the ethylene moieties. The EPR spectrum at 200 K was fairly well simulated by using the parameters given in Table 1. The experimental and simulated EPR spectra are compared in Fig. 5. One of the resulting ^{1}H hyperfine coupling constants is very close to that observed for the mixed-valence radical-anion species $\mathbf{1}^{-\bullet}$, whereas the second one is considerably smaller. Similar behavior has been observed in other polychlorinated bis(triphenylmethyl) systems.[28] When the temperature is increased no evolution is observed confirming that, at least in the temperature range studied, intramolecular electron transfer is not observed because it is slower than the timescale of the EPR experiment. This result, together with the lack of an intervalence band transition in the absorption spectra, suggests that there is a localization effect in the radical-anion species $\mathbf{2}^{-\bullet}$. Previous experimental and theoretical studies performed on diferrocenylbenzenes showed that such localization occurs when the two electroactive centers are connected in the *meta* position, whereas if they are connected in the *para* position, intramolecular electron transfer across the phenylene ring is observed.[29] Similar results have also been detected in polynorbornyl and divinyl alkane systems. Indeed, recent studies have shown that V_{ab} values are markedly larger for polynorbornyl dienes than for the divinyl alkanes, by as much as 35% for the shorter members and 20% for the larger members. These surprising results indicate that simple *n*-alkyl bridges are more effective mediators of through-bond coupling over long distances than the polynorbornyl bridges, even though the chromophore units in the latter are connected by two alkyl relays, rather than one. According to the authors, these results imply the presence of interferences occurring between the various coupling pathways in the polynorbornyl bridge.[30]

2.3 Ring substituent effects

Molecule **3** has the same topology as **2** and they differ only in the substituents on the phenyl ring in the bridge having two octyloxy groups in molecule **3**. These groups were added to impart solubility to the higher members of a series with increasing number of vinylene phenylene groups in the bridge. Before developing the complete series it is important to asses if the rotation around the σ-bonds promoted by the steric hindrance between the substituents in the central rings and the

chlorine substituents in the phenyl rings directly attached to the electroactive site, could originate a decrease of the long-distance electronic coupling between the terminal sites.

2.3.1. Study of diradical 3. The cyclic voltammetry of diradical **3** shows, as expected, only one reversible reduction process at a slightly lower potential ($\Delta E_{1/2} = -0.18$ V *vs.* Ag/AgCl) than biradicals **1** and **2**, which is accounted for by the electron donating character of the substituents in the central ring of **3**.

The UV-Vis spectrum of biradical **3**, recorded in the same conditions as biradicals **1** and **2** is similar to that of the topologically related radical **1**, showing bathochromic shifts of the lowest energetic bands corresponding to the triphenylmethyl radical. Some differences on those bands attributed to the central phenyl ring of the bridge are also observed (See Table 1).

Also similar are the EPR characteristics (Table 1). Indeed, in isotropic CH_2Cl_2 solution, birradical **3** shows three overlapped lines due to the hyperfine coupling with two hydrogen atoms. This fact and the values of the coupling constants are characteristic of a biradical with a magnetic interaction between the two electrons with a magnetic exchange coupling constant J, that fulfils the following condition, $J \gg a_i$.

The absolute values of zero-field splitting parameters, $|D/hc|$ and $|E/hc|$, for diradical **3** obtained from the spectra in frozen toluene : CH_2Cl_2 mixture, are the same of biradical **1** (Table 1) denoting identical extent of dipolar magnetic interactions between the two unpaired electrons in both biradicals. The same results were also obtained by variable temperature measurements in the range between 4 and 100 K of this frozen diluted solution.

2.3.2 Intramolecular electron transfer process. As in the previous cases, both the optically activated and the thermally activated electron transfer processes on the mixed valence species derived from biradical **3** were studied by Vis-NIR and EPR spectroscopies respectively.

As shown in Fig. 6 during the reduction of diradical **3** the sharp band centered at 388 nm, characteristic of the radical, decreases while two new broad and intense bands centred at 523 and 615 grown in, indicating the formation of the anion species. In addition, during the reduction process, a weak and broad band centred at 1420 nm increases until the complete formation of the mixed-valence radical anion species $\mathbf{3}^{-\bullet}$, from where the intensity decreases until it disappears completely when the dianion $\mathbf{3}^{2-}$ is formed. This band was, as previously done, assigned to an intervalence transition. Using the previously described methodology and equations, a V_{ab} coupling parameter of 100 cm^{-1} was determined when the effective separation of the redox sites is considered

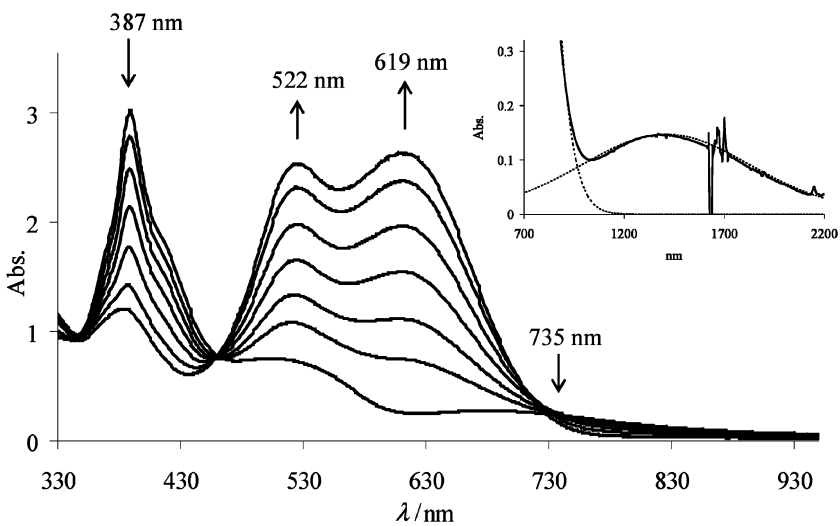

Fig. 6 Evolution of the UV-Vis during the course of the reduction of diradical **3**. Inset shows the intervalence band in the NIR.

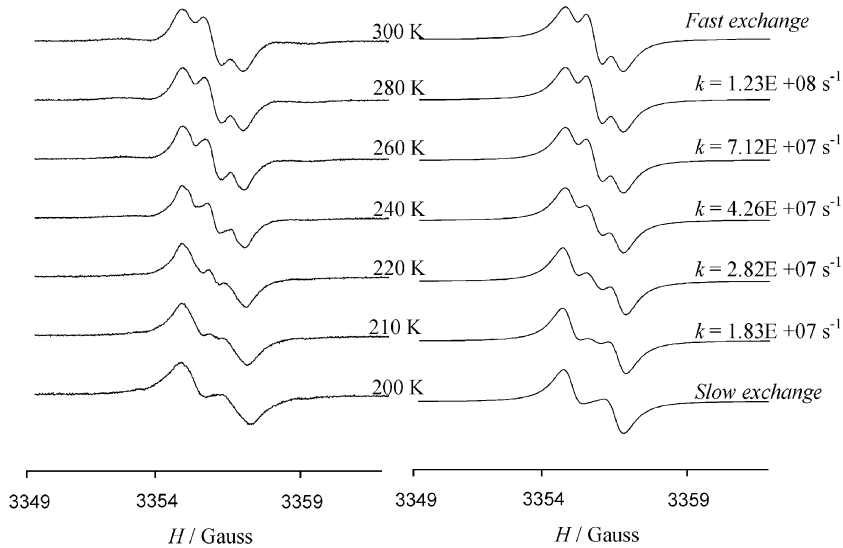

Fig. 7 Experimental (left) and simulated (right) EPR spectra of $\mathbf{3}^{-\bullet}$ at different temperatures in CH_2Cl_2 with 0.1 M of nBu$_4$NPF$_6$. Spectra recorded at the very end of the reduction process. See text for details.

Table 2 Experimental coupling parameters and activation energies corresponding to the electron transfer processes of mixed-valence species derived from biradicals **1** and **3**

Compound	V_{ab}/cm^{-1}	ΔG^*/kcal mol^{-1}
$\mathbf{1}^{-\bullet}$	121	6.0
$\mathbf{3}^{-\bullet}$	100	5.9

to be 19 Å.[31] The V_{ab} value is very close to that of the topologically related mixed valence compound $\mathbf{1}^{-\bullet}$ which suggest that ring substituents effects on electron transfer-rates in this class of "molecular wires" bridging molecules is very small.

This finding was confirmed by the study of the thermal activated process by EPR. Thus, the EPR spectrum of $\mathbf{3}^{-\bullet}$ at 200 K displays two symmetrical lines (Fig. 7) with a ^{1}H hyperfine coupling constant consistent with the localization, at the EPR time scale, of the unpaired electron on one site of the molecule only. As in the case of $\mathbf{1}^{-\bullet}$, when the temperature is increased the evolution of the spectra is consistent with the increase of the electron jump rate from one site to the other of the molecule. The resulting k_{th} values obtained from the spectra simulation gave a linear Eyring plot that permits to calculate the energy barrier for the electron transfer process ($\Delta G^* = 5.9$ kcal mol^{-1}). As in the optically induced process, this value is very similar to the one found for the mixed valence species $\mathbf{1}^{-\bullet}$ (Table 2).

3. Conclusions

Diradicals **1** and **2**, which only differ in their topological connectivity, have been synthesized and characterized. Intramolecular electron transfer phenomena in the mixed-valence radical-anion species $\mathbf{1}^{-\bullet}$ have been observed and studied by a spectroelectrochemical titration and temperature-variable EPR experiments. In contrast to $\mathbf{1}^{-\bullet}$, no electron transfer was observed for $\mathbf{2}^{-\bullet}$, a result that can be ascribed to the localization of frontier orbitals in the latter radical anion because the *meta* connectivity of this non-Kekulé molecule.

A second important point is that the study of the mixed valence species $\mathbf{3}^{-\bullet}$, with the same topology as $\mathbf{1}^{-\bullet}$, reveals that the ring substitution effects on electron transfer rates are very small. This finding is significant since it suggest that adding substituents to the bridges in order to impart

different functionality or simply higher solubility could be readily made without dramatically affecting the electronic coupling along the bridges between the electroactive moieties.

Interestingly, $\mathbf{1}^{-\bullet}$ and $\mathbf{3}^{-\bullet}$ constitutes one of the rare examples of a mixed valence species for which the determination of both the optical and thermal energies for electron transfer is possible.

Acknowledgements

This work was supported by grants from the DGI (Spain), project MAT2003-04699, DGR (Catalunya), project 2001SGR00362, Catalan Network CeRMAE, and COST Chemistry D14 Action "Functional Materials".

References

1 (*a*) R. Metzger, *Acc. Chem. Res.*, 1999, **32**, 950; (*b*) J. M. Tour, *Acc. Chem. Res.*, 2000, **33**, 79; (*c*) R. Lloyd and C. B. Gorman, *Angew. Chem., Int. Ed.*, 2002, **41**, 4378; (*d*) D. M. Adams, L. Brus, C. E. D. Chidsey, S. Creager, C. Creutz, C. R. Kagan, P. V. Kamat, M. Lieberman, S. Lindsay, R. A. Marcus, R. M. Metzger, M. E. Michel-Beyerle, J. R. Miller, M. D. Newtown, D. R. Rolison, O. Sankey, K. S. Schanze, J. Yardley and X. Zhu, *J. Phys. Chem. B*, 2003, **107**, 6668.

2 J. M. Tour, M. Kozaki and J. M. Seminario, *J. Am. Chem. Soc.*, 1998, **120**, 8486.

3 J. M. Seminario and J. M. Tour, in *Molecular Electronics – Science and Technology*, ed. A. Aviram and M. A. Ratner, New York Academy of Science, New York, 1998, p. 69.

4 (*a*) *Electron Transfer in Chemistry*, ed. V. Balzani, Wiley, Weinheim, 2001, vol. I–V; (*b*) M. A. Fox, *Chem. Rev.*, 1992, **92**, 365–490, special issue on electron transfer; (*c*) M. N. Paddon-Row, *Acc. Chem. Res.*, 1994, **27**, 18; (*d*) P. F. H. Schab, M. D. Levin and J. Michl, *Chem. Rev.*, 1999, **99**, 1863; (*e*) J. P. Launay, *Chem. Soc. Rev.*, 2001, **30**, 386.

5 (*a*) J. C. Smart and B. L. Pinsky, *J. Am. Chem. Soc.*, 1980, **103**, 1009; (*b*) J. A. Kramer and D. N. Hendrickson, *Inorg. Chem.*, 1980, **19**, 3330.

6 (*a*) S. F. Rak and L. L. Miller, *J. Am. Chem. Soc.*, 1992, **114**, 1388; (*b*) J. Bonvoisin, J. P. Launay, C. Rovira and J. Veciana, *Angew. Chem., Int. Ed. Engl.*, 1994, **33**, 2106; (*c*) S. F. Nelsen, R. F. Ismagilov and D. A. Trieber, II, *Science*, 1997, **278**, 846; (*d*) S. V. Lindeman, S. V. Rosokha, D. Sun and J. K. Kochi, *J. Am. Chem. Soc.*, 2002, **124**, 843; (*e*) N. Gautier, F. Dumur, V. Lloveras, J. Vidal-Gancedo, J. Veciana, C. Rovira and P. Hudhomme, *Angew. Chem., Int. Ed.*, 2003, **42**, 2765.

7 (*a*) S. Creager, C. J. Yu, C. Bamdad, S. O'Connor, T. MacLean, E. Lam, Y. Chong, G. T. Olsen, J. Luo, M. Gozin and J. F. Kayyem, *J. Am. Chem. Soc.*, 1999, **121**, 1059; (*b*) J. J. Sumner, K. S. Weber, L. A: Hockett and S. E. Creager, *J. Phys. Chem. B*, 2000, **104**, 7449; (*c*) H. D. Sikes, J. f. Smalley, S. P. Dudek, A. R. Cook, M. D. Newton, C. E. D. Chidsey and S. W. Feldberg, *Science*, 2001, **291**, 1519.

8 (*a*) R. E. Homlin, R. F. Ismagilov, R. Haag, V. Mujica, M. A. Ratner, M. A. Rampi and G. M. Withesides, *Angew. Chem., Int. Ed.*, 2001, **40**, 2316; (*b*) R. E. Homlin, R. Haag, R. F. Ismagilov, M. A. Rampi and G. M. Withesides, *J. Am. Chem. Soc.*, 2001, **123**, 5075.

9 (*a*) J. Bonvoisin, J.-P. Launay, C. Rovira and J. Veciana, *Angew. Chem., Int. Ed. Engl.*, 1994, **33**, 2106; (*b*) J. Sedo, D. Ruiz, J. Vidal-Gancedo, C. Rovira, J. Bonvoisin, J -P. Launay and J. Veciana, *Adv. Mater.*, 1996, **8**, 748; (*c*) C. Rovira, D. Ruiz-Molina, O. Elsner, J. Vidal-Gancedo, J. Bonvoisin, J.-P. Launay and J. Veciana, *Chem. – Eur. J.*, 2001, **7**, 240; (*d*) O. Elsner, D. Ruiz-Molina, J. Vidal-Gancedo, C. Rovira and J. Veciana, *Nano Lett.*, 2001, **1**, 117.

10 (*a*) M. Ballester, *Acc. Chem. Res.*, 1985, **297**, 131; (*b*) J. Veciana, J. Riera, J. Castañer and N. Ferrer, *J. Organomet. Chem.*, 1985, **297**, 131; (*c*) O. Armet, J. Veciana, C. Rovira, J. Riera, J. Castañer, E. Molins, J. Rius, C. Miravitlles, S. Olivella and J. Brichfeus, *J. Phys. Chem.*, 1987, **91**, 5608; (*d*) I. Ratera, D. Ruiz-Molina, J. Ensling, K. Wurst, C. Rovira, P. Gutlich and J. Veciana, *J. Am. Chem. Soc.*, 2003, **125**, 1462; (*e*) M. Ballester, C. Miravitlles, E. Molins and C. Carreras, *J. Org. Chem.*, 2003, **68**, 2748; (*f*) D. Maspoch, N. Domingo, D. Ruiz-Molina, K. Wurst, G. Vaughan, J. Tejada, C. Rovira and J. Veciana, *Angew. Chem. Int. Ed.*, 2004, **43**, 1828.

11 (*a*) V. Grosshenny, A. Harriman and R. Ziessel, *Angew. Chem., Int. Ed. Engl.*, 1995, **34**, 1100, and references therein; (*b*) C. Patoux, J.-P. Launay, M. Beley, S. Chodorowski-Kimmes, J.-P. Collin, S. James and J.-P. Sauvage, *J. Am. Chem. Soc.*, 1998, **120**, 3717; (*c*) F. Barigelletti, L. Flamigni, V. Balzani, J.-P. Collin, J.-P. Sauvage, E. C. Constable and A. M. W. Cargill Thompson, *J. Chem. Soc., Chem. Commun.*, 1993, 942; (*d*) F. Barigelletti, L. Flamigni, V. Balzani, J.-P. Collin, J.-P. Sauvage, E. C. Constable and A. M. W. Cargill Thompson, *J. Am. Chem. Soc.*, 1994, **116**, 7692; (*e*) A. C. Benniston, V. Goulle, A. Harriman, J. M. Lehn and B. Marczinke, *J. Phys. Chem.*, 1994, **98**, 7798; (*f*) R. Ziessel, M. Hissler, A. El-Ghayoury and A. Harriman, *Coord. Chem. Rev.*, 1998, **178–180**, 1251.

12 M. Ballester, J. Veciana, J. Riera, J. Castañer, C. Rovira and O. Armet, *J. Org. Chem.*, 1986, **51**, 2472.

13 For other strongly (*E*)-selective reactions, see for example, H. Pommer and A. Nurenbach, *Angew. Chem., Int. Ed. Engl.*, 1977, **16**, 423.

14 H. O. House, *Modern Synthetic Reactions*, Benjamin, Menlo Park, CA, 1972, 2nd edn., 608.

15 (*a*) K. Wurst, O. Elsner and H. Schottenberger, *Synlett*, 1995, **1**, 833; (*b*) J.-G. Rodríguez, A. Oñate, R. M. Martin-Villamil and I. Fonseca, *J. Organomet. Chem.*, 1996, **513**, 71.
16 L. Fitjer and U. Quabeck, *Synth. Commun.*, 1985, **15**, 855.
17 Compound **1**. Anal. calcd. for $C_{48}H_8Cl_{28}$: C, 36.55; H, 0.51; Cl, 62.94; found C, 36.59; H, 0.62; Cl, 62.86%. MS *m*/*z* 1576 (M^+), 1506 ($M^+ - Cl_2$), IR(KBr): $\nu = 3025$, 1624, 1510, 1330, 1255, 960, 810, 800, 800 cm^{-1}. Compound **2**. Anal. calcd. for $C_{48}H_8Cl_{28}$: C, 36.55; H, 0.51; Cl, 62.94; found C, 37.20; H, 0.53; Cl, 62.27%. MS *m*/*z* 1576 (M^+), 1506 (M^+-Cl_2), IR(KBr): ν = 2920, 1510, 1340, 1260, 960, 815, 780, 755 cm^{-1}. Compound **3**. Anal. calcd. for $C_{64}H_{40}Cl_{28}$: C, 41.92; H, 2.19; Cl, 54.13; O, 1,74 found C, 42,12; H: 2,18; Cl, 54.27%. MS *m*/*z* 1572 (M^+), 1762 ($M^+ - Cl_2$), I R(KBr): $\nu = 2918$, 1613, 1508, 1336, 1258, 1202, 967, 814, 734, 710, 665 cm^{-1}.Compound **6**. Anal. calcd. for $C_{48}H_{10}Cl_{28}$: C, 36.51; H, 0.64; Cl, 62.85; found C, 36.56; H, 0.64; Cl, 62.81%. MS *m*/*z* 1579 (M^+), 1544 (M^+-Cl) IR(KBr): $\nu = 3010$, 2920, 1635, 1530, 1510, 1410, 1360, 1335, 1290, 1135, 960, 865, 800, 710, 680, 640, 525, 505 cm^{-1}. ^{1}H-NMR(CCl_4.D_2O): $\delta = 7.25$(4 H, s), 7.00 (6 H, m) ppm.Compound **7**. Anal. calcd. for $C_{48}H_{10}Cl_{28}$: C, 36.50; H, 0.63; Cl, 62.86; found C, 36.63; H, 0.47; Cl, 62.50%. MS *m*/*z* 1579 (M^+), 1544 (M^+-Cl) IR(KBr): $\nu = 3010$, 2920, 1640, 1535, 1520, 1365, 1340, 1295, 1240, 1135, 960, 860, 808, 715, 680, 645, 530, 495 cm^{-1}. ^{1}H-NMR($CDCl_3$): $\delta = 7.67$(1 H, m), 7.53 (3 H, m), 7.12 (4H, m), 7.07 (2H,s) ppm.Compound **8** was not isolated in order to improve the yield of biradical **3**.
18 S. D. McGlynn, T. Azumi and M. Kinoshita, in *Molecular Spectroscopy of the Triplet State*, Prentice Hall, Englewood Cliffs, NJ, 1969.
19 (*a*) MOPAC 93.00: J. J. Stewart, M. J. S. Dewar, E. G. Zoebish and E. F. Healy, *J. Am. Chem. Soc.*, 1985, **107**, 3902; (*b*) M. J. S. Dewar and E. G. Zoebish, *J. Mol. Struct. (THEOCHEM)*, 1988, **180**, 1.
20 It is well known that molecules of the type Ar_3Z, in which three aryl groups (Ar) are bonded to a central Z atom, which have a sp^2 hybridization, are propeller-like in shape. A large number of theoretical studies on the stereochemistry of these propeller-like systems were performed by Mislow *et al.* (K. Mislow, *Acc. Chem. Res.*, 1976, **9**, 26). They demonstrated that in the most simple cases, where the three aryl groups (blades) are not substituted, or else symmetrically substituted around the C_{ar}–Z bond axis of each aryl group (*i.e.*, groups having local C_2 axes), the molecule has always at least two enantiomeric forms due to the intrinsic stereogenic center (helicity) of any propeller that provides chirality to the molecule. If the helix adopts a clockwise sense the enantiomer is called *Plus* (*P*) whereas if it adopts the opposite sense is called *Minus* (*M*). For diradicals **1** and **2** it is straightforward to predict the existence of three stereoisomers, one pair of enantiomers-namely (*P*,*P*)-, and (*M*,*M*)- and a *meso* form—namely (*M**,*P**)—due to the presence of two triphenylmethyl stereogenic centers. (N. Ventosa, D. Ruiz-Molina, J. Sedó, C. Rovira, X. Tomas, J.-J. André, A. Bieber and J. Veciana, *Chem. – Eur. J.*, 1999, **5**, 3533, J. Sedó, N. Ventosa, M. A. Molins, M. Pons, C. Rovira and J. Veciana, *J. Org. Chem.*, 2001, **66**, 1567; J. Sedó, N. Ventosa, M. A. Molins, M. Pons, C. Rovira and J. Veciana, *J. Org. Chem.*, 2001, **66**, 1579). Semi-empirical calculations were done by using initial input molecules with one of the triphenylmethyl units in the *M* form and the other in the *P* form. It was also confirmed that the use of another stereoisomer should not have any influence in the final minimized geometries of the bridges.
21 The upper limit of J^{intra} was determined from the experimental Weiss constant and Bleany-Bowers expression for a dimer using the approximation for the high temperature limit. See R. L. Carlin, *Magnetochemistry*, Springer, Berlin, 1986, p. 76. The lower limit of J^{intra} was deduced from the value of the ^{1}H hyperfine coupling constants. See L. Salem and C. Rowland, *Angew. Chem., Int. Ed. Engl.*, 1972, **11**, 92.
22 A.-C. Ribou, J.-P. Launay, K. Takahashi, T. Nihira, S. Tarutani and C. W. Spangler, *Inorg. Chem.*, 1994, **33**, 1325.
23 S. F. Nelsen, S. C. Blacstock and Y. Kim, *J. Am. Chem. Soc.*, 1987, **109**, 677.
24 It is well known that the unpaired electron of highly chlorinated triphenylmethyl radical and the negative charge of their corresponding carbanions are mainly localized on the α-carbons.[10] Therefore, the two alpha carbon atoms of **1** can be considered in a first approximation as the electron active sites for the electron transfer phenomena. It must also be noticed that as far as intramolecular electron transfer phenomena are concerned, the main distance to be considered is the through-bond distance between the two electron active sites; *i.e.*, the sum of bond lengths corresponding to the conjugated pathway. Such distance, measured from the two radical alpha carbon atoms is 24.1 Å for diradical **1**. However, as shown by EPR spectroscopy, the average distance between the two spins –the average interspin separation- differs from the nominal separation, either through-space or through-bond, between the two radical alpha carbon atoms obtained from the AM1 minimized structures, due to the different extent of the delocalization in both diradicals.
25 J. Bonvoisin, J. P. Launay, M. Van der Auweraer and F. C. De Schryver, *J. Phys. Chem.*, 1994, **98**, 5052.
26 The variation of the intervalence absorption band *versus* the average reduction state can be used to determine the comproportionation constant, K_c, according to eqn. (5), $K_c = [\mathbf{1}^{\bullet-}]^2/[\mathbf{1}][\mathbf{1}^{2-}]$ (6) In the present case, the resulting value of K_c is 7. This value is employed in eqn. (6) for the calculation of the corrected spectra.

$$\varepsilon(\mathbf{1}^{-\bullet}) = \left[\left(2 + \sqrt{K_c}\right)/\sqrt{K_c}\right]\varepsilon(\mathbf{1}^{-\bullet})_{app} - \left(\varepsilon(\mathbf{1}^{\bullet\bullet}) + \varepsilon(\mathbf{1}^{2-})\right)/\sqrt{K_c} \qquad (7)$$

where $(\mathbf{1}^{-\bullet})$ and $(\mathbf{1}^{-\bullet})_{app}$ are the true and the apparent extinction coefficients of the radical anion $\mathbf{1}^{-\bullet}$, and $(\mathbf{1}^{-\bullet})$ and $(\mathbf{1}^{-2})$ are the extinction coefficients of diradical **1** and dianion $\mathbf{1}^{-2}$, respectively. Band

deconvolution of the corrected spectrum of $\mathbf{1}^{-\bullet}$ was performed, assuming Gaussian profiles, in order to separate the intervalence band from other nearby bands (see Fig. 4). This deconvolution procedure has already been described in ref. 21, and has the advantage of giving a better estimate of the Marcus λ value.
27 (*a*) J. Heinzer, *Mol. Phys*., 1971, **22**, 167; (*b*) J. Heinzer, *Quantum Chem. Program Exchange*, 1972, N° 209.
28 O. Elsner, D. Ruiz-Molina, J. Vidal-Gancedo, C. Rovira and J. Veciana, *Chem. Commun*., 1999, 579.
29 C. Patoux, C. Coudret, J. P. Launay, C. Joachim and A. Gourdon, *Inorg. Chem*., 1997, **36**, 5037.
30 (*a*) M. J. Shephard, M. N. Paddon-Row and K. D. Jordan, *J. Am. Chem. Soc*., 1994, **116**, 5328; (*b*) M. N. Paddon-Row, *Acc. Chem. Res*., 1994, **27**, 18, and obtained again, references cited therein.
31 AM1 semiempirical calculations gave the same distances as for diradical **1** and from the EPR parameters the distance is also the same.